A STUDY OF SELENATE REMOVAL FROM WATER BY ADSORPTION ON AN AGED, CARBONATED FRIEDEL'S SALT MATERIAL WITH MASS LOSS CONSIDERATIONS

by

Maryam Rasouli

M.Sc., Institute for Advanced Studies in Basic Sciences, 2009

A THESIS SUBMITTED IN PARTIAL FULFILLMENT OF

THE REQUIREMENTS FOR THE DEGREE OF

DOCTOR OF PHILOSOPHY

in

THE FACULTY OF GRADUATE AND POSTDOCTORAL STUDIES

(Materials Engineering)

THE UNIVERSITY OF BRITISH COLUMBIA

(Vancouver)

November 2019

The following individuals certify that they have read, and recommend to the Faculty of Graduate and Postdoctoral Studies for acceptance, the dissertation entitled:

A study of selenate removal from water by adsorption on an aged, carbonated Friedel's salt material with mass loss considerations

submitted by Maryam Rasouli in partial fulfillment of the requirements for the degree of Doctor of Philosophy in Materials Engineering

Examining Committee:

David Dreisinger, Materials Engineering

Supervisor

Bethan McKevitt, Materials Engineering

Co-supervisor

Edouard Asselin, Materials Engineering

Supervisory Committee Member

Berend Wassink, Materials Engineering

Supervisory Committee Member

Marek Pawlik, Mining Engineering

University Examiner

David G Dixon, Materials Engineering

University Examiner

Additional Supervisory Committee Members:

David G Evans, Beijing University of Chemical Technology

Supervisory Committee Member

Dra Gretchen Lapidus-Lavine, Universidad Autónoma Metropolitana Iztapalapa

Supervisory Committee Member

Abstract

In this work, selenate removal from water was studied using a material from the layered double hydroxide family. This material is a mixture of two hydrocalumite phases, chloro-hydrocalumite $[Ca_4Al_2(OH)_{12}]\cdot[Cl_2\cdot 4H_2O]$ and chloro-carboaluminate hydrocalumite $[Ca_4Al_2(OH)_{12}]\cdot[Cl(CO_3)_{0.5}\cdot 10.8H_2O]$. This material is called aged-FS in this thesis. Aged-FS was obtained by the co-precipitation method followed by an aging process. The aging condition was initial pH 12.0, liquid/solid ratio 20, 65 °C, for 7 days. During aging, a phase transformation from chloro-hydrocalumite in the hexagonal crystal system to chloro-carboaluminate hydrocalumite in the monoclinic crystal system was observed. The aluminum hydroxide impurity was removed and katoite ($Ca_3Al_2(OH)_{12}$) was formed. The formation of well-shaped hexagon crystallites and agglomeration of particles were observed by morphology and particle size studies, respectively. The carbonate content increased during aging from 1.15 to 3.00 wt.%. By aging, ~50% reduction in FS dissolution was recorded. By some modifications in nitrogen purging of the synthesis process, the carbonate content was reduced from 1.15 to 1.01 wt.%.

For selenate removal studies, the effect of initial pH, liquid/solid ratio, time, temperature, agitation, selenate concentration, sulfate and carbonate interference, and container type were studied. The highest loading percentage of selenate and the lowest dissolution of aged-FS was achieved at initial pH 12.0, liquid/solid ratio 200, 30 °C, 24 h, and 150 RPM. A selenate loading isotherm was fitted to the Langmuir model with maximum loading of 71.1 mg Se/g. The intercalated carbonate in aged-FS did not interfere with selenate removal while significant interference was observed from carbonate in solution. The sulfate anion did not interfere with selenate adsorption. The Al dissolution from aged-FS in an adsorption test was suppressed using calcium hydroxide solution. The Al concentration reached to 0.07 ppm; a value lower than the maximum instantaneous value set by a BC guideline. Calcination of aged-FS improved the selenate loading. The lowest level of selenium in solution achieved using the calcined aged-FS (1.84 ppb) met the 2016 US EPA maximum discharge limit of lotic water for Se (<3.1 ppb). Overall, calcined aged-FS is a promising exchanger for selenate removal from calcium sulfate-saturated industrial effluents.

Lay Summary

Selenium in water may pose an environmental problem at elevated concentrations. An adsorbent called Friedel's salt (FS) was prepared by coprecipitation of calcium and aluminum hydroxides. FS was studied for selenate ion removal from water as a function of initial pH, selenate concentration, temperature, liquid/solid ratio, and the presence of other ions such as sulfate and carbonate. FS was found to be effective as an adsorbent and reached a maximum loading of 71.1 mg Se/g.

FS may dissolve in water under some conditions and contaminate the water system. FS dissolution was reduced ~50% by an aging process. At the same time the dissolved aluminum concentration in water containing calcium hydroxide solution reached to values lower than the BC waste water guidelines. The selenate concentration was reduced to values lower than the US EPA maximum discharge limit using calcined-FS material. FS showed a highly selective for selenate over sulfate.

Preface

Two papers from the work presented in this thesis are in the process of being written and submitted. The overall supervision of this research was provided by Dr. Dreisinger. Dr. Bethan McKevitt was the co-supervisor of the project and helped with the experimental design of part of the experiments. Dr. Bé Wassink also assisted with the project.

All of the experiments were developed by the candidate. Bana Batshon was the summer student who helped with the aging and adsorption experiments. The analysis solutions by ICP was carried out by Maureen Soon and Vivian Lai in the Earth and Ocean Sciences department at UBC. Dr. Mati Raudsepp and Jenny Lai from the same department conducted the QXRD analysis. I appreciate all of their kind help.

A conference paper was published in COM 2017 metallurgy conference.

- M. Rasouli, D. Dreisinger, (2017), *New Approach to Selenate Removal by Ion Exchange Methodology with a Review of Ion Exchange Materials and Chelating Exchangers*. COM 2017 hosting World Gold and Nickel-Cobalt 2017. This paper was based on literature review studies by the candidate.

Table of Contents

List of Tables

List of Figures

List of Abbreviations

Aged-FS: Friedel's salt prepared with the aging process

BC: British Columbia

BET: Brunauer–Emmett–Teller method

C_3A: Tri-calcium aluminate

CMA: Diethylenetriamine-N,N,N',N'-polyacetic acid

DI: Deionized water

FS: Friedel's salt

$FS._{sint}$.: Friedel's salt prepared with the sintering-precipitation method in this thesis

FTIR: Fourier Transform Infrared Spectroscopy

HTLc: Hydrotalcite-like compounds

ICP: Inductively Coupled Plasma

ICP-MS: Inductively Coupled Plasma Mass Spectrometry

ICP-OES: Inductively Coupled Plasma Optical Emission Spectrometry

IX: Ion exchange

K_{sp}: Solubility product constant

LBM: Liquid-Based Method

LDH: Layered Double Hydroxide

L/S: Liquid/solid ratio

MB: Mass balance

MCL: Maximum Contamination Limits

MDL: Maximum Discharge Limits

Modified unaged-FS: Friedel's salt prepared with the co-precipitation synthesis under complete nitrogen purging method

PSD: Particle Size Distribution

QXRD: Quantitative X-ray Diffraction

R&D: Research and development

SBM: Solid-Based Method

SEM: Scanning Electron Microscopy

SSA: Specific Surface Area

TDS: Total Dissolved Solid

TIC: Total Inorganic Carbon

US EPA: United State Environmental Protection Agency

Unaged-FS: Friedel's salt prepared with the co-precipitation synthesis process under the partial nitrogen purging method

VWM: Volume-weighted mean (μm)

Wu's $FS._{sint}$.: Friedel's salt prepared with the sintering-precipitation method by Wu

XRD: X-ray Diffraction

List of Symbols

A: Freundlich constant

A_{aq}: Ion A in the aqueous solution

$Al._{LB}$: A method used to calculate Friedel's salt mass loss based on aluminum concentration in solution

Aq.vol.: Aqueous solution volume (mL)

b: Langmuir constant

B_{aq}: Ion B in the aqueous solution

$[Ca^{2+}]$: Concentration of calcium ion in the solution

$Ca._{LB}$: A method used to calculate Friedel's salt mass loss based on calcium concentration in solution

C_e: Pseudo-equilibrium concentration or equilibrium concentration (mM)

C_0: Initial concentration (mM)

ΔH^0: standard enthalpy changes

n: Freundlich constant

Q_m: Maximum capacity of a resin, and Se maximum loading (mg Se/g or mmol/g)

Q_e: Pseudo-equilibrium (or final) loading of Se (mg Se/g or mmol/g)

R: Resin

R-A: Resin loaded with ion A

R-B: Resin loaded with ion B

$Se._L$: Loaded Se from the difference of initial and pseudo-equilibrium concentration in solution (mg Se/g or mmol/g)

$Se._S$: Loaded Se calculated from solid digestion method (mg Se/g or mmol/g)

Se %: Selenium loading percentage

V: Volume (mL)

W: Mass of FS (g or mg)

Acknowledgments

I offer my enduring gratitude to Professor David Dreisinger for his support and guidance.

I owe particular thanks to Dr. Bethan McKevitt for enlarging my vision of engineering and providing helpful advice.

I would like to thank Dr. Berend Wassink and Dr. Edouard Asselin for their guidance.

The assistance of Bana Batshon, who spent two summers working with me in the laboratory, is gratefully acknowledged. I am also thankful to the faculty, staff, and my fellow students at the Materials Engineering department at UBC, who have inspired me to continue my work in this field.

Special thanks are owed to my parents and family who have supported me throughout my education.

Dedicated to my brother

Davood

Chapter 1: Introduction

1.1 Selenium distribution and toxicity

Selenium, with the symbol Se, atomic number 34, and atomic weight 78.96 g/mole, is a metalloid [1]. Selenium shows similar chemical properties to sulfur (S) and tellurium (Te) [2]. Selenium in trace amounts is found in many ores including those of copper, zinc, iron, lead, silver, and gold [1,3]. Selenium abundance in the earth's crust is $5X10^{-6}$ wt.%.

Selenium is discharged into waste waters through various human activities such as the mineral processing of ores, roasting and refining of sulfide deposits [4], gold, silver, and nickel mining [5], coal-mining and combustion [6], metal smelting, petroleum and oil refining, and basic agricultural irrigation from both soil and Se-containing herbicides and insecticides [7]. Table 1 shows the selenium concentration of selected mineral process water sources ranging from a few ppb to more than one thousand ppb in some cases [8]. As seen, mining wastewaters have the highest levels of Se.

Selenium is an essential trace element for humans, fish, and other wildlife (recommended dietary allowance for people ~ 55 µg/day) [9]. However, selenium can be toxic if taken in excess and accumulated in high concentrations. The continuous discharge of selenium in wastewaters can cause bioaccumulation in wildlife species tissues at toxic levels. The pollution of natural waters by selenite- and selenate-impacted industrial effluents has been recognized as a serious concern. Selenium poisoning can result in inflammation of the respiratory and digestive tracts in humans or birth defects/mutations in fish and waterfowl due to interference with normal cellular metabolisms [10,11]. Therefore, the toxicity effects and threats to both human health and wildlife highlight the critical importance of selenium removal from contaminated waters. The Elk Valley in Canada is

an area of concern due to weathering and mobilization of selenium from seleniferous-bearing rocks disturbed in the mining of coal [12,13].

Table 1 Selenium concentration (ppb) in various mineral process water sources

Ash settling pond [3]	87-2700
Mining waste waters [4,6], [11]	3->12000, 15-50, 10-10000
Flue gas desulfurization [3]	1-2, 700
Coal ash slurry [3]	50-1, 500

Growing concern arose from the effects of selenium poisoning on fish and wildlife populations and this prompted the World Health Organization (WHO) to set a very strict Maximum Contamination Level (MCL) for selenium. Based on WHO and the European Union, the Standard MCL in drinking water for Se is 10 ppb, while the US EPA (United State Environmental Protection Agency) recommends a limit of 50 ppb. The US EPA National Ambient Water Quality Criteria for aquatic life was 5 ppb (chronic) and 20 ppb (acute), established in 1987 [8,13]. In more sensitive environments, the US Fish and Wildlife Service recommended 2 ppb to protect fish, waterfowl, and endangered aquatic species. The British Columbia water quality guideline for the protection of aquatic life is 2 ppb [14]. Maximum Discharge Limits (MDL) for industrial effluents in Canada, USA, and Japan are 1, 5, and 100 ppb, respectively. These values are difficult to achieve, especially in the presence of relatively high total dissolved solid (TDS) in impacted water [13].

A new aquatic life ambient water quality criterion for selenium in freshwater was published by US EPA in 2016 [15]. The water quality criteria in this version were based on data and scientific judgments about the relationship between selenium concentration and potential environmental and human health effects. The monthly selenium chronic value for lentic (still water) and lotic (flowing water) waters was <1.5 and <3.1 ppb respectively [15].

1.2 Selenium chemistry

Selenium in water has four common oxidation states: -2, 0, +4, and +6. Selenium aqueous chemistry depends on the pH, the presence of oxidizing or reducing agents (E_h), and the nature of the solution, including factors such as oxygen content, total dissolved solids (TDS) content, and the presence of other ions and microorganisms.

The Pourbaix diagram of the Se-H_2O system at 25 °C and a selenium solute activity of 10^{-4} M is shown in Fig. 1. Selenium species are selenate (SeO_4^{2-}), biselenate ($HSeO_4^-$), selenic acid (H_2SeO_4), selenite (SeO_3^{2-}), biselenite ($HSeO_3^-$), selenious acid (H_2SeO_3), elemental Se, hydrogen selenide (H_2Se), and biselenide (HSe^-). Selenate and selenite, however, are the dominant species in impacted waters. Both selenite and selenate are toxic at elevated concentrations [1].

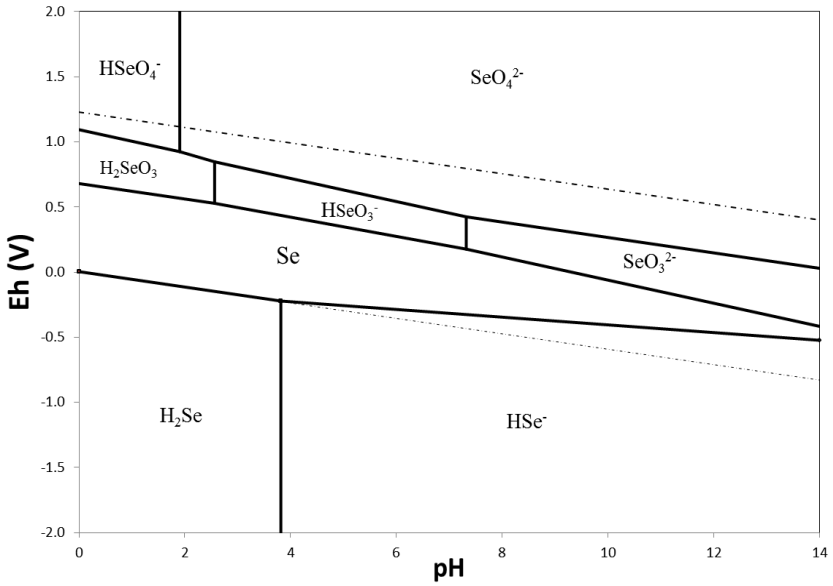

Figure 1 Eh-pH diagram of selenium at 25 °C and selenium activity of 10^{-4} M (Derived from HSC 5.1 software).

Under strongly oxidizing conditions, selenium occurs in the +6 oxidation state. Selenic acid (95%) is a strong acid analogous to sulfuric acid (pk_{a1} -3 and pk_{a2} 1.7) [16]. Singly-protonated biselenate is the dominant species at pH 0 to 1.7 with selenate dominating at higher pH. Selenium

dioxide with a +4 oxidation state (SeO_2) dissolves in water to form selenious acid. The H_2SeO_3 species is a weak acid and selenite is dominant only at pH over 7.3 (Figure 1) [1].

Selenic acid is a much stronger oxidizing agent than sulfuric acid [1]. The oxidation of H_2SeO_3 in acidic solutions by oxygen to both $HSeO_4^-$ and SeO_4^{2-} is thermodynamically favorable (Reaction 1). In highly oxygenated waters, however, selenite exists along with selenate due to the slow oxidation rate of selenite [17]. The efficient oxidizers for the Se^{4+}-Se^{6+} redox reaction are the strong ones (E^0_{red} >>+1.15) such as fluorine, hydrogen peroxide, chromate (CrO_4^{2-}), dichromate ($Cr_2O_7^{2-}$), chlorate (ClO_3^-), and perchlorate (ClO_4^-) used at high temperatures [1].

$SeO_4^{2-} + 2e^- + 4H^+ = H_2SeO_3 + H_2O$ $E^0 = +1.15$, pH=0 Reaction 1

Therefore, the chemistry of selenium in industrial effluents and surface waters (high oxygen content waters) are mainly related to the selenite and selenate species and the protonated forms $HSeO_3^-$, H_2SeO_3, SeO_4^{2-}, and $HSeO_4^-$. The selenate-to-selenite ratio depends on the presence of reducing and oxidizing reagents, kinetic factors, and the pH of the solution.

1.3 Problem definition

Among available technologies for removal of toxic substances from water, the stabilization processes (change of oxidation state) [8,13,18,19] and precipitation (change in solubility) [20,21] have been applied for removal of both selenite and selenate. These techniques have an excellent capacity for selenite capture but are less successful in removing selenate from wastewaters.

The selenate ion can be reduced to lower oxidation states by various reducing agents such as copper metal (Cu), sulfur dioxide (SO_2), hydrogen sulfide (H_2S), ferrous hydroxide ($Fe(OH)_2$), sulfide (S^{2-}), sulfite (SO_3^{2-}), bisulfite (HSO_3^-), and thiosulfate ($S_2O_3^{2-}$) [1,22]. However, the rate at which these processes occur is quite slow. Moreover, harsh experimental conditions, such as the

use of higher temperatures or catalysts, are required for selenate reduction. For instance, selenate can be reduced to selenious acid but by boiling with HCl or HBr [1]. Selenate reduction with a zero-valent iron treatment needs to be enhanced by coupling with a biologically-catalyzed reduction process [6,13].

While the ferrihydrite (Fh) adsorption process is a simple and low-cost process extensively used at full-scale for adsorption of selenite (85-95% recovery), the selenate precipitation by Fh process is weak (only ~10% adsorption) [23].

Therefore, the removal of selenate species from impacted wastewaters is still a big challenge in the mining industry. New research and studies on removal of selenate in both laboratory scale and pilot scale are currently very active. The other issue is the pressure on industries to apply a successful selenium management strategy, which meets the discharge limit guidelines.

The growing concerns arising from selenium in wastewater and the lack of a universal technology for selenate removal motivates the investigation of selenate removal from impacted waters. The efficacy of processes such as crystallization and precipitation for treatment of dilute solutions have been reported to be unsatisfactory [13]. Ion exchange (IX) technology, however, is a feasible method for the treatment of dilute wastewaters. In general, in the majority of commercial uses, dilute solutions, with concentrations of less than 40 equiv/m^3 are treated [24]. In the mining industry, this technology is widely used for the treatment of toxic waste streams prior to disposal and removal of impurities from process streams. Therefore, among all removal technologies, the IX method seems to be a promising alternative method for a selenate removal study.

The ion exchange material selected for this study is called Friedel's salt (FS). This material is also called Friedel phase in Wu's paper [25]. This compound with the general chemical formula of $[Ca_4Al_2(OH)_{12}]\cdot[Cl_2\cdot 4H_2O]$ belongs to the family of layered double hydroxides (LDH). Friedel's salt in this thesis is designated as "**FS**". It was found that the FS in this study always contained some carbonate.

FS was identified as a promising ion exchanger for selenate adsorption by Wu in 2010 [25]. The selenate adsorption by FS material occurs by an ion exchange process. As shown in Reaction 2, every one mole of selenate oxyanion exchanges with two moles of chloride anion from the interlayer space.

$$[Ca_4Al_2(OH)_{12}]\cdot[Cl_2\cdot 4H_2O] + SeO_4^{2-} = [Ca_4Al_2(OH)_{12}]\cdot[SeO_4\cdot 4H_2O] + 2Cl^- \quad \text{Reaction 2}$$

1.4 Thesis layout

This thesis starts with a literature review on layered double hydroxide and Friedel's salt material. The chemical structure, synthesis of FS, literature studies on the aging process, oxyanion adsorption by LDHs and FS are reviewed in Chapter 2. The experimental procedure of synthesis, aging, adsorption and analytical methods are discussed in Chapter 3. In Chapter 4, a description of the preparation of FS in the laboratory and its characterization is provided. The FS material from the synthesis process was found to be partly soluble under the conditions of the adsorption tests. The measurement and control of FS dissolution became one of the objectives of this thesis. In this thesis, the actual dissolution data of FS under all experimental conditions are reported. Such detailed dissolution data for FS is not reported in Wu's work [25]. An aging process after synthesis was applied to as-prepared FS material to minimize the mass loss during the adsorption process. Chapter 5, presents the results of the aging process and the efficiency of the aging process on reducing the FS dissolution. The studies of selenate adsorption by aged-FS material are discussed

in Chapter 6 with a focus on achieving a low residual selenium concentration and determining the selectivity for selenium adsorption in the presence of sulfate and carbonate anions. The understanding of the FS mass loss during adsorption studies affects the utility of FS as a practical adsorbent. Therefore, FS mass loss during adsorption studies is measured and reported for each studied variable. A conclusion and contribution to the knowledge in the field are provided in Chapter 7.

Chapter 2: Literature review

2.1 Introduction to ion exchange (IX)

Ion exchange is the process used in this thesis for selenate removal. As mentioned in 1.3, selenate is removed by FS through the exchange of chloride anions by selenate (Reaction 2). In this section, a short introduction to the ion exchange (IX) process is presented. IX is a well-known technology commonly applied to treat dilute solutions such as waste process and drinking waters for the removal of toxic substances and pollutants [5,24,26]. Reaction 3, shows the reversible and stoichiometric exchange of an ion in solution (B_{aq}) with an ion (A) from an exchanger material (R-A) [24]. Ion exchange technologies use a broad range of materials, including synthetic polymeric resins, modified chelating resins (implemented with metals) [24], layered double hydroxides (LDHs) [25,27–32], clays and cellulose and dextran [24]. Theoretically, the stronger the affinity of R-A for B_{aq}, the more efficient will be the loading. If the exchanging ions both have a positive charge (e.g., Ca^{2+} or Mg^{2+}) the exchanger is called a cationic exchanger. If both are anions (e.g., SeO_4^{2-} or Cl^-), then R-A is an anionic exchanger. FS with exchangeable Cl^- anion in the structure, is an anionic exchanger.

$$R\text{-}A + B_{aq} = R\text{-}B + A_{aq} \qquad \text{(A and B: cation/anion)} \qquad \text{Reaction 3}$$

The maximum capacity of resin for ion B is expressed as Q_m and uses the units mmol/g or mg/g resin. Under experimental conditions, the ion exchanger reaches an equilibrium loading value, Q_e, which is generally lower than the Q_m. The adsorption process is usually studied and presented graphically via an adsorption isotherm. Figure 2 shows a typical adsorption isotherm in which the adsorption increases until it reaches the equilibrium saturation point. The graph shows the loading of B_{aq} (a typical oxyanion) on the adsorbent (any ion exchanger). The equilibrium

loading (Q_e) is usually reported by the mass of oxyanion (mg) over the mass of ion exchanger (g). The remaining equilibrium concentration of oxyanion in the solution C_e can be represented in ppm, ppb, or g/L units. In Figure 2, a ppm concentration is shown as an example.

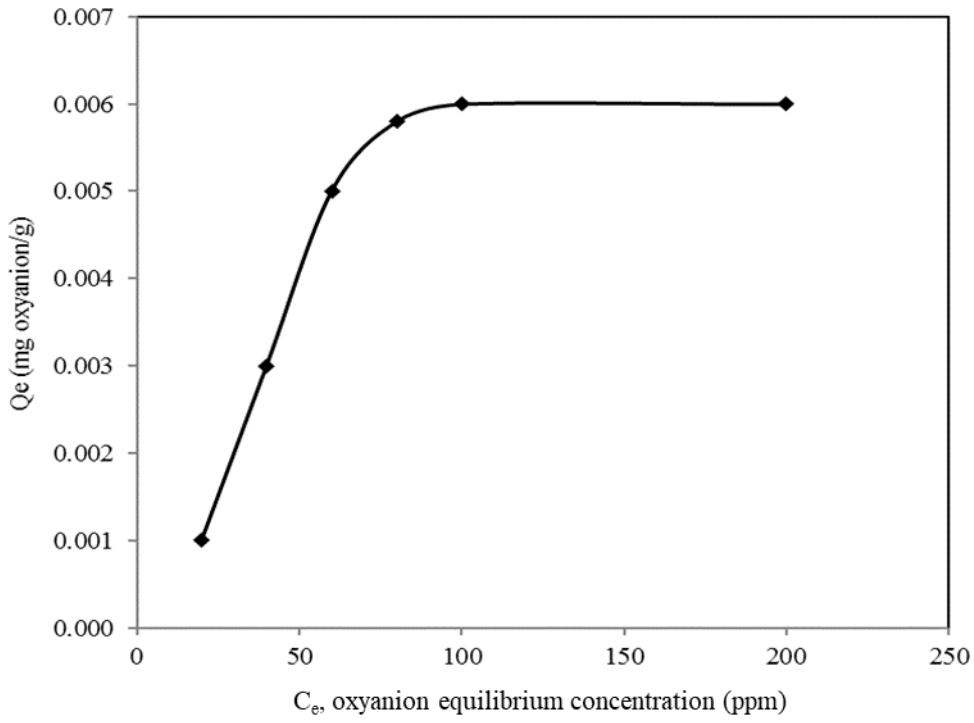

Figure 2 A schematic example of adsorption isotherm for an oxyanion.

A similar adsorption isotherm to Figure 2 is expected for selenate adsorption by FS. The intrinsic dissolution of LDH materials under various experimental conditions, however, imposes a degree of uncertainty on final mass data used for generating the LDH material adsorption isotherms. The inclusion of dissolution data and final mass for most of oxyanion adsorption isotherms by LDHs are not reported (even if determined) [25,33]. In this thesis, the loading percentage of selenate for each individual adsorption test (and therefore adsorption isotherms) is generated by using the actual final mass data. The partial dissolution of FS in all loading data are included. The selenium loading percentage (Se %) is defined by Equation 1.

$$Se\ \% = [(C_0 - C_e))/C_0]*100 \qquad \text{Equation 1}$$

Among all methods applied for toxic species removal, IX provides the advantages of ease of phase separation (if resin beads are used) and high enrichment efficiency, thus reducing the volume (if species is eluted) or mass for further treatment. If the adsorbent is reused, then it is necessary to elute the loaded species. The eluate will be enriched in the target species and may need further treatment (e.g. reduction to elemental Se or immobilization in some other form). IX can suffer from lack of specificity and/or selectivity and interference of other ions with target ion adsorption. For example, the presence of sulfate anion (SO_4^{2-}) may interfere with the loading of selenate (SeO_4^{2-}). This complicates the purification process and increases the secondary waste volume [34,35]. Therefore, treatment of solutions with high sulfate content (ranging from 450 ppm in coal mining waste waters) to reach MDL values set by US EPA in 2016 (<1.5 and <3.1 ppb Se for lentic and lotic waters) is a big challenge in wastewater treatment [4].

Various types of ion exchange materials have been used for removal of both selenite and selenate from selenium-containing solutions. Selenium removal from wastewater solutions using strong base anion exchangers, chelating ligand exchangers and chelating resins pre-loaded with metals have been extensively studied [34,36,37]. These resins have some ability to extract selenium from wastewater.

A short summary of reported studies on selenium removal by strong base anion exchangers, chelating ligand exchangers, and chelating resins loaded with metals is provided in Appendix A. Besides the use of conventional IX materials, selenium adsorption and removal with synthetic nano-magnetite [38] and cement-stabilized wastes are also reported [39–41].

2.2 Structure and chemistry of LDH

This chapter provides a review on layered double hydroxide (LDH) materials, also called hydrotalcite-like (HTLc) compounds. LDHs are synthetic or natural lamellar hydroxides material to which the material used in this thesis, Friedel's salt (FS), belongs to [25,27–32,42,43]. LDH or is presented by a general chemical formula of $[M_{(1-x)}^{2+}N_x^{3+}(OH)_2]^{x+}.[X_{x/n}{}^{n-}.mH_2O]$. It is composed of positively charged layers originating from the substitution of divalent metal ions (M^{2+}) by trivalent metal ions (N^{3+}) and replaceable charge-balancing interlayer anions (X^{n-}) [43,44].

Figure 3, shows a schematic representation of an LDH material. The divalent and trivalent metal ions belong to a wide range of metal ions. A few examples of common metal ions seen in nature also used in LDH preparation are Ca^{2+}, Mg^{2+}, Ni^{2+}, Zn^{2+}, Al^{3+}, Fe^{3+}, and Cr^{3+}. As seen from the LDH chemical formula, the partial substitution of M^{2+} by N^{3+} results in an excess positive charge on the layers [43]. The positive charge of the layers, shown with "x+", is equal to the molar ratio of $N^{3+}/(N^{3+}+M^{2+})$ in the range of $0.2<x<0.33$. Therefore, the higher the trivalent metal ion proportion, the higher will be the positive charge of the layers. The excess positive charge of the layers is balanced with anions from interlayer space.

As shown in Figure 3, the interlayer spacing is the difference of basal spacing (c') and the thickness of the brucite-like sheet of about 4.8 Å. The interlayer spacing depends on the size and orientation of the charge-balancing anions [43]. A wide range of monovalent and divalent anions such as Cl^-, NO_3^-, ClO_4^-, CrO_4^-, F^-, Br^-, I^-, CO_3^{2-}, and SO_4^{2-} are frequently used for LDH preparation. These anions are arranged in the interlayer space through a complex hydrogen bonding network with interlayer water molecules. The intercalated anions and water molecules are shown with light-green circles and blue circles, in Figure 3, respectively. The bonding between anions

and water molecules in interlayer space and brucite layers is associated with a combination of hydrogen bonding and electrostatic effects [43].

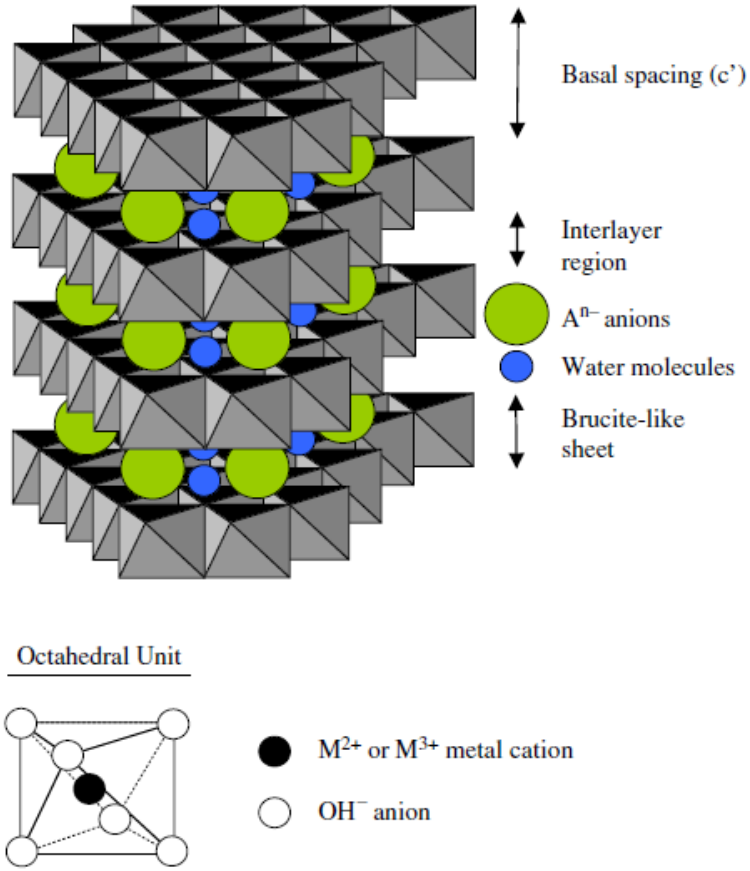

Figure 3 Schematic representation of basal spacing, interlayer region, and brucite-like sheets in LDH (top), and octahedral unit of metal-hydroxide (bottom). Reprinted with permission from [44].

Figure 3, shows the brucite layers with the gray-colored sheets [44]. Inside the brucite layers, the metal ions are located in the center of octahedral units. One octahedral unit is shown as an example in the bottom of Figure 3. The metal ion, M^{2+} or M^{3+}, (shown with a black circle) is bonded to six hydroxyl functional groups (shown with empty circles). These octahedral units form infinite brucite-like layers by edge-sharing of hydroxyl functional groups. From crystallography view, the octahedral units of M^{2+} and N^{3+} metal ions can belong to the hexagonal, monoclinic, or

rhombohedral crystal systems. The crystal systems are fully discussed in Appendix B and C. In general, these crystalline systems differ from each other in terms of O-M-O bond lengths and bond angles [45]. Different stacking arrangements of the brucite layers are also observed. The hexagonal and rhombohedral symmetry have two and three layers in each unit cell, respectively [43,44]. The stacking axis is perpendicular to the brucite sheet.

Hydroxyl groups (-OH), especially the ones bonded to trivalent cations (N^{3+}) are polarized and interact with anions from interlayer space [43]. N^{3+} ion is more electron deficient than M^{2+} ion and therefore withdraws the bonding electrons from oxygen (-N←O-). The polarized -N←O- bonding, in turn, withdraws the bonding electrons from hydrogen, (-N←O←H). As a result, anion from the interlayer space (X^{n-}), bonds to the hydrogen atom through a strong hydrogen bonding. This interaction, in general, can be shown with [$N\text{-}O^{\delta-}\text{-}H^{\delta+}\ldots X^{n-}$].

In this thesis, LDH is shown with the designation M-N-X, an abbreviated term where M, N, and X are a divalent cation, trivalent cation, and interlayer anion, respectively (mostly referring to M/N molar ratio of 2:1). The designation Mg-Al-Cl, for example, refers to a chloride-intercalated LDH with divalent cation Mg^{2+} and trivalent cation Al^{3+} in the layers (Mg/Al molar ratio 2). Some common LDH members found in nature and synthetic cementitious materials are [29,39]:

- Hydrotalcite, the most prominent representative of LDHs, is produced when the bivalent metal ion is Mg^{2+} and the trivalent metal ion is Al^{3+}. Hydrotalcite is shown with a general formula of $[Mg_6Al_2(OH)_{16}]\cdot[CO_3\cdot 4H_2O]$. Using the nomenclature system of this thesis this LDH will be shown by Mg-Al-CO_3.

- Hydrocalumite is an anionic clay mineral with a general chemical formula of $[Ca_4N_2(OH)_{12}]\cdot[X_2\cdot mH_2O]$, N= Al^{3+}, Fe^{3+}, Sc^{3+}, and Ga^{3+}, where X can be Cl^-, OH^-, CO_3^{2-}, and NO_3^- [46]. Aluminum is the most common trivalent ion used in hydrocalumite structure and therefore hydrocalumite is widely introduced with a general chemical formula of $[Ca_4Al_2(OH)_{12}]\cdot[X_2\cdot mH_2O]$ [46]. Hydrocalumite is formed with Ca^{2+} and Al^{3+} cations in a fixed Ca/Al molar ratio of 2:1. It has been assumed that the ordered arrangement of Ca^{2+} and Al^{3+} in a fixed molar ratio of 2:1 is due to the large difference in the ionic radii between Ca^{2+} and Al^{3+} [43,46]. However, the replacement of Al^{3+} with larger metal ions such as Ga^{3+}, Fe^{3+}, and Sc^{3+}, did not show any loss of cation ordering [46]. This indicated that the fixed Ca:Al molar ratio of 2:1, in the hydrocalumite phase is related to the large size and noticeable anisotropy of the coordination sphere of Ca^{2+} ion [43,46].

  Friedel's salt (FS) with a chemical formula of $[Ca_4Al_2(OH)_{12}]\cdot[Cl_2\cdot 4H_2O]$ and hydrocalumite-hydroxide with a chemical formula of $[Ca_4Al_2(OH)_{12}]\cdot[(OH)_2\cdot 6H_2O]$ both belong to the hydrocalumite family. Hydrocalumite forms as secondary precipitates during the hydration of fly ash and mainly presents in the hydrated cement paste [25,47]. Using the nomenclature system of this thesis the hydrocalumite and Friedel's salt materials will be shown by Ca-Al-X and Ca-Al-Cl, respectively, with a Ca/Al molar ratio of 2.0. The experimental Ca/Al molar ratio in a hydrocalumite phase might differ slightly from the ideal value of 2.0, due to the presence of minor Ca- or Al-containing impurities in the material.

- Ettringite with a chemical formula of $[Ca_6Al_2(OH)_{12}]\cdot[(SO_4)_3\cdot 26H_2O]$ is a well-known primary constituent of hydration of Portland cement concrete [40,41]. Using the nomenclature system of this thesis ettringite will be shown by Ca-Al-SO_4, with a Ca/Al molar ratio of 3.0.

2.2.1 Structure and chemistry of Friedel's salt (FS)

Friedel's salt (henceforth referred to as **FS**) with a chemical formula of $[Ca_4Al_2(OH)_{12}]\cdot[Cl_2\cdot 4H_2O]$ belongs to the hydrocalumite family $[Ca_4Al_2(OH)_{12}]\cdot[X_2\cdot mH_2O]$, where $X=Cl^-$ and m=4 [25,33,48–50]. In 1897, Friedel's salt was mentioned for the first time by Friedel who was performing experiments on the reactivity of lime with aluminum chloride [51]. In 1962, the ordinary Portland cement and sulfate resistant Portland cement was shown to be capable of adsorbing chloride anions [52]. A few researchers two decades later reported that the chloride containing cement was Friedel's salt. FS also forms through the reaction of calcium and alumina which are available in cementitious matrices in the presence of chloride [49].

The following are some structural features of FS. Firstly, FS is a chloro-hydrocalumite with a chemical formula of $[Ca_4Al_2(OH)_{12}]\cdot[Cl_2\cdot 4H_2O]$ and a fixed Ca/Al molar ratio of 2:1. In a study on chromate removal by Friedel's salt, the synthesized material was reported to match well with Friedel's salt XRD pattern [33]. The sample had an approximate formula of $[Ca_{3.6}Al_{2.0}(OH)_{11.2}]\cdot[Cl_{1.9}(CO_3)_{0.05}\cdot 3.8H_2O]$ with a Ca/Al molar ratio of 1.8, slightly deviated from the ideal value of 2.0.

The second feature of a pure FS material is the chloride anion being the only host interlayer anion. The carbonate oxyanion, if intercalated makes bi-anionic FS. A series of bi-anionic hydrocalumite compounds with partial substitution of Cl^- with CO_3^{2-} in FS structure were prepared by Mesbah [53]. The origin of intercalated-carbonate in FS can be from manual addition of Na_2CO_3 to the synthesis slurry [53] or from the dissolution of $CO_{2(g)}$ from the air [25,33]. Since this thesis, deals with both pure FS and carbonated-FS the following labeling is used for these materials. FS material with a chemical formula of $[Ca_4Al_2(OH)_{12}]\cdot[Cl_2\cdot 4H_2O]$, a pure FS material, is called *chloro-hydrocalumite* phase. The carbonated-FS phase with a general chemical formula of

$[Ca_4Al_2(OH)_{12}]\cdot[Cl_{2(1-x)}(CO_3)_x\cdot(4+x)H_2O]$ is called *chloro-carboaluminate hydrocalumite* phase [54]. The hemi-carboaluminate and mono-carbonate hydrocalumite phases terms are used for the half-carbonated and fully-carbonated hydrocalumite phases, respectively.

Figure 4 shows a schematic representation of Friedel's salt. FS is represented with a chemical formula of $[Ca_4Al_2(OH)_{12}]\cdot[Cl_2\cdot4H_2O]$. An alternative chemical formula used for FS in literature is $3CaO\cdot Al_2O_3\cdot CaCl_2\cdot10H_2O$ [47]. The positively-charged layers of FS are composed of $[Ca_4Al_2(OH)_{12}]^{2+}$ units with an ordered arrangement of calcium and aluminum ions seven-and six-coordinated, respectively, in a fixed ratio of 2:1. These brucite layers are shown with light gray columns in Figure 4. The negatively-charged interlayer space with the composition of $[Cl_2\cdot4H_2O]^{2-}$ is arranged parallel to the brucite layers (seen as dark gray columns in Figure 4). This alternative arrangement of brucite layers and interlayer space maintains the total charge of FS balanced.

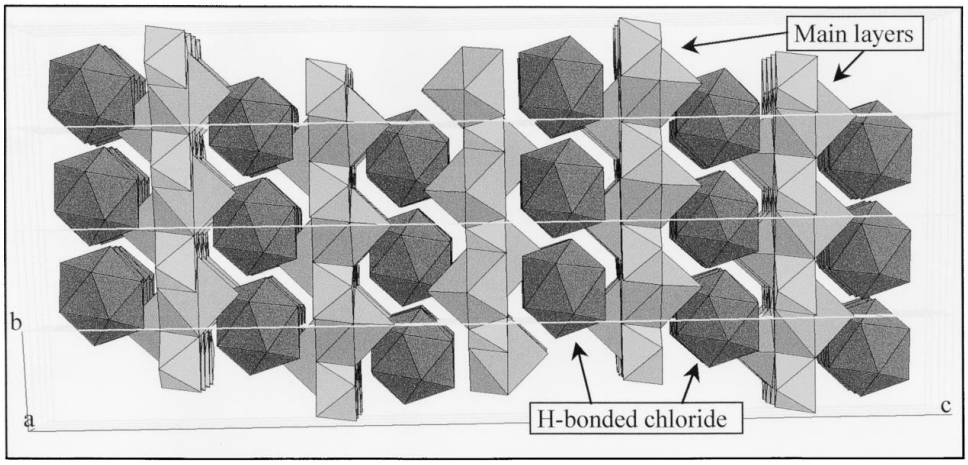

Figure 4 Perspective polyhedral representation of Friedel's salt. Reprinted with permission from [47].

The single crystal study of Friedel's salt by Renaudin et al. in 1999, revealed more complexity of this layered structure. Firstly, the intercalated chloride anions were bonded to water molecules and hydrogen atoms of hydroxyl groups from layers through hydrogen bonding (see Figure 5) [47]. Secondly, all water molecules from interlayer space were directly bonded to the

layers through Ca atoms (no space filling water). Calcium ions in the layers were also bonded to six hydroxyl functional groups in an octahedral unit, therefore making seven-coordinated calcium units. This calcium unit of FS is called Ca-framework and is shown with $[OH\text{-}Ca\text{-}OH]._{FS}$ in this thesis. Al ions, on the other hand, were only bonded to six hydroxyl functional groups from layers without any direct bonding to the interlayer space, making six-coordinated aluminum units. Al units bond to the interlayer space through hydrogen bonding (Al-O-H…Cl). Aluminum unit of FS in this thesis is called Al-framework and is shown with $[OH\text{-}Al\text{-}OH]._{FS}$. The Ca- and Al-framework terminology was used by Wu as well [25].

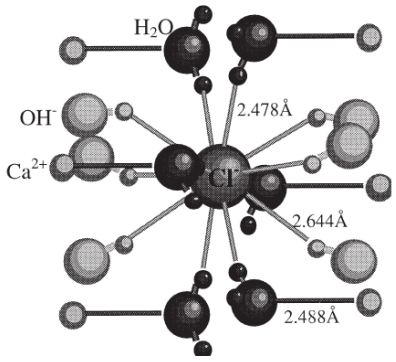

Figure 5 Hydrogen environment of chloride anions in Friedel's salt. Reprinted with permission from [47].

Renaudin et al. studied the phase transformation of Friedel's salt at various temperatures [47]. From Renaudin's study two polymorphs were detected for Friedel's salt; monoclinic system (the low-temperature phase) and rhombohedral system (the high-temperature phase). The monoclinic and rhombohedral crystal systems are called low-temperature and high-temperature phases of Friedel's salt. See Appendix B and C for more details on monoclinic, hexagonal and rhombohedral crystal systems.

2.3 LDH synthesis

Many studies have been reported for LDH preparation by different methods in the literature [27,47,55]. There are several approaches for the synthesis of LDHs in the literature including co-precipitation [25,30,32,55,56], the urea hydrolysis method [57,58], ion exchange [59], the hydrothermal method [31], mechanochemical methods [60,61] and microwave radiation [62].

Co-precipitation is the most commonly used procedure for LDH synthesis. In this method, an aqueous solution of metals (M^{2+} and N^{3+}) is added to the reactor containing the desired anion (X) that is to be incorporated into the LDHs. M^{2+} and N^{3+} are the divalent and trivalent metals respectively. The desired anion, can be added with the metal salt precursors (e.g., Cl^- from $CaCl_2 \cdot 6H_2O$ salt) or separately (e.g., CO_3^{2-} added as sodium carbonate). It is necessary to provide supersaturation condition by addition of an alkaline solution simultaneously. This will ensure the pH control and simultaneous precipitation of metal cations and anion. In the absence of proper supersaturation condition (poor pH control), the trivalent metal hydroxide, $N(OH)_3$, will precipitate. The solubility product constant of trivalent metal hydroxide is smaller than the bivalent metal hydroxide ($K_{sp}\ M(OH)_2 >> K_{sp}\ N(OH)_3$) [63].

In order to ensure the purity of the as-prepared LDHs, the use of the de-carbonated water and nitrogen purging in the slurry during the synthesis process are necessary. The dissolution of $CO_2(g)$ from the air in the alkaline solution can form carbonate anion (CO_3^{2-}) during the synthesis process [25,42,64]. Among all anions, carbonate is known to have a high tendency for intercalation in LDHs. This oxyanion with a planar geometry (sp^2 space group), easily intercalates into the interlayer space and is tenaciously held between the layers [53,65]. Carbonate intercalation can reduce the adsorption capacity of the target oxyanion [42].

Some examples of the synthesis methods in the published literature are reviewed in this section. Zn-Fe-SO_4 LDH with sulfate in the interlayer space was prepared by the following co-precipitation process [66]; a mixed salt solution of $ZnSO_4 \cdot 7H_2O$ and $FeSO_4 \cdot 7H_2O$ (a mix of Fe^{2+} and Fe^{3+}) and a 1.25 M NaOH solution, was added to a volume of water with controlled addition rate to maintain the pH at 7.0. The resulting suspension was aged at 38 °C for 24 h. The solid was filtered, washed and dried. The XRD analysis confirmed the formation of Zn-Fe-SO_4 LDH.

Erickson in 2005, studied the preparation of an LDH with a chemical formula of $[Zn_6Al_2(OH)_{16}] \cdot [CO_3 \cdot 4H_2O]$ by the urea method [58]. A mixed solution of 0.165 M Al^{3+} (as $AlCl_3 \cdot 6H_2O$) and 0.335 M Zn^{2+} (as $ZnCl_2 \cdot 6H_2O$) were prepared. To this solution, 1.65 M of urea ($CO(NH_2)_2$) was added and dissolved. Urea is an effective chemical agent in precipitation of metal ions. The mixed solution was heated to 90 °C for 24 h, then filtered and washed several times. The formation of the LDH product was confirmed by X-ray diffraction.

In a study by Zhang in 2003, a Ca-Al-X LDH was precipitated by the addition of calcium hydroxide and mono-calcium aluminate to an oxyanion stock solution [56]. The stock solution contained 10 ppm of each B, Cr, Mo, and Se oxyanions. With this synthesis method, Ca-Al-X LDH synthesis and oxyanion incorporation processes occurred simultaneously. This is not a usual adsorption study for LDH materials. In most LDH-related studies, the LDH is synthesized first and then used for oxyanion removal study from synthetic water [25,33,66].

LDH materials prepared by co-precipitation methods are usually a mixture of poorly crystalline and crystalline phases [44]. The preparation of pure single crystals of LDH materials was performed by hydrothermal synthesis methods. In this method, the initial reactants are mixed and exposed to heat and pressure in a silver capsule, usually for a long period [47,67,68]. Francois

in 1998 synthesized Ca-Al-CO_3 LDH with a chemical formula of $[Ca_4Al_2(OH)_{12}]\cdot[CO_3\cdot 5H_2O]$ using hydrothermal synthesis [68]. The single crystal of this carbonated-LDH was prepared as follows; the starting powders $Ca(OH)_2$, $Al(OH)_3$ and $CaCO_3$ in a 3.5:2:0.5 ratio was mixed with water (solid/water ratio: 0.5) and loaded into a silver capsule (length 100mm, diameter 5mm, thickness 0.1 mm) sealed under normal atmosphere. This experiment was performed over a period of one month at 120 °C and 2 Kbar (1 mbar = 100 Pa). From single-crystal data, the structural information such as oxygen-atom environments of Ca^{2+} and Al^{3+} cations and hydrogen bonding network of carbonate anions in the interlayer were studied.

In a similar study, Renaudin prepared single crystals of Friedel's salt, the Ca-Al-Cl LDH by hydrothermal synthesis [47]. In this experimental procedure, the starting chemicals $Ca(OH)_2$, $Al(OH)_3$, and $CaCl_2\cdot 6H_2O$ in a molar ratio of 3/2/1 were mixed in a silver capsule for a period of one month at 120 °C at 2 Kbar. As mentioned before in 2.2.1, single crystals of FS were analyzed for phase transformations studies at 0 to 40 °C.

Beside co-precipitation and hydrothermal methods, a less common mechanochemical method is used for LDH synthesis [32,61]. In contrast to the co-precipitation method, this process involves the activation of the starting materials by only the grinding of chemicals. This method is reported to be free from aqueous-related issues such as different precipitation rates of metals, carbonate-free LDH formation, and pH control. Ferencz in 2015, prepared Ca-Al-OH LDH using a mechanochemical process [61]. This method included manual grinding of aluminum hydroxide ($Al(OH)_3$) and calcium hydroxide ($Ca(OH)_2$) with water (in mortar and pestle for 5 minutes) followed by grinding in presence of NaOH solution for an additional hour. A method similar to this was performed in a mixing mill. The precursors were put in grinding jars and mixed for an hour (dry milling) followed by a controlled wet-milling process (addition of water/NaOH

solution). The X-ray diffraction of products formed by two methods shows that even though LDH could be produced by manual grinding it was clearly far from being complete (a minor phase was formed). The initial metal hydroxide precursors were the major phases in the XRD pattern. On the other hand, the two-step milling procedure provided adequate energy for the transformation of precursors to Ca-Al-OH LDH.

In 2017, Fahami et al. reported a low-cost approach to the synthesis of hydrocalumite with short processing time [69]. Specific amounts of $CaCl_2$, $AlCl_3$, and NaOH were milled at 30-300 minutes in a high energy ball mill under air atmosphere. The composition of the Ca-Al-LDH product at the selected time intervals was detected using the X-ray diffraction method. Based on the XRD pattern, a pure material Ca-Al-LDH (free from carbonate) was prepared after 30 minutes, but the expansion of time to 60 minutes resulted in a higher crystallinity. With increasing the milling time, the basal spacing of Ca-Al-LDH increased, and shift toward lower 2θ was observed. This was related to the carbonate insertion in the interlayer space over time. FTIR spectrum confirmed the presence of carbonate in the prepared samples.

Another ultrasonically-enhanced mechanochemical synthesis method was used to prepare Ca-Al-X LDHs with X: CO_3^{2-}, F^-, Cl^-, Br^- and I^- [60]. The procedure was started with milling $Al(OH)_3$ and $Ca(OH)_2$, with the Ca/Al molar ratio to 2, in a mixer mill. The mill was operated at fixed ball/sample weight ratio and grinding frequency, but varying milling time. The milled hydroxides were transferred to glass centrifuge tubes followed by addition of distilled water containing the appropriate anions (CO_3^{2-}, F^-, Cl^-, Br^- and I^-). Then, these tubes were placed into a thermostated glass vessel, where the suspensions were subjected to ultrasound, at various temperatures and durations. Finally, the solid materials were filtered and dried at 60 °C. The LDH preparation was prepared under N_2 purging, to avoid the intercalation of the carbonate.

Linares et al. in 2016 reported a fast synthesis process for the preparation of a carbonated-hydrocalumite by using microwave radiation [62]. The Ca and Al nitrates were used in a basic solution (sodium hydroxide and sodium carbonate) to prepare a gel. The gel was heated in a domestic microwave for only 2.5 minutes. The obtained solid was washed and dried. The characterization study by XRD method confirmed the formation of a carbonated Ca-Al-LDH and a minor calcite phase. This method had the advantage of quick preparation compared to the conventional hydrothermal synthesis method.

2.3.1 FS synthesis

In general, the synthesis of FS was carried out by different methods including sintering-precipitation [25,33], co-precipitation [55], and hydrothermal methods [47]. Some of the synthesis processes of FS are highlighted in this section.

Dai et al. in 2009, prepared FS by the sintering-precipitation process [33]. In this method, the precursor tri-calcium aluminate (C_3A) was prepared by sintering at 1400 °C followed by preparation of FS through mixing of C_3A with $CaCl_2$ solution. The as-prepared FS was used for the study of chromate removal from water. It needs to be mentioned that the material prepared by Dai was a carbonated Friedel's salt with a chemical formula of $[Ca_{3.6}Al_2(OH)_{11.2}]\cdot[Cl_{1.9}(CO_3)_{0.05}\cdot 3.8H_2O]$. The synthesized material was called pure Friedel's salt by Dai. However, using the naming convention used in this thesis, the material would be reported as a chloro-carboaluminate hydrocalumite phase.

Wu et al. in 2010, used the sintering-precipitation method for a selenate removal study [25]. The C_3A was prepared by sintering of a 3:1 molar ratio of calcium carbonate and alumina at 1400 °C. In the next co-precipitation process, the synthesized C_3A was slowly added to $CaCl_2\cdot 6H_2O$ in a sealed water-jacketed reactor. The milky mixture was stirred at 45 °C for 24 h.

The slurry was filtered and the as-prepared Ca-Al LDH was washed with DI water. The material was used for selenate removal study from water and was shown to have a high capacity for selenate. The FS material used by Wu and prepared by sintering-precipitation method is called Wu's $FS._{sint}$ in this thesis. The FS material prepared in this thesis by sintering-precipitation method is called $FS._{sint}$.

Rousselot et al. in 2002, prepared FS by a co-precipitation method using decarbonated water under nitrogen gas to avoid contamination by carbonate anion [46]. According to the synthesis procedure, a 10 mL aliquot of a mixed solution of $CaCl_2$ and $AlCl_3$ was added dropwise to a reactor with pH controlled at 11.5 by addition of 2.0 M NaOH solution. The reacting flask (250 mL) was filled with 2:3 volumetric ratio water and ethanol. After the complete addition of the metal solution, the slurry was aged in mother liquor for 24 h. After filtration, the solid was dried under vacuum and stored in a desiccator. The prepared FS had a chemical formula of $Ca_2Al(OH)_6Cl{\cdot}2H_2O{\cdot}0.29H_2O{\cdot}0.31CO_2$. The amount of chloride anion was reported to exactly balance the charge of positive layers. This indicated that CO_2 was physically adsorbed on the outer surface of the crystallites rather than intercalation into hydrocalumite phase in the carbonate form.

Tóth et al. in 2014, prepared FS with two different co-precipitation methods [55]. In the first method, the metal ion solution containing both $CaCl_2$ and $AlCl_3$ was added dropwise to 3.0 M NaOH solution at 60 °C. In a second modified co-precipitation method, $CaCl_2$ solution was added slowly to the alkaline solution containing NaOH and $Al(OH)_4^-$ solutions. The carbonate-free conditions were assured by using a nitrogen atmosphere during each preparation. The preparation of Ca-Al-Cl LDH was successful in both cases.

Jiang et al. in 2015, prepared FS by co-precipitation method to study the removal of Cr(VI) [32]. The $CaCl_2$ powder was dissolved in deionized water. Subsequently, $Ca(OH)_2$ was added to

the solution with constant stirring and ultrasonic treatment (40 KHz, 360 W) for dispersion. After mixing, mono-calcium aluminate was added slowly with constant mixing for 20 minutes. The mixture was sealed and transferred to a thermostatic water bath oscillator (150 RPM) at 40 °C for 72 h. The final product was filtered and dried at 65 °C in an air oven.

As explained earlier in 2.2.1, single crystals of FS were synthesized by hydrothermal synthesis [47]. FS was prepared with mixing allocated proportions of blast furnace slag, clinker, and sodium chloride as well [48].

2.4 Aging of LDH materials and quantification of its efficiency in minimization of LDH dissolution

In general, co-precipitation under supersaturation conditions is associated with complex nucleation, crystal growth, agglomeration, and breakage processes of particles. The formation of large numbers of crystallization nuclei from the co-precipitation process may result in a material with a low degree of crystallinity. Hydrothermal treatment and the aging process are applied on freshly precipitated LDH materials to achieve the following [28,44,70]:

1- transform the small crystallites of LDH into coarser particles of crystalline LDH
2- transform amorphous/poor crystalline precipitates into higher crystalline LDH

Hydrothermal treatments are generally performed at temperatures higher than 100 °C, under pressure in a silver or gold capsule or a stainless steel autoclave. A conventional aging treatment is performed at temperatures below 100 °C. The aging process usually occurs over a few hours or several days [27,70].

Various aging processes on LDH materials are reported in the literature with a focus on structural studies. Aging has been shown to affect the LDH properties such as particle morphology, particle size distribution, and the degree of crystallinity of the LDH material [28,71–73]. On the

other hand, LDHs are known to suffer from partial dissolution in water especially at low-pH range solutions [44]. As mentioned, the dissolution of FS in the early stages of this thesis was a big drawback in the continuation of more adsorption tests. The correlation of an aging process to controlling the intrinsic dissolution of LDH materials (and quantification of this control) seems a promising research study on addressing the LDH dissolution.

In general, the aging studies on quantification of LDH dissolution control for the benefit of using a less-soluble material in adsorption tests are not widely investigated [71]. In this thesis, the FS material was aged after filtration from the synthesis-mother liquor and washing with DI water for impurity removal. By applying an aging process after the synthesis process, the impact of that aging process on the reduction of mass loss can be quantified. Some examples of aging studies in the literature are highlighted in this section.

Xu et al. in 2006, reported the preparation of a stable homogenous suspension of Mg-Al-Cl LDH by fast co-precipitation followed hydrothermal treatment under various time and temperature conditions [71]. The effect of heating duration and temperature on particle size and dispersion of LDH agglomerates were studied. The results of this study showed that as the treatment time increased (from 2 to 48 h), the Mg-Al-Cl LDH particle size was increased from 69±15 nm to 159±29 nm at 100 °C, indicating the particle growth over hydrothermal treatment. The increase in temperature from 80 to 150 °C (8 and 16 h) in an autoclave almost doubled the primary particle size of Mg-Al-Cl LDH as well. The suspension obtained after hydrothermal treatment at 100 °C for 16 h, had a narrower particle size distribution (45-250 nm) than freshly prepared LDH (particle size distribution of 320-2300 nm). This showed that the dispersion of LDH agglomerates into individual particles occurs during hydrothermal treatment. From the results of hydrothermal treatment in Xu's work, a question naturally arises as to what extent this

hydrothermal treatment process could have an impact on the dissolution of Mg-Al-Cl LDH material (the product of fast co-precipitation)? If Mg-Al-Cl LDH samples (before and after hydrothermal treatment), were used for a typical oxyanion removal study how much of each material will be dissolved? How much of the material after hydrothermal treatment is expected to be saved in comparison with the material before hydrothermal treatment?

Various carbonate-containing LDHs (Mg-Al LDH, Mg-Al/In LDH, and Mg-In LDH) were prepared with separate nucleation and subsequent aging process [72]. A mixed metal solution with $Mg^{2+}/(Al^{3+}+In^{3+})$ molar ratio 3 and a $NaOH/Na_2CO_3$ solution was simultaneously added to a reactor rotating at 3000 RPM and mixed for 2 min. The resulting slurry was aged for 6 h at 80 °C. The aging slurry was filtered and solid was dried at 60 °C overnight. LDH samples were calcined at 500 °C in air for 5 h. The properties of as-prepared LDH and calcined product were studied. X-ray analysis showed that the product was a well-crystallized single phase. Calcination of the LDH materials increased the surface area (from 99.7 m^2/g to 146.7 m^2/g for Mg-Al/In LDH). The calcined Mg-Al LDH with the highest density of base sites (OH^- sites) showed the highest catalytic activity for phenol loading from cyclohexane solution.

Zhao et al. in 2002, have proposed a synthesis method for Mg-Al-CO_3 LDH involving separate nucleation and aging steps [28]. The key features of this method were a rapid mixing and nucleation process in a colloid mill followed by a separate aging process. A colloid mill is a machine that is used to reduce the particle size of a solid in suspension in a liquid. The nucleation process in the colloid mill was rapid and particles did not have time for aggregation of nuclei. When the resulting mixture was aged in a separate process, well-formed crystallites with a similarly narrow particle size range resulted. The same question regarding the effect of the separate aging process on the dissolution of Mg-Al-CO_3 LDH remains unanswered here. How much of Mg-

Al-CO_3 LDH mass loss can be prevented by this separate aging process? To what extent this separate aging process will be helpful in controlling the dissolution of Mg-Al-CO_3 LDH (coming directly from rapid mixing and nucleation) in exposure to an oxyanion removal study?

Non-conventional aging techniques such as the use of microwave and ultrasound have been used because of their unique features compared with conventional aging processes [73]. The microwave aging technique allows the use of the concentrated solution and reduces aging time significantly. Aging of FS was studied using microwave irradiation or conventional heating and by refluxing or in an autoclave with the aim of decreasing the aging times. FS material was prepared by the co-precipitation method at constant pH and was then exposed to different temperatures (80 °C and 180 °C) for various times (1-24 h) using either conventional or microwave heating. Results showed that aging with microwave heating resulted in faster crystal growth while the use of autoclave improved crystallinity as observed by X-ray diffraction. The sample with the highest crystallinity was the aged sample obtained with microwave irradiation and autoclaving at 180 °C for 1 h. The effect of these applied aging conditions on controlling FS dissolution during a typical adsorption study seems an interesting future work for this study.

In summary, the correlation of all above-mentioned aging studies to controlling/quantification of such a control of the natural dissolution of LDH materials in an adsorption process seems a new direction for the usage of aging studies. If aging could impact the LDH properties such as morphology, particle size, and the degree of crystallinity, to what extent could it minimize the dissolution problem observed in the early stages of this thesis? To what extent could an aging process assist in preparing a more stable material for an adsorption process? With this perspective to aging process, the aging of LDH particles in the mother liquor of synthesis process, is ignored for simplicity. The material prepared by synthesis (e. g., co-precipitation

process) is “an unaged LDH”. The unaged LDH after treatment by an aging process is “an aged LDH”.

2.5 Oxyanion adsorption on LDHs

LDHs have attracted attention due to their low cost and medium-high adsorption capacity for removal of oxyanions from water-based solutions [44,74]. LDHs with a surface area (0.02-0.12 m^2/g) and high thermal stability show a comparable anion exchange capacity with resins (2-3 meq/g) and a relatively higher capacity than clay materials (1 meq/g) [4,74,75]. The average capacity of 2-5 mmol/g is reported for adsorption of oxyanions by LDHs [44].

According to the literature, the capacity of LDHs is affected by the positive charge of the layers, the basal spacing, the nature of metal components, type of oxyanion, and competition of other oxyanions [44]. Das, for example, showed that the partial substitution of Zr^{4+} by Al^{3+} in Mg-Al-CO_3 LDH increased the dichromate adsorption capacity [74]. In the absence of any Zr^{4+}, 55.5% of dichromate was removed by Mg-Al-CO_3 LDH (initial Cr^{6+}:10 ppm, LDH dose: 0.5 g/L, pH 6, 30 °C, and 2 h). By 30% of Zr^{4+}substitution for Al^{3+}, under an identical experimental condition, dichromate loading increased to 67.4%. The addition of zirconium, presumably, increased the positive charge of the layers and thereby increased the dichromate adsorption capacity.

The removal of several harmful oxyanions by LDHs has been widely reported. Selenate removal by LDH, however, is less studied [5,6]. Table 2 shows the reported capacity of LDHs for variety of oxyanions reported by Goh in 2008 [44]. Arsenate shows higher adsorption with LDH than any other oxyanion. The LDHs for this purpose is usually calcined and uncalcined M–N LDHs where M=Mg, Ni, Ca and N=Fe, Al with various oxyanions. Calcined LDHs are prepared by heating of LDHs. Yang described the differences of calcined and uncalcined LDHs under the same

adsorption conditions for arsenate and selenite removal. The calcined LDHs had a higher capacity for oxyanion loading than the uncalcined materials [64].

Table 2 LDH capacity for oxyanions [44]

Oxyanion	Arsenite	Arsenate	Chromate	Phosphate	Selenite	Borate	Nitrate
Capacity (mg/g)	0.1-87.5	5-615	9-160	7.3-81.6	29-270	14-20	2.3-4.6
Capacity (mmol/g)	0.00093-0.82	0.035-4.4	0.077-1.4	0.076-0.86	0.23-2.1	0.24-0.34	0.037-0.074

2.5.1 Selenate and selenite adsorption with different LDHs

As the focus of this thesis was selenate removal, the removal of selenium oxyanions (both selenate and selenite) from water by different LDHs is covered in this section. Most of the LDHs used for adsorption studies were prepared with the co-precipitation method.

The type of LDHs used (M-N-X), selenium concentration range, and adsorption capacity are summarized in Table 3. The common metal ions used for LDH preparation in Se-adsorption studies are divalent and trivalent transition metals such as Ca^{2+}/Mg^{2+} and Fe^{3+}/Al^{3+}. In some studies, however, Zr^{4+} was used to prepare mixed LDHs. All the samples provided in Table 3 have M/N molar ratio of 2.0, except one example (Mg-Al-Cl LDH) which was prepared by M/N molar ratio of 2.0 and 4.0 [42].

You, et al. in 2001, prepared a series of Mg-Al-Cl and Zn-Al-Cl LDHs using the co-precipitation method for selenite and selenate adsorption studies [42]. The time-dependent adsorption process, pH effect, and competing anions effect were studied. Adsorption experiments with the L/S ratio of 250, pH 9, 12 h of shaking, and ppm concentration were applied (see Table 3 for feed properties). In addition, the M/N molar ratio effect was studied by changing the Mg/Al ratio from 2-4. As is shown in Table 3, selenite adsorption with Mg-Al-Cl LDH is higher than Zn-Al-Cl LDH. Maximum loading of selenite on Mg-Al-Cl LDH and Zn-Al-Cl LDH was 118.4 and 98.7 mg Se/g respectively. This finding shows that the type of LDH generally affects the

adsorption capacity for a specific anion. The metals composing the layers affect the thickness of layers, basal space, and charge density of layers, resulting in, different affinities of LDHs for selenite. The adsorption of selenate from 0-180 ppm selenate feed solution (0-1.27 mM Se) was studied with Zn-Al-Cl, Mg-Al-Cl (Mg/Al ratio: 2 and 4) LDHs. Results showed that the adsorption behaviors of selenite and selenate on Zn-Al-Cl and Mg-Al-Cl (Mg/Al ratio of 2) LDHs are similar. The capacity of Mg-Al-Cl (Mg/Al ratio: 4) for selenate, however, was slightly lower than for that selenite. Mg-Al-Cl (Mg/Al ratio: 4) has a lower portion of aluminum cations in the brucite layers than Mg-Al-Cl (Mg/Al ratio: 2), thus resulting in lower positive charge density in layers and lower loading for selenate.

Das et al. in 2004, studied selenite adsorption with Zr^{4+} substituted Mg-Al-CO_3 and Zn-Al-CO_3 LDHs [74]. The (Al+Zr)/Zn and (Al+Zr)/Mg were prepared by the co-precipitation method. The LDHs were calcined in air at 450 °C for 5 h. The calcined LDHs were kept in a desiccator over $CaCl_2$. The adsorption of selenite and dichromate was studied with prepared LDHs. Selenite adsorption with Mg-Al-Zr (30% of Zr substitution for Al^{3+}), showed 29 mg/g maximum loading and the results were fitted to the Langmuir model. This value is very close to values reported for the uncalcined Mg-Al-CO_3 (29 mg/g). The capacity of LDHs for selenite removal is reported to be 29-270 mg/g (Table 2). The zirconium incorporation in the Mg-Al LDH (30% of Zr substitution for Al^{3+}) increased the adsorption of dichromate from 55.5% to 67.4% (11.1 and 13.5 mg/g respectively). A similar increase in adsorption was observed when 10% of Zr was substituted for Mg^{2+} (a 63.0% increase compared to zero-Zr incorporation). The zirconium incorporation increased the surface area up to 30%. The increase in capacity may also be related to the increase in the positive charge of the layers.

Table 3 Different LDHs used for selenite and selenate removal

LDH type (M-N-X)	Feed concentration	Loading of Se (mg Se/g)	Reference
Mg-Al-Cl Zn-Al-Cl	0-1610 ppm selenite/0-12.7 mM Se	118.4 98.7	You, 2001[42]
Mg-Al-Cl [a] Zn-Al-Cl [b] Mg-Al-Cl *[c]	0-180 ppm selenate/0-1.27 mM Se	[a, b] Selenate loading similar to selenite capacity [c] Selenate loading lower than selenite capacity	You, 2001[42]
Zr-Mg-Al-CO_3 (calcined at 450 °C)	402 ppm selenite/3.17 mM Se	29	Das, 2004[74]
Mg-Fe-CO_3 (uncalcined)	50 ppm selenite/0.39 mM Se	Temperature 30 °C=2.92 50 °C=2.22 60 °C=1.69	Das, 2002[76]
Zn-Fe-SO_4 Mg-Al-CO_3	50 ppm selenate/0.35 mM Se	Loading after 60 minutes: 9.76 mg Se/g 4.5 mg Se/g	Hongo, 2008[66]
Mg-Al-CO_3	0.01-0.3 ppm selenite/$7.88X10^{-5}$ - $2.36X10^{-3}$ mM Se	0.140 mg Se/g calcined 0.07 mg Se/g uncalcined	Yang, 2005[64]
Ca-Al-OH Ca-Al-SO_4	20.94 ppm selenate/0.15 mM Se	0.50 mg Se/g 0.43 mg Se/g	Zhang, 2003[56]
Ca-Al-Cl (Friedel's salt or FS)	1086 ppm selenate/7.6mM Se	108 mg Se/g 1.37 mmol/g	Wu, 2010[25]

*Mg/Al ratio: 4

Das et al. also studied the removal of selenite with Mg-Fe-CO_3 LDH [76]. The LDH material was synthesized with the co-precipitation method using the sodium hydroxide and sodium carbonate addition. No calcination process was applied and adsorption with uncalcined Mg-Fe LDH was performed. The effect of the initial pH on adsorption showed that loading increases as pH decreases. Figure 6 shows that selenite removal increased as pH decreased. The effect of temperature (30-60 °C) on the capacity of Mg-Fe-CO_3 for loading of selenite was also studied (see Table 3, Mg-Fe-CO_3 uncalcined). As the temperature decreased, the maximum loading of selenite increased. This was related to the exothermic nature of the ion exchange process in agreement with the calculations of standard enthalpy changes ($\Delta H°$).

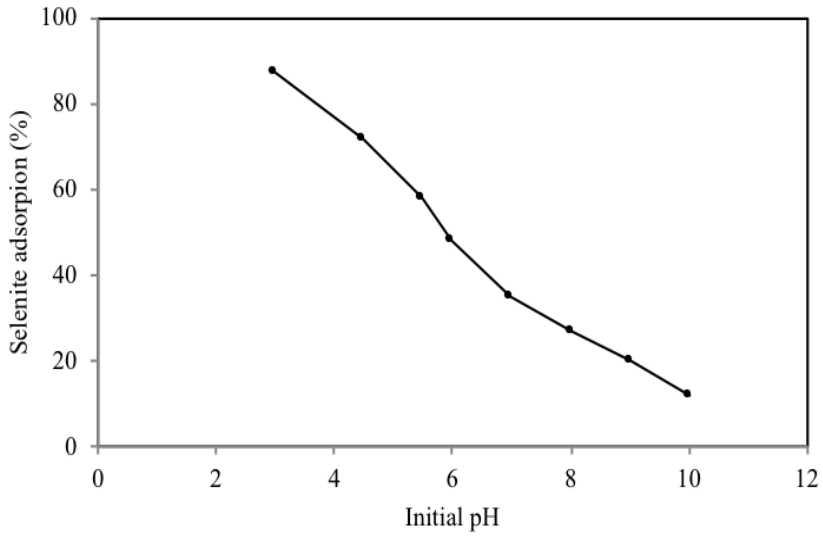

Figure 6 Adsorption of selenite by Mg-Fe-CO_3 LDH as a function of initial pH (selenite 50 ppm, LDH dose 1 g/L). Reprinted with permission from [76]

A Zn-Fe-SO_4 LDH with sulfate as the interlayer anion was prepared by Hongo to study the removal of selenate and some other oxyanions [66]. The Zn-Fe-SO_4 affinity for adsorption of selenate from 50 ppm feed solution at L/S 200 and 1 hour of shaking was studied at pH 2.3-14. The phosphate had the highest adsorption percentage (~100%). The removal of selenate was higher than chromate and arsenate oxyanions (9.76 mg Se/g). Borate showed the lowest adsorption percentage (~10%) and fluoride was not removed. Adsorption affinity of Zn-Fe-SO_4 for oxyanions was compared with Mg-Al-CO_3 LDH. The intercalated carbonate in Mg-Al-CO_3 LDH was interfering with the removal of oxyanions. Zn-Fe-SO_4 LDH was a more efficient adsorbent than Mg-Al-CO_3 LDH, for removal of phosphate, selenate, and chromate oxyanions.

Yang et al. studied the removal of selenite and arsenate with calcined and uncalcined Mg-Al-CO_3 [64]. The LDH was prepared with the co-precipitation method using $Mg(NO_3)_2.6H_2O$, $Al(NO_3)_3.9H_2O$ and Na_2CO_3. A selenite solution of 10-200 ppb with the initial pH of 4.2 to 5.4 was shaken with the LDH at 150 RPM for 5 days. The effect of the initial pH, adsorbent dosage,

and the presence of competitive anions on selenium adsorption was studied. The loading of selenite (mg/g) is shown in Table 3. Selenite adsorption with Mg-Al-CO_3 LDH was temperature dependent for calcined Mg-Al but independent for uncalcined Mg-Al-CO_3 LDH. Calcined Mg-Al showed higher capacity than uncalcined Mg-Al-CO_3 LDH for both selenite and arsenate. Calcined material had a higher specific surface area than the uncalcined material, as well. FTIR studies also showed that there is less intercalated-carbonate in layers of calcined LDH. Calcination also affects the pH-dependency behavior of the oxyanion's adsorption. Selenite adsorption with uncalcined Mg-Al-CO_3 LDH decreased as pH increased over the initial pH range 4-10. However, adsorption with calcined Mg-Al was constant at pH 4-10.

Zhang et al. in 2003, studied the removal of selenate, borate, molybdate, and chromate with hydrocalumite-hydroxide with a chemical formula of $[Ca_4Al_2(OH)_{12}]\cdot[(OH)_2\cdot 6H_2O]$ and ettringite with a chemical formula of $[Ca_6Al_2(OH)_{12}]\cdot[(SO_4)_3\cdot 26H_2O]$ [56]. The incorporation of these oxyanions into both LDH materials was studied by directly precipitating LDH materials from a solution containing low concentrations of the oxyanions (initial solution pH 12.5). The selenate uptake by hydrocalumite was larger than that by ettringite (see Table 3). In his work, hydrocalumite reduced Se concentration from 11.57 ppm to <0.100 ppm (L/S 44:1) over a 1-day adsorption test (99.1% removal). Under similar conditions (L/S 40:1), 1.81 ppm Se remained in the solution after adsorption with ettringite (84.3% removal).

Baur et al. in 2003, studied the removal of selenate and selenite by ettringite and monosulfate materials [40,41]. Ettringite and monosulfate are sulfate-containing LDHs with a chemical formula of $[Ca_6Al_2(OH)_{12}]\cdot[(SO_4)_3\cdot 26H_2O]$, and $[Ca_4Al_2(OH)_{12}]\cdot[SO_4\cdot 8H_2O]$ respectively. The sorption isotherm for selenate and selenite oxyanions was determined on 390 ppb<Se total<789 ppm (L/S 520) after shaking for 30 days. Selenite was adsorbed by surface

reactions, and for ettringite, a sorption maximum of 0.03 mmol/g was determined. The selenate amount adsorbed on LDH/amount in solution in the equilibrium was 0.03 and 2.06 m^3/kg with ettringite and monosulfate respectively.

2.6 Oxyanion adsorption on FS

FS was used for removal of selenate oxyanion from solution by Wu (Reaction 2) [25]. Wu et al. proposed using this chloride containing LDH for selenate removal. According to his study, the kinetics of selenate adsorption was very fast and a large amount of selenate was rapidly adsorbed over a wide pH range of 4-10. The adsorption of selenate from 0.25, 1.25, and 5 mM selenate feed solutions (19.7, 98.7, and 395 ppm Se) with 2.0 g/L FS (L/S 500) was 98, 82, and 48% in accordance with 9.5, 40.3, and 94.7 mg Se/g capacity. The highest practical capacity for selenate loading at an initial pH of 8 was reported to be 108 mg Se/g equal to 1.37 mmol Se/g at 7.6 mM Se feed solution (600 ppm Se). This loading was lower than the theoretical capacity of pure FS (140.5 mg Se/g or 1.78 mmol/g), likely due to the LDH contamination with carbonate. It will be more accurate to compare the experimental loading to the theoretical capacity of carbonated-FS (as Wu was not dealing with pure FS). The exact carbonate content was not reported by Wu, however, the FTIR peak at 1442 cm^{-1} was reported as possibly being due to an anti-symmetric stretching vibration of carbonate. Wu related the carbonate content to the $CO_{2(g)}$ capture from the air during the FS synthesis. FS showed the highest adsorption capacity among all LDH materials studied (see Table 3). Selenate elution from Wu's $FS._{sint}$. was studied with 0.1 M sodium chloride solution (70-80% recovery). In Wu's paper, no dissolution data was reported while the dissolution of Ca^{2+} and Al^{3+} ions as a result of the buffering capacity of the material was mentioned (see 5.3.1). Therefore, some degree of mass loss in the final mass of Wu's $FS._{sint}$. was observed by Wu. It is unclear if the actual final mass of Wu's $FS._{sint}$. was used for a maximum capacity of 1.37 mmol

Se/g. LDH materials are generally unstable at low pH region (metal ions hydration in acidic solutions), and therefore the dissolution data for low pH studies are even more crucial [44].

FS was studied for chromate removal [32,33,48]. The sintering-precipitation method was used to prepare FS to study Cr(VI) removal from 32 to 600 ppm Cr solution. Cr(VI) was effectively adsorbed by FS in the initial pH range of 4-10. The maximum adsorption of Cr(VI) 1.3-1.4 mmol/g was reported to be similar to the selenium capacity reported by Wu (1.37 mmol/g) [33].

2.6.1 Gaps in the literature regarding LDH dissolution report during oxyanion adsorption studies

The chemical and mechanical stability of an adsorbent in an IX process is a key property if the adsorbent is used industrially. The LDHs are partially soluble and the dissolution of LDHs during adsorption studies are not reported as a challenge for industrial use [44,57]. Many laboratory adsorption studies that used LDHs synthesized with metals such as Ca, Al, Zn, Cr, Ni, Mn, Co, Cu, Cd, etc., did not report the metal ions dissolution data [25,44,77]. However, LDH dissolution as an inherent feature of these materials can be critically high under harsh experimental/industrial conditions (e.g. highly acidic solutions of acid mine drainage) [44]. Goh et al. in a review paper published on LDH materials state that "*If the precursor metals in the brucite-like sheets are to be released into the solution, it would be important to ensure that they exist below the levels harmful to the environment, or otherwise the LDHs should be free of toxic metals. Though some of the precursor metals are not currently regulated, they potentially pose a health concern if used for drinking water treatment*" [44]. Based on British Columbia (BC) water quality criteria, the concentration of dissolved aluminum in freshwater aquatic life, should not exceed 0.10 ppm when the pH is greater than or equal to 6.5 (maximum at any time) [78]. A drinking water quality

criterion for aluminum is recommended to be 0.2 ppm dissolved aluminum (maximum at any time).

In addition to what Goh mentioned in his paper, we emphasize that if the precursor metals in the brucite-like sheets are to be released into the solution, then it would be important to measure and report the dissolution data. In summary, it is important to know how much of LDH mass is lost in an adsorption experiment; note that metal ions dissolution results in material loss.

Therefore, more dissolution minimization studies on LDH before and during adsorption tests are needed in this field. In addition to the environmental concerns, an ion exchanger with the possibility of significant mass loss during adsorption is not considered an efficient and feasible material in the engineering field. The polymeric resins have been frequently used in industrial plants with minimal material loss concerns for decades [24].

In comparison with a polymeric resin, in which the polymeric matrix is constructed with strong crosslinks and is essentially insoluble, LDHs are constructed of the positively charged brucite layers and negatively charged interlayer regions (see Figure 3). The positive charge of layers is balanced with a negative charge from interlayer space. The anions and water molecules in the interlayer space facilitate hydrogen bonding between the layers, which is weaker than covalent crosslinks in the resins. As shown in the bottom of Figure 3, the metal ions are located in the octahedral units. Any crystalline defects in these octahedral units (e. g., lattice vacancies, substitution by impurity atoms, or dislocations in hexagonal units), can contribute to a less stable structure in which metal ions are more susceptible to release from the layers into solution.

While solubility data at equilibrium for LDHs can be helpful in understanding the dissolution behavior of these materials, the dissolution of LDHs during oxyanion adsorption studies is also of great importance [63]. In a solubility study on pure Friedel’s salt, the solubility

product of material was studied as follows: the solid was dispersed in decarbonated DI water for 180 days at 20 °C [49]. The slurry was filtered and the solution composition was analyzed by ICP. The equilibrium concentration values were calculated to be 9.03 mM Ca^{2+}, 4.87 mM Al^{3+}, 4.92 mM Cl^-, and 10.51 mM OH^- (average of four experiments). The solubility product constant (K_{sp}) of pure FS was calculated to be $10^{-27.10}$ using $K_{sp}=[Ca^{2+}]^4[Al(OH)_4^-]^2[Cl^-]^2[OH^-]^4$. As seen, the time required reaching equilibrium for K_{sp} calculations for Friedel's salt was 180 days. This time is significantly longer than the usual time an LDH material is exposed to water in an adsorption process. Therefore, the metal ions concentration values obtained from K_{sp} values, will not be accurate estimates of metal ions concentration in adsorption experiments. In another study performed by Gácsi et al., K_{sp} of hydrocalumite-hydroxide with a chemical formula of $[Ca_4Al_2(OH)_{12}]\cdot[(OH)_2\cdot 6H_2O]$ was estimated to be $10^{-11.4}$ and $10^{-12.1}$ at 25 and 75 °C, respectively [79]. In this study, K_{sp} was calculated from hydrocalumite-hydroxide precipitation in an aqueous mixture of NaOH, $Ca(OH)_2$ and $NaAl(OH)_4$. The equilibrium constant expression for hydrocalumite-hydroxide is $[Ca^{2+}]^2[Al(OH)_4^-][OH^-]^3$. The concentration of Ca^{2+} dissolved from hydrocalumite-hydroxide in a typical adsorption process, will not be necessarily the equilibrium concentration values obtained by Gácsi. Equilibrium and adsorption studies have two different experimental conditions. The dissolution values for adsorption tests are expected to be lower than the equilibrium values, as the dissolution of metal ions to reach equilibrium usually needs a long period of time (e. g., 180 days for FS).

Although many studies have been conducted on the removal of oxyanions from wastewater by LDH materials, relatively little attention has been focused on the significant issue of dissolution of the adsorbent and the potential for secondary contamination of the wastewater. Ferreira reported that magnesium ion release from Mg-Al-NO_3 and Mg-Fe-NO_3 LDH was pH-dependent [80]. The

amount of Mg^{2+} released from the LDHs increased with decreasing initial pH as is expected for LDH materials. In addition, it was shown that the type of trivalent metal ion in LDH affects the dissolution of Mg^{2+} from these LDHs. The amount of Mg^{2+} released from Mg-Fe-NO_3 LDH was smaller than from Mg-Al-NO_3 LDH.

Zhang in a study on removal of various B, Cr, Mo and Se oxyanions by hydrocalumite or ettringite stated that "the most important limitation in using these calcium aluminate phases to control contaminant oxyanion levels in water is pH" [56]. A high pH condition must be maintained in a disposal or treatment environment (pH 12.5 was used) because of the instability of hydrocalumite and ettringite at low pH values. Zhang did not report the dissolution data of hydrocalumite or ettringite during oxyanion adsorption at pH 12.5 (and low pH values). This still represents uncertainty in what one should expect for hydrocalumite or ettringite loss at any oxyanion adsorption test performed at pH 12.5. It was wise to report a dissolution value for at least selected pH of 12.5?

Yang in a study on selenate and arsenate removal by Mg-Al-CO_3 LDHs reported a mass loss at pH lower than 4 using the ICP-MS analysis of solutions [64]. Mg^{2+} and Al^{3+} ions were present in the final solutions. However, again, no quantitative mass loss data was reported for Mg-Al-CO_3 LDH over a wide experimental pH range of 4-10. Das in a study on selenite removal by Mg-Fe-CO_3 LDH gives us a similar hint on mass loss from LDH [76]. As the presence of Mg^{2+} in solution at pH lower than 6 was reported by solution analysis, pH 6 was used for experiments. Again, it is not reported how much of Mg-Fe-CO_3 LDH mass was dissolved at pH<6, or even more importantly, how much of this LDH dissolved at the selected pH of 6. Was the dissolution of Mg-Fe-CO_3 LDH, nil or significant at pH 6?

As mentioned Friedel's salt was used by Wu [25], and Dai [33], for selenate and chromate removal, respectively. In neither of these adsorption studies was the actual mass loss of FS for each individual adsorption experiment reported. Wu's study lacks the dissolution data for FS during the selenate adsorption tests [25]. It is not reported how much of FS dissolves under L/S 500 and pH 8 experimental conditions that were used. The Ca and Al ions dissolution at various pH values were attributed to a buffering capacity of FS (explained in 5.2), however, the dissolution data were not provided.

In Dai's study, the initial pH impact on dissolution is reported; a high dissolution of FS material at pH 6 was reported (data not provided) and therefore an initial pH 10 was selected as the optimum value [33]. The chromate adsorption tests were performed at an initial pH of 10, L/S 250, 25±1 °C, 150 RPM agitation rate and 24 h with Cr(VI) feed solutions of 0.1-8.0 mM. The optimization of other adsorption variables (especially L/S) for mass loss considerations of FS was not reported. The concentration of Ca in the solution for these adsorption tests was reported to be 1-2 mM. On the other hand, a series of fixation stability tests were performed using the chromate-loaded FS. The fixation stability of chromate tests was designed to measure the chromate release form chromate-loaded FS under various initial pH conditions (pH 4-10). The Ca and Al concentration an initial pH 10 was reported to be 1-2 mM and 0.1-0.2 mM, respectively. The leaching data of Ca and Al from chromate-loaded FS were called "unpublished data" in Dai's study [33].

As seen, in Dai's study [33], similar to many LDH related studies, the metal precursor dissolution from FS, was only addressed by avoiding the low pH region [44]. It seems that the metal ions dissolution during adsorption is considered a natural property of these materials and not

a barrier to their effective application. No effort on optimization of other adsorption variables for lowering the FS dissolution was reported.

In an attempt at minimization of adsorbent dissolution Baur et. al, in 2003, recommended the use of pre-saturated LDH solutions [40]. LDH materials used were ettringite and the monosulfate LDH with chemical formulas of $[Ca_6Al_2(OH)_{12}]\cdot[(SO_4)_3\cdot 26H_2O]$ and $[Ca_4Al_2(OH)_{12}]\cdot[SO_4\cdot 8H_2O]$, respectively. The pre-saturated solutions were prepared by equilibrating suspensions of ettringite and the monosulfate LDH (0.7 g L-1 ettringite and 1.1 g L-1 monosulfate) for 7 days at 25 °C using a rotary shaker (150 RPM). The selenium oxyanion was added later to this suspension for oxyanion removal studies. Here, it is not clear how much of ettringite and monosulfate LDH mass losses were prevented by the application of this pre-treatment procedure. However, it is also unknown how serious the extent of metal ions release into solution is either, and therefore whether the effluent is at all suitable for discharge or would have to be further treated. On the other hand, the author of this paper mentioned that the dissolution was needed to be minimized. This implies that the original dissolution was a problem and the effluent was not safe for the discharge.

In summary, the LDH mass losses during adsorption tests and studies related to the reduction of dissolution before adsorption have not reported. For an ion exchange process, one of the most important considerations is the adsorbent stability. The solubility product data (K_{sp}) provided for LDH materials in literature can be considered in adsorption experiments. However, it is important to provide the actual dissolution data for LDH materials used in adsorption studies, simply because the adsorption tests can be run under non-equilibrium conditions. The collection of actual mass loss data for LDH materials will be a helpful database for the usage of these

materials for any industrial plant design. In this thesis, FS mass loss for every individual adsorption test is reported.

In an attempt to minimize LDH dissolution before a typical adsorption process, various strategies including conventional aging or hydrothermal treatment processes can be applied [70]. In most of LDH studies, the impact of aging (separate from synthesis process) on minimization of dissolution is not quantified [44,70]. In general, aging and hydrothermal treatments are potentially applicable treatments for the purpose of dissolution minimization [44,70]. In this thesis, the usage of one optimized aging condition for minimization of FS dissolution is developed.

2.7 Objectives of research

The removal of selenate from wastewater is currently a significant issue affecting many industries and more research and focus on this particular field is required. The general objective of this work was to study selenate removal from water with the ion exchange method. Friedel's salt (FS) from the layered double hydroxide family was selected as an ion exchange material in this research since this material has been reported to have high capacity and fast loading kinetics [25]. It was found early in this work that FS exhibits significant dissolution in water during selenate removal studies. This behavior limits the use of FS for water treatment in industrial plants so another general objective was to minimize the dissolution of FS to make it more suitable for selenate removal.

In fact, this thesis targets the study of selenate adsorption by FS with a consideration of the FS dissolution issue. The specific objectives are divided into three parts as follows;

<u>Part one: synthesis, characterization and carbonate minimization of FS during synthesis</u>

The first objective was to see if incorporation of carbonate into FS from the air in the co-precipitation process could be minimized by use of a nitrogen atmosphere in the experimental FS preparation. Carbon analysis was used to determine carbonate content.

Part two: an investigation into the structure to minimize dissolution by the aging process

The second objective was to investigate and minimize FS dissolution by an aging process before studying anion adsorption. The phase transformation of the material was studied by QXRD analysis.

The third objective was to investigate the minimization of FS dissolution during studies of anion adsorption in a simulated industrial wastewater matrix by using a non-saturated calcium hydroxide solution.

Part three: optimization of selenate loading in association with minimization of dissolution of FS. Mass loss was reported for all selenium loading studies. The effects of competing ions commonly present in industrial plant solutions were studied.

The fourth objective was to investigate the maximization of FS capacity by a calcination process.

The fifth objective was to measure the selectivity of selenate adsorption over sulfate and carbonate oxyanions as the industrial wastewaters frequently contain high concentrations of both of these anions. The interference of carbonate anion was studied for both added carbonate oxyanion in the feed solution and intercalated-carbonate during synthesis.

Chapter 3: Experimental

3.1 Materials and equipment

3.1.1 Chemicals and reagents

Deionized (DI) water used for all the experiments, including co-precipitation, aging, adsorption-simulation, and adsorption. The water was boiled for 10-15 minutes for decarbonation, cooled under nitrogen gas purging and stored in a sealed container before use.

Reagents and analytical grade materials were obtained from commercial suppliers and used without further purification. Certified calcium chloride hexahydrate ($CaCl_2 \cdot 6H_2O$), certified sodium hydroxide (NaOH) 0.995-1.005 M, and Na_2SeO_4 salt (99.8% purity) were purchased from Fisher Scientific. Carbonate-free sodium hydroxide was purchased from Electron Microscopic Sciences. Reagent grade aluminum chloride hexahydrate ($AlCl_3 \cdot 6H_2O$) was purchased from the Alfa Aesar Company. Certified A.C.S. grade calcium carbonate ($CaCO_3$) with 99.88% purity and α-alumina (Al_2O_3), with 99.85% purity and 150 nm particle size were purchased from Fisher Scientific and Inframat Advanced Materials, respectively. The analytical standard solutions of calcium, aluminum, sodium, and selenium were purchased from Fisher Scientific.

3.1.2 Experimental and instrumental equipment

For the synthesis of FS, the following equipment was used: A 4-neck water-jacketed reactor (designed and supplied by Cansci Glass Company) was used for the co-precipitation experiments. High-Na tolerance pH probes designed by Cole-Parmer and a pH meter/controller (model number 501-3400) manufactured by Barnant Company were used for pH measurements and control. Masterflex Cole-Parmer pumps and Tygon tubing (compatible with alkaline solutions) were used for reagent injection into the reactor. Industrial nitrogen gas (99.99% purity) was used for purging

nitrogen into the solution. The Pyrex glass container, polypropylene plastic (PP) and high-density polyethylene (HDPE) containers were used in adsorption tests.

A Thermo Scientific shaking water bath (model number SWB25) and a water bath (model Grant JB Nova), IKA heater-stirrer (model C-MAG H57 digital) was used for adsorption and aging experiments. Nalgene filter units, Fluoropore^{TM} filter membranes (0.45 μm alkaline compatible), SARSTEDT centrifuge tubes, and syringe filter heads were used for slurry filtration. An oil-sealed vane vacuum pump, liquid nitrogen trap, and a desiccator were used for drying solids. Pyrex glass container was used for aging and adsorption tests.

3.1.3 Analytical equipment for characterization

The synthesized FS materials were identified with Multiflex 2kW X-ray Diffractometer (XRD). The morphological images were recorded with scanning electron microscopy (SEM) technology using a HITACHI S3000N secondary electron beam detector. The Malvern Mastersizer 2000 was used for particle size distribution analysis (PSD) of FS samples. A LECO analyzer at the ALS Geochemistry laboratory located in North Vancouver was used for carbon analysis of FS samples. CoKα radiation on a Bruker D8 Advance Bragg-Brentano diffractometer equipped with Fe monochromator foil was used for quantitative X-ray diffraction (QXRD). Inductively coupled plasma optical emission spectrometry (ICP-OES Varian 725-ES Optical Emission Spectrometer) and inductively coupled plasma mass spectrometry (ICP-MS Agilent 7700x) were used for selenium, calcium, aluminum, and sodium analysis in solution.

3.2 FS synthesis by co-precipitation method at constant-pH under partial nitrogen purging (unaged-FS synthesis)

DI water used for all synthesis experiments was decarbonated by purging nitrogen gas for 10-15 minutes. The Ca-Al metal mixture solution was prepared with $CaCl_2.6H_2O$ (0.66 M) and

$AlCl_3.6H_2O$ (0.33 M) dissolution in decarbonated DI water. The total metal concentration was adjusted at 1 M with calcium to an aluminum molar ratio of 2:1. A solution of 1 M sodium hydroxide was used for pH adjustment and pH was monitored and controlled using the pH meter/controller. The mixed metal solution and the sodium hydroxide solution were separately purged with nitrogen gas for 20 minutes before addition into the reactor.

Figure 7 shows one of the co-precipitation equipment arrangements for the preparation of FS. The mixed metal and sodium hydroxide solutions were added to the 4-neck water-jacketed reactor containing water with an initial pH of 12.1 at adjusted rates. It is necessary to carry out the synthesis under conditions of supersaturation, to ensure the simultaneous precipitation of metal ions. The supersaturation condition can be reached by careful pH control. The pH of slurry during synthesis must be maintained at higher than or equal to the one at which the most soluble hydroxide precipitates [27]. The pH was controlled at a set value of 11.3 by the addition of 1 M sodium hydroxide. The slurry was mixed at a high stirring rate and the addition was continued. Once the pH dropped to less than 11.3, the sodium hydroxide pump turned on automatically, increasing the pH to the target value. Peristaltic pumps and alkaline-resistant Nalgene tubing were used for pumping the sodium hydroxide solution from the bottle to the reactor. The pumping rate was adjusted with the speed controller. Under constant-pH conditions, metals and sodium hydroxide solutions were mixed for 72 hours at a high stirring rate. The temperature was controlled at 30 °C with the water bath. Nitrogen gas was purged into the reactor for the whole experiment (average 0.5 L/min).

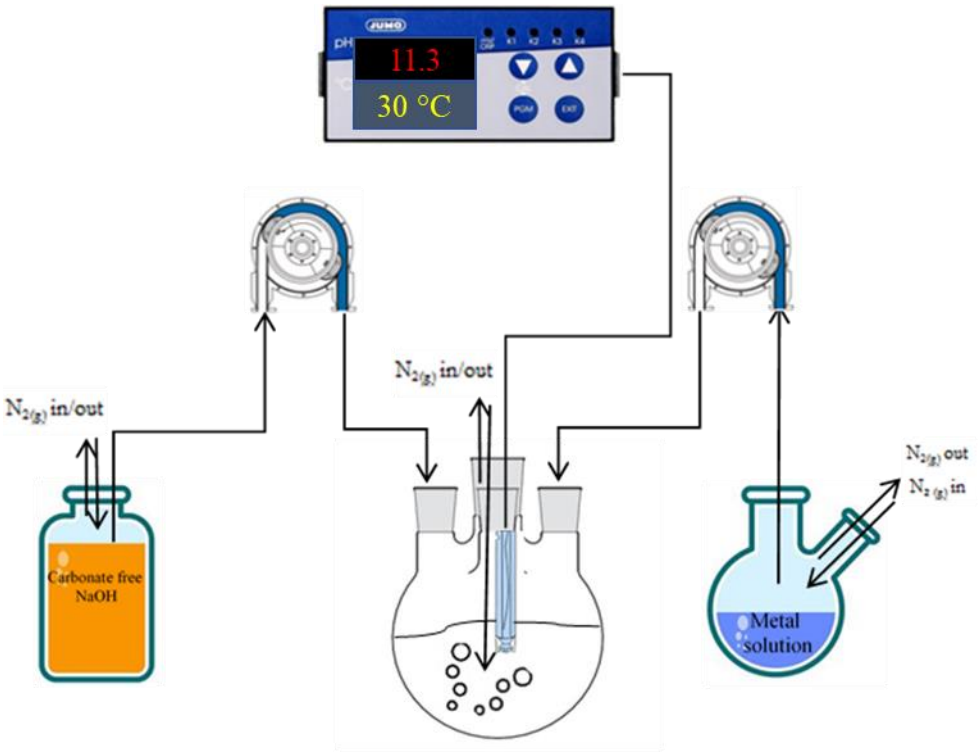

Figure 7 Co-precipitation experimental arrangement for precipitation of FS at the constant-pH method under partial nitrogen purging.

The white slurry formed during synthesis was filtered with a 3.0 μm Fluoropore ™ filter membrane (alkaline compatible) using pressure filtration. No nitrogen gas was purged during the filtration process. The solid was washed with cold water and dried in an oven at 100 ºC exposed to air. The clear filtrate was collected, the final pH was recorded, and the solution was analyzed with ICP-OES for Ca, Al, Na concentrations. The solid was characterized by XRD, SEM, QXRD, PSD, and ICP-OES analysis. A large amount of FS sample was collected by replication of this co-precipitation process in the laboratory. The nitrogen purging method applied in this procedure is called a partial nitrogen purging method. In this method, nitrogen purging is limited to the slurry mixing during the synthesis process. No effort was done to isolate the wet sample from the air during the following filtration, washing, and drying processes.

3.2.1 The labeling system of FS samples prepared by partial and complete nitrogen purging method in the co-precipitation process

The carbonate oxyanion (CO_3^{2-}) is present in alkaline solutions due to the dissolution of $CO_{2(g)}$ from the air. The carbonate oxyanion is known to intercalate easily in LDH composition and lower the oxyanion adsorption capacity [44,64]. Therefore, the co-precipitation method performed under partial nitrogen purging (Figure 7), was modified to determine if the carbonate loading from solution during synthesis could be better controlled.

In general, the nitrogen gas purging in the co-precipitation process was performed in two different ways. Table 4 describes each method, the name of the product obtained by each method, and also highlights the main differences between the two methods in terms of nitrogen purging. The two nitrogen purging methods are called "partial nitrogen purging" and "complete nitrogen purging" methods.

Table 4 Similarities and differences of the partial and complete nitrogen purging methods in the co-precipitation process (decarbonated DI water used for all synthesis tests)

	Reactor purging	**Chemical purging**	**Slurry transfer under positive pressure**	**Filtration with positive pressure / Head-purging to the filter unit**	**Drying method**	**Product name**
Partial $N_{2(g)}$ purging	Yes	Yes	No	Yes/No	Oven dried in air (100 °C)	***Unaged-FS***
Complete $N_{2(g)}$ purging	Yes	Yes	Yes	Yes/Yes	Desiccator/ drying under high vacuum	***Modified unaged-FS***

In the partial nitrogen purging method, the mixed metal solution was purged with nitrogen gas 20 minutes before addition into the reactor (see Figure 7). The carbonate-free sodium hydroxide solution was used for the partial nitrogen purging method. The headspace of the sodium hydroxide bottle was purged with nitrogen gas for the duration of the synthesis step. Nitrogen gas

purging was maintained during the synthesis process. The slurry was filtered using nitrogen gas pressure otherwise the filtration process was extremely slow. However, no effort was made to exclude air during the filtration process. The wet solid was dried in an oven at 100 °C. As mentioned, the FS sample prepared by partial nitrogen purging is called “unaged-FS”. An adequate portion of unaged-FS (~150 g) was collected by the repetition of several batches of co-precipitation synthesis under partial nitrogen purging.

The complete nitrogen purging method was the most complete nitrogen purging method that could be applied using available laboratory equipment. Similar to partial nitrogen purging the carbonate-free sodium hydroxide solution was used for complete nitrogen purging. Figure 8 shows the experimental set up used in complete nitrogen purging in details.

Use was made of the nitrogen positive pressure to transfer the slurry into the Nalgene filtration unit. The Nalgene unit receiver was purged with nitrogen during filtration. The solid was washed with cold DI water under nitrogen purging. After filtration, the filtration unit was opened; solid was collected on a watch glass and transferred to the desiccator quickly.

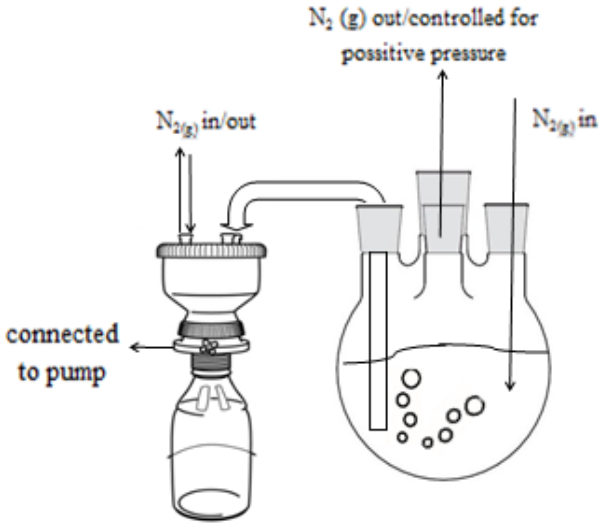

Figure 8 The complete nitrogen purging method filtration set-up (slurry transfer and filtration of FS under a nitrogen atmosphere).

Drying was carried out under vacuum using an oil-sealed pump. Figure 9 shows the drying setup. Wet solid collected from the filtration step was put in the desiccator over $CaCl_2$ granules, NaOH pellets and silica in order to avoid adsorption of $CO_{2(g)}$ and moisture from the atmosphere. The desiccator under the vacuum was connected to a glass trap which was immersed in a liquid nitrogen Dewar flask. The glass trap from the other side was connected to an oil-sealed vacuum pump. All moisture removed from FS passed through liquid nitrogen and were condensed as ice. Overall weight loss of 62.5% was recorded after 18 h. The completely dry sample was collected and analyzed.

Figure 9 The complete nitrogen purging method drying set-up (vacuum pump, liquid nitrogen trap, and vacuum desiccator used for drying).

The product of the complete nitrogen purging process is called “modified unaged-FS”. The unaged-FS and modified unaged-FS samples were analyzed by carbon analysis to measure the carbonate contents of samples. In general, the unaged term was selected for all products of co-precipitation process to differentiate them from the products of additional aging processes. Therefore, unaged-FS and modified unaged-FS are the direct products of co-precipitation

processes with no aging treatment applied to them. The FS term is still used if it refers in general to Friedel's salt material.

3.2.2 Sintering-precipitation method; FS.$_{sint}$. preparation

The sintering-precipitation method was the early method used in the laboratory for preparation of FS. The experimental conditions reported by Wu were used [25]. This method was comprised of two individual steps: C_3A synthesis and FS precipitation.

In the first step, C_3A was synthesized by the sintering of calcium oxide and alumina pellets at 1400 °C in a Pt crucible. Micropyretics Heater International Inc. (MHI) furnace was used for sintering of samples at high temperatures. For the preparation of pellets, a press machine (Instron model 3369), steel dye, and ball mill were used.

Sintering-grinding-pellet-making cycles were repeated until lime content was lowered to <0.6% [81]. In the next step, FS was synthesized with the addition of C_3A to the $CaCl_2 \cdot 6H_2O$ solution in the water-jacketed reactor [25]. The mixed suspension was aged at 45 °C for 24 h under stirring. The precipitate was then collected via filtration, thoroughly washed with deionized water and dried at 100 °C in an oven. FS material prepared with sintering-precipitation in this thesis is designated as FS.$_{sint}$. to distinguish it from Wu's FS.$_{sint}$., the material prepared by Wu.

3.2.3 Primary synthesis method

Among sintering and co-precipitation methods, co-precipitation was selected for experimental convenience. The main material prepared in a larger batch and used in this study was prepared by co-precipitation using the partial nitrogen purging method (see Table 4). A large amount of unaged-FS was prepared in frequent small and large co-precipitation batches. The unaged-FS was used for characterization and aging studies.

3.2.4 Analytical methods for characterization of FS samples

The following analytical and characterization methods were used for phase identification and solid structural analysis of both unaged-FS and aged-FS materials: XRD, QXRD, SEM, and PSD. Both samples were also digested with concentrated nitric acid and analyzed with ICP-OES for chemical analysis. Calcium, aluminum, sodium, and selenium contents were measured. The Ca/Al molar ratio was calculated for solid samples.

3.2.4.1 XRD analysis

The unaged-FS samples prepared from the co-precipitation processes and aged-FS samples were all identified with XRD analysis. The XRD detection limit is reported to be <1-5 wt.%. In the XRD analysis, the solid powder was well ground with a mortar and pestle. A thin film of powder was put on a glass sample holder and mounted in the XRD machine. For analysis with the Rigaku MultiFlex instrument, a continuous scan with a 0.01-degree sampling window was used. The instrument was equipped with a fine focus copper X-ray tube using Ni-filtered Cu Kα (λCu Kα = 0.154186 nm radiation at 40 kV and 20 mA) over the 2θ range of 10-80° (scan speed: 2° per minute, and step size: 0.04°). Step-scan X-ray powder-diffraction data were collected over a range of 3-80° 2θ.

The system is equipped with an incident and diffracted beam Soller slits, a graphite monochromator or the receiving side tuned to Copper K_α, and a scintillator detector. The 1/2 degree divergence and scattering slits, a 0.3 mm receiving slit, and a 0.8 mm monochromator receiving slit were used for XRD analysis. It also only needs a few milligrams of the sample. Jade and Match software were used for solid phase characterization.

3.2.4.2 QXRD analysis

For QXRD, at least 4 g of each sample was required. The QXRD method uses a corundum standard (α-Al_2O_3) with a sample preparation technique that homogenizes the sample and reduces the preferred orientation. The sample was ground to the optimum grain-size range (<5 μm) by grinding under ethanol in a vibratory McCrone Micronising Mill (McCrone Scientific Ltd., London, UK) for 5 minutes. A 20 wt.% addition of highly crystalline corundum was initially added as an internal standard to quantitatively measure the crystalline and amorphous components of the FS samples. Negative values were obtained for the amorphous content of the samples. Therefore, QXRD method failed to identify any amorphous content in the prepared samples.

Step-scan X-ray powder-diffraction data were collected over a range 3-80° 2θ with CoKα radiation on a Bruker D8 Advance Bragg-Brentano diffractometer equipped with a Fe monochromator foil, 0.6 mm (0.3°) divergence slit, incident- and diffracted-beam Soller slits, and a LynxEye-XE detector. The long fine-focus Co X-ray tube was operated at 35 kV and 40 mA, using a take-off angle of 6°. PDF4+ 2016 software program was used for QXRD analysis. Different crystal variations of FS (called hydrocalumite as a general family name) were identified using this software. An uncertainty of 5-10 wt.% is considered for results.

3.2.4.3 Software programs used for XRD and QXRD analysis of FS

Table 5 shows the software parameters used for XRD and QXRD analysis including the software database name, hydrocalumite name, hydrocalumite formula for single crystal, and the lattice parameters. For XRD analysis, Jade software was used in which the FS database belongs to the monoclinic system with an *A2/*n space group. The crystal lattice parameters for this pattern was extracted from Jade software. The reference paper used for this database was unavailable in Jade software.

For QXRD analysis, the database from PDF4+ 2016 software was used to fit the experimental patterns. These databases were extracted from relevant powder and single crystal XRD studies in the literature [46,53]. All the lattice parameters from reference phases are summarized in Table 5.

The QXRD experimental patterns of synthesized FS samples in this thesis were fitted with two phases from literature: a chloro-hydrocalumite phase with a hexagonal crystalline system and a chloro-carboaluminate hydrocalumite with a monoclinic crystalline system. As shown in Table 5, the carbonated hydrocalumite phase is a hemi-carboaluminate hydrocalumite phase and not a fully carbonated phase.

The first reference compound was a chloro-hydrocalumite with a hexagonal phase and space group $R\bar{3}$ published by Rousselot in 2002 [46]. This phase with the chemical formula of $[Ca_4Al_2(OH)_{12}]\cdot[Cl_2\cdot 4H_2O]$ was the pure Friedel's salt and showed a good match the experimental patterns of prepared samples. The isotropic atomic displacement factors used for Rousselot's study were those for Friedel's salt high-temperature structure with $R\bar{3}$-c space group studied by Renaudin [47]. $R\bar{3}$ and $R\bar{3}$-c space group both belong to the hexagonal family and have different stacking pattern of layers.

Although pure Friedel's salt was detected in synthesized samples, it was not the only hydrocalumite phase. The material was multiphase and an additional chloro-carboaluminate phase was also detected in the samples. This phase showed a good match with a hydrocalumite phase studied by Mesbah et al. in 2011 [53]. The hydrocalumite material had a chemical formula of $[Ca_4Al_2(OH)_{12}]\cdot[Cl(CO_3)_{0.5}\cdot 10.8H_2O]$ and belonged to the monoclinic crystalline system with a space group of *P*2/*c*. The lattice parameters of both hexagonal phase with space group $R\bar{3}$ and monoclinic phase with space group *P*2/*c* is shown in Table 5. For more discussion on the

descriptions of lattice crystal systems and rotation axis for each point groups see Appendix B and C, respectively.

It appears from the quantitative phase analysis that the monoclinic chloro-carboaluminate hydrocalumite phase interrelates with carbonate-rich part of the samples prepared in this thesis, while the hexagonal chloro-hydrocalumite phase interrelates with chloride-rich part of the samples.

It needs to be mentioned that the low-temperature phase of Friedel's salt (monoclinic phase, with no carbonate in the composition) from PDF4+ 2016 software database was used for data matching, but did not fit with any of the experimental patterns. This showed that the second phase matching the experimental patterns was actually a carbonated-FS.

Table 5 Hydrocalumite lattice parameters from Jade and PDF4+ 2016 database software used for XRD and QXRD analysis

Hydrocalumite name, crystal system, space group, PDF #	**Software single crystal formula**	**a, b, c (Å)**	**α, β, γ (°)**	**V (Å³)**	**XRD analysis, Jade software**	**QXRD analysis, PDF4+ 2016 Database**	**Reference**
Friedel's salt, Monoclinic, *A*2/n, 01-078-1219	$[Ca_4Al_2(OH)_{12}]\cdot[Cl_2\cdot 4H_2O]$	9.979 5.751 16.32	90 104.53 90	906.6	✓		Not Available
Hydrocalumite, Hexagonal, $R\bar{3}$, 04-010-4677	$[Ca_4Al_2(OH)_{12}]\cdot[Cl_2\cdot 4H_2O]$	5.7487 5.7487 23.492	90 90 120	672.34		✓	Rousselot, et al.[46]
Hydrocalumite, Monoclinic, *P*2/*c*, 04-014-9938	$[Ca_4Al_2(OH)_{12}]\cdot[Cl(CO_3)_{0.5}\cdot 10.8H_2O]$	10.020 11.501 16.286	90 104.2 90	1819.2		✓	Mesbah, et al.[53]

3.2.4.4 Carbon analysis

The total inorganic carbon (TIC) content of the synthesized FS was analyzed by a LECO analyzer at the ALS Geochemistry laboratory. The sample was heated in the LECO furnace to approximately 1350 °C while a stream of oxygen gas passed through it. Carbon was removed as carbon dioxide gas and measured by an infrared detection system. The lower and upper limit of carbon analysis is 0.01 and 50 wt.%, respectively, with an accuracy of is 3.54%.

3.2.4.5 SEM analysis

A Hitachi S3000N VP-SEM with EDX was used for SEM analysis. The Hitachi S3000N is a conventional tungsten hairpin filament source SEM with variable pressure capability. The small amount of solid sample was coated with a thin gold layer and mounted on a holder in the chamber of the SEM machine.

3.2.4.6 Particle size distribution (PSD)

A Malvern Mastersizer 2000 was used for the measurement of the particle size of the FS samples. Sample preparation is an important stage of this measurement. The FS sample was dispersed in ethanol (5 wt.%) and the slurry was injected into the optical bench in the Malvern instrument. The light scattering pattern from the prepared sample was captured. The particle size was calculated from the pattern using the Mie theory and reported via the Malvern software output.

3.2.4.7 ICP

In this thesis, ICP-OES and ICP-MS analytical methods were frequently used for the elemental analysis of solutions and solids. ICP-OES was used in solution analysis of calcium and aluminum for aging solutions, adsorption solutions, and aged-solid digestion solutions. ICP-OES was also used for the analysis of sodium in FS washing experiments and selenium analysis in the ppm range for adsorption experiments. For selenium analysis in the ppb range of concentration, ICP-MS was used.

Al and Ca have different adsorption wavelengths in ICP-OES with no interference on the accuracy of analysis for each other. A selected volume of solution (usually 1 mL) was pipetted and diluted with a 2 wt.% nitric acid solution. The prepared sample solution was analyzed by ICP-OES analysis for Ca and Al concentrations. Ca and Al detection limit by ICP-OES is 0.2 ppm. The ICP solutions were prepared in the range of 20-50 ppm. In this range, Ca and Al analytical error is 5%. For solid analysis, samples (usually 40-50 mg) were digested with concentrated nitric acid and diluted to 100 mL using 2 wt.% nitric acid solutions.

All ICP standard solutions of calcium, aluminum, sodium, and selenium were prepared from standard solutions (1000±1 ppm) by the serial dilution procedure. Calcium, aluminum, and sodium standards were prepared in the range of 0.125, 0.625, 1.25, 10, 40, 80, and 160 ppm. Selenium standard solutions for ICP-OES analysis were prepared in the range of 2, 5, 10, 50, and 100 ppm. Selenium standard solutions for ICP-MS analysis were prepared in the range of 5, 25, 50, 100, 400, and 800 ppb.

Se detection limit by ICP-OES is 0.5 ppm. The ICP solutions were prepared in the range of 10-70 ppm. In this range, Se analytical error is 5%.

In general, when multiple replicates of one aging/adsorption experiment were performed to evaluate repeatability, only one sample from each experiment was analyzed by ICP. Here, the data (mass loss percentage values or Se loading data) are reported by the average value. The range of analytical values is shown in brackets next to this average value. For example, the average selenate removal by FS sample at a certain adsorption condition was 94.2% (92.6-95.5%). 94.2% is the average selenate removal value and 92.6% to 95.5% is the range of selenate removal for multiple replicates.

However, in some cases, only one single aging/adsorption experiment was performed. Here, two to three final solution samples were prepared for ICP analysis. For this case, the average ICP

reading is reported. The ICP-OES replicates were found to have very high reproducibility. For calcium and aluminum, the ICP solutions were prepared in the range of 20-50 ppm and were found to have variability in the range of +/- 0.01-0.07 ppm for Ca and +/- 0.01-0.07 ppm for Al. This is much lower than the analytical error of 5% expected in this range, so only the average ICP reading was reported. For selenium, the ICP-OES and ICP-MS solutions were prepared in the range of 10-70 ppm and 10-100 ppb and were found to have variability in the range of +/- 0.001-0.04 ppm for ICP-OES and +/- 0.05-0.07 ppb for ICP-MS. This is much lower than the analytical error of 5% expected in this range, so only the average ICP reading was reported.

3.2.4.7.1 FS mass-loss determination

The as-prepared FS material was partly dissolving in water and therefore the mass loss was calculated in every individual experiment. However, FS was a fine powder and collecting this material from filter units was challenging and prone to incomplete recovery. The FS-related slurries were initially centrifuged and filtered using syringe filter heads. As collecting FS was technically difficult with this equipment eventually, Durapore® filter membrane (0.45 μm) and Nalgene filter units were used. All filtration equipment is shown in Figure 10. Despite using various filtration equipment for FS collection, the estimation of final mass was still difficult, as FS (in dry and wet states) was sticking to the filter units. The direct weighing of solid by analytical scale is called a solid-based method (SBM). SBM is rarely used for mass calculations in the thesis.

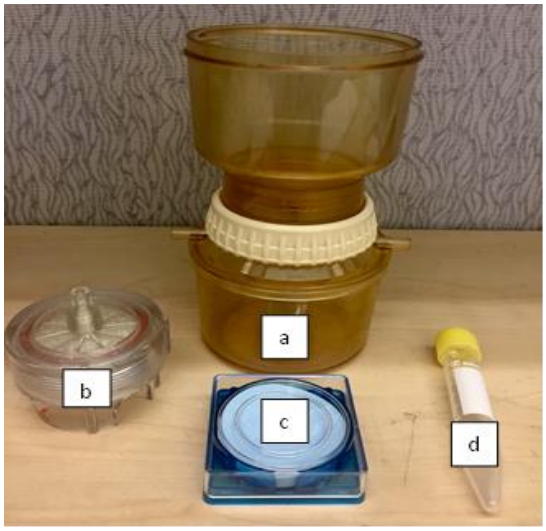

Figure 10 Filtration equipment, a: Nalgene filter unit, b: syringe filter head, c: Durapore ® Filter membrane and d: centrifuge tube.

3.2.4.7.2 Liquid-based method (LBM) for mass loss calculations

As a result of the technical difficulty of SBM, an alternative method was used for final mass calculations. The method is called the liquid-based method (LBM) since the FS mass loss calculations were based on the analysis of the liquid phase rather than weighing the recovered solid. Unless otherwise noted the LBM method was used to estimate the final FS mass for all experiments involving aging, dissolution and adsorption tests. In LBM, the solution analysis by ICP-OES was used to provide an indirect measure of the final FS mass (Equation 2). The ICP analysis of the solutions provides the moles of Ca^{+2} and Al^{+3} dissolved. From the stoichiometry of the FS solid, the moles of FS dissolved can be estimated. The calculation is illustrated in Equation 3 for the example of pure Friedel's salt, $[Ca_4Al_2(OH)_{12}]\cdot[Cl_2\cdot 4H_2O]$

FS final mass (W) = FS initial mass – mass loss (based on dissolved Ca & Al in solution) Equation 2

$$Mass\ FP\ dissolved = \frac{[Ca^{+2}]\ ^{g}/_{L}}{40.08\ ^{g}/_{mol\ Ca^{+2}}} \times Aq.vol.L \times \frac{1\ mol\ FP}{4\ mol\ Ca^{+2}} \times 561.34\ ^{g\ FP}/_{mol\ FP}$$ Equation 3

$$[Ca_4Al_2(OH)_{12}]\cdot[Cl_2\cdot 4H_2O] = 4Ca^{2+} + 2Al^{3+} + 12OH^- + 2Cl^- + 4H_2O$$ Reaction 4

The mass loss of FS was reported as weight percentages based on final Ca and Al concentrations in solution (Reaction 4). These values are called $Ca._{LB}$ and $Al._{LB}$ respectively, as indicated by Equations 4 and 5. Table 6, summarizes the mass loss calculation methods using Ca and Al concentrations.

$$Ca._{LB} = \frac{\text{FS mass loss (g) using Ca concentration in solution}}{\text{initial FS mass (g)}} * 100$$ Equation 4

$$Al._{LB} = \frac{\text{FS mass loss (g) using Al concentration in solution}}{\text{initial FS mass (g)}} * 100$$ Equation 5

The real FS materials used in this work were not pure Friedel's salt, but rather a mixture of chloride- and carbonate-containing materials. This complicates the decision about which formula weight to use for the FS material in Equation 3.

3.2.4.7.3 Se-loading calculations

As shown in Table 6, for Se loading data, the difference of initial selenium mass in feed solution and the final selenium mass in the filtrate solution was measured. This method is called $Se._{L}$ method in the thesis. ICP-OES and ICP-MS methods were used for solution analysis in ppm and ppb level of Se respectively. ICP-OES and ICP-MS detection limit for Se was 0.5 ppm and 1.0 ppb Se respectively. All ICP samples were prepared with appropriate dilution factors to ensure a concentration level ~2-100 times above the detection limits. At this range, Se analytical error is 5%.

Table 6 The mass loss calculations (LBM), Se-loading data, and adsorption capacity calculations used in the thesis

To be calculated value, ICP method	Method	Symbols (units)	Description
Mass loss (%) and final FS mass (g), ICP-OES	Liquid-Based Method **(**LBM**)***	$Ca._{LB}$ (%)	FS mass loss using Ca concentration in solution
		$Al._{LB}$ (%)	FS mass loss using Al concentration in solution
	Solid-Based Method	SBM (%)	FS mass measured with the final weight of solid
Se-loading data ICP-OES and ICP-MS	Solution analysis	$Se._{L}$ (mg Se or mmol Se)	Se loaded using the difference of initial and final Se concentration (C_0-C_e)
	Solid analysis	$Se._{S}$	Se loaded by digestion of solid
Adsorption capacity of FS (mg Se/g or mmol/g)	From a combination of LBM and $Se._{L}$	Q_e	Se loaded per gram of FS

*ICP data also used for calculation of Ca/Al molar ratio of solid samples

The digestion of solid for Se content calculations was also performed for some of the solid samples. This method is called $Se._{S}$ method in the thesis. In this method, the selenium content of the solid was measured by digestion of 40-50 mg sample with concentrated nitric acid followed by dilution with 2 wt.% nitric acid for ICP analysis. In this thesis, $Se._{L}$ is the main method used for Se loading data. In the case of using the alternative method, $Se._{S}$ for loading calculations, it is mentioned. In general, solution analysis was a more convenient method than solid digestion.

The digestion of FS solids was performed to measure the Ca and Al contents, for some samples. In this method, 40-50 mg sample was digested by concentrated nitric acid followed by dilution with 2 wt.% nitric acid for ICP analysis.

3.2.4.7.4 Pseudo-equilibrium adsorption loading

In this thesis, the amount of Se loaded at pseudo-equilibrium on aged-FS is expressed as Q_e (mg Se/g) or Q_e (mmol/g) using Equation 6. It should be mentioned that the final Se loading after 24-h shaking is considered the pseudo-equilibrium loading value. A 24-h shaking time is considered to be enough for reaching close to the equilibrium.

$Q_e = ((C_0 - C_e).V)/W = Se._L/W$ Equation 6

C_0 and C_e are initial and the pseudo-equilibrium concentration of selenium in solution, respectively (ppm or ppb). V is the final volume of solution (L) measured with a graduated cylinder. The difference between C_0 and C_e is the $Se._L$ value calculated from Se-ICP analysis. W is the final mass of aged-FS (g) calculated from the average of $Ca._{LB}$ and $Al._{LB}$ values (see Table 6). As explained in 3.2.4.7.2, the pure FS molar mass was used for mass loss calculations in adsorption studies. One of the contributions of this work is the usage of the actual final mass of LDH material (aged-FS) in pseudo-equilibrium loading isotherms. To the best of our knowledge, this thesis is the first publication in LDH materials filed, reporting and using the mass loss data in adsorption isotherms.

The pseudo-equilibrium adsorption isotherms were obtained by plotting the Q_e, pseudo-equilibrium loading (mg Se/g or mmol/g) on the y-axis versus pseudo-equilibrium solution Se concentration (ppm or ppb) on the x-axis.

3.2.4.7.5 Importance of including dissolution data in adsorption loading from engineering perspectives

In this thesis, the loading is calculated from two values; $Se._L$: the mass of loaded-Se (appears in the numerator as “mg Se” or “mmol Se”) and W: the final mass of FS. It is important to note that the different FS materials have different extents of dissolution. This has to be considered in any application for selenium removal from an engineering perspective. Therefore, in an industrial plant, the stability of an ion exchanger is of critical importance alongside the preference for high loading. Furthermore, a material with low mass-loss and moderate loading is preferred to an unstable material with high loading. An example of the importance of mass loss reporting for loading data comparisons to engineering considerations is discussed in section 6.3.5.

3.3 Aging process

The unaged-FS as-prepared could not be used for the selenate adsorption experiments due to its high dissolution. Therefore, an aging process was designed to age the unaged-FS material under variable conditions. The aging process was studied by variation of initial pH, time, temperature, and L/S. One experiment was carried out to study the effect of time, temperature, and L/S followed by several ICP replicate assays. For the initial pH effect, four to six individual experiments were performed. See 3.2.4.7 for the method used to report these analytical data in the thesis. The target was to age the material and eventually prepare an aged material with lower dissolution.

DI water used for all aging tests was decarbonated by purging nitrogen gas for 10-15 minutes. The unaged-FS material (prepared from the co-precipitation process, see Table 4) was added to decarbonated DI water (at initial pH 8.0 and 12.0) under various liquid over solid ratios (L/S 20-200). The bottle containing water and FS was closed tightly and the milky slurry was shaken vigorously by hand. Solids settled slowly as shown in Figure 11. The container was put in the water bath at a specific temperature (30, 65, and 85 °C), without any further mechanical agitation for a specific period of time (2, 4, and 7 days).

Figure 11 FS suspension in an aging experiment (decarbonated DI water was used for aging tests).

After each experiment, the slurry was filtered and analyzed for calcium and aluminum by ICP-OES. The concentration of Ca and Al in each solution and FS mass loss in each test was calculated as explained in 3.2.4.7.1. The mass of Ca and Al in aged solids were analyzed and the Ca/Al molar ratio was calculated by solid digestion method. A 40-50 mg sample of FS was digested with concentrated nitric acid followed by dilution with 2 wt.% nitric acid for ICP analysis.

3.3.1 Time effect on the aging process

The aging time applied in the literature varies from a couple of hours to a few days [44,71]. In these experiments, an aging period of 2, 4 and 7 days was selected for the duration of aging. Three aging slurries were prepared as follows; A 0.5 g sample of unaged-FS material was added to 25 mL of water with pH adjusted to 8.0 (L/S 50) in each container. Three bottles containing water and unaged-FS were closed tightly, shaken by hand and put in the water bath at 65 °C. The experiment was stopped for a first, second and third container after 2, 4, and 7 days. The slurries were filtered. The concentration of Ca and Al in each solution was measured. The weight loss under each aging condition was calculated using $Ca._{LB}$ and $Al._{LB}$, as explained in 3.2.4.7.1.

3.3.2 Effect of temperature on the aging process

For these experiments, three aging slurries were prepared as follows; A 0.5 g unaged-FS material was added to 10 mL of water with pH adjusted to 8.0 (L/S 20) in each container. Three bottles containing water and unaged-FS were closed tightly, shaken by hand and put in the water bath for 7 days at 30, 65, and 85 °C. The slurry was filtered and analyzed for calcium and aluminum by ICP-OES. The mass loss for each sample and the Ca/Al molar ratio of final solids were calculated.

3.3.3 L/S effect on the aging process

A critical parameter that affects the dissolution of any solid material in water is the “water-to-solid ratio”. A known volume of water was added to 0.5 g of unaged-FS, adjusting the L/S ratio at 20 to 200

(Table 7). The initial pH of the water was adjusted to 8.0, using 1 M sodium hydroxide. Each container was put in the water bath at 65 °C for 7 days. The slurry was filtered and analyzed for calcium and aluminum by ICP-OES. The mass loss for each sample and the Ca/Al molar ratio of final solids were calculated.

Table 7 Liquid over solid ratio in L/S studies (initial pH 8.0, 65 °C, and 7 days)

L/S	Water (mL)	Unaged-FS (g)
20	10	0.5
50	25	0.5
200	100	0.5

3.3.4 Effect of initial pH on the aging process

The initial pH of the water to which LDH is exposed is a critical parameter affecting LDH stability [44]. In general, LDHs are less stable in low-pH range. In addition, dissolution of Ca and Al is a pH-dependent process. In these aging experiments, the initial pH of the water was adjusted to 8.0 and 12.0 with sodium hydroxide solution. A sample of 0.5 g unaged-FS was added to 10 mL of water (L/S 20) at 65 °C and aged in this solution for 7 days. The slurry was filtered and analyzed for calcium and aluminum by ICP-OES. The final pH of the solution was recorded. The mass loss for each sample and the Ca/Al molar ratio of final solids were calculated.

3.3.5 A labeling system for FS samples

Table 8 summarizes all FS samples prepared from synthesis and aging process used in this thesis. Sample abbreviated IDs, full names, synthesis, and aging methods are described. From aging studies, one aging condition was selected, the general name of “aged-FS” is given to that sample. That one sample was aged at initial pH 12.0, L/S 20, 65 °C, and 7 days. The reason for selection of this aging condition will be explained later in section 5.5.1.

Therefore, “aged-FS” sample was prepared with co-precipitation synthesis process under partial nitrogen purging method followed by aging at initial pH 12.0, L/S 20, 65 °C, and 7 days. No nitrogen was applied in the aging process.

Table 8 Summary of FS samples prepared in this work

Abbreviated IDs	Full name	Synthesis method	Aging
Aged-FS*	Aged Friedel’s salt	Prepared by the co-precipitation method under ***partial*** nitrogen purging	Aged at the selected aging condition: initial pH 12.0, L/S 20, 65 °C, and 7 days (without N_2 purging)
Unaged-FS	Friedel’s salt		Not aged
Modified unaged-FS	Friedel’s salt	Prepared by the co-precipitation method under ***complete*** nitrogen purging	Not aged
$FS._{sint.}$**	Friedel’s salt	Prepared by the sintering-precipitation method	-

*used for selenate adsorption experiments, ** used only for a few preliminary adsorption tests

The unaged-FS and modified unaged-FS samples were prepared by co-precipitation synthesis process under partial and complete nitrogen purging methods, respectively. No aging was applied to these samples. FS samples were characterized by XRD, QXRD, and carbon analysis. Among all samples, more studies were performed on aged-FS as it was the main material used in selenate adsorption tests. $FS._{sint.}$ was the sample prepared by the sintering-precipitation method in the early stages of the work, and was only used for a few preliminary adsorption tests.

3.3.6 Dissolution of aged-FS compared to unaged-FS

In the next step, after preparation of aged-FS under the selected aging process of initial pH 12.0, L/S 20, 65 °C, and 7 days, the dissolution of the aged-FS sample was studied. The dissolution test was designed to study if the aged-FS was dissolving less than unaged-FS. For this purpose, in addition to aged-FS sample, the unaged-FS sample was used for comparison. In fact, the results of this test could quantify the effects of the aging process on reducing the dissolution of unaged-FS material.

The dissolution test was performed at an initial pH of 12.5, L/S 200, 30 °C, agitation (150 RPM), and 24 h. The solution matrix was selected to be selenate-free to monitor the dissolution process independent from the IX process. The initial pH of the water was adjusted at 12.5 and 20 mL of this solution was added to 0.1 g of FS sample (L/S 200) in a Pyrex glass container. The sealed container was shaken at 150 RPM in the water bath at 30 °C for 24 h. The slurry was filtered and analyzed for calcium and aluminum by ICP-OES.

The mass loss for each sample was calculated using $Ca._{LB}$ and $Al._{LB}$, as explained in 3.2.4.7.1. For the dissolution test, chemical formula and molar mass of aged-FS sample were used for mass loss of aged-FS material. Similarly, chemical formula and molar mass of unaged-FS sample were used for mass loss of unaged-FS material.

3.4 Selenate adsorption by aged-FS

In this thesis, aged-FS was the main FS material used for selenate adsorption experiments. The synthesis of this material is summarized in Table 8. Several consecutive large batches of FS material were prepared by co-precipitation followed by aging at initial pH 12.0, L/S 20, 65 °C, and 7 days (collected mass: ~150 g).

Selenate adsorption tests were conducted using synthetic solutions made up in ppm and ppb concentrations of Se. The concentrated stock solutions (100-600 ppm Se) were prepared by dissolution of Na_2SeO_4 salt in water (99.8% purity). The dilute solutions (400-800 ppb Se) were prepared by dilution of the concentrated feed solution. For concentration study experiments, feed solutions as high as 1539 ppm Se were prepared.

A Pyrex glass container was filled with a known volume of selenate solution with a specific concentration (ppm or ppb level). The initial pH was adjusted by addition of sodium hydroxide solution and a known amount of aged-FS was added to this solution. The bottle containing selenate

solution and aged-FS was closed tightly and the milky slurry was shaken vigorously by hand (similar to an aging slurry in Figure 11). The tightly sealed container was shaken in a Thermo Scientific shaking water bath for a selected period at a specific temperature.

The slurry was filtered using a Durapore® filter membrane (0.45 μm) and Nalgene filter units (see Figure 10). The solid was washed with water and dried in an oven at 100 °C.

The clear filtrate solution and the washing water were analyzed for selenium content by ICP. The ppb Se solutions were analyzed with ICP-MS and ICP-OES was used for ppm Se solutions. The final pH of the filtrate was recorded. The loaded-Se (mg Se), the mass loss (wt.%), and the final mass (g of FS) were calculated as explained in Table 6 (labeled as $Se._{L}$, $Ca._{LB}$, and $Al._{LB}$). The final pH of the solution was measured using high-sodium tolerance pH probes. The pH probe with temperature compensation was calibrated using pH buffer solutions 10.0 and 12.45 before any experiment.

The effect of various parameters on selenate adsorption including initial pH of selenate solution, L/S ratio, time, temperature, shaking rate, selenate initial concentration, oxyanion interference, container type, and medium composition was studied.

3.4.1 The initial pH study experiments

The initial pH of the Se feed solution (134 ppm and 460 ppb Se) was adjusted to 8-14 using either 1 or 10 M sodium hydroxide solutions. A 50 mL sample of selenate solution with an adjusted initial pH was mixed with 0.25 g of aged-FS (L/S 200). The container was placed in the shaking water bath at 30 °C and was shaken at 150 RPM for 24 h. The milky slurry was filtered. The solution was analyzed for selenium, calcium and aluminum contents.

3.4.2 L/S study experiments

For these experiments, weighed amounts of aged-FS (0.08 to 2.5 g) were mixed with 50 mL of Se feed solution (460 ppb Se) adjusting the L/S range at 20-1200 (Table 9). The initial pH was adjusted at 12.0

and the slurry was mixed for 24 h at 30 °C at 150 RPM shaking. The milky slurry was filtered. The solution was analyzed for selenium, calcium and aluminum contents as explained in 3.2.4.7.1.

Table 9 Mass of aged-FS and Se solution volume used at L/S studies of adsorption tests

L/S	Aged-FS (g)	Se solution (mL)
20	2.5	50
50	1.0	50
100	0.5	50
200	0.25	50
400	0.13	50
800	0.13*	100
1200	0.08*	100

*The mass was weighed by scale readability of 0.001 g

3.4.3 Time study experiments

For this series of experiments, the initial pH of the Se feed solution (637 ppb Se) was adjusted at 12.0. A 50 mL of Se solution was added to 0.25 g aged-FS (L/S 200). Eight of these containers were placed in a water bath at 30 °C and mixed at 150 RPM for 20 minutes to 48 h. The first container was taken out of the shaker and quickly filtered after 20 minutes. Other experiments were stopped at 45 minute, 1.5, 3, 6, 12, 24, and 48 h. The milky slurry was filtered. The solution was analyzed for selenium, calcium and aluminum contents.

3.4.4 Temperature study experiments

For this series of experiments, the pH of Se solution (468 ppb Se and 753 ppb Se) was adjusted at 12.0. A 50 mL of Se solution was added to 0.25 g aged-FS (L/S 200). The container was put in a shaking water bath stirred for 24 h at 150 RPM. The temperature of the water bath was adjusted at 30, 60, and 85 °C temperatures. The milky slurry was filtered. The solution was analyzed for selenium, calcium and aluminum contents.

3.4.5 Effect of container type on selenate adsorption by aged-FS

The selenate adsorption by Pyrex glass container, polypropylene (PP) and high-density polyethylene (HDPE) plastic containers was studied. A 50 mL of 495 ppb Se feed at initial pH 12.0 was added to each of the containers. No aged-FS was added to these containers to monitor the adsorption by container material exclusively. The container was put in the shaking water bath at 30 °C and stirred at 150 RPM for 24 h. The final concentration of Se solution was analyzed by ICP-MS for each experiment.

3.4.6 Agitation rate experiments

For this series of experiments, the pH of Se solution (753 ppb Se) was adjusted at 12.0. A 50 mL of Se solution was added to 0.25 g aged-FS (L/S 200). The container was put in a shaking water bath stirred at 30 °C for 24 h at agitation rates of 100, 150, and 175 RPM. These experiments were performed at 100 and 150 RPM with Thermo Scientific shaking water bath. The mechanical restriction of this shaker limited its applications at higher RPM. Therefore, the experiments at 175 RPM were performed with a Lab-Line orbit environ-shaker. The milky slurry was filtered. The solution was analyzed for selenium, calcium and aluminum contents.

3.4.7 Effect of initial concentration on selenate adsorption by aged-FS

For this series of experiments, the initial concentration of feed solution was adjusted in the range of 1, 2, 5, 10, 20, 50, 100, and 200 ppm Se. The initial pH of the selenium solution was adjusted to 12.0 by 1 M sodium hydroxide solution. A 0.5 g sample of aged-FS was added to 50 mL of selenium solution. The container was put in the shaking water bath at 30 °C, stirred at 150 RPM for 24 h. The clear filtrate solution was collected and analyzed for selenium with ICP-MS and ICP-OES (see 3.2.4.7.2 and 3.2.4.7.3).

3.4.8 Oxyanion interferences; sulfate and carbonate competition with selenate

The interference of sulfate and carbonate oxyanions with selenate were studied, as these oxyanions often exist in high concentrations in selenate-impacted wastewaters [3,4,6,11]. For the sulfate interference experiments, a calcium sulfate solution was prepared by the addition of 2 and 10 g $CaSO_4 \cdot 2H_2O$ into 1000 mL of DI water. The solution was mixed overnight and left on a bench for an additional 24 h. No precipitation was observed for the 2 g/L solution but the 10 g/L solution contained residual solids. This solution was filtered and observed for 1 day to ensure that there was no additional precipitation. No more precipitation occurred.

The mixed sulfate-selenate solutions were prepared with the addition of a specific amount of concentrated selenate solution into a volumetric flask. The solution was made up to a final volume using the as-prepared sulfate feed solutions (Se feed 763 ppb Se). The molar ratio of sulfate-to-selenate in solution was adjusted to 800, 1500, and 3000. The pH of the solution was adjusted to 12.0 by 1 M sodium hydroxide solution. A 0.25 g sample of aged-FS was added to 50 mL of as-prepared selenate-sulfate mixed solution (L/S 200). The container was put in the shaking water bath at 30 °C, stirred at 150 RPM for 24 h. Each experiment was repeated three times. The clear filtrate solution was collected and analyzed for selenium with ICP-MS and ICP-OES (see 3.2.4.7.3).

For the carbonate interference experiments, Na_2CO_3 was dissolved in water to prepare 2 and 14 g/L solutions. Sodium carbonate was fully soluble. The sodium carbonate solution was used as-prepared for making selenium solutions. Similar to the sulfate solution experiments, adsorption of selenate from synthetic carbonate-selenate mixed solutions was studied. The molar ratio of carbonate-to-selenate was adjusted to 700, 1400, and 2800. Initial pH of the solution was adjusted to 12.0 using 1 M sodium hydroxide solution. A 0.25 g sample of aged-FS was added to 50 mL of as-prepared selenate-carbonate mixed solution (L/S 200, Se feed 763 ppb Se). The container was put in the shaking

water bath at 30 °C, stirred at 150 RPM for 24 h. Each experiment was repeated three times. The clear filtrate solution was collected and analyzed for selenium with ICP-MS and ICP-OES (see 3.2.4.7.3).

3.4.8.1 The effect of increased intercalated-carbonate content during aging on Se loading

Aged-FS was the main material used for the selenate adsorption tests. Adsorption by unaged-FS, the material that did not go through the aging process, was also studied in three experiments. The purpose of these studies was to figure out the effect of an increase in intercalated-carbonate on the loading of Se. In these experiments, the initial pH of the selenate feed solution (219 ppm Se) was adjusted to 12.0 with 8 M sodium hydroxide solution. A 0.25 g unaged-FS sample was added to 50 mL (L/S 200), the slurry was put in shaking water bath at 30 °C, stirred at 150 RPM for 24 h. After filtration, the solid was dried in an oven at 100 °C. The mass loss and Se-loading for each adsorption experiment were reported by LBM and $Se._L$ calculations (see 3.2.4.7.1, Table 6). The adsorption experiments under identical experimental conditions were performed with aged-FS. The Se-loading and dissolution data were compared for two materials.

3.4.9 Calcium hydroxide solution experiment; industrial wastewater's solution matrix

The adsorption of selenate from a calcium hydroxide solution was performed for application to industrial wastewater solutions. The mentioned waste water can be for instance industrial wastewater after a lime precipitation circuit. It was thought that the FS dissolution can be minimized in the presence of high Ca concentrations. The calcium hydroxide feed solution was prepared by dissolving 1.73 g $Ca(OH)_2$ in 1000 mL DI water ($K_{sp}=6.5X10^{-6}$). The mixture was mixed overnight and left on the bench for a couple of days. A thin layer of solid (most likely calcite) formed on the surface of the solution was removed by filtration. The final clear solution was analyzed for calcium content by ICP-OES. The calcium concentration was 708 ppm. The solution is called "calcium hydroxide feed solution".

The selenate feed solution (498 ppb Se) was prepared by dissolving the sodium selenate salt in the so-prepared calcium hydroxide feed solution. No sodium hydroxide was required for the pH adjustment since the calcium hydroxide solution was alkaline (pH 12.3). A 50 mL aliquot of this feed solution was added to the 0.25 g of aged-FS (L/S 200). The slurry was mixed for 24 h at 30 °C and 150 RPM. The experiment was repeated twice. The slurry was filtered. The selenate concentration in solution was analyzed by ICP and the selenate loading percentage was measured by $Se._{L}$ method. The FS mass loss was calculated by aluminum concentration in solution ($Al._{LB}$). The calcium concentration could not be used as Ca was already present in high concentrations in solution.

3.4.10 Calcination of aged-FS

A selected amount of aged-FS was weighed and heated in a ceramic crucible at temperatures of 300-800 °C for 5 h in the furnace. The solid was collected, sealed in a sample tube and stored in a desiccator over $CaCl_2$ granules, NaOH pellets and silica in order to avoid adsorption of $CO_{2(g)}$ and moisture from the atmosphere. The solid was characterized by XRD and used for selenate adsorption experiments.

3.4.10.1 Effect of calcination on selenate adsorption

Adsorption of selenate by calcined aged-FS was studied for loading-comparison purposes of aged-FS and its calcined forms. In these experiments, the initial pH of the selenate solution was adjusted to 12.1 with 8M sodium hydroxide solution. A 0.25 g solid sample was added to 50 mL (L/S 200) of the selenate solution concentration of 753 ppb Se. The temperature and shaking rate were adjusted to 30 °C and 150 RPM. The mixture was shaken for 24 h followed by filtration and solid drying in an oven (100 °C). The mass loss for each adsorption experiment was reported by LBM. The clear filtrate solution was collected and analyzed for selenium, calcium, and aluminum content with ICP-MS and ICP-OES (see Table 6).

Chapter 4: FS synthesis by co-precipitation method at constant-pH under partial nitrogen purging (unaged-FS synthesis)

The synthesis of FS was best accomplished by the co-precipitation method at constant-pH. Early work was performed using the sintering-precipitation method reported by Wu for preparation of FS_{sint}. [25]. This method was laborious and time-consuming and was therefore replaced by the co-precipitation method. The following sections illustrate the procedures used in the co-precipitation synthesis.

4.1 Co-precipitation method; precipitation at constant pH

The co-precipitation at constant-pH method was used to prepare fresh FS. This procedure describes the synthesis method using a partial nitrogen purging method (see 3.2). The product of this method is called "*unaged-FS*". It was subjected to aging later.

The complete nitrogen purging method is a similar synthesis procedure with the main differences being in the filtration and drying steps (see 3.2.1). The product of this synthesis method in the nomenclature of this thesis is referred to as "*modified unaged-FS*".

The key parameter for FS synthesis by co-precipitation is the pH used to control the precipitation. An initial experiment was performed at pH 10. This was difficult to control and resulted in aluminum hydroxide precipitation and not FS.

The successful synthesis of FS required a higher pH set point. For example, in the general experiment, the initial pH of the solution was set to 12.1 instead. The Ca-Al metal solution (total metal concentration 1 M) was added at 0.25 mL/min to the pH 12.1 aqueous NaOH solution in the reactor under partial nitrogen purging conditions (see 3.2 and 3.2.1). A 1 M sodium hydroxide solution with a maximum of 20 mL/min flow rate was used to control the pH of the slurry at 11.3 during the experiment. Figure 12 shows the change in the pH of the slurry over the time of the metal addition.

The pH was maintained successfully during the whole experiment. The initial pH of 12.1 dropped sharply to 11.2 at the moment of the metal addition to the reactor and remained within the range of about 11.2 to 11.5 throughout the experiment. It is necessary to control the pH to provide a supersaturation condition for preparation of FS material free from metal hydroxides [63]. Aluminum hydroxide forms at pH 3.9 (at 10^{-2} M) and pH 8.0 (at 10^{-4} M) [27]. The temperature for the co-precipitation process was kept at 30 °C.

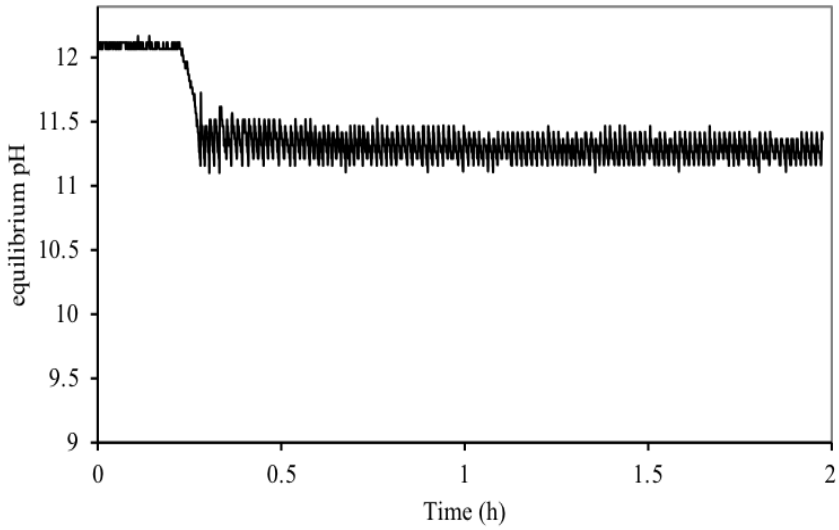

Figure 12 pH control in the co-precipitation method at constant pH method (initial pH 12.1, set pH 11.3).

The slurry was mixed for 72 hours at a high stirring rate. The pH was unchanged over the three days reaction period. The solid and liquid phases were separated by filtration and the precipitated solid was washed with cold water to remove contamination. For this, DI water was boiled, cooled to room temperature under nitrogen gas, and cooled down to 0 °C in the fridge. An aliquot of cold DI water (L/S 10) was used for washing. For example, 50 g wet solid, was washed with ~500 mL of cold water. The water was added as a displacement wash to the filter cake. The wash water was sampled, diluted with 2 wt.% nitric acid and, analyzed for sodium content by ICP-OES.

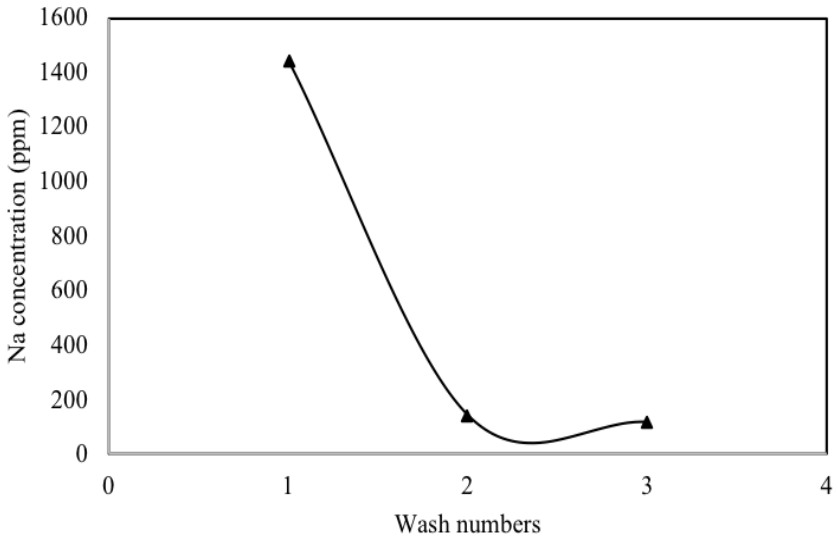

Figure 13 Sodium concentration in wash water as a function of washing (cold DI water at L/S 10).

Figure 13 shows the sodium concentration after each washing step. Sodium release into the wash water for the second and third washing step was low and nearly constant. Therefore, only one wash with cold water and L/S 10 was sufficient. The analysis for FS after washing indicated 0.37% Na.

The co-precipitation experiment was repeated in several batches and phase analysis of all the solids confirmed the formation of Friedel's salt. The XRD pattern of the unaged-FS sample prepared with partial nitrogen purging in the large batch is shown in Figure 14. As seen, the experimental pattern of solid matched with Friedel's salt XRD pattern from the Jade software database with reference number 78-1219 and chemical formula of $[Ca_4Al_2(OH)_{12}]\cdot[Cl_2\cdot 4H_2O]$. A typical XRD pattern of an LDH displays three major reflections; the one with the highest intensity appears around 2θ 11° value. This high-intensity basal reflection corresponds to the successive orders of basal spacing. The other two low-intensity non-basal reflections appear at higher 2θ values. The presence or lack of these reflections was used in the thesis to determine whether Friedel's salt was formed or not. The high intensity of diffraction peaks shows that crystalline material was formed.

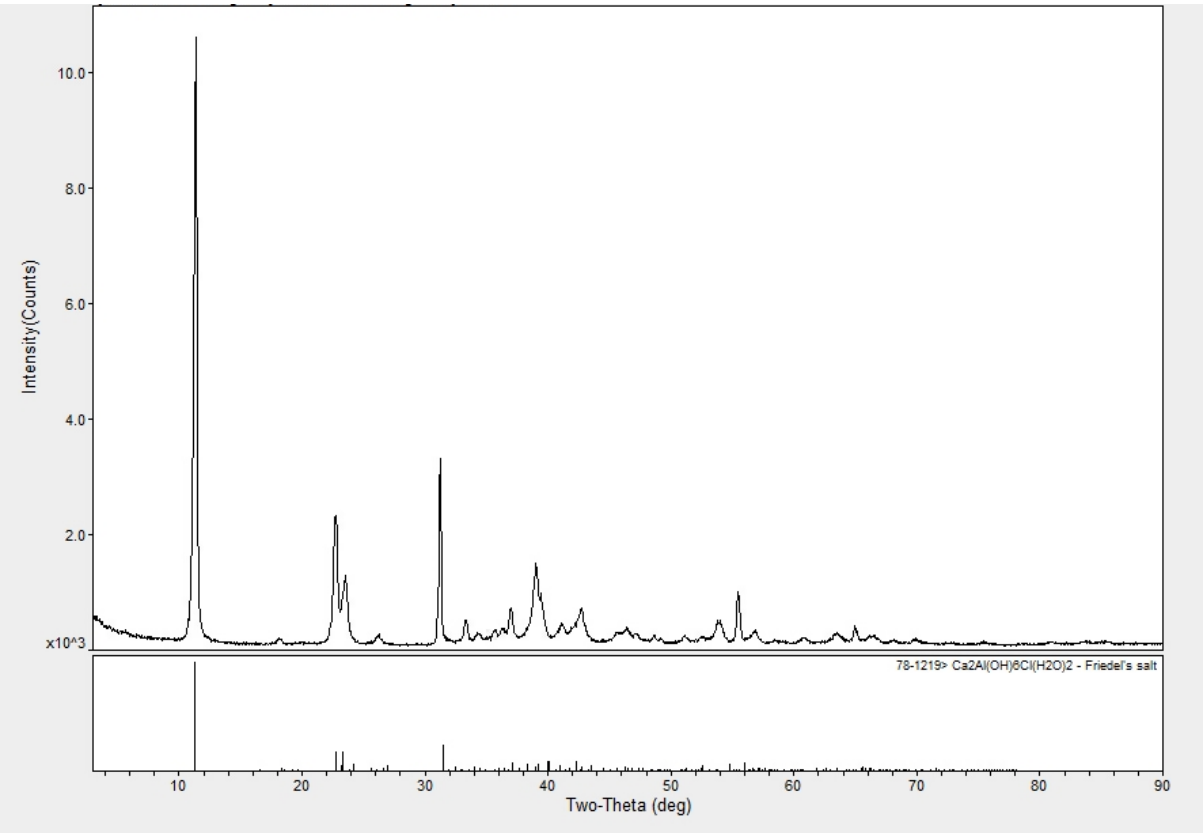

Figure 14 XRD pattern of the unaged-FS sample prepared with co-precipitation method at constant-pH method under partial nitrogen purging (initial pH 12.1, setpoint pH 11.3, room temperature, NaOH and the metal solution flow rates of 20 and 0.25 mL/min). The lower pattern belongs to the Friedel's salt pattern from Jade software.

4.2 General procedures for preparation of FS samples

Figure 15, shows a general flowsheet for preparation and evaluation of FS samples. First, the freshly precipitated unaged-FS was used for preliminary adsorption tests. In the early stages of using the unaged-FS material for preliminary Se adsorption tests, it was found out that the material was partially soluble in water. This issue was a critical drawback for the adsorption studies and could limit the efficiency of adsorption studies if not addressed. After studying the literature, a conventional aging treatment was selected for the study to try to reduce material loss [28,70,71]. The aging process was carried out after the original FS was prepared by co-precipitation, filtered and washed and dried. The section number of each experiment and the relevant result is also shown, for more clarifications.

Secondly, as large amounts of unaged-FS were required for aging studies and further characterization, several large batches of co-precipitation synthesis FS at constant pH under partial nitrogen purging conditions were carried out (see experimental section: 3.2 and Table 4). Next, one homogenized sample was prepared (~150 g). This sample was also called unaged-FS and was used for aging tests (see experimental section:3.3) and characterization studies. The product of aging was called aged-FS and was used for selenate adsorption tests (see experimental section: 3.4).

After synthesis and characterization discussions in Chapter 4, the aging process is discussed in details in Chapter 5 of the thesis. The selenate adsorption tests carried out by aged-FS is discussed in Chapter 6 of the thesis.

The complete nitrogen purging method was used in the co-precipitation process to see if the carbonate content of the precipitated FS could be reduced by controlling nitrogen purging (see experimental section: 3.2.1) [44,64].

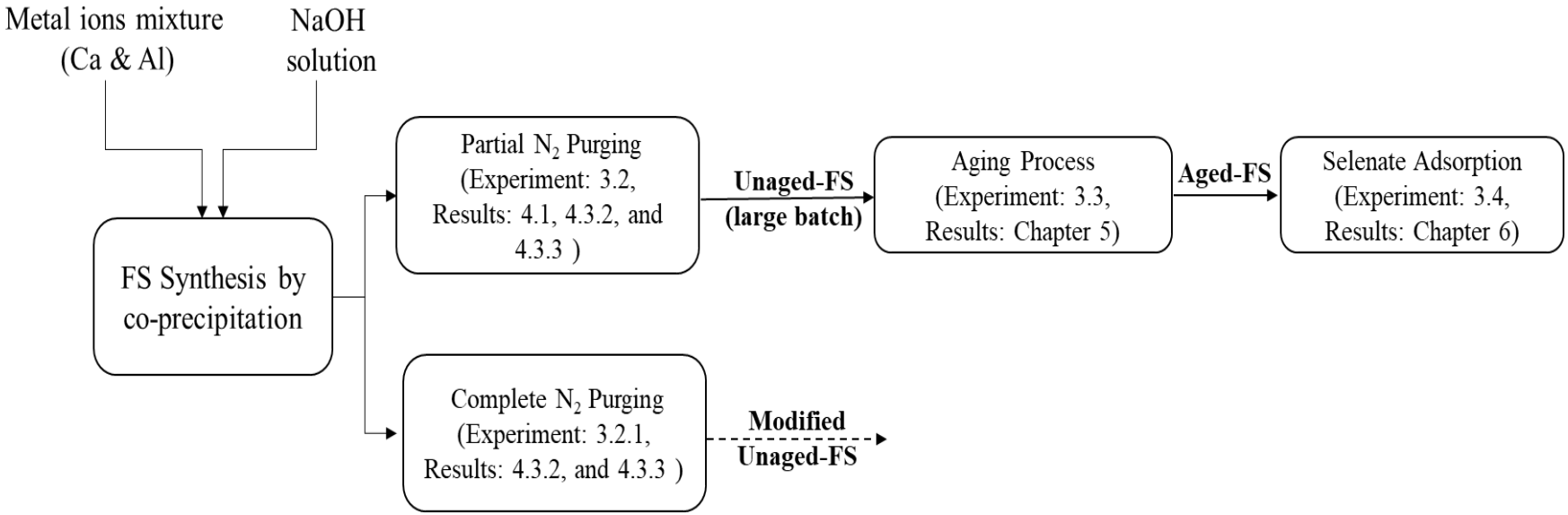

Figure 15 General flowsheet for preparation of unaged-FS, modified unaged-FS and aged-FS in the thesis.

4.3 Characterization of unaged-FS

As shown by XRD study, the unaged-FS sample matched well with Friedel's salt pattern from Jade software with a chemical formula of $[Ca_4Al_2(OH)_{12}]\cdot[Cl_2\cdot 4H_2O]$ (see Figure 14). The as-prepared unaged-FS material was further analyzed by solid digestion and ICP-OES, carbon analysis, and QXRD methods. The solid digestion followed by ICP-OES determined the calcium and aluminum content of the sample. The carbon analysis was used for carbonate content. QXRD analysis was used for phase analysis. The results of each analytical method are discussed in the following sections.

4.3.1 Solid digestion; calcium and aluminum content of unaged-FS

To determine the calcium and aluminum content of the unaged-FS sample, three homogenized samples were taken from a large batch co-precipitation product. These samples were digested with concentrated nitric acid and each was analyzed for Ca and Al with ICP-OES. The concentrations and weight percentage of Ca and Al for each sample are shown in Table 10. Based on three digestion tests, the average amount of calcium and aluminum of 0.1030 and 0.0549 mmol were calculated. The average Ca/Al molar ratio of solids was calculated to be 1.88. The average calcium and aluminum weight percentages were 25.3 and 9.03%, respectively.

XRD analysis suggested the formation of Friedel's salt. The measured Ca/Al molar ratio (1.88) was less than the expected value of 2.0 based on the stoichiometry of FS. For hydrocalumite family with a chemical formula of $[Ca_4Al_2(OH)_{12}]\cdot[X_2\cdot mH_2O]$, Ca^{2+} and Al^{3+} cations are arranged in a fixed Ca/Al molar ratio of 2:1 (as a result of the large size and noticeable anisotropy of the coordination sphere of Ca^{2+} ion) [43,46]. Therefore, this deviation from the ideal value of 2.0 was presumably related to some minor phases undetectable by XRD analysis. The detection limit for XRD is 5 wt.%. Therefore, further investigation by quantitative XRD analysis was required.

Table 10 Ca and Al content of unaged-FS sample from solid digestion analysis

Unaged-FS Sample	Ca wt.%	Al wt.%	Ca/Al molar ratio in unaged-FS solid
1	27.4	9.90	1.86
2	24.5	8.73	1.89
3	24.0	8.62	1.87
Average	25.3	9.08	1.88±0.01

4.3.2 The reduction of carbonate content with complete nitrogen purging method; carbon analysis of unaged-FS and modified unaged-FS

To measure the amount of carbonate in FS samples, the carbonate content of unaged-FS and modified unaged-FS samples were measured by a LECO carbon analyzer. The carbon analysis results of both samples are shown in Table 11. As seen, the unaged-FS sample prepared by partial nitrogen purging contained 1.15 wt.% carbonate. A composite sample was collected from several batches of co-precipitation products.

In most of the literature studies, the carbonate content of as-prepared LDH materials is reported [33,53]. However, the tracking of carbonate content in LDH by variation of synthetic methods is not widely reported. In this thesis, in addition to partial nitrogen purging method, a synthesis process was performed under a more complete nitrogen purging method to minimize the carbonate content of the precipitated FS sample (3.2.1). The product of the complete nitrogen purging method, called modified unaged-FS, was analyzed for carbonate content. The carbonate content of the material obtained by this method is shown in Table 11. As shown, the modified unaged-FS sample had actually lower carbonate content than the unaged-FS sample. The complete nitrogen purging method reduced the carbonate content from 1.15 to 1.01 wt.%. Although the difference looks small, it will be seen later that this reduced the molar content of carbonate significantly (section 4.3.3.14.3.3). Further reduction in the carbonate content of the sample was

not achievable under the applied experimental conditions (complete nitrogen purging method). The exposure of the wet sample to $CO_{2(g)}$ from the air during the transfer of solid to the desiccator was unavoidable and therefore a 1.01 wt.% carbonate was the lowest carbonate content achieved in the laboratory. One might expect to achieve carbonate contents lower than 1.01 wt.% by performing the complete nitrogen purging method in a glove box.

Table 11 Carbonate content of unaged-FS samples from co-precipitation process

	Unaged-FS (partial nitrogen purging)	**Modified unaged-FS (complete nitrogen purging)**
Carbonate content wt.(%)	1.15	1.01

4.3.3 QXRD analysis of unaged-FS and modified unaged-FS

Qualitative XRD analysis involves the identification of phases in a sample by comparison with "standard" patterns (i.e., data collected usually from single crystals) and relative estimation of proportions of different phases in multiphase specimens by comparing peak intensities attributed to the identified phases. From the XRD analysis of the unaged-FS sample, the material was shown to be mainly a chloro-hydrocalumite phase (Figure 14). To determine the exact proportion of chloro-hydrocalumite phase and presence of any other minor phases (undetectable by XRD), the FS samples prepared with co-precipitation synthesis in partial and complete nitrogen purging methods were analyzed with quantitative XRD analysis. QXRD applies an internal standard (Al_2O_3) and uses mathematical methods to "fit" the XRD pattern to the solid phases identified in order to come up with a quantitative measure of the phase fractions present. QXRD analysis provided further pieces of information about the unaged-FS sample. Firstly, the material was shown to be a two-phase hydrocalumite material and not a single hydrocalumite phase. Secondly, a minor impurity phase was detected. This showed that XRD analysis could not distinguish two hydrocalumite phases because the XRD patterns were very similar to each other. Only the

mathematical deconvolution of the patterns achieved by QXRD was able to show that two phases were present.

As mentioned previously in 3.2.4.2, the QXRD analysis did not show any unaccounted phase fraction that could be assigned to an amorphous or non-crystalline phase. All the unaged-FS samples by co-precipitation processes were reported to be crystalline materials. Table 12 summarizes the QXRD results for two unaged-FS samples prepared by the co-precipitation method under partial nitrogen purging. As explained in 3.2.4.3, two phases from the literature were used for data matching; a chloro-hydrocalumite phase with a hexagonal crystalline system and a chemical formula of $[Ca_4Al_2(OH)_{12}]\cdot[Cl_2\cdot 4H_2O]$ along with a chloro-carboaluminate hydrocalumite with a monoclinic crystalline system and a chemical formula of $[Ca_4Al_2(OH)_{12}]\cdot[Cl(CO_3)_{0.5}\cdot 10.8H_2O]$ [46,53]. The carbonated hydrocalumite phase found in samples of this study were all hemi-carboaluminate phases, the half-carbonated hydrocalumite (not the fully carbonated). PDF4+ 2016 software was used to match the experimental patterns. Note that all the phases in QXRD reports are kept in the table even when a phase was not found in the sample, to maintain the consistency of the reports.

The unaged-FS samples 1 and 2 were prepared under partial nitrogen purging in large and small batches respectively. Both samples are labeled as unaged-FS for simplicity. As seen, sample 1 was composed of 74 wt.% chloro-hydrocalumite and 24 wt.% chloro-carboaluminate hydrocalumite phase. For unaged-FS sample 2, a similar proportion of 68 wt.% chloro-hydrocalumite and 20 wt.% chloro-carboaluminate hydrocalumite phase was observed. The proportion of chloro-carboaluminate hydrocalumite (monoclinic phase) was similar for both samples (24 and 20 wt.%). Both unaged-FS samples prepared under partial nitrogen purging had some portion of intercalated carbonate in the hydrocalumite phase. The carbonated hydrocalumite

portion of FS in a partial nitrogen purging method was almost constant for small and large scales; average of 22 wt.% (20-24 wt.%). The chloro-hydrocalumite phase proportion in two unaged-FS samples was an average of 71 wt.% (68-74 wt.%).

As seen in Table 12, the unaged-FS sample 1 contains 2 wt.% $Al(OH)_3$ as a minor phase. This sample was analyzed previously by solid digestion and ICP-OES (4.3.1). The sample was shown to have a Ca/Al molar ratio of 1.88, lower than what is expected for an ideal hydrocalumite. The $Al(OH)_3$ impurity most likely is the reason for the deviation of experimentally determined Ca/Al molar ratio from the ideal value. This is further discussed in the next section.

Table 12 QXRD phase analysis of FS samples obtained from the co-precipitation process with partial nitrogen purging (unaged-FS) and complete nitrogen purging methods (modified unaged-FS)

Phase name	**Software single crystal formula**	**Phase fraction (wt %)**		
Sample name, Sample number		**Unaged-FS**		**Modified unaged-FS (Sample 3)**
		Sample 1*	**Sample 2**	
Synthesis method/ nitrogen purging method		**Co-precipitation/ partial nitrogen purging**		**Co-precipitation/ complete nitrogen purging**
Hydrocalumite, Hexagonal crystal system, $R\bar{3}$ space group, PDF#: 04-010-4677	$[Ca_4Al_2(OH)_{12}]\cdot[Cl_2\cdot 4H_2O]$	74	68	86
Hydrocalumite, Monoclinic crystal system, *P2/c* space group, PDF#: 04-014-9938	$[Ca_4Al_2(OH)_{12}]\cdot[Cl(CO_3)_{0.5}\cdot 10.8H_2O]$	24	20	11
Katoite	$Ca_3Al_2(OH)_{12}$	-	-	-
Calcite	$CaCO_3$	trace	2	2***
Bayerite	$Al(OH)_3$	2	3	-
Halite	NaCl	-	7**	1
Quartz	SiO_2	-	-	<0.5
Total wt.%	-	100	100	100

*sample studied by solid digestion and carbon analysis ** from an incomplete washing process, *** 0.98% calcite, and 1.48% vaterite

For unaged-FS sample 2, incomplete washing resulted in 7% NaCl impurity. This shows the importance of solid washing after filtration in controlling impurities and tracking of sodium content in washing filtrate by ICP-OES (as shown in Figure 13). Trace quartz was present due to

possible contamination from abrasion of micronizer pellets in QXRD experiments. Calcite also is present in trace levels. As seen, adsorbed carbonate from the air was intercalated in the FS structure rather than precipitating as calcite. The complete exclusion of carbonate oxyanion from FS structure in co-precipitation process under partial nitrogen purging was unavoidable.

It needs to be noted that the presence of hydrocalumite-hydroxide with a chemical formula of $[Ca_4Al_2(OH)_{12}]\cdot[(OH)_2\cdot 6H_2O]$ was not detected by QXRD. At aqueous chloride concentrations of more than 2 mM in the synthesis process, the chloride-hydrocalumite formation is favored over hydroxide-hydrocalumite formation [49]. The concentration of chloride in an aqueous solution of all co-precipitation tests was 2.3 M much higher than the reported value. Therefore, the co-precipitation experimental conditions ensured the formation of a chloro-hydrocalumite over hydrocalumite-hydroxide phase.

4.3.3.1 The experimental chemical formula of unaged-FS

As seen from QXRD analysis, the unaged-FS material sample 1 was composed of 74 wt.% chloro-hydrocalumite (hexagonal system), 24 wt.% chloro-carboaluminate hydrocalumite phase (monoclinic system) and 2 wt.% aluminum hydroxide. The experimental chemical formula of the unaged-FS sample is calculated using the molar mass of above-mentioned phases. Sample 2 from Table 12 was discarded due to high halite impurity.

As shown in Table 13, the phase analysis data from QXRD studies were used to calculate the elemental content of the unaged-FS sample. With the inclusion of $Al(OH)_3$ minor phase the experimental formula of unaged-FS is close to $[Ca_{3.88}Al_{2.09}(OH)_{12.1}]\cdot[Cl_{1.73}(CO_3)_{0.10}\cdot 5.27H_2O]$. The unaged-FS material is a partially carbonated hydrocalumite with a Ca/Al molar ratio of 1.86 (from the chemical formula). This ratio is similar to the average experimental value obtained by solid digestion and ICP-OES analysis of the sample (1.88 in Table 10). Moreover, Ca and Al weight percentages based on the experimental chemical formula are 26.8 and 9.71 %, respectively. These values are in adequate agreement with the solid digestion data of unaged-FS samples shown in Table 10 (25.3 and 9.03 % for Ca and Al, respectively). With the exclusion of $Al(OH)_3$ minor phase the experimental formula of unaged-FS will be $[Ca_{3.88}Al_{1.93}(OH)_{11.6}]\cdot[Cl_{1.73}(CO_3)_{0.10}\cdot 5.27H_2O]$. In this case, a Ca/Al molar ratio of 2.0 will be obtained for the hydrocalumite sample, as expected for the hydrocalumite family. In conclusion, the aluminum hydroxide impurity was causing the observed deviation of experimental Ca/Al molar ratio from the ideal value of 2.0.

Table 13 Unaged-FS experimental chemical formula calculations

			Moles per 100 g					
Phase formula	**Phase proportion (wt.%)**	**Molar mass (g/mole)**	**Ca**	**Al**	**OH**	**Cl**	**CO_3**	**H_2O**
$[Ca_4Al_2(OH)_{12}]\cdot[Cl_2\cdot 4H_2O]$	74%	561.3	0.53	0.26	1.58	0.26	-	0.53
$[Ca_4Al_2(OH)_{12}]\cdot[Cl(CO_3)_{0.5}\cdot 10.8H_2O]$	24%	678.4	0.14	0.07	0.42	0.04	0.02	0.38
$Al(OH)_3$	2%	78.0	-	0.03	0.08	-	-	-
		total moles	0.67	0.36	2.08	0.30	0.02	0.91
Molar mass: 579.76 g/mole		moles per one mole of FS	3.88	2.09	12.1	1.73	0.10	5.27

4.3.3.2 The reduction of chloro-carboaluminate phase content with the complete nitrogen purging method

The FS sample prepared under a complete nitrogen purging method (called modified unaged-FS sample 3 in Table 12) was analyzed by QXRD. The phase analysis of this sample showed a different proportion of chloro-hydrocalumite and chloro-carboaluminate phases. The chloro-carboaluminate phase weight percentage in modified unaged-FS was significantly lower than in the unaged-FS samples. The average chloro-carboaluminate phase content in the unaged-FS sample was 22 wt.% while modified unaged-FS contained only half as much (11 wt.%) of this phase. The proportion of chloro-hydrocalumite phase, the phase with no carbonate in the structure, was significantly increased using complete nitrogen purging method (86 wt.% vs average 71 wt.% in unaged-FS samples). The complete nitrogen purging method reduced the intercalated carbonate portion and consequently increased the pure Friedel's salt portion of synthesized samples.

The QXRD pattern of the modified unaged-FS sample with more details is shown in Figure 47 in Appendix D. In this QXRD pattern, a small legend on the top right corner shows all the phases with different colors. The experimental pattern is shown in blue. All the phases detected by QXRD are shown with other colors (e. g., hexagonal and monoclinic phases are shown with orange and pink colors respectively). The gray line shows the difference between the experimental and the total detected phases. The calcium carbonate minor phase (2 wt.%) is actually composed of 0.98 wt.% calcite and 1.49 wt.% vaterite. Vaterite belongs to the hexagonal crystal system, whereas calcite is trigonal.

Using the weight percentages of two hydrocalumite phases (Table 13) and the experimental formula of $[Ca_{3.88}Al_{2.09}(OH)_{12.1}]\cdot[Cl_{1.73}(CO_3)_{0.10}\cdot 5.27H_2O]$, the carbonate weight percentage in

unaged-FS was calculated. The results are shown in Table 14. As seen, the calculated result is close to the carbonate content reported by carbon analysis.

Table 14 Carbonate content of unaged-FS calculated from QXRD analysis and carbon analysis

	From QXRD results	**From carbon analysis**
Carbonate wt.%	1.06 wt.%	1.15 wt.%

In summary, the QXRD results in association with carbon analysis results showed that the carbonate content of the FS sample can be reduced by a complete nitrogen purging condition. The complete nitrogen purging condition will be favored over partial nitrogen purging method if there is a need to use the maximum capacity of the material in an adsorption process. The intercalated-carbonate interference with selenate will be further discussed in 6.3.3.

4.4 Summary of unaged-FS synthesis and characterization

FS was synthesized by co-precipitation method at a constant pH of 11.3 under partial nitrogen purging method. The FS product from this synthesis is referred to as “unaged-FS”. The synthesis of unaged-FS was conducted at a larger scale with consistent results.

The unaged-FS sample (from large scale co-precipitation synthesis, sample 1 in Table 12) was characterized by, solid digestion, carbon analysis, and QXRD analysis. The solid digestion data, phase analysis from QXRD studies, and carbon analysis data were all in agreement with each other.

QXRD results showed that the sample was not a pure Friedel’s salt. It was composed of two hydrocalumite phases, a chloro-hydrocalumite phase (74%) from the hexagonal crystal system and a chloro-carboaluminate phase (24%) from the monoclinic crystal system.

For a hydrocalumite material, a Ca/Al molar ratio of 2.0 is expected based on the chemical formula of $[Ca_4Al_2(OH)_{12}]\cdot[X_2\cdot mH_2O]$. Based on the experimental chemical formula obtained for unaged-FS the Ca/Al molar ratio was 1.86. With the exclusion of minor $Al(OH)_3$ phase, the Ca/Al molar becomes identical to the hydrocalumite family (2.0). The digestion of unaged-FS sample confirmed the Ca/Al molar ratio of 1.86 obtained from an experimental chemical formula.

In fact, the minor phase impurities (mainly aluminum hydroxide) causes the Ca/Al molar ratio of hydrocalumite materials (unaged-FS material in this case) to differ slightly from the ideal value. In a study by Dai, FS material with a chemical formula of $[Ca_{3.6}Al_2(OH)_{11.2}]\cdot[Cl_{1.9}(CO_3)_{0.05}\cdot 3.8H_2O]$ and Ca/Al molar ratio of 1.8 was synthesized [33]. As QXRD data was not provided in Dai's study, it is unclear if the prepared FS was free from any minor impurity or if the Ca/Al molar ratio in hydrocalumite phase deviated from ideal values of hydrocalumite family.

Chapter 5: Aging process; preparation of aged-FS and quantification of mass loss prevention by the aging process

As mentioned in Chapter 4, the sintering-precipitation method reported by Wu was discarded due to the technical difficulty in the repeatability of experiments [25]. It was difficult to synthesize large portions of $FS._{sint}$. needed for this work. Additionally, some preliminary adsorption tests performed using $FS._{sint}$. showed that the material was partially dissolving. In the early stages of this study, an adsorption experiment was conducted based on an adsorption test reported in Wu's paper [25]. A sample of 0.1 g of $FS._{sint}$. was placed into 50 mL of 730 ppm Se solution at initial pH 8.0 at 30 °C and was shaken for 24 h. After solid-liquid separation, the solid was recovered, dried and weighed. The final FS mass (by SBM) was lower than the initial mass; a FS mass loss of 18.5% was indicated. The experiment was repeated and a 19.2% mass loss was noted (average SBM: ~19.0%). This amount of mass loss was not viewed as acceptable for an application of this material for selenium adsorption process. Selenium adsorption was 23.5% (21.6-25.3%) by the $Se_{.L}$ method. Although Wu reports some 'minor dissolution' of FS, Wu apparently did not consider this dissolution to be a significant concern. However, from an engineering perspective, the dissolution was a barrier to further adsorption experiments in this thesis (see 2.6.1). The partial dissolution of Ca and Al, at low and high pH ends, was mentioned by Wu with respect to buffering effects [25]. The buffering capacity of FS is discussed in 5.3.1.

The preliminary adsorption test performed with unaged-FS also showed significant mass loss (~18.0% SBM, at initial pH 10, L/S 250, 156 ppm Se, for 24 h, and at 25 °C). In general, the dissolution of FS ($FS._{sint}$. or unaged-FS) was an impediment to the continuation of adsorption experiments. Due to the dissolution problem in the early stages of the work, the direction of the thesis was changed. First, the synthesis process was switched from sintering-precipitation (Wu's

method) to the co-precipitation at constant pH. The latter technique was a simpler process in making larger amounts of FS material. It needs to be emphasized that the sintering-precipitation method was replaced by co-precipitation, not due to partial dissolution of $FS._{sint}$., but because the repetition of the method was technically too challenging. The co-precipitation process is the most common method for the preparation of LDH materials. Secondly, attention was turned towards reducing the dissolution of unaged-FS as more adsorption experiments with substantially soluble material were untenable.

As mentioned in 2.4, literature studies showed that the aging process affects the physiochemical properties of LDH materials including particle size distribution, particle size growth, dispersion of agglomerates, and nanostructure evolution [70,72,73,82,83]. However, the quantitative effects of these aging processes on minimization of LDH dissolution have not been reported. At this point in the project, a new series of aging experiments were designed. The material used for aging studies was the unaged-FS material prepared by co-precipitation at constant pH under partial nitrogen purging conditions (see Table 8). The aging process was carried out after the original unaged-FS was prepared by co-precipitation, filtered, washed and dried. The sodium chloride impurities were washed out from the wet FS (see Figure 13). The purpose of the aging process was to minimize the unaged-FS dissolution in adsorption experiments. More importantly, the aging efficiency on the prevention of mass loss could be quantified. Since the aging tests were applied on one homogenized initial material (unaged-FS), several aging conditions could be compared knowing that one uniform starting sample was used for all tests. It is believed that, in the aging-related literature, the efficiency of an aging process (separate from the synthesis step) for controlling the partial dissolution of LDH material in an adsorption test is not quantified or studied in detail. This poses a lack of important information about the hydrolytic stability of these

materials. In many LDH studies, the mass loss that can be expected during adsorption tests is unclear [25]. In mining industries, it is crucial to have a reliable platform for FS mass-loss expectations in a typical wastewater treatment using FS material [44,80].

Among different aging variables, the effect of initial pH, L/S, time, and temperature were studied. In summary, unaged-FS material was aged by adding to aqueous NaOH solutions (initial pH set at 8.0 or 12.0) under specific L/S ratios for specific periods of time and at a specific temperature (see Figure 11). DI water used for all aging tests was decarbonated by purging nitrogen gas for 10-15 minutes. All aging tests were performed in sealed bottles without further nitrogen gas purging. The amount of CO_2 in the gas phase was calculated as being negligible and therefore not a major concern with respect to carbonation. In general, most of the aging experiments were carried out once with two or three replicate ICP analyses (see 3.2.4.7).

The tracking of crystallinity of material over aging was not pursued since QXRD studies showed that the unaged-FS sample itself was a crystalline material (see 4.3.3). The purpose of aging in this thesis was to figure out if unaged-FS dissolution could be lowered by any purification of material (removal of minor impurity) or any other physical/chemical changes such as particle growth or any phase transformation. The FS mass loss as a result of aging tests was reported for all aging tests using $Ca._{LB}$ and $Al._{LB}$.

The selection of aging variables such as time, temperature, and L/S was made based on finding a low mass-loss aging condition. The initial pH effect was also studied by tracking the dissolution of Ca and Al. It was mentioned in 4.3.3.1, that aluminum hydroxide was the minor impurity in unaged-FS material. Ca/Al molar ratio of unaged-FS material was deviated from the ideal value of 2.0, due to 2 wt.% aluminum hydroxide impurity. Therefore, special attention was

given to an aging condition resulting in more Al dissolution in solution alongside forming an aged solid with Ca/Al ratio of 2.0. Later, further analytical studies including QXRD were performed on aged material.

5.1 Mass loss calculations in aging tests

It was mentioned earlier in 3.2.4.7.2 that mainly LBM is used for FS mass loss calculations for the experiments in this thesis. As shown in Equation 3, a chemical formula and molar mass of FS involved in any specific experiment were required. In the case of aging tests, this FS material was an unaged-FS sample. Various characterization methods showed that the unaged-FS sample with an experimental chemical formula of $[Ca_{3.88}Al_{2.09}(OH)_{12.1}]\cdot[Cl_{1.73}(CO_3)_{0.10}\cdot 5.27H_2O]$ was not a pure, single FS (see 4.3.3.1), but rather mainly a mixture of two FS phases. The average molar mass of the two main FS phases could be used. On the other hand, the analytical studies showed that the unaged-FS composition was close to the composition of pure FS; 74 wt.% pure chloro-hydrocalumite (see 4.3.3.1) and its calculated average molar mass is only slightly higher than that of pure FS (579.76 g/mole vs 561.34 g/mole, respectively). Therefore to estimate the mass loss during aging tests the material was assumed to be mainly pure FS with a molar mass of 561.34 g/mole. It was also assumed in this calculation that chloro-hydrocalumite and chloro-carboaluminate hydrocalumite phases dissolve to the same extent. Later in section 5.5, it will be shown that the degree of dissolution for the two phases are different. For simplicity, however, both phases are assumed to have equal dissolution in initial mass loss calculations of aging (and adsorption) tests.

5.2 Selection of aging variables (time, temperature, L/S) based on low mass loss

In some preliminary aging experiments designed before pH studies, unaged-FS was added to water under specific L/S ratios for specific periods of time and at specific temperatures. An aging test

was performed once for each set of variables. Three solutions for ICP analysis were prepared from each final aging solution. Only the average ICP result is reported (see 3.2.4.7). The FS mass losses (wt.%) using $Ca._{LB}$ and $Al._{LB}$ for all variables is summarized in Table 15. The best aging variables were selected based on low mass-loss condition. In this way, the material loss during the subsequent pH-effect studies was minimized.

Table 15 FS dissolution under aging variables. The selected values are in bold for clarity.

Aging variable	**Aging conditions held constant**	**Test values for aging variable**			**Selected variable**	**Ca/Al molar ratio of aged solid**
	Mass loss method (LBM)	$Ca._{LB}$, $Al._{LB}$				
Time	L/S 50, initial pH 8.0, and 65 °C	2 days	4 days	**7 days**	7 days	1.85
	Mass loss $Ca._{LB}$, $Al._{LB}$	8.96%, 4.05%	8.73%, 3.20%	8.62%, 2.62%		
Temperature	L/S 20, initial pH 8.0, and 7 days	30 °C	**65 °C**	85 °C	65 °C*	1.88
	Mass loss $Ca._{LB}$, $Al._{LB}$	2.80%, 2.13%	3.10%, 2.14%	6.54%, 2.14%		
L/S (mL/g)	Initial pH 8.0, 65 °C, and 7 days	**20**	50	200	20	1.84
	Mass loss $Ca._{LB}$, $Al._{LB}$	3.1%, 2.4%	7.2%, 4.8%	26%, 23%		

*more preliminary tests were performed at 65 °C

The aging time data presented in Table 15, showed that there was a very little variation in FS dissolution using $Ca._{LB}$ over the range tested. The average of calcium dissolution in this period of time was 8.77% (8.62-8.96%). Aluminum dissolution from material over 7 days of aging was almost similar, however, a slight decrease was observed as aging time was extended from 4 to 7 days (3.20% vs 2.62%). The average of aluminum dissolution in 7 day-aging periods was 3.29% (2.62-4.05%), where Ca always dissolved more than Al. At initial pH 8.0, calcium always dissolved more than Al. Therefore, seven days of aging was selected because of lower Al dissolution than that measured at other times (2.62%). There was also a desire to minimize the

experimental time frame for the project, therefore, time periods longer than 7 days were not studied.

The Ca and Al dissolution over the temperature change from 30 to 65 °C was almost constant. As the temperature of the aging process increased from 65 to 85 °C, the average Ca dissolution increased from 3.10% to 6.54%. The temperature of 85 °C was avoided because of higher material dissolution at this temperature. The temperature of 65 °C was selected as this was the baseline value used in the time and L/S series experiments. The temperature 65 °C was selected as a baseline since in a report by Rousselot in 2002, a better crystallinity was expected at this temperature for Ca-Al-LDH [46]. In general, the interaction of different variables was beyond the scope of this work.

In contrast to the time and temperature variables, FS dissolution was highly L/S-dependant. As seen in Table 15, FS dissolution (using $Ca._{LB}$) sharply increased from 3.1% at L/S 20 to 26% at L/S 200. Aging at L/S 20 was selected for initial pH studies because of lower mass loss than other L/S conditions.

In summary, the aging of unaged-FS for 7 days, the temperature of 65 °C and L/S 20 ensured a low mass-loss outcome for the aging process.

In conclusion, the dissolution of Ca^{2+} ions was always higher than Al^{3+} ions, resulting in solids with Ca/Al molar ratios lower than the original material (1.88 for unaged-FS). This is related to the initial pH value of these experiments (pH 8.0) and is discussed in the next section. The aged solid samples obtained from aging variables in Table 15 were digested with nitric acid. The Ca/Al molar ratio of aged solids at selected aging variables of time (7 days), temperature (65 °C) and L/S (20) were 1.85, 1.88, and 1.84, respectively (see Table 15). For more reproducibility of L/S data in aging tests see Appendix E.

5.3 The initial pH effect in aging tests

The pH of the aqueous NaOH solutions used in these aging tests was adjusted to 8.0 and 12.0. The initial pH studies of aging tests were performed at selected aging variables of L/S 20, 65 °C, and 7 days, under which mass loss was controlled at minimum values. The dissolution of Ca and Al ions by pH variation was tracked.

Four and six individual aging tests were performed at an initial pH of 8.0 and 12.0, respectively. The FS dissolution data using $Ca._{LB}$ and $Al._{LB}$, Ca and Al contents in solution, final pH values, and Ca/Al molar ratio of aged solids from initial pH studies are shown in Table 16. As shown, different amounts of Ca and Al were dissolved at an initial pH of 8.0 and 12.0. At initial pH of 8.0, an average of 3.05% (2.37-3.32%) and 2.35% (1.25-2.97%) FS was dissolved using $Ca._{LB}$ and $Al._{LB}$, respectively. On the other hand, once the initial pH of the aging slurry was increased to 12.0, significantly lower Ca in solution observed. Due to the higher initial pH, the average extent of Ca dissolved decreased from 3.05% to 0.173% ($Ca._{LB}$).

Table 16 FS dissolution percentage $Ca._{LB}$ and $Al._{LB}$, relative metal ion contents, Ca/Al molar ratio of aged solid and final pH in initial pH studies of aging tests (aging conditions: L/S 20, 65 °C, and 7 days).

	Mass loss (%)			**Mass loss (%)**		
Test number	**$Ca._{LB}$%**	**$Al._{LB}$%**		**$Ca._{LB}$%**	**$Al._{LB}$%**	
Unaged-FS Ca/Al molar ratio 1.88 (from solid digestion)	Initial pH 8.0		Final pH	Initial pH 12.0		Final pH
1	3.28	1.25	10.6	0.199	3.54	11.1
2	3.25	2.42	10.9	0.170	5.50	11.2
3	3.32	2.76	11.3	0.171	5.20	11.9
4	2.37	2.97	11.2	0.163	3.54	11.9
5	-	-	-	0.170	5.50	12.0
6	-	-	-	0.171	5.20	11.8
Average	**3.05**	**2.35**	11.0	**0.173**	**4.75**	11.6
Ca/Al molar ratio in aged solid (from solid digestion)	1.84 (1.82-1.87)			2.02 (1.95, 2.03, 2.03 and 2.08)		

In comparison, due to the higher initial pH of 12.0, the average Al dissolution rose from 2.35% to 4.75% ($Al._{LB}$). This opposite tendencies of Ca and Al dissolution caused the average aluminum content in solution to be 13.1 times higher than the average Ca content.

Based on the aluminum speciation diagram, the dissolution of Al^{3+} is highly pH-dependant [84]. The higher Al dissolution at initial pH 12.0, was related to the dissolution of aluminum hydroxide impurity in the form of aluminate. At high pH values (9.0-12.0), aluminum hydroxide redissolves via formation of soluble aluminum species such as aluminates ($Al(OH)_4^-$) [27]. Aging at an initial pH 12.0 removed the aluminum hydroxide minor impurity.

The minor aluminum hydroxide impurity was shown to be the reason for the deviation of Ca/Al molar ratio of unaged-FS from 2.0 (section 4.3.3.1). If aluminum hydroxide impurity was dissolved over aging at initial pH 12.0, then a change in Ca/Al molar ratio of aged solid from 1.88 to 2.0 was expected. Three solids aged at initial pH 12.0 were digested and analyzed by ICP-OES. An average Ca/Al molar ratio of 2.02 (1.95-2.08) was indicated for the sample. The solid analysis result was also indicative of aluminum hydroxide removal.

5.3.1 Final pH and the buffering effect

The final pH values for the pH study of aging tests are shown in Table 16. In addition, Ca and Al metal ions content in the aging solution for each initial pH is shown. In this section, the correlation of final pH change to the metal ions content in solution is discussed. As discussed previously in QXRD studies (see Table 12) the unaged-FS is composed of hydrocalumite phases (chloro- and chloro-carboaluminate phases) and aluminum hydroxide. Here, it is assumed that the Ca dissolved in the solution is coming from hydrocalumite phases while Al dissolved in the solution is from aluminum hydroxide and hydrocalumite phases. Note that both Ca and Al ions dissolve at initial pH of 8.0 and 12.0, however, the extension of dissolution is different for these metal ions.

At an initial pH of 8.0, Ca content of the solution was 4.1 times the Al content, and the final pH of the solution jumped to 10.6-11.3. At an initial pH of 12.0, the Al content in the solution was 13.1 times the Ca content, and the final pH of the filtrate was measured to be 11.1-12.0. From the final pH values and the Ca and Al contents in the solution, the following possible explanation can be provided: At initial pH 8.0, according to Reaction 5, a portion of the Ca-framework of FS ($[OH\text{-}Ca\text{-}OH]._{FS}$) dissolved preferably, resulting in a final pH jump to around 11.0 (10.6-11.3).

$$[OH\text{-}Ca\text{-}OH]._{FS} = Ca^{2+} + 2OH^{-} \quad \text{Reaction 5}$$

At an initial pH of 12.0, the Al content in the solution was 13.1 times higher than the Ca content and Ca dissolution compared to initial pH 8 was reduced significantly. Compared to initial pH 8.0, Al dissolution increased presumably due to the formation of highly soluble aluminate species (Reactions 6 and 7). Tetra-hydroxy aluminate with a chemical formula of $Al(OH)_4^-$ is the dominant aluminum species at high pH [84]. Aluminate formation consumed hydroxide anions and reduced the final pH to the average value of 11.6 (11.1-12.0).

$$Al(OH)_3 \text{ (or } [OH\text{-}Al\text{-}OH]._{FS}) = Al^{3+}_{(aq)} + 3OH^{-} \quad \text{Reaction 6}$$

$$Al^{3+}_{(aq)} + 4OH^{-}_{(aq)} = [Al(OH)_4]^{-}_{(aq)} \quad \text{Reaction 7}$$

In summary, Ca or Al dissolved depending on the initial pH of the solution. This way the final pH of the solution was maintained in a medium point (11.0-11.6) for both low and high initial pH solutions. This suggests the possibility of buffering. Aqueous Ca^{+2} and Al^{+3} in contact with solid FS might be buffering the solution pH. Wu reported a similar buffering capacity for his $FS._{sint}$. and selenate-loaded Wu's $FS._{sint}$. during selenate adsorption tests and chemical stability tests, respectively [25]. For selenate adsorption tests, the final pH of the solution at an initial pH of 4.0, 7.0, and 10.0 jumped to 10.25-12.0. For chemical stability tests, selenate-loaded Wu's $FS._{sint}$. (0.28

mmol Se/g) was added to water (L/S 20) at an initial pH of 4.00, 7.00, 10.00 and 13.0 [25]. Wu reported that the final pH of the solution for the initial pH 4.00, 7.00, and 10.00 was 10.70±0.3. The final pH of the solution was 11.60±0.3 when the initial pH was 13.00. The final pH was maintained in the 10.70-11.60 region for Wu's $FS._{sint}$. material. The buffering capacity of FS synthesized in this study during aging was similar to the buffering capacity of Wu's $FS._{sint}$. in selenate adsorption studies of Wu.

To better understand the possible changes on the unaged-FS material over the selected aging process, further characterization of aged-FS properties was performed.

5.4 Characterization of aged-FS

For characterization studies, particularly QXRD, more aged material was needed. A larger batch was prepared. The whole quantity of as-prepared unaged-FS (~150 g) was aged under the best aging condition (initial pH 12.0, L/S 20, 65 °C and 7 days). The aged-FS was collected and stored in a desiccator. Three homogenous samples were analyzed by digestion and ICP-OES to determine the Ca/Al molar ratio. An average value of 2.02 (2.01-2.05) was obtained.

5.4.1 QXRD analysis of aged-FS; phase transformation during the aging process

Table 17 shows the phase analysis of aged-FS by the QXRD analysis. The phase composition of unaged-FS is also shown for comparison. As seen from the QXRD results, aged-FS was composed of 28 wt.% chloro-hydrocalumite in a hexagonal crystal system, 70 wt.% chloro-carboaluminate hydrocalumite in a monoclinic crystal system, and 2 wt.% a calcium aluminum hydroxide minor phase called katoite.

The selected aging process was associated with the following chemical transformations and phase transformation of unaged-FS. First of all, as expected from previous discussions in 5.2, the minor $Al(OH)_3$ impurity (2 wt.%) was dissolved through aging. However, a new minor phase

katoite with a chemical formula of $Ca_3Al_2(OH)_{12}$ was formed (2 wt.%). Apparently, along with the $Al(OH)_3$ dissolution, the hydrocalumite phase partly dissolved, as calcium was detected in solution. The dissolved Ca^{2+} and Al^{3+} ions all were re-precipitated in the form of a katoite phase as shown by Reaction 8. Katoite is the most stable calcium aluminate hydroxide phase [85]. The aging process dissolved the unstable aluminum hydroxide phase in favor of a more stable phase.

$$3Ca(OH)_{2(aq)} + 2Al(OH)_{3(aq)} = Ca_3Al_2(OH)_{12} \quad \text{Reaction 8}$$

Secondly, during the aging process, much of the chloro-hydrocalumite in the hexagonal crystal system ($R\bar{3}$) was transformed into the chloro-carboaluminate hydrocalumite phase in the monoclinic crystal system (*P*2/*c*). Previously the QXRD analysis of unaged-FS showed that the hydrocalumite phase was composed of 74 wt.% chloro-hydrocalumite in the hexagonal crystal system ($R\bar{3}$) and 24 wt.% chloro-carboaluminate hydrocalumite in the monoclinic crystal system (*P*2/*c*, see Table 12). The phase transformation during aging alongside with other phase transformations of Friedel's salt and carbonated Friedel's salt samples in the literature are summarized in Table 34, Appendix G.

Table 17 QXRD results of unaged-FS and aged-FS samples

Phase name	**Software single crystal Formula**	**Unaged- FS**	**Aged-FS**
Hydrocalumite, Hexagonal crystal system, $R\bar{3}$ space group, PDF#: 04-010-4677	$[Ca_4Al_2(OH)_{12}]\cdot[Cl_2\cdot 4H_2O]$	74	28
Hydrocalumite, Monoclinic crystal system, *P*2/*c* space group, PDF#: 04-014-9938	$[Ca_4Al_2(OH)_{12}]\cdot[Cl(CO_3)_{0.5}\cdot 10.8H_2O]$	24	70
Katoite	$Ca_3Al_2(OH)_{12}$	-	2
Bayerite	$Al(OH)_3$	2	-
Calcite	$CaCO_3$	trace	-

By aging, the dominant hydrocalumite phase became the chloro-carboaluminate hydrocalumite phase ($[Ca_4Al_2(OH)_{12}]\cdot[Cl(CO_3)_{0.5}\cdot 10.8H_2O]$) in the monoclinic crystal system (*P2/c*, 70 wt.%). Aging was performed without any nitrogen purging, and $CO_{2(g)}$ dissolved from the air in the aging slurry was adsorbed into the aged-FS composition in the form of carbonate. In addition, the increase in the proportion of chloro-carboaluminate phase shows that carbonate was intercalated in the interlayer space rather than surface physical adsorption.

Feng et al. in 2016 showed that the formation of carbonated hydrocalumite in monosulfate phase ($[Ca_4Al_2(OH)_{12}]\cdot[X_2\cdot mH_2O]$, $X=SO_4^{2-}$) depends on the amount of carbonate present in the synthesis solution [65]. In the absence of carbonate, the monosulfate phase was the only phase present. The carbonate content in the solution was increased up to 0.018 mol $CaCO_3$/kg water at pH 12.5-14.0. With the increase in the carbonate content, a phase transformation from monosulfate phase to hemi-carboaluminate (half-carbonated) and mono-carbonate (fully-carbonated) hydrocalumite phases was observed. At carbonate concentration range 0.006-0.01 mol $CaCO_3$/kg water, the proportion of both hemi-carboaluminate and mono-carbonate phases increased. At sufficiently high carbonate dosage (0.018 mol $CaCO_3$/kg water), the mono-carbonate was a major phase and monosulfate was a minor phase.

The results of Feng are consistent with the formation of more of chloro-carboaluminate hydrocalumite phase during aging [65]. The carbonate level in the solutions used for aging was not significant enough to form a fully carbonated Friedel's salt. However, it was high enough to increase the proportion of hemi-carboaluminate phase ($[Ca_4Al_2(OH)_{12}]\cdot[Cl(CO_3)_{0.5}\cdot 10.8H_2O]$). Feng showed the carbonated hydrocalumite is a more stable phase than the carbonate-free hydrocalumite, in the presence of carbonate.

5.4.1.1 The experimental chemical formula of aged-FS

The experimental formula of the aged-FS sample was calculated using the molar masses of above-mentioned phases. As shown in Table 18, the phase analysis data from the QXRD studies were used to calculate the elemental content of the aged-FS sample. With the inclusion of $Ca_3Al_2(OH)_{12}$ the experimental formula of aged-FS is $[Ca_{4.02}Al_{2.03}(OH)_{12.1}]\cdot[Cl_{1.30}(CO_3)_{0.33}\cdot 8.40H_2O]$. The aged-FS material is a carbonated hydrocalumite with a Ca/Al molar ratio of 1.98. This ratio is very similar to the average experimental value obtained by the solid digestion of this sample (2.02). Moreover, Ca and Al weight percentages suggested by the chemical formula are 25.2 and 8.55 %, respectively. These values are in fair agreement with the solid digestion and analysis data for aged-FS samples (28.0 and 9.1 % for Ca and Al, respectively). With the exclusion of $Ca_3Al_2(OH)_{12}$ minor phase the experimental formula of aged-FS will be $[Ca_{3.88}Al_{1.93}(OH)_{11.6}]\cdot[Cl_{1.30}(CO_3)_{0.33}\cdot 8.40H_2O]$, with a Ca/Al molar ratio of 2.0 as expected for hydrocalumite family.

Table 18 Aged-FS experimental chemical formula calculations

			Moles per 100 g					
Phase formula	**Phase proportion (wt.%)**	**Molar mass (g/mole)**	**Ca**	**Al**	**OH**	**Cl**	**CO_3**	**H_2O**
$[Ca_4Al_2(OH)_{12}]\cdot[Cl_2\cdot 4H_2O]$	28 %	561.3	0.20	0.10	0.60	0.10		0.20
$[Ca_4Al_2(OH)_{12}]\cdot[Cl(CO_3)_{0.5}\cdot 10.8H_2O]$	70 %	678.4	0.41	0.21	1.24	0.10	0.05	1.11
$Ca_3Al_2(OH)_{12}$	2 %	378.3	0.02	0.01	0.06	-	-	-
		Total moles	0.63	0.32	1.90	0.20	0.05	1.31
Molar mass: 639.61 g/mole		Moles per one mole of FS	4.02	2.03	12.1	1.30	0.33	8.40

5.4.2 Carbonate adsorption through aging; carbon analysis

The carbonate content of aged-FS was measured by carbon analysis. The results of the carbonate content of aged-FS (and unaged-FS for comparison) are shown in Table 19. During the aging process, carbonate content increased from 1.15 to 3.00 wt.%. The carbonate content based on the chemical formula ($[Ca_{4.02}Al_{2.03}(OH)_{12.1}]\cdot[Cl_{1.30}(CO_3)_{0.33}\cdot 8.40H_2O]$) would be expected to be 3.10%. The analyzed carbonate content and that obtained from the chemical formula derived from QXRD analysis are reasonably close. A higher carbonate content in aged-FS shows that $CO_{2(g)}$ dissolved from the air in the aging slurry was adsorbed into the aged-FS composition in the form of carbonate. In this aging process, the decarbonated water (initial 20-minutes nitrogen purging) was used, however, no nitrogen gas was purged during 7-days of aging.

Table 19 Carbonate content increase over selected aging measured by carbon analysis (aging condition: initial pH 12.0, L/S 20, 65 °C and 7 days)

	Unaged-FS	**Aged-FS**
Carbonate (wt.%)	1.15	3.00

The aged-FS material similar to unaged-FS was contaminated with carbonate oxyanion. As shown with the QXRD results, the increase in intercalated carbonate content changed the interlayer composition of FS material. The carbonate content increased, and therefore the chloride anion content decreased.

5.4.3 Morphology change over aging; SEM results

Figure 16 shows the morphologies of the as-prepared FS particles before and after aging at initial pH 12.0, L/S 20, 65 °C for 7 days. The aged-FS SEM images are illustrated in pictures 1 and 2, and the unaged-FS SEM images are shown in pictures 3 and 4. The aged-FS crystallites appear as flat crystals with a well-defined geometry of hexagonal crystals with sharp edges. In comparison, the unaged-FS plates had no specific geometry and were mostly composed of stacked flat plates

with chipped and broken edges. The broken edges are expected because the metal-OH bonds in the hexagonal units of brucite layers do not continue at the crystal edges [24].

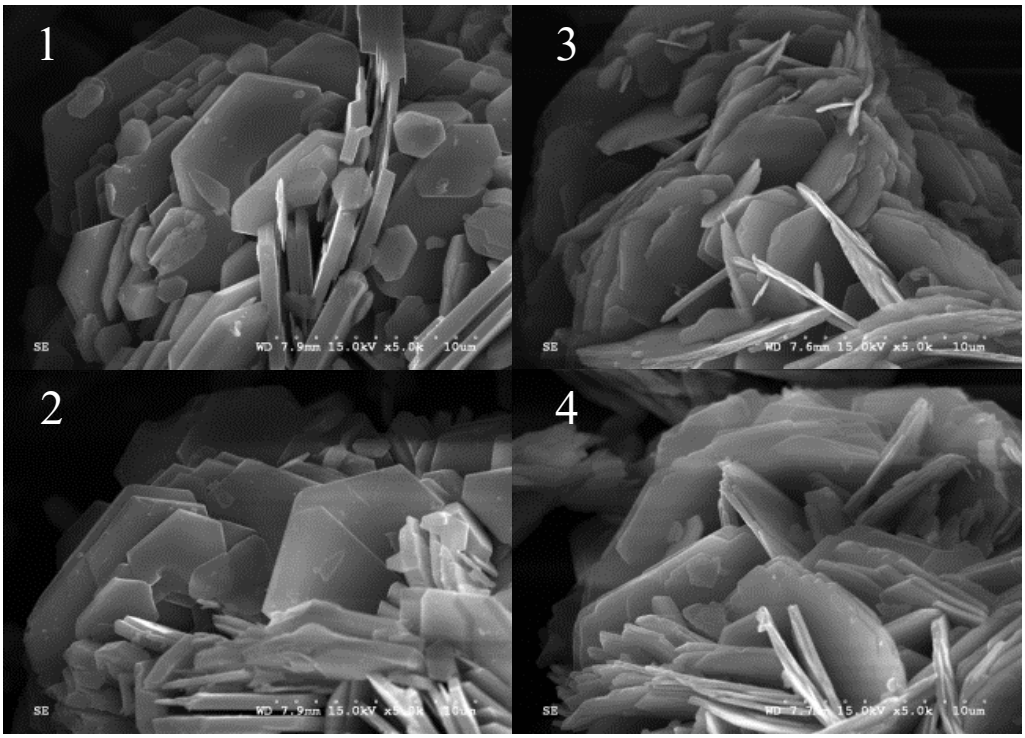

Figure 16 SEM images of aged-FS (1 and 2) and unaged-FS (3 and 4), 5.0 k magnification (aging condition: initial pH 12.0, L/S 20, 65 °C and 7 days).

As seen in the schematic representation of LDH materials in Figure 3, in a perfectly crystalline LDH, the brucite layers are composed of repetitive hexagonal units of [OH-Ca-OH].$_{FS}$ and [OH-Al-OH].$_{FS}$, called Ca- and Al-frameworks, respectively. The sharp hexagonal edges formed during aging is possibly indicative of dissolution and re-crystallization of hexagonal units on the edges of layers. The recrystallized aged-FS material is composed of Ca and Al ions in well-organized octahedral units on the edges. The dissolution of Ca and Al ions from those octahedral units is most likely less than dissolution from broken plates.

5.4.4 Particle growth over aging; PSD results

In general, an aging process involves a series of complex processes such as crystal growth, agglomeration, and breakage. Particle size growth during aging or hydrothermal treatment has been reported widely in the literature [27,71]. The time period of the aging process was shown to have an important influence on the particle size distribution. As discussed earlier in section 2.4, the effect of heating duration on Mg-Al-Cl LDH showed that the particle size increased from 69±15 nm to 159±29 nm as the treatment time increased from 2 h to 48 h (100 °C); an indication of particle growth during hydrothermal treatment [71].

A co-precipitation process results in a larger PSD than a rapid mixing/aging process [70]. In the co-precipitation procedure, not all of the precipitated particles experience the same nucleation or crystal growth times. The nuclei formed at the onset of precipitation grow larger than the ones formed at the end of the process. In comparison, in a rapid mixing or aging procedure, all particles experience almost the same crystal growth time and so the particle size distribution will be narrower. Therefore, it is difficult to control the particle size and distribution of LDHs using a traditional co-precipitation method [27].

In Table 20, the particle size distribution and volume-weighted mean (VWM) of unaged-FS and aged-FS are compared. The particle size distribution is shown with $d_{(0.1)}$, $d_{(0.5)}$, $d_{(0.8)}$, and $d_{(0.9)}$ values which are standard "percentile" readings from the PSD analysis. For example, $d_{(0.9)}$ is the size of the at which 90% of the sample is smaller and 10% is larger than this size. The VWM value is an arithmetic average of data, calculated by Malvern Mastersizer laser instrument using the weight of the sphere particles (Equation 7, where r: diameter, ρ: density) [86]. In these calculations, particles are assumed to be spherical and non-porous.

Weight of particles: $\frac{4}{3}\pi r^3 * \rho$ Equation 7

For VWM value, the analyzer cubes the diameters of particles (r_1 to r_n), sums the cubed diameters, divides by the number of particles (n), and finally takes a cube root (Equation 8). The resultant value is the volume-weighted mean diameter (VWM).

$$\text{Volume-weighted mean} = \frac{\sqrt[3]{(r1^3+r2^3+r3^3+\cdots+rn^{3)}}}{\text{n}} \qquad \text{Equation 8}$$

The unaged-FS was prepared over a 72-h co-precipitation time as explained in section 4.1. The aged-FS was prepared by the aging of unaged-FS at initial pH 12.0, L/S 20, 65 °C for 7 days. Each data point shown in Table 20 is the average of three repeated analyses. The range of analytical values is shown in brackets next to this average value.

Table 20 The particle size distribution, volume weighted mean and specific surface area of unaged-FS and aged-FS (selected aging: initial pH 12.0, L/S 20, 65 °C and 7 days).

	Unaged-FS	**Aged-FS**
$d_{(0.1)}$ (μm)	4.70 (4.10-5.80)	6.11 (5.00-6.68)
$d_{(0.5)}$ (μm)	18.2 (15.4-19.9)	23.1 (21.8-23.9)
$d_{(0.8)}$ (μm)	36.0 (35.0-37.4)	48.2 (46.3-51.1)
$d_{(0.9)}$ (μm)	50.7 (47.5-53.9)	78.7 (73.2-82.7)
Volume-weighted mean (μm)	29.5 (27.6-31.3)	42.5 (40.5-45.2)
Specific surface area (m^2/g)	0.535 (0.466-0.604)	0.338 (0.208-0.407)

As shown in Table 20, the particle size distribution for the aged-FS sample is larger than the unaged-FS sample. The unaged-FS particles were distributed in the range of 4.70-50.7 μm. After aging, the particle size distribution was increased to 6.11-78.7 μm. For example, as a result of aging, the $d_{(0.5)}$ was increased from 18.2 to 23.1 μm. The $d_{(0.8)}$ was increased from 36.0 to 48.2 μm. Similarly, the $d_{(0.9)}$ value was increased from 50.7 to 78.7 μm. The VWM value was increased from an average of 29.5 μm to 42.5 μm. The aged-FS particles mean diameters were larger than that of unaged-FS particles, indicative of agglomeration during the aging process. The specific

surface area (SSA) of FS material as reported by Malvern Mastersizer was reduced from 0.535 m^2/g to 0.338 m^2/g, as a result of aging. As a result of agglomeration, particles stick to one another and result in a material with smaller calculated surface area. If the SSA is used, it is important that the density of the material is defined. Malvern Mastersizer assumed a density of 1 for these calculations.

The reversibility of agglomeration by application of ultrasound is shown with details in Appendix F, Table 33. The results showed that the coarse agglomerates formed through the aging process were broken by the application of ultrasound.

5.5 Solubility of aged-FS (dissolution comparison to unaged-FS)

Next, the effectiveness of the selected aging process on controlling the dissolution of the aged material was investigated. The purpose of the dissolution experiment was to determine if aged-FS was a less soluble material than unaged-FS. After all, the ultimate purpose of the aging process was minimizing the FS dissolution in a real selenate adsorption test. Any positive impact of this compositional change on lowering the dissolution of FS material during selenate adsorption tests could be a step forward towards lowering metal ions release from LDH materials into solution. Figure 17, shows a general schematic of synthesis, aging, dissolution and adsorption tests in the thesis.

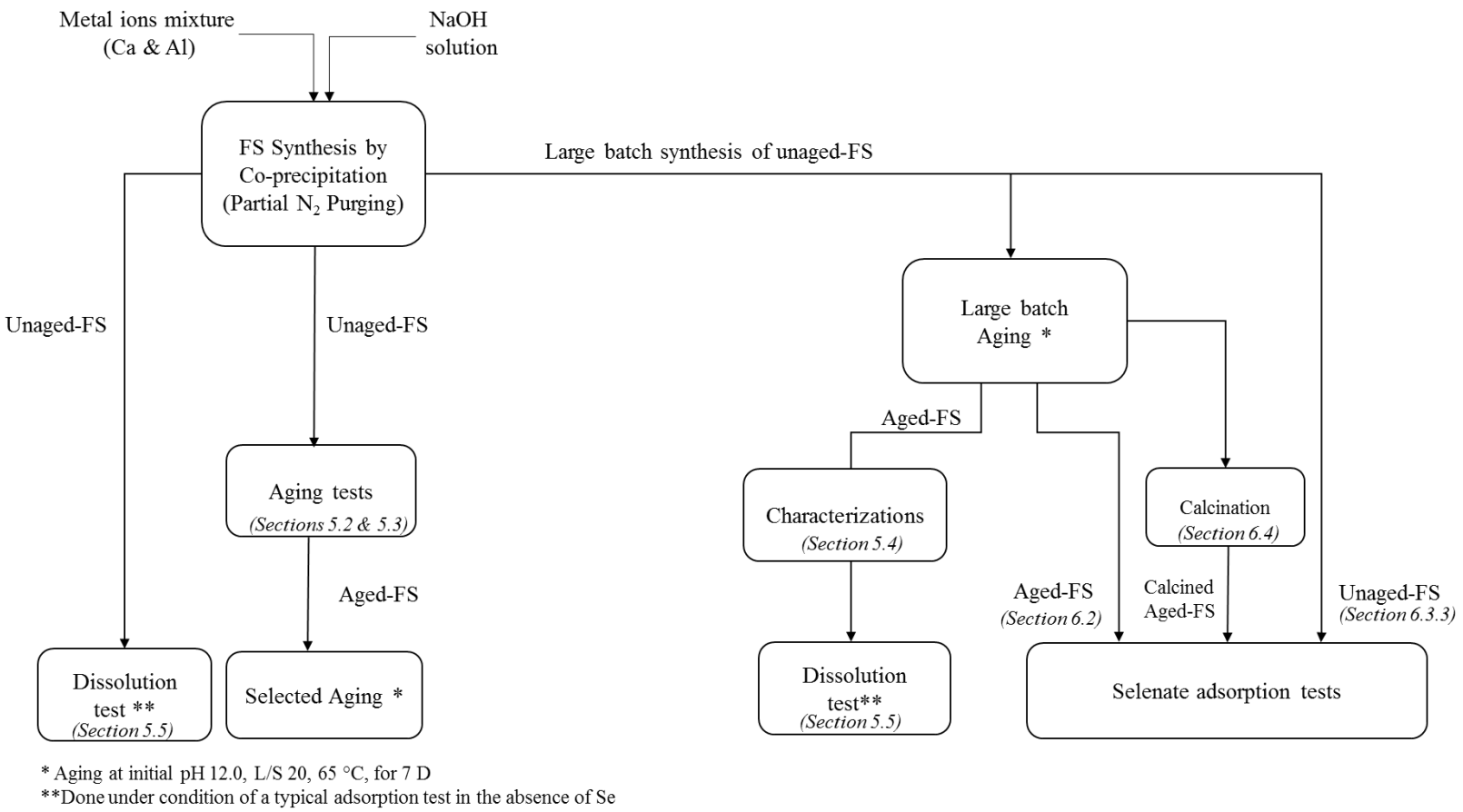

Figure 17 General flowsheet for aged-FS preparation and testing.

5.5.1 Aged-FS dissolution under conditions of a typical adsorption test using Se-free solution

As seen from the analytical results (5.4.1 to 5.4.4) aging caused a series of changes in the FS material. Next, the effect of aging on the dissolution of the material was investigated. The dissolution of aged-FS was examined by its exposure to a typical adsorption experiment. The unaged-FS sample was used for comparison. For mass loss calculations of aged-FS in dissolution tests, the molar mass value of 639.61 g/mole for aged-FS with chemical formula of $[Ca_{4.02}Al_{2.03}(OH)_{12.1}]\cdot[Cl_{1.30}(CO_3)_{0.33}\cdot 8.40H_2O]$ was used in Equation 3 (see 3.2.4.7.2). Similarly, for mass loss calculations of unaged-FS in dissolution tests, the molar mass of 579.76 g/mole for unaged-FS with chemical formula of $[Ca_{3.88}Al_{2.09}(OH)_{12.1}]\cdot[Cl_{1.73}(CO_3)_{0.10}\cdot 5.27H_2O]$ was used in Equation 3 (see 3.2.4.7.2).

The experimental conditions for the dissolution test were similar to a typical adsorption test, simply because the final goal was the minimization of dissolution in a real adsorption test. In the dissolution test, low initial pH was avoided as LDHs are unstable in the low-pH region. L/S 200 was selected to parallel industry applications, as treatment would usually be applied to large volumes of water with low concentrations of the adsorbate. A 50 mL sample of DI water with pH adjusted to 12.5 was added to 0.25 g FS sample, stirred at 150 RPM and 30 °C for 24 h. The slurries in dissolution tests were shaken at 150 RPM to simulate real adsorption tests. Three dissolution tests were carried out on both unaged-FS and aged-FS. The solution after filtration was analyzed for Ca and Al concentrations for mass loss calculations.

Figure 18 shows the solution results after contact with aged-FS and unaged-FS. The FS dissolution percentage using $Al._{LB}$ and $Ca._{LB}$ for the experiments is shown with filled triangle and empty triangles, respectively (see Equations 2 and 3). The error bars for dissolution data in Figure 18 represent the uncertainty or error in ICP analysis (±5%).

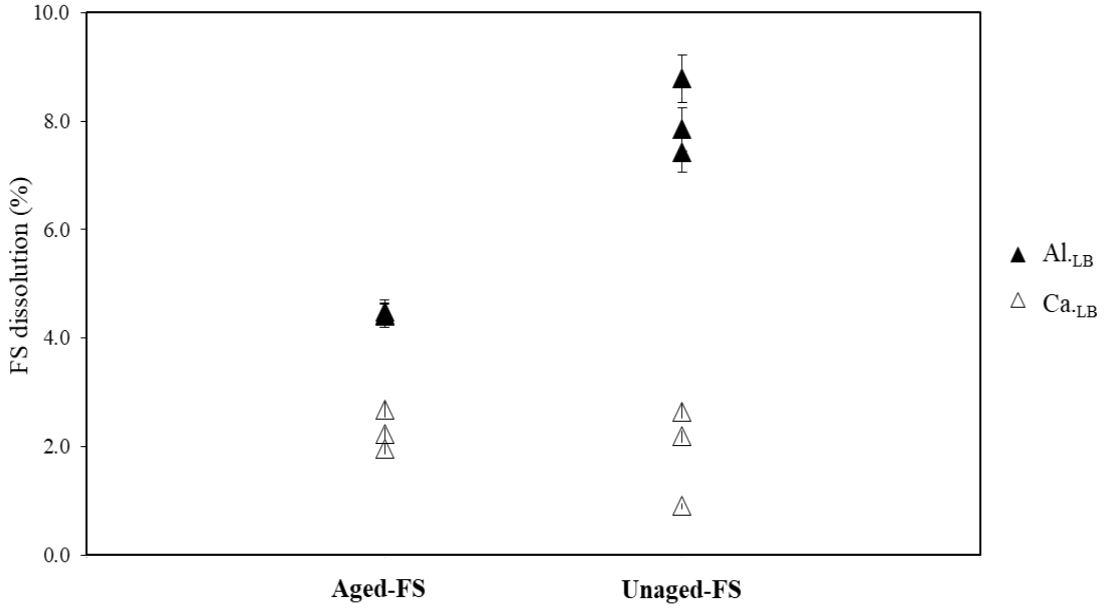

Figure 18 FS dissolution for aged and unaged material reported as $Al._{LB}$ and $Ca._{LB}$. (experimental condition: initial pH 12.5, L/S 200, 30 °C, 150 RPM, and 24 h; Se-free solution).

The following finding can be concluded from the comparison of the aged-FS and unaged-FS samples. As seen in Figure 18, the selected aging condition reduced the amount of Al^{3+} ions released into the solution. The average $Al._{LB}$ dissolution for aged-FS at 4.44% (4.41-4.48%) was lower than that of unaged-FS at 8.02% (7.42-8.79%) by a factor of not quite 2 (44.6% reduction). The average Al^{3+} ions concentration dissolved from aged-FS was 19.1 ppm (19.0-19.3 ppm), lower than that of unaged-FS, 39.3 ppm (36.4-42.9 ppm). $Ca._{LB}$ was perhaps slightly higher for aged-FS than for unaged-FS, or about the same. The average $Ca._{LB}$ dissolution for aged-FS at 2.29% (1.95-2.67%) was similar to that of unaged-FS at 1.91% (0.90-2.65%). The average Ca concentration dissolved from aged-FS 29.0 ppm (24.7-33.9 ppm) was similar to the amount dissolved from unaged-FS 25.8 ppm (12.1 ppm-35.7 ppm). In general, reduction in the dissolution of even one of metal ions is an achievement, both from environmental aspects and material mass loss view.

As mentioned before, low initial pH was avoided for the dissolution test, as LDHs are unstable in the low-pH region. However, the results of some dissolution tests at a lower initial pH showed interesting results. A few similar experiments were performed using aged-FS and unaged-FS at initial pH 8.0 (L/S 200, 30 °C, 150 RPM, and 24 h; Se-free solution). For this test, the average $Ca._{LB}$ dissolution from the aged-FS sample 14.9% (13.9-15.5%) was lower than that of the unaged-FS sample, 29.3% (27.2-31.8%). The average $Ca._{LB}$ dissolution from the FS material was reduced by a factor of ~50%, as a result of aging. The average $Al._{LB}$ dissolution from the aged-FS sample 16.2% (16.0-16.4%), was also lower than that of the unaged-FS sample, 21.1% (17.1-24.2%). The average $Al._{LB}$ dissolution from the FS material was reduced by a factor of 23.0%, as a result of aging.

In summary, from the results of dissolution tests at initial pH 12.5 and 8.0, followings can be concluded; aged-FS was a more stable material than unaged-FS. Compared to unaged-FS, a lower amount of metal ions were dissolved from aged-FS material into solution. Upon using a high pH range (initial pH 12.5), aged-FS showed lower $Al._{LB}$ dissolution (by a factor of ~45%) than unaged-FS. $Ca._{LB}$ dissolution for two materials was about the same. However, using a lower pH range (initial pH 8.0), lower Ca and Al dissolution was observed for aged-FS (compared to unaged-FS). $Ca._{LB}$ dissolution was lowered by a factor of ~50% and $Al._{LB}$ dissolution was lowered by a factor of 23%. This shows that aged-FS material is a better candidate than unaged-FS for adsorption tests, as lower material loss and lower dissolution of metal ions is expected.

The higher Al^{3+} ions dissolution from unaged-FS compared to aged-FS (at initial pH 12.5), was mainly related to the dissolution of minor aluminum hydroxide from this material. Based on the mass balance calculations of Al, the total amount of aluminum dissolved from unaged-FS (1.7 mg Al) was more than the amount of Al from aluminum hydroxide in this sample (0.34 mg Al).

This means that aluminum dissolved into solution was both from aluminum hydroxide and hydrocalumite phases.

The minor phase in aged-FS material was katoite phase; a stable calcium-aluminum hydroxide phase. In general, lower Al ions was expected to dissolve from katoite phase (see Table 17). Note that the unstable aluminum hydroxide phase was transformed into stable katoite phase by the aging process. In fact, dissolution of Al^{3+} ions from aged-FS was simply lower than that of unaged-FS, as the minor Al-containing phase was more stable. At initial pH 8.0, dissolution of both Ca and Al ions from the aged-FS sample were lowered. In general, this test shows that Ca and Al ions in the brucite layers of aged-FS are held with stronger bonding that those in the composition of unaged-FS. The higher the structural stability of brucite layers, the lower the dissolution of metal ions. Note that lower metal ions dissolution means lower material loss.

This test also showed the importance of pH control during the synthesis process. The aluminum hydroxide impurity needs to be maintained at its lowest possible value otherwise it will dissolve, causing the material loss and more importantly discharge of Al^{3+} ions into adsorption effluent. As explained earlier in section 4.1, the pH of the slurry was maintained at 11.3, during synthesis experiment. With a careful pH control, only 2 wt.% aluminum hydroxide was formed. In the preliminary co-precipitation tests at initial pH of 10.0 ($[Al^{3+}]$: 0.33 M), aluminum hydroxide was precipitated and no FS was formed. Therefore, a careful pH control at set pH values of $\geq$11.3 is necessary. In most of the adsorption studies, the amount of minor impurities in the LDH materials (if present), are not reported [25]. QXRD analysis of LDH material similar to this study will be helpful in a better estimation of the metal ions dissolution under various experimental conditions. The temporary failure in the function of the alkaline agent pump during the synthesis

process can also result in poor pH control and the proportion of aluminum hydroxide might increase.

It needs to be highlighted that aging did not fully prevent the dissolution of the material. Aged-FS material still showed some partial dissolution.

5.5.2 Aging impact on minimization of dissolution

The selected aging process reduced the dissolution of metal ions from FS, depending on the initial pH. The aging process reduced the dissolution of Al^{3+} ions from FS, at an initial pH of 12.5. The concentration of Al^{3+} in solution was reduced from an average of 39.3 ppm (for unaged-FS) to 19.1 ppm (for aged-FS). At initial pH 8.0, the aging process reduced the dissolution of Ca^{2+} and Al^{3+} ions from FS. The concentration of Ca^{2+} in solution was reduced from an average of 376 ppm (for unaged-FS) to 205 ppm (for aged-FS). The concentration of Al^{3+} in solution was reduced from an average of 78 ppm (for unaged-FS) to 60 ppm (for aged-FS). This higher stability of aged-FS with respect to its dissolution in water can be related to several factors. It is hard to separate the impact of these variables from each other and therefore, lower dissolution of aged-FS is probably due to a combination of the following factors.

The higher stability of aged-FS is likely due to the phase and chemical transformation of much of the chloro-hydrocalumite to the chloro-carboaluminate hydrocalumite (see 5.4.1). It was explained before in 2.2, that anions in the interlayer space and brucite layer are connected through a complex hydrogen bonding and electrostatic interactions. The intercalation of more carbonate anions during aging has changed the anion ordering of the interlayer space. This change in interlayer space has imposed some new changes to the brucite layers and the crystal systems of brucite layers has changed. Before aging, the Ca and Al ions were mostly in the hexagonal system while after aging the monoclinic systems was dominant. Carbonate oxyanion favored the

monoclinic crystalline system over the hexagonal system. Apparently, Ca and Al ions in the monoclinic phase are held stronger, hence dissolving less. For O-M-O bond lengths and O-M-O angles of hexagonal and monoclinic phases see Appendix B and C. The phase transformation from rhombohedral phase to the monoclinic phase by an increase in the intercalated-carbonate content was reported by Mesbah [53]. For more details on this study see Appendix G.

It was shown by Feng that the carbonated hydrocalumite is a more stable phase than the carbonate-free hydrocalumite [65], and therefore, is expected to have reduced solubility in solution. In this work, it was shown that when the carbonate content of the FS was increased, the solubility of the material was reduced. The extent of reduction in solubility of Ca and Al depends on the initial pH.

A single crystal study was performed by Mesbah to investigate the chemical structure of a chloro-carboaluminate compound with a chemical formula of $[Ca_2Al(OH)_6]\cdot[Cl_{0.52}(CO_3)_{0.24}\cdot 2.33H_2O]$ [53]. Figure 19 presents the structural features of this compound. As seen, Ca and Al are located in octahedral units with seven and six coordination numbers, respectively (shown in blue and green). Carbonate and chloride anions (shown in red and yellow) are distributed statistically in the interlayer space, shared with the water molecules. Carbonate oxyanions and chloride anions are also bonded to the hydroxyl anions from brucite layers. The water molecules are bonded to Ca from the main layer bridging between the layers and interlayer space (gray points). As seen the carbonate oxyanion with a planar molecular geometry easily intercalates in the center of interlayer space instead of just physically adsorbing on the surface of layers [53].

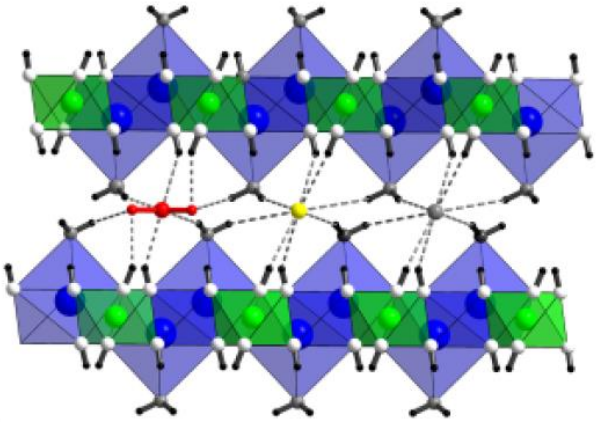

Figure 19 Structure description of $[Ca_2Al(OH)_6]\cdot[Cl_{0.52}(CO_3)_{0.24}\cdot 2.33H_2O]$ and a general representation of chloro-carboaluminate structure (white, gray, red, yellow spheres represent, respectively, hydroxyl anions, water molecules, carbonate, and chloride anions. Blue and green are sevenfold Ca polyhedra and sixfold Al polyhedra). Reprinted with permission from [53].

The structure shown in Figure 19, was reported to be a general representation of chloro-carboaluminate compounds. In another study on chloro-carboaluminate phase, a different possibility for carbonate location in chloro-carboaluminate was also proposed. Carbonate oxyanion was either inserted parallel to the brucite layers at the center of the interlayer (similar to Figure 19) or connected to the brucite layers via bonding to Ca^{2+} [54]. The experimental evidence was obtained via Raman spectroscopy with CO_3^{2-} symmetric stretching vibrations at 1068 or 1086 cm^{-1}. Carbonate intercalation in the interlayer space of aged-FS, either parallel to the brucite layers or connected to the brucite layers via bonding to Ca^{2+}, reduced the dissolution of the material.

In addition to more carbonate intercalation, the elimination of the minor amount of aluminum hydroxide and formation of katoite might be also involved in lowering the metal ions dissolution. Aluminum hydroxide is unstable at high pH while katoite is a stable calcium aluminum hydroxide phase [85]. Since the aluminum hydroxide minor impurity dissolves at high initial pH in an adsorption process, it is important to have a careful pH control in the synthesis process and

minimize the formation of aluminum hydroxide. With an increase in aluminum hydroxide impurity content of FS, the amount of Al dissolved into solution during the adsorption process will increase. It is advised to age the FS material to remove the minor aluminum hydroxide impurity before using use in the adsorption process. This method will guarantee more control over Al dissolution (for FS and in general hydrocalumite) during adsorption.

This study shows that the characterization of LDH in adsorption process by quantitative XRD can be more informative than characterization by qualitative XRD. The QXRD analysis of LDH materials used for adsorption studies, are not generally reported. In industrial plants, an ion exchanger material with lower dissolution such as aged-FS is preferred over a less-stable material such as unaged-FS.

Finally, the formation of larger agglomerates of aged-FS with well-shaped hexagons is probably contributing to a material with higher stability with respect to dissolution.

In general, it is difficult to relate a specific magnitude to the importance of above-mentioned factors on minimization of dissolution. However, as the change in interlayer region composition, has a direct influence on the strength of metal ions bonding in the brucite layers, this factor is most likely playing a more critical role than other ones.

5.6 Summary of aging

In summary, the aging process lowered the metal ion dissolution from FS material. The higher stability of aged-FS than unaged-FS was related to a series of changes imposed on this material during aging. A simple illustration in Figure 20, is used to show the changes imposed on FS material by the aging process. LDH structural details are not shown in this figure.

The chloro-hydrocalumite phase with the chloride in the interlayer space is shown with the light gray color. The chloro-carboaluminate hydrocalumite phase with chloride and carbonate anions in the interlayer space is shown with the dark gray color. Chloride and carbonate anions are shown with blue and green circles, respectively. The aluminum hydroxide and katoite phases are shown with orange and red colors, respectively.

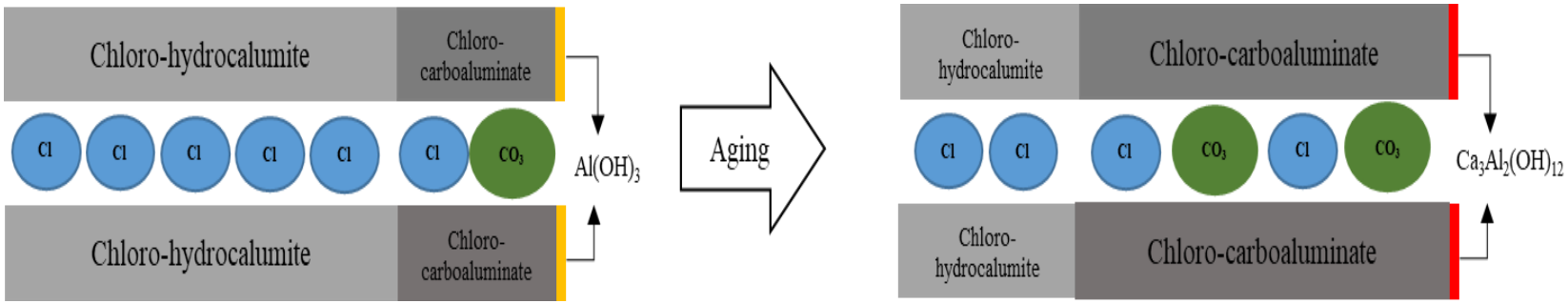

Figure 20 A simple illustration of aging impact on FS material, light gray: chloro-hydrocalumite [$Ca_4Al_2(OH)_{12}$]·[Cl_2·$4H_2O$], dark gray: chloro-carboaluminate hydrocalumite phase [$Ca_4Al_2(OH)_{12}$]·[$Cl(CO_3)_{0.5}$·$10.8H_2O$], orange: aluminum hydroxide, red: katoite phase, blue circles: chloride anions, and green circle: carbonate anions. The proportion of each phase is a rough estimate of the actual data. The structural details are not shown.

As shown in Figure 20, the increase in intercalation of carbonate in the interlayer space during aging, transformed the chloro-hydrocalumite phase (light gray) to the chloro-carboaluminate hydrocalumite phase (dark gray). Since, the carbonated-hydrocalumite phases are generally more stable than non-carbonated phases [65], the higher stability of aged-FS can be related to the increase in the proportion of the chloro-carboaluminate hydrocalumite phase. It needs to be noted that the higher proportion of carbonated hydrocalumite will eventually reduce the capacity for Se loading [25,31,64]. The exchange of carbonate by selenate anion is more difficult than the exchange of chloride anion. The impact of increased carbonate on loading of selenate is discussed in section 6.3.3.

In addition to the phase transformations of hydrocalumite phases, the minor aluminum hydroxide impurity (orange-colored phase in Figure 20) was converted to the katoite phase (red-colored phase in Figure 20) during aging. Aluminum hydroxide is an unstable phase at high pH region and easily dissolves (pH 9.0- 12.0). Aging removed the unstable aluminum hydroxide phase and replaced it with a more stable katoite phase. Aged-FS with no aluminum hydroxide is a more stable material than unaged-FS. Finally, the electronic microscopy study (SEM) showed that aged-FS particles were well-shaped hexagon crystals while unaged-FS was composed of broken plates. The well-shaped hexagons are most likely composed of well-organized Ca- and Al- hexagonal units in the edges of brucite layers, contributing in a less dissolution of the material. The particle size study showed an increase in volume-weighted mean (VWM) of particles over aging. The VWM value for aged-FS was larger than unaged-FS (42.5 μm vs 29.5 μm). In general, larger agglomerates dissolve less than small particles.

In summary, dissolution of Ca and Al ions from aged-FS and unaged-FS depends on the initial pH of the solution. At high initial pH (pH 12.5), dissolution of Al ions from aged-FS was lower than that of unaged-FS. Ca dissolution was almost the same for two materials. At low pH (pH 8.0), dissolution of both Ca and Al ions were suppressed.

Chapter 6: Selenate adsorption by aged-FS

Aged-FS material showed lower metal ions dissolution than the unaged-FS sample in the dissolution tests and was, therefore, a better candidate for selenate adsorption experiments.

6.1 Mass loss calculations in adsorption tests

It was mentioned earlier in 3.2.4.7.2 that mainly LBM is used for FS mass loss calculations for the experiments in this thesis. As shown in Equation 3, a specific chemical formula and molar mass value of FS are required. In the case of adsorption tests, this FS material was an aged-FS sample. Various characterization methods showed that aged-FS sample with an experimental chemical formula of $[Ca_{4.02}Al_{2.03}(OH)_{12.1}]\cdot[Cl_{1.30}(CO_3)_{0.33}\cdot 8.40H_2O]$ was a not pure, single FS (see 5.4.1), but rather mainly a mixture of two FS phases. The average molar mass could be used. On the other hand, some preliminary calculations showed that the mass loss calculations assuming aged-FS has an average molar mass equal to that of pure FS were suitably close to the mass loss calculations using the average molar mass of aged-FS (see Appendix H and Appendix I). Therefore to estimate the mass loss during adsorption tests the molar mass of aged-FS was assumed to the same as that of pure FS with a molar mass of 561.34 g/mole. As mentioned in section 5.1, dissolution of chloro-hydrocalumite and chloro-carboaluminate hydrocalumite phases are assumed to be equal, for simplicity. SBM data for some adsorption experiments can be found in Appendix J to Appendix N. The likely error margins for LBM using the concentrations of Ca and Al are ±0.01 and ±0.03%.

In this thesis, the mass loss of aged-FS is reported for each individual adsorption test. The mass-loss data for LDH materials during adsorption experiments are generally missing from the literature [44,64,76]. While the partial dissolution of LDH is a natural property of this material (see 2.6.1) and equilibrium concentration values (K_{sp} data) are widely reported for them, the dissolution of LDH in adsorption experiments still needs to be reported.

6.2 Effect of various experimental parameters on selenate adsorption by aged-FS

The effect of experimental parameters that can influence selenate loading was studied. These critical factors include the initial pH of selenate solution, liquid to solid ratio (L/S), time, temperature, agitation rate, selenate concentration, the presence of other oxyanions in solution, and the type of container used. The selenium feed solutions were prepared in both ppb and ppm ranges (400 ppb-~1600 ppm Se), as selenium in industrial wastewater solutions ranges from a few ppb to the ppm range (Table 1). The high ppm concentration feeds (>200 ppm), were used for generation of adsorption isotherms. All adsorption tests were performed without nitrogen gas purging. Most of the selenate adsorption experiments were performed two to six times each. Where only one experiment was performed, two or three final solution samples were prepared to replicate ICP analysis.

6.2.1 Effect of initial pH on selenate adsorption by aged-FS

The initial pH of the solution is a critical variable affecting the oxyanion loading and stability of LDH materials. The initial pH effect on selenate adsorption by aged-FS from ppm and ppb level Se solutions was studied (Figure 21). The purpose of this study was to find the optimized pH value based on maximum loading and minimum dissolution of the material.

In general, the oxyanion adsorption is lower at high initial pH value; at sufficiently high initial pH, a significant concentration of hydroxyl anion is present in solution, competing with the target anion for adsorption sites [66]. A few exceptions to this trend were observed for LDH materials [44]. Figure 21, shows that the concentrated feed solution (134 ppm Se) actually follows this trend. Adsorption from the dilute feed solution (460 ppb Se), showed a different trend. The selenate removal from ppm and ppb level feed solutions are separately discussed in 6.2.1.1 and 6.2.1.2.

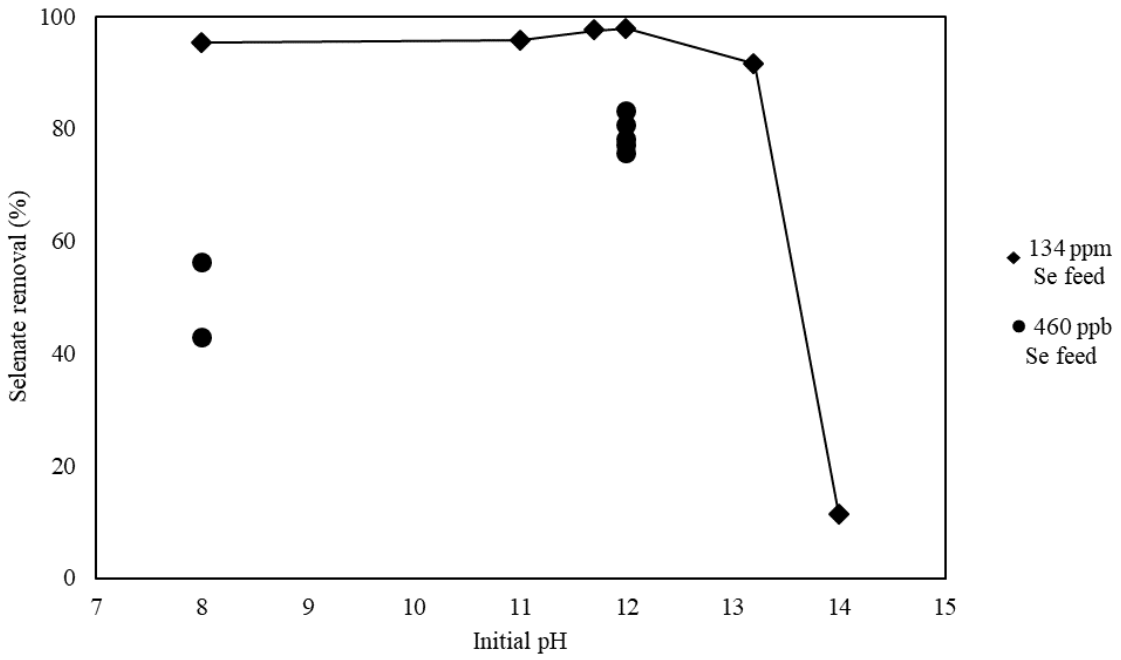

Figure 21 The initial pH effect on selenate removal percentage ($Se._L$ method) by aged-FS from Se 134 ppm feed (black diamonds) and 460 ppb feed (black circles) at L/S 200, 150 RPM, 24 h, and 30 °C.

6.2.1.1 Adsorption from ppm level Se feed solution

The initial pH of the solution was adjusted to 8.0, 11.0, 11.7, 12.0, 13.2, and 14.0 with the addition of 1 and 10 M sodium hydroxide. Most experiments were repeated 2-3 times (see Appendix J). As seen in Figure 21, from 134 ppm Se solution, as initial pH increased from 8.0 to 12.0, the average selenium adsorption was fairly constant. The Se adsorption results show that an excess of hydroxide anion eventually competes with selenate adsorption. At high hydroxyl concentrations (at pH≥13.2), selenate adsorption started to drop. Selenate removal percentage at an initial pH of 13.2 was 91.4% (91.2-91.7%, average of two repetitive experiments). Over initial pH increases to 14.0, the selenate loading dropped dramatically to 11.2%.

6.2.1.2 ppb level Se feed solution; surface loading vs interlayer loading

The effect of initial pH on selenate adsorption from 460 ppb Se feed solution is shown with black circles in Figure 21. The average selenate loadings at initial pH 8.0 and 12.0 were lower: 49.5%

(42.8-56.2%, two repetitive experiments) and 78.9% (75.2-83.2%, six repetitive experiments), respectively. It is apparent that, at a given pH, the extent of selenate removal from the ppb-level feed solution was lower than from a ppm feed solution.

This adsorption trend is not typical for synthetic exchangers such as polymeric resins [24]. In polymeric resins, the removal percentage from low-concentration feed solutions is higher than from high concentration feed solutions. The different behavior of aged-FS from synthetic resins can be explained by the structural differences between the two types of exchangers. As shown in Figure 22, polymeric resins consist of polymers connected in a three-dimensional framework through covalent cross-linkages (seen on the left side of Figure 22) [24]. The fixed functional groups are attached to the resin skeleton and the exchange of a target ion with exchangeable resin ions occurs inside the polymeric network. There isn't a significant difference in types of ion exchange sites. The distribution of exchange sites in an LDH material, however, is substantially different.

The structure of a typical LDH is shown on the right side of Figure 22. As seen, an LDH is composed of positively charged brucite layers $[M_{(1-x)}^{2+}N_x^{3+}(OH)_2]^{x+}$ and interlayer anions and water molecules $[X_{x/n}{}^{n-}\cdot YH_2O]$. As proposed for hydrocalumite-like adsorbents, the oxyanions loading can involve both *surface and interlayer anion exchange* sites. Kinetic investigations showed that adsorption starts with loading on surface sites and is continued into the interlayer sites via intra-particle mass transfer [25,44].

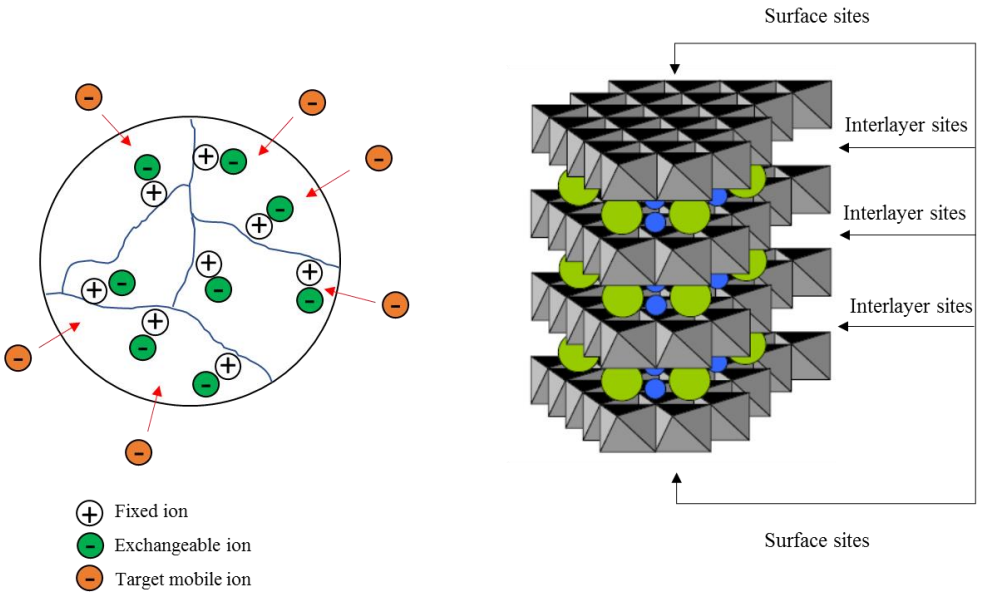

Figure 22 Structural differences of a polymeric resin and LDH [44].

In ppb Se feed solution, the selenate concentration is low and loading probably occurs mainly through the exchange of selenate ions with surface chloride ions. As surface sites are a small proportion of the total available adsorption sites, the removal percentage from 460 ppb level Se feed was low. This might also be due to very slow reaction rate at low concentrations, as 24 h was enough time to reach only to a pseudo-equilibrium and not a full equilibrium. Low concentration would make diffusion into the interlayer region much slower.

At higher selenate concentrations (134 ppm), however, selenate oxyanions penetrate into the interlayer space and a significant exchange with interlayer sites occurs. The surface sites are saturated and the loading continues into interlayer space with the diffusion of selenate from the bulk of the solution. As a result, higher loading was achieved from 134 ppm feed solution. In general, the dominant loading mechanisms for ppb and ppm feed solutions are surface and interlayer loadings, respectively. The initial pH effect, in this thesis, was studied at low and high feed concentrations (460 ppb and 134 ppm Se), which revealed the general loading mechanisms

of LDH family. In Wu's paper, the initial pH effect was studied at one constant concentration of [SeO_4^{2-}]: 7.60 mM [25].

The surface and interlayer loading mechanisms in most of LDH studies are investigated by kinetic studies or XRD analysis [25,33]. The loading mechanisms using XRD patterns of selenate-loaded aged-FS samples will be further explained in 6.2.7.3.

As seen in Figure 21, by increasing pH from 8.0 to 12.0, the average removal of selenate in 460 ppb Se feed solution showed a rise (from 49.5% to 78.9%). The oxyanion loading increase with pH is unusual and opposite to the behavior reported for LDHs. Only a few studies report this pH effect in the literature [44]. One explanation was provided by Das [76]. In this case, the possibility for the incorporation of chemical and electrostatic interactions together was suggested. In the ppb range study, the chemical interaction between selenate and hydroxyl functional groups from the surface of FS might proceed through the formation of a monodentate or multidentate complex over pH increase from 8.0 to 12.0. A possible complexation might be bonding of –OH group from brucite layers to selenate (most likely through Se center).

6.2.1.3 Aged-FS dissolution in initial pH effect studies of adsorption tests

It was explained earlier in 6.1 that for mass loss calculations in adsorption tests, the molar mass of pure FS was used for aged-FS. Figure 23 shows aged-FS dissolution using LBM (for 134 ppm Se and 847 ppb Se feed solutions) at pH 8.0-14.0. The dissolution of aged-FS decreased with increasing pH as expected based on FS dissolution behavior in water. At higher concentration of hydroxide anion, the dissolution of Ca and Al from FS decreases as the metal ions hydration is forced backward at high hydroxide concentrations (Reaction 4, 3.2.4.7.2). In general, LDH materials are more stable at high pH [44].

At an initial pH of 8.0, 17.9 and 17.4% aged-FS was dissolved using $Ca._{LB}$ and $Al._{LB}$ (134 ppm of Se feed, seen on the left side of Figure 23). The dissolution was constant until pH 11.0 but dropped with further increase in pH. At an initial pH of 11.7 and 12.0, $Ca._{LB}$ was 15.0 and 12.0 %, respectively *(*$Al._{LB}$: 13.9 and 11.6 %, respectively). As initial pH increased to 13.2, Al dissolution slightly increased relative to Ca (5.70% $Al._{LB}$ and 4.26% $Ca._{LB}$). At an initial pH of 14.0, $Al._{LB}$ dissolution exceeded the $Ca._{LB}$ dramatically (8.38 % vs 2.22%).

As discussed in the aging studies section, FS material has the buffering capacity (see 5.3, Table 16). The final pH of adsorption solutions showed a similar pattern to the aging solutions. In 134 ppm feed solution, at an initial pH of 8.0, the final pH was increased to 10.5 (Ca dissolution was dominant), while at initial pH 12.0, the final pH was slightly higher (12.2-12.6). The final pH for initial pH 13.2 and 14.0, decreased to 12.7 and 13.2, respectively (Al dissolution was dominant); the final pH was always adjusted at the medium pH region for both low and high initial pH.

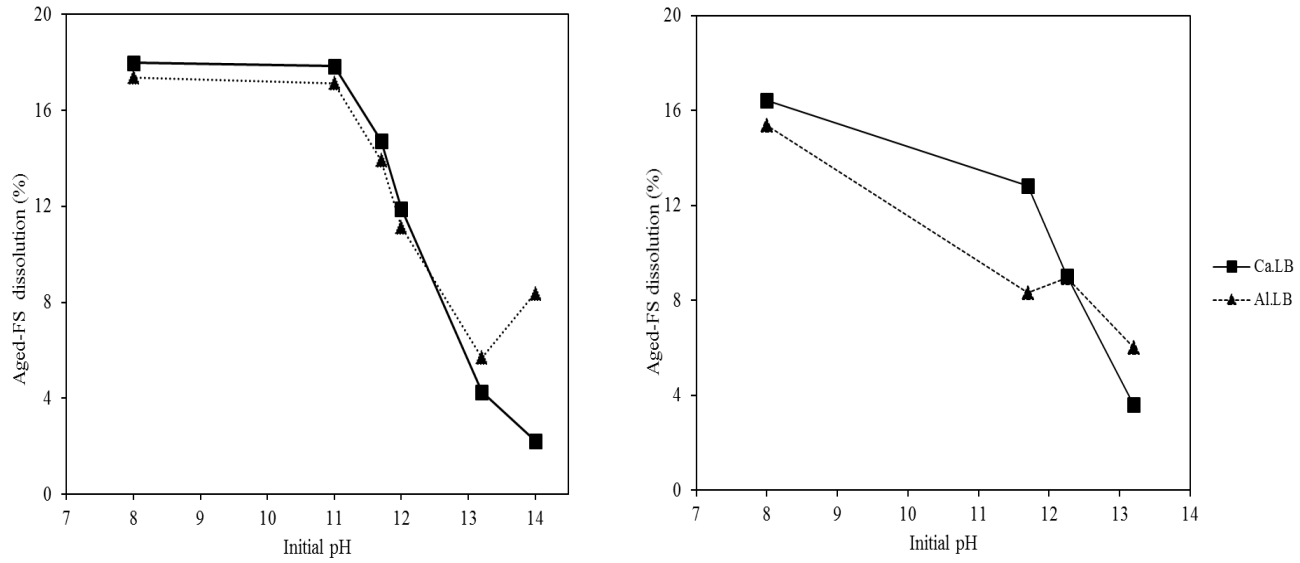

Figure 23 Aged-FS dissolution (%) in pH studies of adsorption tests (experimental condition: L/S 200, 150 RPM, 24 h and 30 °C), 134 ppm Se feed (left) and 847 ppb Se feed (right).

In Wu's study, the adsorption isotherm of selenate was mentioned to be independent of the initial pH (4–10) because pH jumped to above 10 in a minute and rose to a value of 10.5–12.0 [25]. Wu reported a similar buffering effect and trend in pH changes for chemical stability tests of selenate-loaded Wu's $FS._{sint}$. samples [25]. The final pH of solutions for initial pH 4.00, 7.00 and 10.00 was 10.70±0.3. The final pH of the solution was 11.60±0.3 when the initial pH was 13.00. The final pH was 10.70-11.60 for Wu's $FS._{sint}$. material.

Aged-FS dissolution in 847 ppb Se feed at initial pH 8.0, 11.7, 12.2, and 13.2 is shown on the right side of Figure 23. At an initial pH of 8.0, FS dissolution was 16.4% and 15.4% using $Ca._{LB}$ and $Al._{LB}$, respectively (similar to corresponding dissolution values of 134 ppm Se feed in the left figure). The $Ca._{LB}$ was higher than $Al._{LB}$ up to initial pH 11.7 ($Ca._{LB}$: 12.8% and $Al._{LB}$: 8.31%). $Ca._{LB}$ and $Al._{LB}$ dissolution at initial pH 12.2 was similar, 9.02% and 8.94%, respectively. The dissolution at initial pH 13.2 was 3.60% and 6.03% for $Ca._{LB}$ and $Al._{LB,}$ respectively. FS dissolves to some extent, and more of Al stays in the solution because of complexation, whereas more of calcium precipitates possibly as katoite. See Appendix J for dissolution data for 460 ppb Se feed solution in which a similar dissolution trend with pH was observed.

In summary, one of the aspects of this study is providing mass loss data for every individual adsorption experiment. For most of the LDH-related studies, the dissolution of the adsorbents is not quantified [44,76]. Das reports that 85% of selenite is adsorbed with Mg-Fe LDH at pH 4. The possibility of disordering the LDH structure was confirmed by the detection of Mg in the resulting solution at pH 4, and therefore, the optimized initial pH was selected to be 6.0. However, quantitative data on mass loss was not provided [76]. Wu also performed selenate removal studies with his $FS._{sint}$. at an initial pH range of 4-8. The mass loss data for Wu's $FS._{sint}$. material at the studied pH range was not reported despite the reference to its buffering capacity [25]. The partial

dissolution (as a matter of buffering capacity) was not been considered a problem by Wu. In a similar study by Dai, Friedel's salt was used for Cr(VI) removal at an initial pH of 10.0 instead of 6.0 [33]. The reason for this pH selection was reported to be much higher mass loss of Friedel's salt at pH 6.0 (not quantified). In Dai's study, however, Ca and Al concentrations of 1-2 mM and 0.1-0.2 mM, respectively, were reported for the final solution at initial pH 10.0 [33]. The material dissolution at this level was not reported to be a problem or issue for the usage of Friedel's salt in Cr(VI) removal. Similar to many LDH related studies, Dai avoided the adsorption tests at low pH range which is a common strategy for lowering the dissolution of LDHs [33]. No effort was reported on optimizing of adsorption variables other than pH for minimizing the dissolution and maximizing the loading. It is unclear if adsorption variables other than pH (e. g., L/S) were optimized for mass loss considerations. An L/S of 250 was used by Dai for all adsorption tests and the dissolution data by Dai were indicated as "not published data" [33]. The material loss of LDH in industrial plants dealing with any oxyanion-removal can be a serious problem (especially if no industrial solution for minimization of intrinsic dissolution is recommended). In this thesis, an industrial strategy using calcium hydroxide solution is recommended to minimize the mass loss from FS (discussed in 6.3.6).

Table 21 summarizes the aged-FS dissolution from ppm and ppb level Se feed solutions at an initial pH of 8.0 and 12.0. As seen, within experimental uncertainty ranges for $Ca._{LB}$ and $Al._{LB}$ many of the dissolution values are close. It is hard to claim a difference. The lower LBM dissolution for 847 ppb Se feed solution than other two feed solutions is related to slightly higher initial pH in this experiment (initial pH: 12.2). In general, the average aged-FS dissolution at initial pH of 12.0-12.2 range using average LBM of three feed solutions in Table 21 is 11.0%.

Table 21 Aged-FS dissolution using LBM for different feed solutions at pH studies of Se adsorption tests (experimental conditions: L/S 200, 150 RPM, 24 h and 30 °C)

	Se Feed Solution		
Initial pH	**460 ppb**	**847 ppb**	**134 ppm**
8.0	$Ca._{LB}$: 17.5%, (16.5-18.5%) $Al._{LB}$: 18.1%, (17.3-18.8%) Average LBM: 17.8%	$Ca._{LB}$: 16.4%, (16.4-16.5%) $Al._{LB}$: 15.4%, (all 15.4%) Average LBM: 15.9%	$Ca._{LB}$: 17.9% $Al._{LB}$: 17.4% Average LBM: 17.6%
12.0	$Ca._{LB}$: 12.3%, (11.4-13.6%) $Al._{LB}$: 12.4%, (11.6-13.8%) Average LBM: 12.3%	*(initial pH 12.2)* $Ca._{LB}$: 9.00% $Al._{LB}$: 8.91% Average LBM: 8.96%	$Ca._{LB}$: 12.0%, (11.9-12.1%) $Al._{LB}$:11.6%, (11.1-12.0%) Average LBM: 11.8%

6.2.1.4 Pseudo-equilibrium adsorption loading for pH studies

The final mass of aged-FS for each pH-study experiment was calculated, using the LBM data provided in 6.2.1.3. The selenate pseudo-equilibrium loading (Q_e) for 134 ppm Se feed solution, was calculated by a combination of these final mass values and $Se._L$ data from 6.2.1.1. The results are presented in Table 22 as $Se._L/Ca._{LB}$ and $Se._L/Al._{LB}$.

Table 22 Adsorption pseudo-equilibrium loading of aged-FS from 134 ppm feed solution (experimental conditions: L/S 200, 150 RPM, 24 h, and 30 °C)

Initial pH	**Q_e: $Se._L/Ca._{LB}$ (mg Se/g)**	**Q_e: $Se._L/Al._{LB}$ (mg Se/g)**	**Average Q_e: $Se._L$/LBM (mg Se/g)**
8.0	31.4	31.2	31.3
11.0	31.3	30.9	31.1
11.0	31.3	30.8	31.1
11.7	30.8	30.4	30.6
11.7	30.7	30.3	30.5
12.0	30.3	29.9	30.1
12.0	29.2	28.8	29.0
13.2	25.9	26.3	26.1
13.2	25.6	25.9	25.8
14.0	3.17	3.39	3.30

Since Q_e results from $Se._L/Ca._{LB}$ showed good agreement with Q_e results from $Se._L/Al._{LB}$, the average value of Q_e was taken. This shows that the concentration of both metal ions can be

used to calculate the final mass for initial pH experiments. The average Q_e at pH 8.0 to 12.0 remained almost constant at 31.3 mg Se/g and 29.6 mg Se/g, respectively. The average loading of Se dropped to 25.9 mg Se/g at pH 13.2. At an initial pH of 14.0, only 3.30 mg Se/g was loaded.

The Q_e and solid digestion data ($Se._S$) results for other feed solutions are shown in Appendix J. The average Q_e using $Se._L$/LBM for 460 ppb Se feed is 0.055 and 0.084 mg Se/g at initial pH 8.0 and 12.0. The increase in loading with initial pH agreed with the observed trend for loading from 460 ppb Se feed solution in Figure 21.

6.2.1.5 Actual dissolution data vs equilibrium solubility values of pure FS from K_{sp} studies

As discussed in 2.6.1, the equilibrium concentrations of Ca and Al for pure Friedel's salt from K_{sp} studies were reported to be 9.03 and 4.87 mM, respectively [49]. It was emphasized that the actual amounts of metal precursors dissolved during adsorption tests, might be different from equilibrium values and therefore needed to be reported. The average and range of Ca and Al molar concentrations for initial pH 12.0 and 134 ppm Se and 847 ppb Se feed adsorption tests are summarized in Table 23. The actual concentrations are compared to the equilibrium values of pure FS; however, a more precise comparison needs to be done with the equilibrium values of aged-FS. The aged-FS material is mainly a chloro-carboaluminate hydrocalumite phase. It is composed of only 24 wt.% pure FS. Therefore the equilibrium concentration values for aged-FS are expected to be different from that of pure FS provided in Table 23.

Table 23 Actual Ca and Al concentration for pH studies of adsorption test at L/S 200, 150 RPM, 24 h and 30 °C vs Ca and Al equilibrium concentration data extracted from K_{sp} of Friedel's salt

	Actual concentrations		**Equilibrium concentrations from K_{sp} studies for pure FS** [49]
	134 pm Se initial pH 12.0	847 ppb Se initial pH 12.2	
Ca (mM)	4.23 mM, (4.12-4.29 mM)	3.15 mM, (3.14-3.17 mM)	9.03
Al (mM)	1.98 mM, (1.91-2.01 mM)	1.59 mM (both solutions 1.59 mM)	4.87

As shown in Table 23, the actual concentrations are indeed different from equilibrium values for pure FS. The average Ca concentrations in final solutions after loading from 134 ppm Se feed and 460 ppb Se feed were 4.23 and 3.15 mM, respectively. Both values are lower than the equilibrium value of 9.03 mM Ca for Friedel's salt [49]. A key reason may be that the material used in this study was a mixture of phases and mainly the chloro-carboaluminate hydrocalumite phase. Similarly, the Al ion concentrations were lower than the corresponding equilibrium concentration of Al using pure FS. These comparisons show that the equilibrium solubility values are not necessarily an accurate representation of metal ion dissolutions in adsorption experiments. For K_{sp} studies, pure FS sample was exposed to double distilled decarbonated water for 180 days (final pH >12) [49]. In this thesis, selenate adsorption studies were performed for only 24 hrs at various initial pH values. It is also possible that equilibrium (with respect to solubility of the phases) was not attained. Therefore, from the beginning, the Ca and Al ion concentrations were expected to be far from equilibrium values. The difference between the adsorption tests and K_{sp} studies in the literature convinced us to track the concentration of each of the metal ions in all adsorption tests. In summary, the adsorption experimental conditions are quite different from equilibrium solubility studies and mass loss during adsorption studies needed to be reported. To the best of our knowledge, this thesis, in an LDH-adsorption field, is the first work on reporting, and considering the metal precursor ions concentrations after adsorption.

Researchers in this field are advised to include the actual dissolution data of LDH used for adsorption studies. This will be helpful in providing a realistic platform for LDH material usage and adsorption isotherms for any future applications (such as drinking water purification or industrial wastewater treatments).

6.2.1.6 Summary of pH studies

In summary, from the results of pH studies, initial pH 12.0 was selected as an optimized pH variable for further studies. This selection was made based on considering maximum Se-loading (from Figure 21) and minimizing dissolution of aged-FS (Figure 23). The initial pH 13.2 has the bonus of lower mass loss, however, the selenate adsorption starts to drop at this pH, and therefore it is better to avoid it. At the initial pH of 12.0, the average Se removal was 97.8% (97.7-98.0%) for 134 ppm Se feed and 78.9% (75.2-83.2%) for 460 ppb level feed solutions. The average LBM aged-FS dissolution at initial pH of 12.0-12.2 was 11.0%.

The initial pH for adsorption process in a wastewater plant should be selected considering the pH of wastewater and data provided by both Figure 21 and Figure 23 for Se loading and FS dissolution, respectively. It means that, for example, an initial pH of 11 can also be a suitable choice since it provides similar loading percentage to initial pH of 12 and a lower material dissolution.

6.2.2 Effect of L/S ratio on selenate adsorption by aged-FS

To obtain an adsorption isotherm for selenate loading, the effect of selenate solution to aged-FS mass ratio (L/S) was studied by varying L/S from 20 to 1200 using 460 ppb Se feed solution. Figure 24 shows the removal percentage of selenate at various L/S ratios (experimental conditions: initial pH 12.0, 150 RPM, 30 °C, and 24 h). Each experiment was performed once, except the experiment at L/S 200, which was performed a total of six times to establish reproducibility.

As shown, removal of selenate decreased with increasing L/S ratio. The extent of Se removal at L/S 20 was 96.8%. As the L/S ratio increased from 20 to 50 and 100, removal dropped from 96.8% to 94.0 and 89.0%, respectively. The average removal percentage at L/S 200 was 78.9% (75.7-83.2%). The selenate removed continuously decreased over the L/S 200-800 region.

The Se removal almost leveled off at L/S 800-1200. The selenate removal percentage was 35.0, 18.5 and 13.2% at L/S 400, 800 and 1200, respectively.

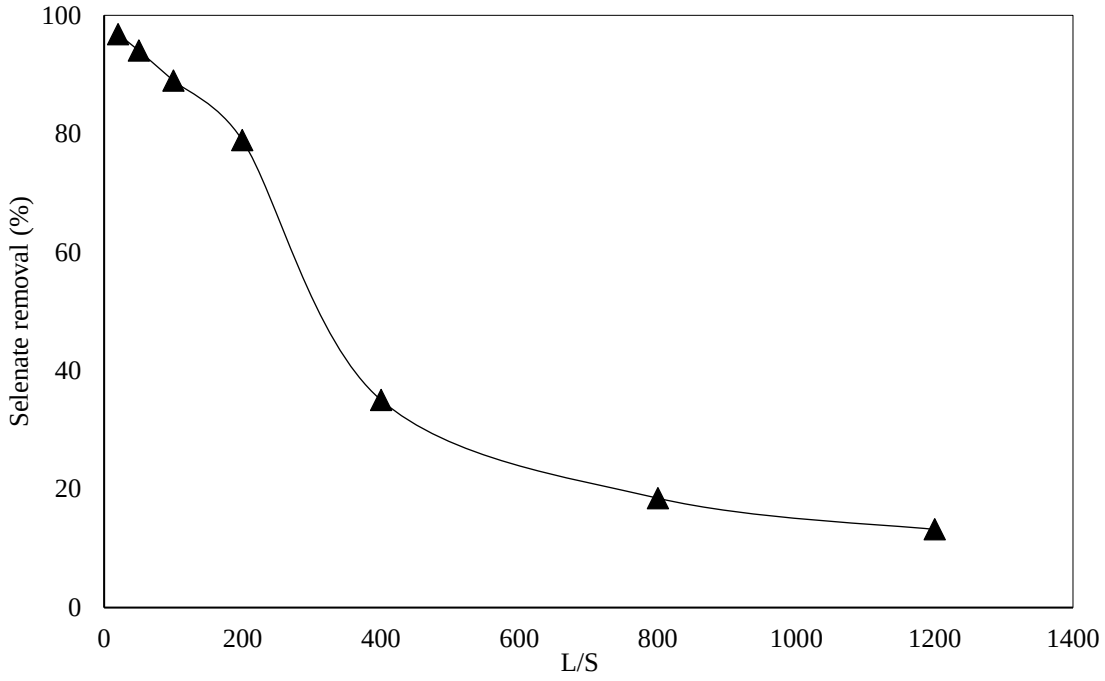

Figure 24 Selenate removal percentage ($Se._L$ method) by aged-FS vs L/S ratio (experimental condition: 460 ppb Se, initial pH 12.0, 150 RPM, 24 h and 30 °C).

As L/S increased, the fraction of selenate removed decreased, since the amount of selenate mass in solution was much higher than the available exchange sites in aged-FS to adsorb it. This resulted in a final solution Se concentration approaching the starting concentration at the highest L/S ratio. The final Se concentration change with L/S ratio is shown in Figure 25. The pseudo-equilibrium concentration at L/S 400 was 298 ppb Se (equal to 35.2% $Se._L$). The final concentration at L/S 600-1200 was 358-399 ppb range. The remaining selenate at L/S 1200 was 399 ppb, closest value to the initial feed concentration (460 ppb), indicative of a low removal percentage. For more loading data of L/S experiments see Appendix K.

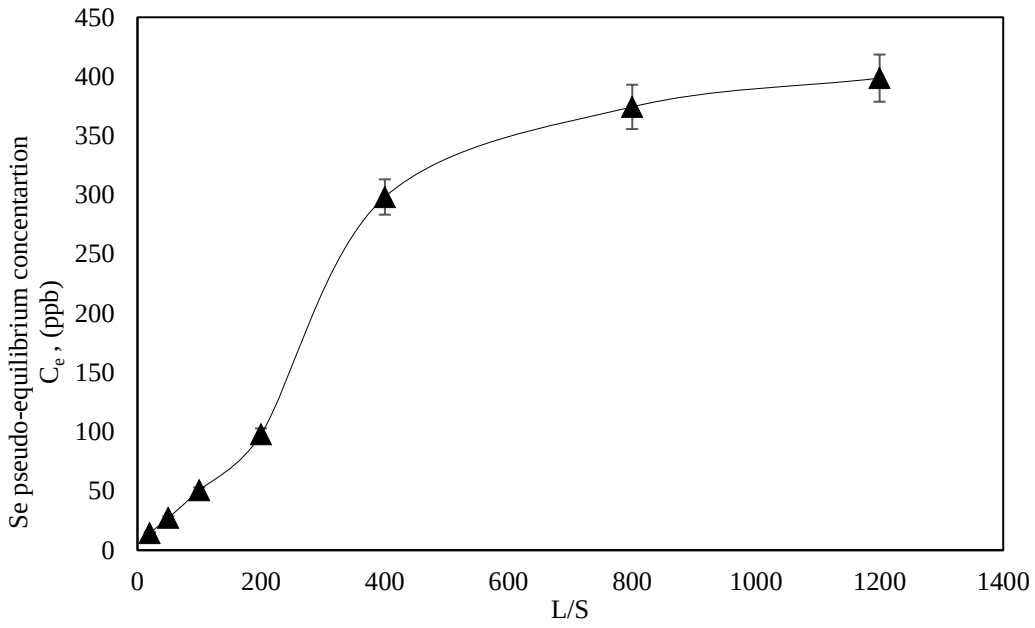

Figure 25 Selenium pseudo-equilibrium concentration (C_e) vs L/S (experimental condition: 460 ppb Se, initial pH 12.0, 150 RPM, 24 h and 30 °C loading by aged-FS), ICP error ±5%.

6.2.2.1 Aged-FS dissolution in L/S studies of adsorption tests

It was explained earlier in 6.1 that for mass loss percentage calculations in adsorption tests, the molar mass of pure FS was used. Aged-FS dissolution was very dependent on L/S as shown in Figure 26. Wu used L/S of 500 for selenate removal studies; no attempt was performed by Wu for finding a suitable L/S regarding the material dissolution [25].

Aged-FS dissolution using $Al._{LB}$ and $Ca._{LB}$ methods are shown in Figure 26. A good agreement was observed between $Al._{LB}$ and $Ca._{LB}$ at L/S 20-400. In general, aged-FS dissolution increased significantly as the L/S ratio increased. The dissolution of aged-FS using $Ca._{LB}$ was 1.93% and 12.1 % at L/S 20 and 200, respectively. A much higher mass loss of 29.2% and 34.1% $Ca._{LB}$ occurred at L/S 800 and 1200, respectively.

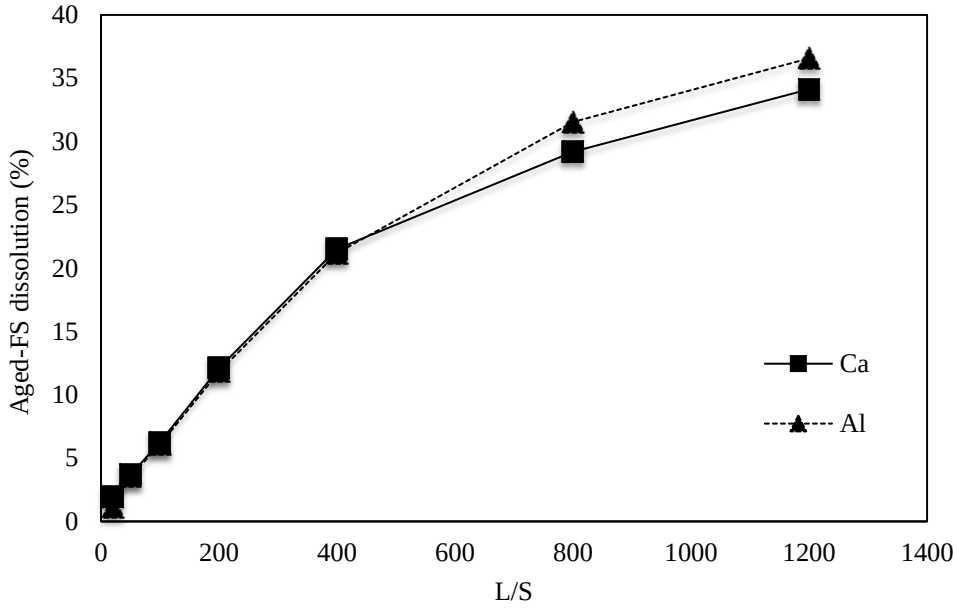

Figure 26 Aged-FS dissolution (%) in L/S studies of adsorption tests (experimental condition: 460 ppb Se, initial pH 12.0, 150 RPM, 24 h and 30 °C).

6.2.2.2 Pseudo-equilibrium adsorption isotherm for L/S studies

The selenate adsorption isotherm for L/S studies is shown in Figure 27 (460 ppb Se, initial pH 12.0, 150 RPM, 24 h and 30 °C). The pseudo-equilibrium adsorption of Se (Q_e) was calculated using $Se._L$ adsorption data and average LBM mass loss data. More Se loading data using $Se._S$ for L/S studies is provided in Appendix K.

As seen, the experimental loading of Se on aged-FS increased from 0.009 mg Se/g at L/S 20 to 0.04 mg Se/g at L/S 100. The experimental loading kept increasing with L/S and reached 0.08 mg Se/g at L/S 200. Loading was constant beyond this up to L/S 400 (loading 0.08 mg Se/g). After reaching a plateau, there was a rise in loading again, as experimental L/S was increased to 800-1200. The second rise in loading is related to the transition of surface loading to interlayer loading.

As L/S was increased from 20 to 200, the loading on the surface sites increased (shown as surface loading area in Figure 27). At L/S 200-400, loading on surface sites reached saturation and no more loading was observed (shown as surface saturation area in Figure 27). As L/S was increased to 800-1200, the available Se concentration in solution increased. At higher selenate concentration, the mass transfer of selenate was forced into the interlayer space. As a result, a higher proportion of selenate was adsorbed by the interlayer loading mechanism. Selenium loading in solid increased from 0.08 mg Se/g to 0.11 mg Se/g (shown as interlayer loading area in Figure 27). The increase in loading as a result of interlayer adsorption was modest. This suggests that the interlayer sites might not be as active as the surface sites. The distinct surface and interlayer loading mechanisms were confirmed by pH studies data earlier (see 6.2.1.2). The XRD pattern of Se-loaded samples after different extents of loading will be discussed further in 6.2.7.3.

The error bars for Se loading data in Figure 27 represent the uncertainty or error in ICP analysis (±5%). The analytical errors can be higher at higher L/S ratio (e. g., L/S 800 and 1200) because of the small difference in concentrations between the initial and final solutions. The final concentration of Se at high L/S is very close to the initial concentration (e.g. final: 399 ppb and initial: 460 ppb at L/S 1200). Therefore, the ICP error could be significantly amplified because the difference between two similar values was used to calculate loading.

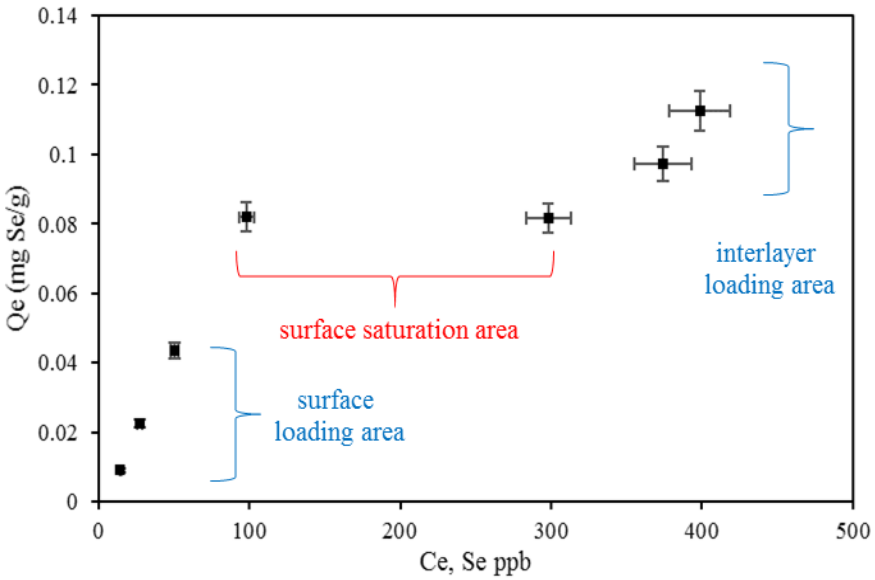

Figure 27 Pseudo-equilibrium adsorption isotherm of selenate by aged-FS for L/S studies (experimental condition: 460 ppb Se, initial pH 12.0, 150 RPM, 24 h and 30 °C).

The maximum loading of 0.11 mg Se/g was achieved at L/S 1200. Considering the mass loss issue at high L/S ratios, adsorption experiments at L/S ratios higher than 400 is not advised (mass losses of 21.2-35.4% for L/S 400-1200). L/S 200 was selected for future adsorption studies since a high Se loading along with a low mass loss was guaranteed under this L/S ratio. An experimental L/S with a lower mass loss is preferred, even with a low Se loading, because of lower metal ions dissolution.

Selenium experimental loading of 0.08 mg Se/g equal corresponding to an average Se loading of 78.9% (75.2-83.2%) was measured while the average aged-FS dissolution of 11.9% (12.1 and 11.8% $Ca._{LB}$ and $Al._{LB}$, respectively) was obtained.

6.2.2.3 Pseudo-equilibrium adsorption isotherm models

As explained in 3.2.4.7.4, the pseudo-equilibrium adsorption loading (Q_e) for Se was calculated using Se aqueous concentration data ($Se._L$ method) and the final mass of FS (average of $Ca._{LB}$ and

$Al._{LB}$). In this thesis, the Langmuir and Freundlich adsorption isotherms were used to model the experimental data. These models were applied to the experimental data obtained from L/S and concentration studies (6.2.2.2 and 6.2.7.2). Langmuir and Freundlich models correlate the Se-loaded on the FS (Q_e) to the pseudo-equilibrium concentration of selenate in solution (C_e).

The Langmuir and Freundlich isotherms are expressed mathematically with Equation 9 and Equation 10, respectively. Q_e is the pseudo-equilibrium adsorption loading of Se on aged-FS (mg Se/g or mmol/g). C_e is the pseudo-equilibrium concentration of selenate. The quantities **A** and **b** are the Freundlich and Langmuir constants, respectively; **A** is related to the adsorption capacity. The quantity **1/n** is another constant related to the energy or intensity of adsorption in the Freundlich isotherm. The quantity $\mathbf{Q_m}$ is the maximum amount of selenate that can be adsorbed in the Langmuir model [25,44].

$Q_e = (Q_m b C_e)/(1+bC_e)$ Langmuir equation — Equation 9

$Q_e = AC_e^{1/n}$ Freudlich equation — Equation 10

In the Langmuir model, the adsorbent is assumed to have an ideal solid surface composed of homogenous and distinct sites capable of binding the adsorbate. This does not perfectly apply here since there are distinctive surface and interlayer adsorption sites. The Freundlich model, however, describes the adsorption of a non-homogenous adsorbent to which layers of adsorbate can bind [24].

6.2.2.4 Pseudo-equilibrium adsorption isotherm fit with models for L/S studies

Figure 28 shows the adsorption isotherms for L/S studies in the range of L/S 20 to 1200 for the initial concentration of 460 ppb Se. The Langmuir model and the Freundlich model were applied to the experimental data by changing the constant values of each isotherm using the Microsoft

Excel solver routine. Table 24 shows the adsorption constants of two isotherm models. The Q_m value was selected close to the maximum experimental loading for a series of experiments. The b value was varied so to match the experimental loading and isotherm with the minimum possible errors.

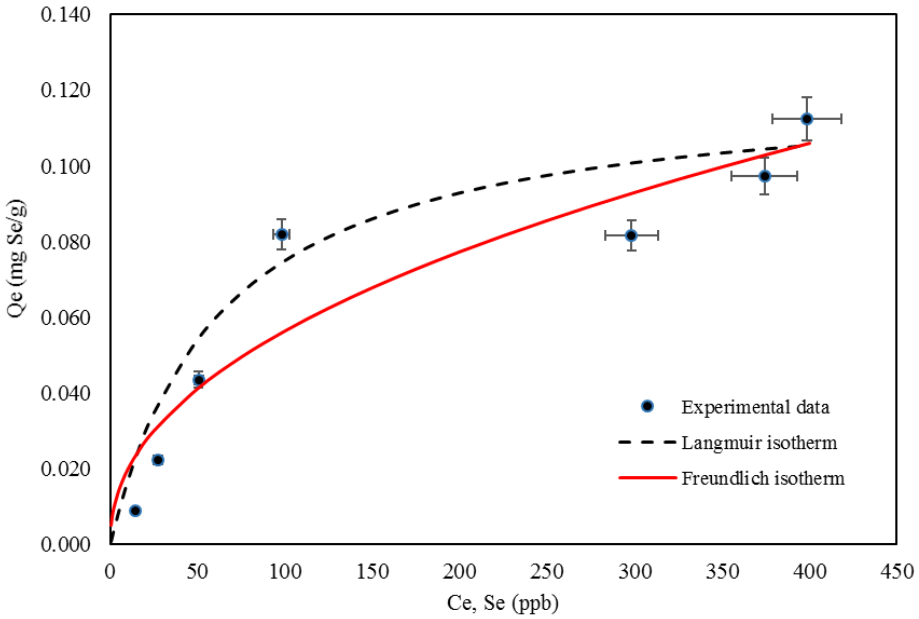

Figure 28 Pseudo-equilibrium adsorption isotherm fit with models for L/S studies (460 ppb Se, L/S 20-1200, initial pH 12.0, 150 RPM, 24 h and 30 °C).

Table 24 Langmuir and Freundlich constants for selenate loading on aged-FS in L/S study

Langmuir constants		**Freundlich constants**		
Q_m (mg Se/g)	b (mM^{-1})	A (mg/g)	1/n	n
0.12	0.02	0.01	0.45	2.22

The negative charge of selenate anions makes the multilayer adsorption (Freudlich model) unreasonable unless some positive counter ions (Ca^{2+}, and Al^{3+} or Na^{+} present in solution) are

involved. In the entire L/S range of 20-1200, both surface and interlayer loading mechanisms were involved and therefore one isotherm did not fit with all the experimental data.

6.2.2.5 Selenium mass balance

Selenium mass balance for the L/S series of adsorption experiments is shown in Table 25. The Se in the solid mass at the end of the experiment was calculated based on analysis of final solid ($Se._S$ method) and calculation of the total mass of solid at the end using an average of $Ca._{LB}$ and $Al._{LB}$ (LBM). In general, the reliability of mass balance calculations LBM was higher than SBM. The direct weighing of final solid was associated with some inaccuracies. See Appendix J to Appendix N for all mass balance data of adsorption tests.

Table 25 Mass balance of selenium for L/S tests ($Se._S$ and an average of $Ca._{LB}$ and $Al._{LB}$ used for calculations)

L/S ratio	Added Se mass in (mg)	Se mass in solution (mg)	Se mass in solid (mg) (From Se.s)	Mass balance (%)
20	0.023	0.0007	0.022	101
50	0.023	0.0014	0.024	110
100	0.023	0.0025	0.015	76
200	0.023	0.0049	0.020	107
200	0.025	0.0082	0.013	84
400	0.023	0.0149	0.006	92
400	0.025	0.0174	0.006	93
800	0.046	0.0374	0.005	91
800	0.051	0.0435	0.006	97
1200	0.046	0.0399	0.003	94

As shown, the mass balance for most of the experiments is in the range of 91-110%. For a few adsorption experiments, mass balance closure values between 76, 82 and 84% were observed. The errors might be due to solid digestion process errors. Once the experiment with low mass balance closure was repeated better results were obtained (e.g., a repeat of the L/S 200 test with the mass balance of 84% resulted in a mass balance of 107%).

6.2.2.6 Summary of L/S studies

Aged-FS dissolution was highly L/S-dependant and experimental conditions at L/S>400 are not recommended for selenate adsorption studies. In summary, L/S 200 was selected as suitable L/S ratio, from pseudo-equilibrium adsorption isotherm of L/S studies (L/S: 20-1200, 460 ppb Se, initial pH 12.0, 150 RPM, 24 h and 30 °C). At L/S 200, the maximum pseudo-equilibrium loading of 0.082 mg Se/g and minimum average aged-FS dissolution of 11.9% was achieved.

6.2.3 Effect of time on selenate adsorption by aged-FS

The adsorption profile of selenate on FS over 20 minutes to 48 hours is displayed in Figure 29 (637 ppb Se, initial pH 12.0, L/S 200, 150 RPM, and 30 °C). The selenate loading (Q_e) is illustrated using $Se._L/Ca._{LB}$ and $Se._L/Al._{LB}$. As shown, selenate loading increased sharply initially but slowed down with time. In general, this type of initial fast adsorption was previously reported for LDHs, similar to ion exchange reactions in soils and clay minerals [44]. The surface adsorption of oxyanions on LDH material likely takes place quickly. However, the diffusion of oxyanion into the interlayer space requires a longer time [25].

As seen in Figure 29, there is a good agreement between $Se._L/Ca._{LB}$ and $Se._L/Al._{LB}$ loading values. Therefore, an average of $Se._L/Ca._{LB}$ and $Se._L/Al._{LB}$ is used for reporting the loading data. Adsorption by aged-FS was fast. At 20 minutes, 27.8% adsorption occurred corresponding to 0.037 mg Se/g. After 45 minutes, 47.8% selenate was removed corresponding to 0.064 mg Se/g. At longer exposure time, adsorption continued but at a slower rate. After 3 h, 62.4% of Se corresponding to 0.084 mg Se/g was adsorbed. The Se loading reached to 0.120 mg Se/g after 12 h (85.2% adsorption). Selenate loading reached to 0.129 and 0.137 mg Se/g after 24 and 48 h of exposure time. The contact time of 24 h seemed enough to reach to pseudo-equilibrium and therefore was used for subsequent adsorption studies. It was also explained in 3.2.4.7.4, the final

concentration of Se after 24 h loading was considered the pseudo-equilibrium concentration for all adsorption experiments in this thesis. The average aged-FS LBM dissolution was 12.7% (12.4-13.0%). See Appendix L for more details on dissolution data of time studies.

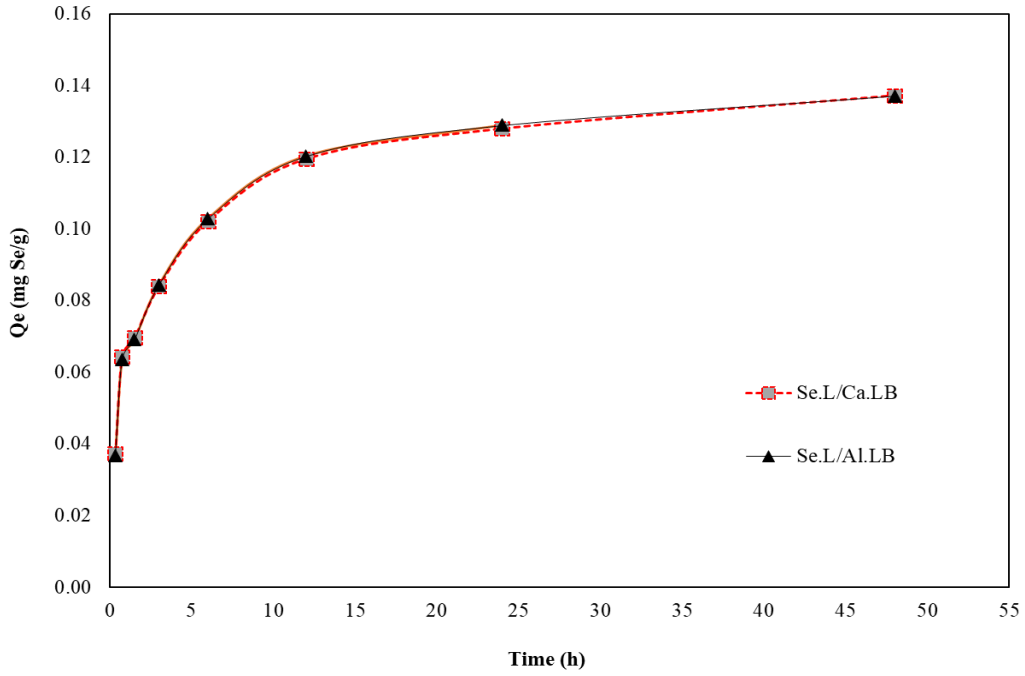

Figure 29 Effect of time on selenate loading by aged-FS (experimental condition: 637 ppb Se, initial pH 12.0, L/S 200, 150 RPM, and 30 °C).

6.2.4 Effect of temperature on selenate adsorption by aged-FS

To measure the effect of temperature on selenate adsorption by aged-FS, the temperature of the adsorption process was adjusted at 30, 60 and 85 °C. A 0.25 g aged-FS sample was added to 50 mL of selenate solution at selected temperatures under following experimental conditions; initial pH 12.0, L/S 200, 150 RPM, and 24 h. The effect of temperature on selenate removal from 468 ppb Se feed is displayed with a solid black line in Figure 30. As shown, from 30 to 60 °C, selenate adsorption increased from an average of 78.9% (75.2-83.2%, six repetitive experiments) to an average of 99.1% (98.6-99.5%, three repetitive experiments). A slight drop in adsorption was observed as the temperature was increased from 60 to 85 °C. The average selenate removal at 85

°C was 97.0% (96.7-97.5%, three repetitive experiments). A similar trend was observed for loading from 753 ppb Se feed solution (dashed black line in Figure 30). The average fractions of selenate removed at 30, 60 and 85 °C were as follows; 73.0% (72.2-73.8%), 99.21% (99.18-99.24%), and 95.9% (95.1-97.1%).

The adsorption of oxyanions with LDHs is usually an exothermic process and therefore oxyanions uptake decreases with increasing temperature [44]. In the case of aged-FS, the selenate adsorption appears to be an endothermic process (at least for predominantly surface loading). The selenate adsorption was higher at 60 °C, however, the physical attack of glassware container with sodium hydroxide solution limits the use of glass at higher temperatures. Since the glass container was etched at high temperatures, it was impractical to operate under these conditions. Therefore, a temperature of 30 °C was used for subsequent adsorption experiments. Selenate adsorption at higher temperatures should be studied using a sodium hydroxide-resistant container. Low and high-density polyethylene (LDPE and HDPE) bottles are reported to show little or no damage after 30 days at 20-50 °C with even 50% sodium hydroxide [87].

The average FS dissolution at 60 °C using $Ca._{LB}$ and $Al._{LB}$ was 12.4% (all three samples 12.4%), and 4.43% (3.83-5.18%), respectively. The average FS dissolution at 85 °C using $Ca._{LB}$ and $Al._{LB}$ was 10.2% (9.95-10.4%), and 2.87% (2.44-3.34%), respectively (see Appendix M). The slightly lower dissolution of material at 85 °C than 60 °C, might be related to a higher stability of Se-loaded hydrocalumite phase at 85 °C.

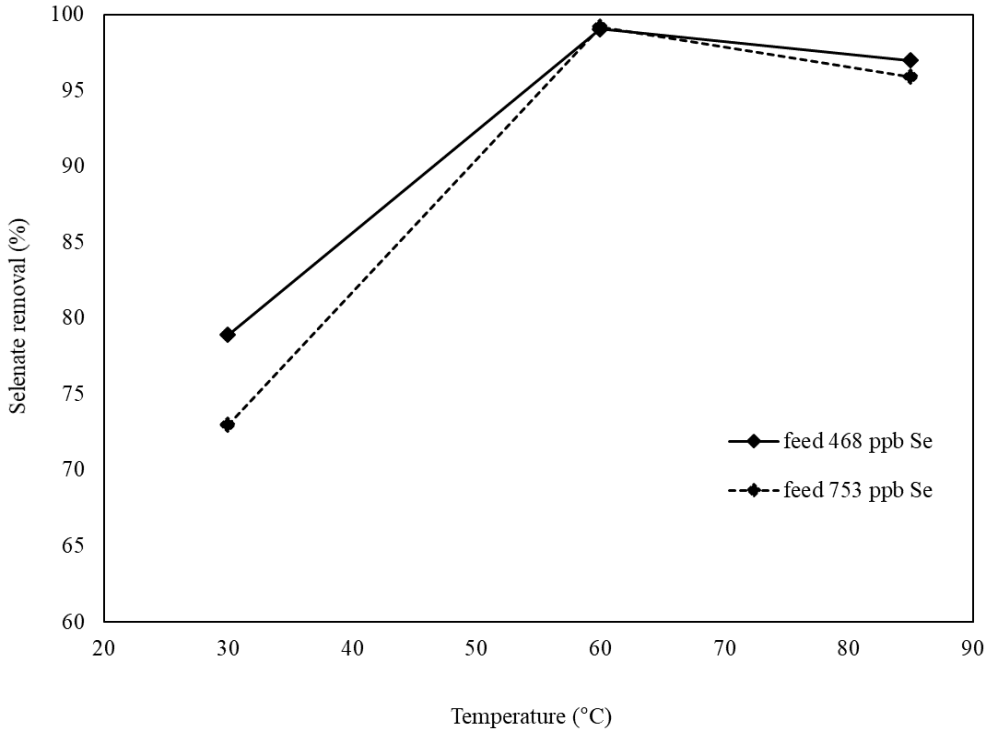

Figure 30 Effect of temperature on selenate removal by aged-FS (experimental condition: initial pH 12.0, L/S 200, 150 RPM, and 24 h).

6.2.5 Effect of container type on selenate adsorption by aged-FS

For ppb Se level solutions, the surface adsorption of oxyanion by the container used in the adsorption experiment can cause interferences with the main adsorption process. Selenate adsorption by different containers such as Pyrex glass, polypropylene (PP) and high-density polyethylene (HDPE) plastic containers from 495 ppb Se was investigated. The experiments were performed in the absence of aged-FS to monitor the surface adsorption exclusively by the container materials. Table 26 shows the final Se concentration in the solution for each test. No significant change in selenate concentration was observed in Pyrex and HDPE containers ($Se._L$: 1.3% and 0.0%, respectively). The PP container, however, showed some surface adsorption for selenate (6.9% adsorption) and is not recommended for selenate-loading experiments. HDPE containers

seem to be a more suitable container than Pyrex glass due to resistance to etching by hydroxide and zero-interference for selenate loading.

Table 26 Final Se concentration in different containers (feed: Se 495 ppb, pH 12.0, 30 °C, 150 RPM, for 24 h)

Container	Final Se (ppb)
Pyrex glass	488
PP	460
HDPE	495

6.2.6 Effect of agitation rate on selenate adsorption by aged-FS

Three individual adsorption tests were performed at 100, 150, and 175 RPM in 753 ppb Se feed solution to study the effect of agitation speed on the removal percentage. These experiments were performed at 100 and 150 RPM with a shaking water bath. However, the experiments at 175 RPM were performed with an orbital shaker.

The selenate removal results from all tests are displayed in Figure 31. Selenate adsorption remained constant as the shaking rate was raised from 100 to 150 RPM. The $Se._L$ results indicated that at 100 RPM, agitation speed was not limiting the loading rate. Average removal of selenate at 100 and 150 RPM was 74.4% (72.6-75.9%) and 73.9% (70.4-76.4%), respectively. The average removal at 175 RPM was 80.7% (80.0-81.7%) slightly higher, but since two shakers had different shaking patterns, the interpretation of results was complicated. It is possible that the particle size of the material might have been reduced and in turn, caused increased the loading. A shaking rate of 150 RPM using a shaking water bath was selected for the rest of the experiments.

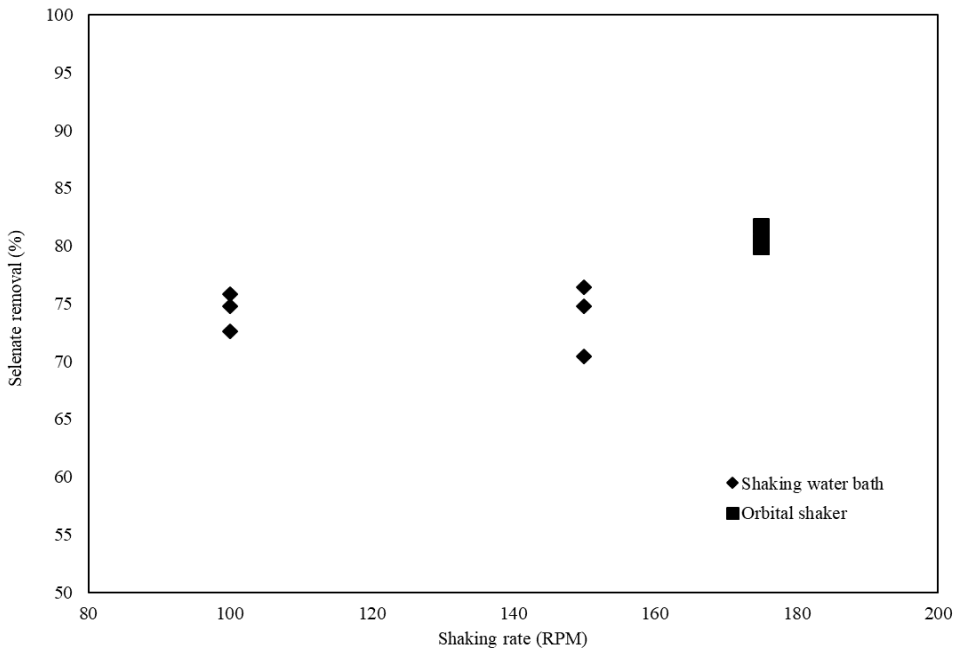

Figure 31 Shaking rate effect on selenate adsorption (experimental condition: 753 ppb feed, initial pH 12.0, L/S 200, 30 °C, and 24 h).

6.2.7 Effect of initial concentration on selenate adsorption by aged-FS

One of the important parameters for determining the oxyanion adsorption capacity is the initial concentration of oxyanion in solution (C_0). For the effect of initial concentration two series of concentration ranges were studied: 0.5 to 200 ppm and >200 ppm. The purpose of performing the experiments over a wide range of selenate concentrations was to obtain the loading isotherm. As mentioned in 3.2.4.7.4, pseudo-equilibrium loading (Q_e) was calculated using $Se._L$ and the final mass of FS (W). The difference of initial (C_0) and Se final concentrations (C_e), is labeled as $Se._L$. Final mass of FS (W) is the average of $Ca._{LB}$ and $Al._{LB}$ using LBM. For more dissolution data in concentration studies, see Appendix N.

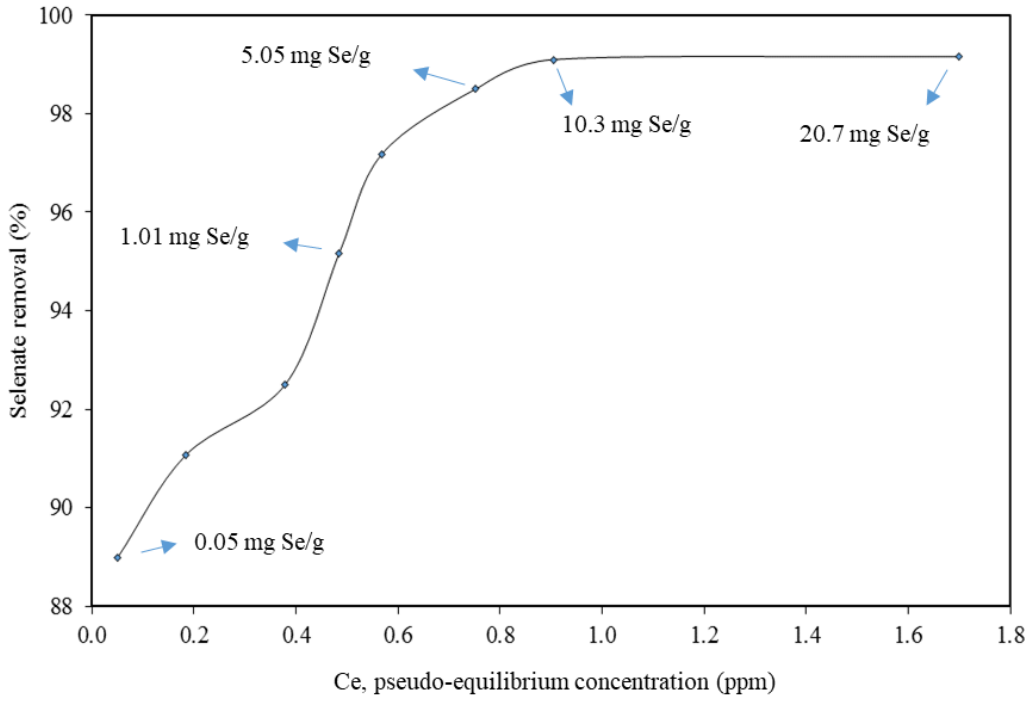

Figure 32 Selenate removal as a function of Se pseudo-equilibrium concentration (C_e) on adsorption by aged-FS (0.5-200 ppm Se, initial pH 12.0, L/S 100, 30 °C, 24 h, and 150 RPM). The loading data pointed with the blue arrows are $Se._L$/average LBM dissolution data.

Figure 32 displays selenate loading vs the pseudo-equilibrium Se concentration in the range of 0.5 to 200 ppm initial Se concentration. As shown, at an initial concentration of 0.5 ppm Se, the adsorption was 89.0% with remaining 0.055 ppm Se in the final solution. The pseudo-equilibrium loading (Q_e) was 0.05 mg Se/g at this point. As the initial concentration was increased from 0.5 to 10 and 50 ppm, loading increased to 95.2 and 98.5%, respectively. The pseudo-equilibrium loading (Q_e) was 1.01 and 5.05 mg Se/g at these data points. The pseudo-equilibrium concentration in the solution for these experiments was 0.38 and 0.75 ppm Se, respectively.

As the initial concentration was increased from 50 to 100 and 200 ppm higher loading was observed. The fraction adsorbed reached 99.1% at 100 ppm initial Se concentration (Q_e:10.3 mg Se/g). Adsorption from the 200 ppm solution was 99.2% with pseudo-equilibrium loading of 20.7

mg Se/g. The Se pseudo-equilibrium concentration in solution was 0.9 and 1.7 ppm Se for 100 and 200 ppm initial concentrations, respectively. The average of aged-FS dissolution (LBM) was 2.58% at 200 ppm. Note that in concentration studies L/S of 100 is used. It was lower than the L/S used in pH studies (L/S 200). Therefore, a lower dissolution (2.58%) than the average dissolution of pH studies (11.0%, see 6.2.1.6), was measured.

As can be seen, loading was still increasing even after contact with 200 mg/L Se, indicating that saturation had not been achieved. To obtain the maximum capacity of aged-FS for selenate, higher initial concentrations than 200 ppm Se were required. Therefore, in the second series of concentration studies, loading from initial concentrations of 514, 870, 1258, and 1539 ppm Se were performed (one experiment each). Figure 33, shows selenate removal for all concentration data points including the first series (0.5-200 ppm Se) and the second series (514-1539 ppm Se).

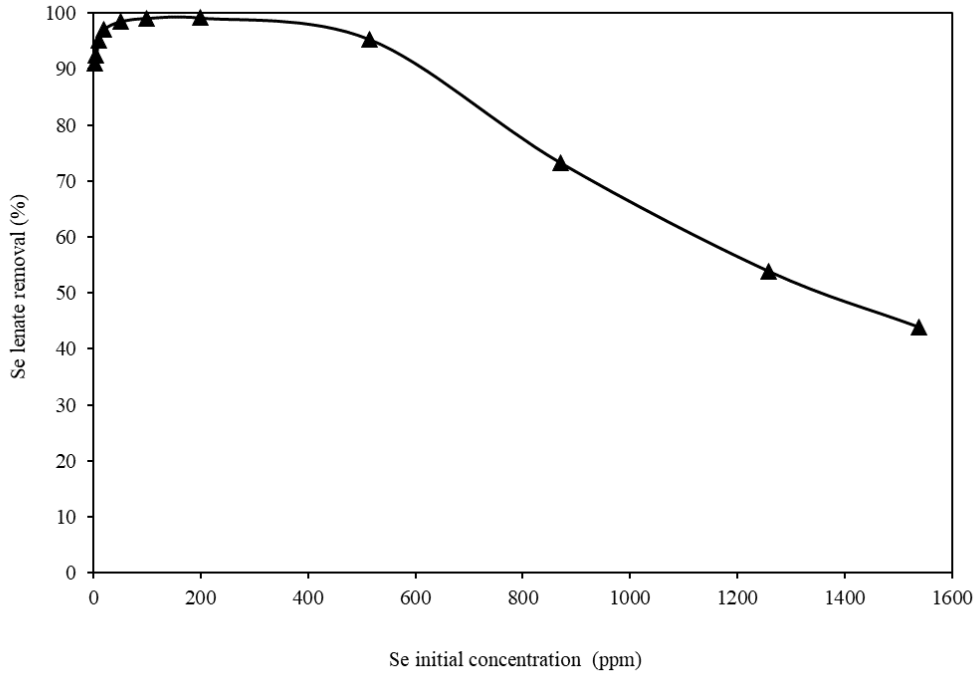

Figure 33 Selenium removal percentage vs Se initial concentration in this study (experimental condition: 0.5-1539 ppm Se, initial pH 12.0, L/S 100, 24 h, and 30 °C).

As shown, at concentrations higher than 200 ppm, the fraction adsorbed started to drop. Se removal at initial concentrations of 514, 870, 1258 and 1539 ppm Se were 95.3, 73.3, 53.9, and 43.9%, respectively. Similar to the discussion in 6.2.2 section (L/S studies), a decrease in the fraction of selenate loaded is expected as the amount of selenium available in solution increases. Note that a much wider concentration of Se was covered in this thesis (500 ppb to 1539 ppm Se) compared to Wu's study (20-600 ppm Se), since the selenate feed solutions in ppb range are of great importance in industrial wastewater plants [25].

6.2.7.1 Pseudo-equilibrium adsorption isotherm for concentration studies

As explained in 6.2.2.3, adsorption isotherms are used to calculate the Se maximum loading (Q_m) using a plot of the final loading (Q_e) and final aqueous concentration (C_e). Similar to the adsorption isotherm obtained from the L/S studies (Figure 27), another adsorption isotherm was investigated using the data from the variation in initial Se concentration study. Figure 34 shows the isotherm for selenate loading in the initial concentration range of 0.5-1539 ppm Se. The graph shows the final loading in units of mg Se/g on the left axis. The pseudo-equilibrium loading in units of mmol/g is shown on the right axis. As seen, selenate loading increased sharply from 0.05 to 50.3 mg Se/g (equal to $5.70X10^{-4}$ to 0.64 mmol/g) as initial Se concentrations were varied from 0.5 to 514 ppm Se. Selenate loading further increased up to 64.3 mg Se/g from an initial concentration of 870 ppm Se and leveled off at 70.2 mg Se/g. The initial Se concentration was 1258 ppm Se at this point. At an initial concentration of 1539 ppm Se, 71.1 mg Se/g was adsorbed corresponding to 43.5% selenate removal. The selenate loading of 71.1 mg Se/g (0.90 mmol/g) was considered the maximum experimental loading of aged-FS for selenate. Based on the chemical formula of aged-FS ($[Ca_{4.02}Al_{2.03}(OH)_{12.1}]\cdot[Cl_{1.30}(CO_3)_{0.33}\cdot 8.40H_2O]$), the maximum capacity for selenate

loading is 1.02 mmol/g, assuming that only chlorides are exchanged. Note that, the theoretical loading capacity of aged-FS was based on the chloride content.

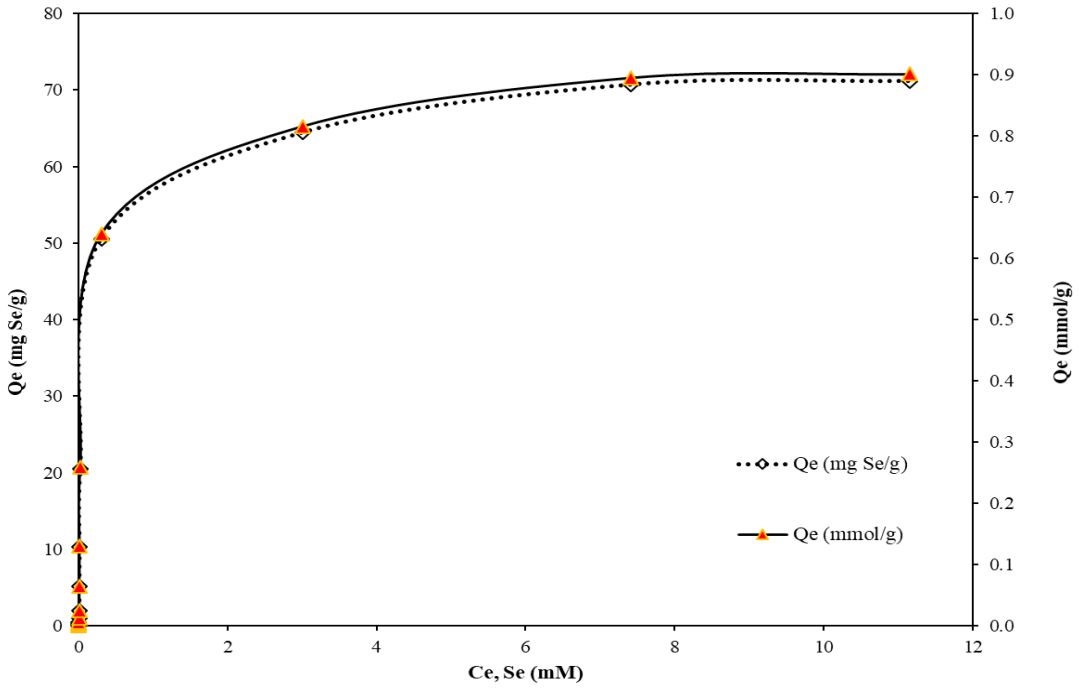

Figure 34 Adsorption isotherm of selenate by aged-FS obtained from concentration studies (Se initial concentration: 0.5-1539 ppm, initial pH 12.0, L/S 100, 24 h, and 30 °C).

6.2.7.2 Adsorption isotherm models fit with concentration data points

The Langmuir and Freundlich models were applied to the concentration data in the range of 0.5-1539 ppm, as shown in the left side of Figure 35. The logarithmic isotherm is shown on the right side of Figure 35. From the left side figure, the experimental data points fit better to the Langmuir model rather than the Freundlich model. However, the logarithmic isotherm on the right side shows that the Langmuir isotherm matches better for high- concentration data points (the last four data points at initial concentration 514 to 1539 ppm Se). In L/S studies, it was shown earlier that the Langmuir model matched better with experimental data points at low L/S region 20-200 (the first four data point in Figure 28). It appears that the surface of aged-FS was covered with a monolayer

of selenate oxyanions instead of stacks of selenate layers at high concentrations. As was discussed before for the pH-effect studies (6.2.1.2), that at higher concentrations, the principal loading mechanism is most likely ion exchange in the interlayer space. At higher concentrations, selenate replaced almost all of the chloride anions in the adsorption sites of the interlayer space, resulting in a good fit with the Langmuir model. In the low-concentration range, loading of selenate in the interlayer region is not still complete and chloride anions are only partly replaced by selenate. In this region loading of selenate does not really fit with a Langmuir model. In summary, the Langmuir model fit with the experimental data of the concentrations studies is limited to the low L/S and high concentration region. This is illustrated better by plotting a complete adsorption isotherm in the next section.

Table 27 shows the adsorption constants for the Langmuir model. The b parameter in the Langmuir model was calculated to be 0.14. This parameter refers to the strength of adsorption.

Table 27 Langmuir and Freundlich constants for selenate loading on aged-FS in Se concentration studies (0.5-1539 ppm Se)

Langmuir constants		**Freundlich constants**		
Q_m (mg Se/g)	b(mM^{-1})	A (mg/g)	1/n	n
69.4	0.14	12.3	0.28	3.62

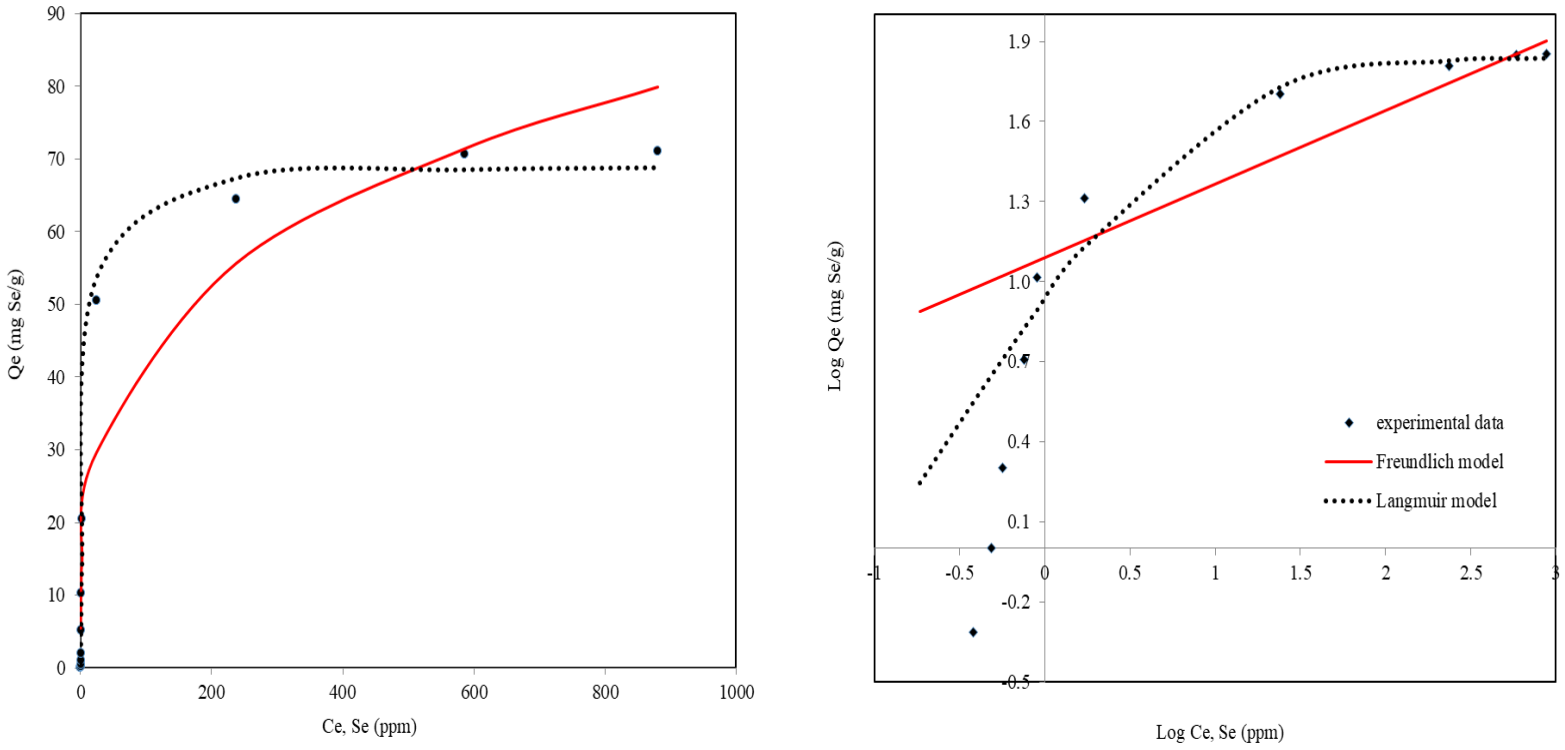

Figure 35 Adsorption isotherm fit with models at concentration studies (0.5-1539 ppm Se, initial pH 12.0, L/S 100, 24 h, and 30 °C).

6.2.7.3 Complete adsorption isotherm

Figure 36, shows an entire adsorption isotherm for selenate loading by a combination of L/S (diamonds) and concentration data points (crosses). As explained before, the Langmuir isotherm was a better fit than Freundlich isotherm, therefore here only the former is applied to the data. Overall, as seen in Figure 36, the two sets of data points did not fit with one single Langmuir isotherm.

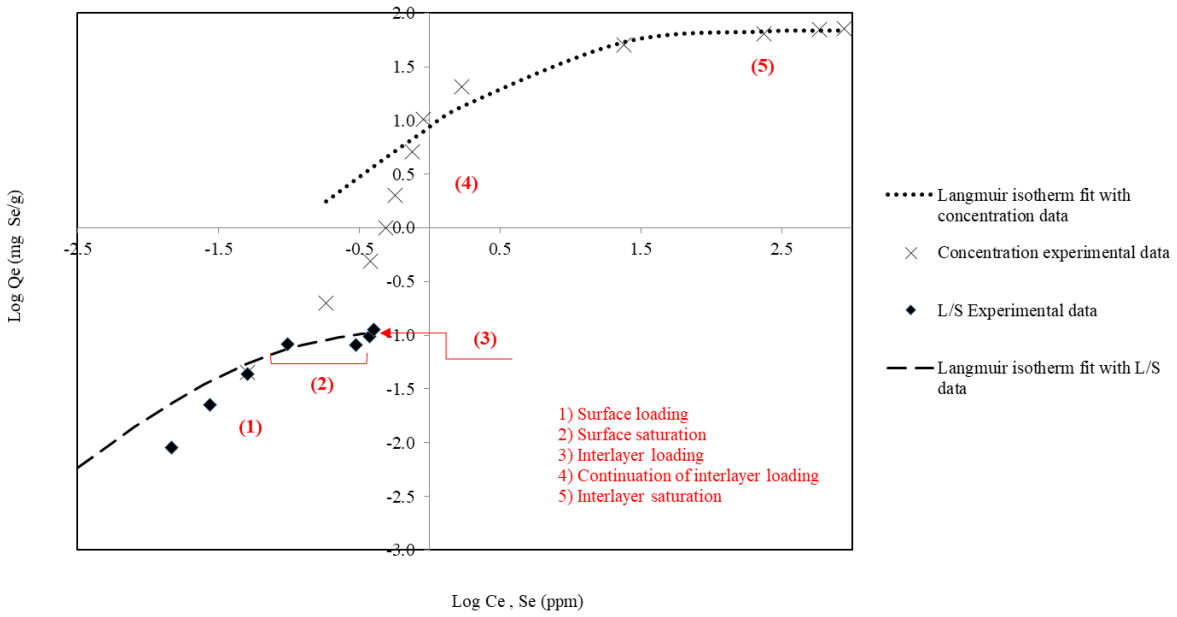

Figure 36 Complete adsorption isotherm fit with the Langmuir models (L/S 20-200, concentration 0.5-1539 ppm, initial pH 12.0, 30 °C, and 24 h).

As discussed before in 6.2.2.4, the Langmuir isotherm fit with low L/S region data points (dashed line in Figure 36). The high-concentration data points continued smoothly from the initial ppb-level data points, to reveal an S-shaped curve. The three closely clustered points at log $Q_e \approx -1$ (ppb-level points; diamonds) appear to be below the combined isotherm curve. This suggests that loading in these cases did not attain the expected levels. By this point in the loading process, the surface layers appeared to be nearly saturated; further loading would have had to access the

interlayer sites. With the very low concentrations of Se available in solution, the driving force for diffusion into the interlayer region might not have been sufficient to achieve this within the reaction time available. At high concentration of selenate in solution, a new Langmuir isotherm started to fit the experimental data (dotted line in Figure 36). As just suggested, this division of loading into two distinct regimes can be explained by surface adsorption and interlayer loading mechanisms of LDH materials [25,33].

Region (1) in Figure 36, corresponds to the ppb range (low L/S) data (L/S 20-200). The probable loading mechanism in this area is the surface loading. For ppb concentrations of Se, the concentration of Se in the solution are very low and loading mainly occurs on the surface of the aged-FS material. A monolayer of selenate oxyanions forms on the surface, which fits with the Langmuir isotherm (dashed line in Figure 36). As L/S was increased, the loading on the surface increased until it reached saturation (L/S 200-400, area (2) in Figure 36). After surface saturation, the adsorption on interlayer sites started (L/S 400-1200, area (3) in Figure 36) and loading increased again.

With the continued increase in C_e, the interlayer loading continued. The experimental data points in the area (4) in Figure 36 did not match with any isotherm. At high solution Se concentration (area labeled (5)) in Figure 36, the saturation of selenate loading in the interlayer space probably forms a monolayer of selenate oxyanions in the interlayer space. In this region, the experimental data fitted again to a new Langmuir isotherm (shown as a dotted line in Figure 36).

The XRD patterns of Se-loaded FS samples obtained from ppb Se feed solution are shown in Figure 37. The XRD pattern of aged-FS is shown at the bottom of Figure 37 for comparison. As seen, in general, the XRD patterns of FS samples after selenate loading (in L/S 20-1200 region)

are similar to the diffraction pattern of aged-FS. The diffraction peak at low 2θ is representative of basal spacing (c') in LDHs (see 2.2). The intensity of this diffraction peak (labeled * in Figure 37), remained unchanged with increased Se loading. For all samples, this peak exhibited a slight shift to the lower 2θ values, the effect being greatest for samples from L/S 400, 800 and 1200 experiments.

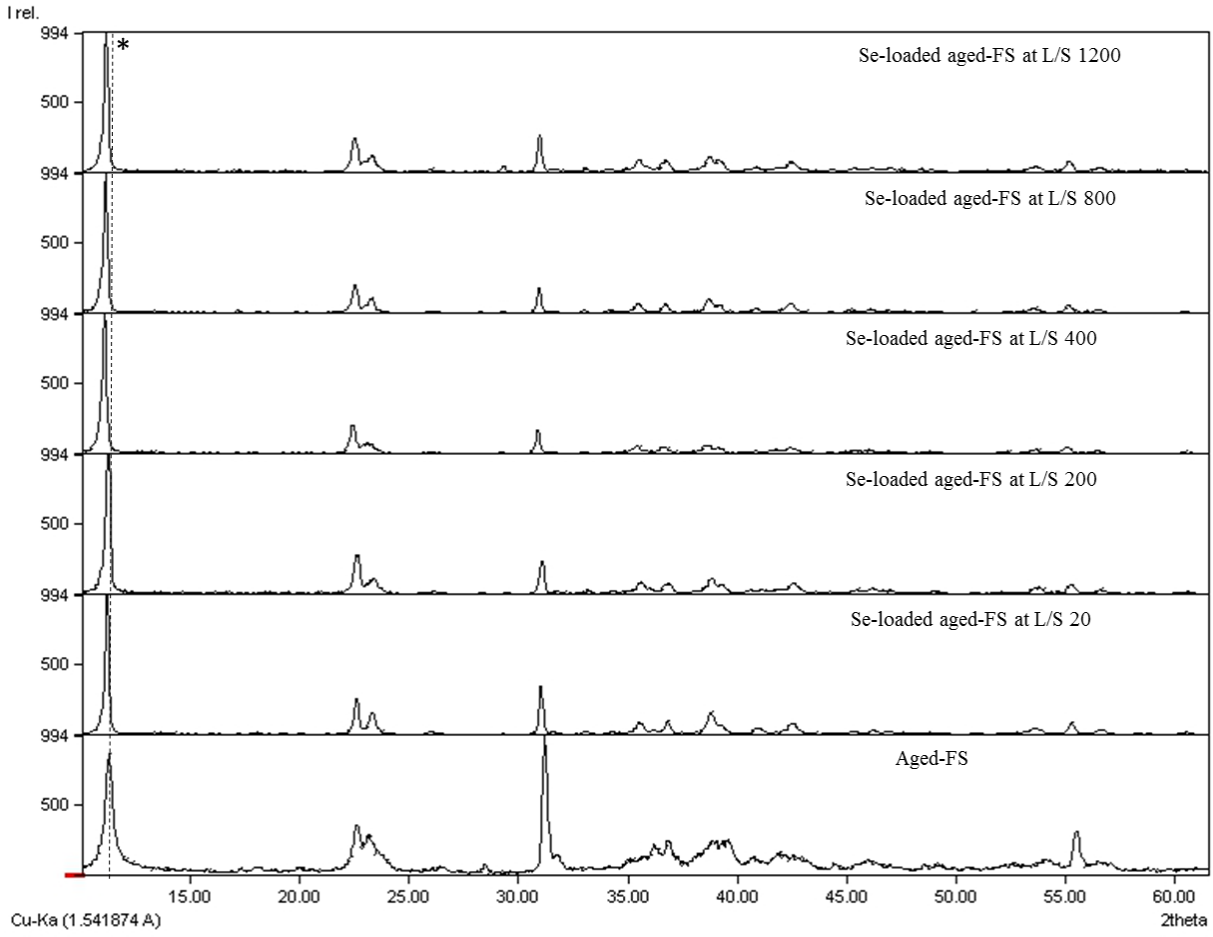

Figure 37 XRD patterns of aged-FS samples loaded by Se at L/S 20-1200 in ppb range Se feed solution (460 ppb Se, initial pH 12.0, 150 RPM, 24 h and 30 °C).

The XRD patterns of Se-loaded FS samples from ppm-level solutions (concentration studies) were different than those of the ppb-level tests. The results are shown in Figure 38. As seen, an obvious broadening of basal spacing diffraction peak (labeled * in Figure 38) and the non-

basal diffraction peak (at 2θ 23°) occurred. Selenate loading from ppm Se feed solution is associated with a larger loading of selenate oxyanions in the interlayer space. Compared to Figure 37, the diffraction peaks shifted more to lower 2θ region. This shift is related to the different van der Waal's diameters of selenate and chloride [25]. The chloride and selenate anions have van der Waal's diameters of 0.3 nm and 0.5 nm, respectively. The exchange of the smaller chloride anions for the larger selenate anion in the interlayer region resulted in the expansion of interlayer spacing (c') and shifted the basal spacing diffraction peak to lower 2θ values [25].

In conclusion, the shift of basal spacing diffraction peak to lower 2θ values for Se-loaded FS samples from ppm solution (Figure 38) was more than that for the Se-loaded FS samples from ppb-level solution (Figure 37). This indicates that the basal spacing expanded more as a result of more selenate loaded in the interlayer region. This is consistent with loading first on surface sites, followed by loading on interlayer sites.

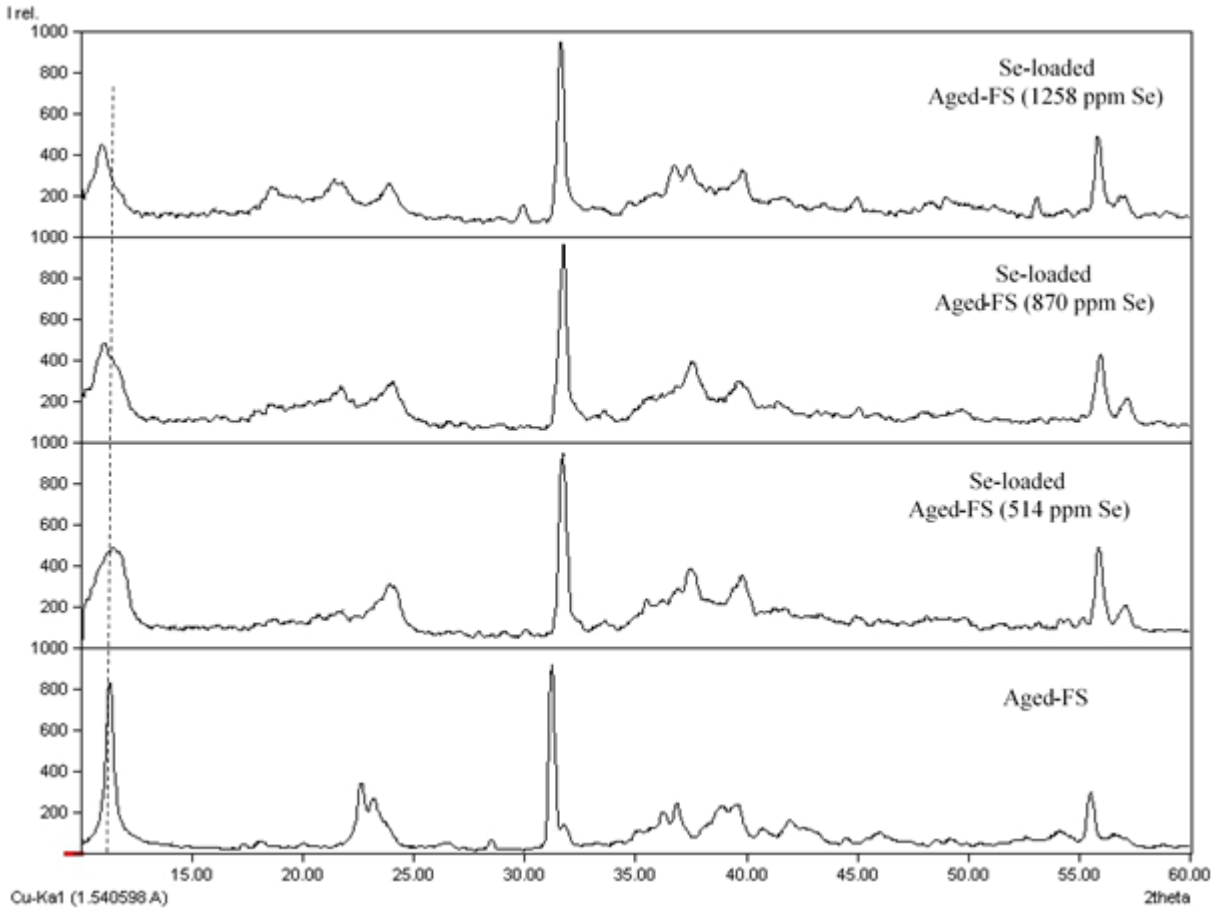

Figure 38 XRD patterns of aged-FS samples loaded by Se at concentration studies (initial pH 12.0, L/S 100, 24 h, and 30 °C).

6.2.8 Comparison of Se loading by aged-FS and loading data of Wu's FS.$_{sint}$. (from Wu's work)

In this section, the selenate adsorption by aged-FS and loading data from Wu's study are compared. In the upper part of Table 28, the selenate removal experimental conditions from Wu's study are shown (20-600 ppm Se, 30 °C, L/S 500, 150 RPM, and initial pH 8.0) [25]. Selenium removal was reported to be 98.0, 82.0 and 48.0% at initial concentrations of 20, 99 and 395 ppm Se, respectively. The loading data were derived from Wu's work and corresponds to Se_L in this work, with the assumption of no dissolution of the adsorbent [25]. Since there was no report on

dissolution data of Wu's FS.$_{sint}$. during adsorption experiments, the final mass of Wu's FS.$_{sint}$. in Q_e term had to be assumed to be equal to its initial mass.

Table 28 Selenate loading data in Wu's work (L/S 500, initial pH 8.0, 1 h, 150 RPM, and room temperature) [25]

Selenate loading by Wu's FS.$_{sint.}$ (from Wu's paper)						
Initial Se (mM)/ppm	Se.$_L$%	Se mass loaded (mg)	Experimental loading (Q_e) assuming no dissolution (mg Se/g)	Maximum available loading if 100% Se adsorbs, assuming no dissolution (mmol/g)	Experimental loading (Q_e) assuming no dissolution (mmol/g)	Experimental loading (Q_e) with dissolution included (mmol/g)
0.25/20	98.0	0.970	9.67	0.13	0.12	not available
1.25/99	82.0	4.05	40.5	0.63	0.51	
5.00/395	**48.0**	**9.48**	**94.8**	**2.5**	**1.2**	
7.60/600	36.1	10.8	108	3.8	~1.4*	
Results of one loading test with aged-FS under conditions used by Wu (refer to parameters in bold above).						
Initial Se (mM)/ppm	Se.$_L$%	Se mass loaded (mg)	Experimental loading (Q_e) assuming no dissolution (mg Se/g)	Maximum available loading if 100% Se adsorbs assuming no dissolution (mmol/g)	Experimental loading (Q_e) assuming no dissolution (mmol/g)	Experimental loading (Q_e) with dissolution included** (mmol/g)
5.1/403	21.2	4.27	42.7	2.55	0.55	0.78

*: Maximum experimental capacity reported for Wu's FS.$_{sint.}$,

**: Average of Ca.$_{LB}$ and Al.$_{LB}$ used for final mass (32.6% dissolution)

Assuming no Wu's FS.$_{sint.}$ dissolved, Q_e was calculated to be 9.67, 40.5, and 94.8 mg Se/g, respectively for Wu's adsorbent. The maximum experimental loading was 108 mg Se/g equal to ~1.4 mmol/g [25]. The maximum experimental loading of selenate by Wu's FS.$_{sint}$. was higher than the maximum experimental loading of aged-FS (71.1 mg Se/g equal to 0.90 mmol/g).

Wu's FS.$_{sint}$. did have a higher loading than aged-FS. While Wu did not report the dissolution of material to be an issue, it was clearly mentioned that Ca and Al dissolved as evidenced by the buffering capacity of the material [25]. Therefore, the assumption that none of the adsorbents dissolved is invalid; actual loading might be higher.

The lower loading of aged-FS than Wu's $FS._{sint.}$ can possibly be related to a higher carbonate content of the aged-FS material. Aged-FS has 3.0 wt.% carbonate but the carbonate content of Wu's $FS._{sint.}$ was not reported (likely very low). The experimental loading of Wu's $FS._{sint.}$ was probably about or slightly above 1.37 mmol Se/g (Table 28; assuming no dissolution of the adsorbent). This is still lower than the theoretical capacity for pure FS (the chloro-hydrocalumite) of 1.78 mmol/g. It suggests the possibility of some carbonate in Wu's $FS._{sint.}$ material. Wu showed that his $FS._{sint.}$ contained some carbonate (by FTIR) [25]. It is believed that the experimental loading of 1.37 mmol/g should be compared to the theoretical capacity of Wu's $FS._{sint.}$ (based on the chloride content) the material with loaded carbonate and not pure FS. It is the chloride ions that are exchangeable.

The exact composition of FS material Wu was dealing with is not clear to us (in terms of chloride and carbonate proportion). The material is FS, but the exact carbonate intercalated in the composition is unclear. Therefore, it is hard to know if the materials we were dealing with (aged-FS) is the same/very similar to the FS material, used by Wu. Next, there was an attempt to find a better way to compare the loadings of two materials, and therefore, one experiment from Wu's work was performed using aged-FS.

At the bottom part of Table 28, selenate removal by aged-FS under one experimental condition from Wu's paper is shown. The experiment involved an initial concentration of 395 ppm Se (5 mM Se), selected for replication of one of Wu's sets of conditions (L/S 500, initial pH 8.0, 2 h, 150 RPM, and room temperature). A feed solution was prepared by the dissolution of sodium selenate in DI water. The feed solution was analyzed by ICP and reported to contain 403 ppm Se, close enough to the target value. Initial pH was adjusted to 8.0 by addition of 1 M sodium hydroxide. A 0.1 g sample of aged-FS was added to 50 mL of this solution and agitated at 150

RPM for 2 h. After phase separation, it was found that 21.2% of the Se loaded. Selenate loading of 48.0% was reported by Wu under very similar experimental conditions. As shown in Table 28, the experimental loading (Q_e) assuming no dissolution of the adsorbent for Wu's $FS._{sint}$. and aged-FS were 1.20 and 0.55 mmol/g, respectively. Aged-FS exhibited lower loading than Wu's $FS._{sint}$. regardless of the final masses of the adsorbents. The experimental loading (Q_e) including consideration of dissolution for aged-FS was 0.78 mmol/g. This data is not available for Wu's $FS._{sint}$. material.

As mentioned in 3.2.4.7.5, in addition to selenate loading, the mass loss of the ion exchanger is also of great importance. For the adsorption test with aged-FS reported in Table 28, an average LBM mass loss of 32.6% ($Ca._{LB}$: 34.1 and $Al._{LB}$: 31.2%) was calculated. This is very substantial and probably not acceptable for industrial applications. The extent of dissolution of Wu's $FS._{sint}$. material under the experimental conditions of Table 28 is not known.

6.2.9 Summary of selenate adsorption by aged-FS

Aged-FS material prepared in this work showed a maximum selenate loading of 0.90 mmol/g (71.1 mg Se/g) from solutions with up to 1539 ppm Se. The following experimental conditions are recommended for selenate adsorption with aged-FS based on the trying to maximize *loading* and *minimize dissolution*: initial pH 12.0, L/S 200, 30 °C, 24 h, and adequate agitation (150 RPM).

a. Initial pH of 12.0 is recommended in order to lower dissolution. Higher pH decreased loading due to interference from hydroxide. The maximum selenium loadings from 134 ppm and 460 ppb Se solutions were ~98% and ~79%, respectively. As seen, the affinity of aged-FS for selenate in very dilute solutions is high. This is a potentially positive outcome for using these materials in selenate impacted wastewaters particularly the ppb levels solutions.

b. A liquid-solid ratio of L/S = 200 was selected as suitable L/S for maximum loading and minimum dissolution. Selenium loading from very dilute Se feed solutions (460 ppb Se), resulted in 0.082 mg Se/g adsorbed (79% removal) while the average aged-FS dissolution of 11.9% under these conditions, was measured. An L/S of more than 400 is not recommended for selenate adsorption studies due to the substantial dissolution of aged-FS.

c. Temperatures higher than 30 °C can be applied only if alkaline-resistant containers are used. Adsorption of selenate reached to a pseudo-equilibrium after 24 h, and at a stirring rate of 150 RPM. More time for the reaction was not deemed to be of significant benefit. Polypropylene containers are not recommended for selenate-loading experiments due to adsorption losses to the container walls. HDPE containers seem to be more suitable than Pyrex glass for higher temperature work.

6.3 Oxyanion interferences; sulfate and carbonate competition with selenate (surface loading region)

One of the important aspects of the IX process is the interference of other ions with the adsorption of the target ion. Selenium IX methods frequently suffer from low loading capacities due to competing ions, especially sulfate. Generally, the anion interference depends on the type, charge, concentration of the anion, LDH type (e.g. calcined or uncalcined), and the type of target oxyanion [44,64]. The interference of carbonate and chloride with chromate oxyanion adsorption on Friedel's salt was reported by Dai [33]. At a carbonate-to-chromate molar ratio of 1:1 (2 mM $NaHCO_3$), a 7.2% reduction in chromate adsorption was observed (from 97% to 90%; pH 10, L/S 250, 30 °C, and 24 h). At a chloride-to-chromate molar ratio of 1:1 (2 mM NaCl), chloride showed no interference with chromate loading. The material prepared by Dai was a modestly carbonated Friedel's salt with a chemical formula of $Ca_{3.6}Al_2(OH)_{11.2}Cl_{1.9}(CO_3)_{0.05}(H_2O)_{3.8}$ [33], which he

called pure Friedel's salt [33]. It would be better to call it a chloro-carboaluminate hydrocalumite phase.

In general, multivalent anions have more affinity for LDH materials than monovalent anions. Among the monovalent anions, the competition of hydroxyl anion with selenate loading for adsorption on aged-FS was observed at $[OH^-] \geq 0.16M$ (pH≥13.2, see Figure 21). Sulfate is the main interfering anion of concern and may exist at several orders of magnitude higher concentration than the Se concentration in mining wastewaters (e. g., 100-300 ppb Se and 1400-2000 ppm SO_4^{2-} in coal mining wastewater) [88]. Carbonate can also exist in industrial mine treatment applications. The interference of sulfate and carbonate with selenate loading on aged-FS was studied at various molar ratios.

6.3.1 Sulfate competition with selenate

The effect of sulfate oxyanion on the removal of selenate from solution was studied by the addition of calcium sulfate to the solution. Many industrial (mining) waste solutions are high in calcium sulfate content. In principle, the Ca^{+2} in solution should also lower solubility of the aged-FS. This is discussed later in 6.3.6. The aged-FS dissolution is not studied in oxyanion competition experiments.

The selenate removal change by aged-FS over increasing the sulfate concentration is shown with black circles in Figure 39. Selenate loading in the presence of various sulfate concentrations showed that sulfate has a minor interfering effect on the adsorption of selenate by aged-FS. Sulfate was added to the solution.

In the absence of any sulfate oxyanion, the selenate adsorption from a 760 ppb solution was 78.9%. The addition of sulfate at 800 times the molar concentration of selenate, lowered the selenate adsorption to 71.4% (only a 9.5% reduction). Selenate adsorption from solutions having

sulfate-to-selenate molar ratios of 800-3,000 was further reduced only slightly. At a sulfate-to-selenate molar ratio of 3,000 times (~2,500 ppm SO_4^{2-}), 67.3% loading of selenate was observed.

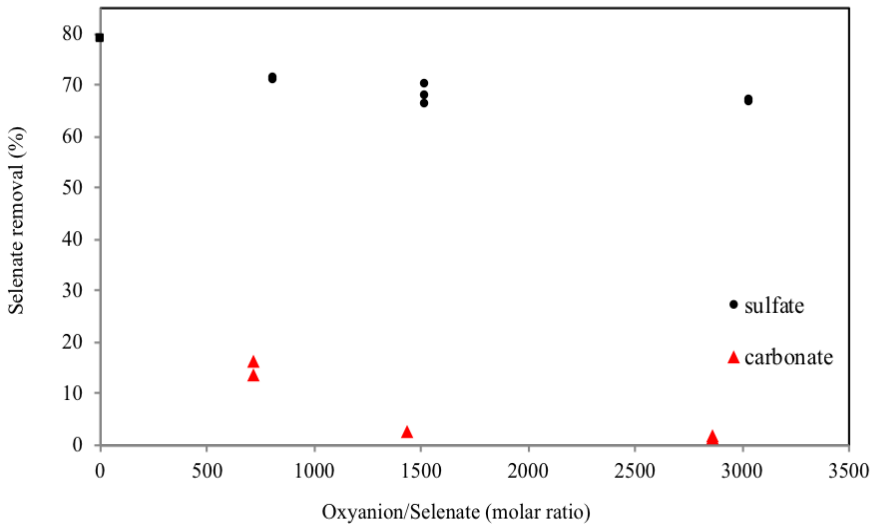

Figure 39 Oxyanion interference with selenate adsorption by aged-FS (Se feed: 763 ppb Se, initial pH 12.0, L/S 200, 24 h, 150 RPM, and 30 °C)

The competition of sulfate and selenate for adsorption on LDH materials is compared with literature studies next. In a study on cement hydrate products, performed by Baur et., al., the substitution of sulfate in a monosulfate-rich cement by selenate was reported [40]. The monosulfate with a chemical formula of $[Ca_4Al_2(OH)_{12}]\cdot[SO_4\cdot 8H_2O]$ is a sulfate-hydrocalumite. The study showed that adsorption of selenate by the sulfate-hydrocalumite was favorable, which is indicative of sulfate substitution by selenate. On the other side, sulfate substitution from an ettringite phase by selenate was reported to be less favorable. This ettringite phase ($[Ca_6Al_2(OH)_{12}]\cdot[(SO_4)_3\cdot 26H_2O]$) has a column-like structure in which the sulfate oxyanion is located in the inter-channel spaces [40,89]. The monosulfate phase, as said before, belongs to the hydrocalumite family with a layered hexagonal structure. Compared to the ettringite structure, in which the sulfate oxyanion is held strongly in the column-like structure, the sulfate oxyanion in

the monosulfate is intercalated in the interlayer space. The sulfate in the monosulfate LDH is, therefore, more amenable to the substitution by selenate.

In agreement with Baur's study [40], the aged-FS hydrocalumite material showed a higher affinity for adsorption of selenate over sulfate. Aged-FS can tolerate as high as 3,000:1 sulfate-to-selenate molar ratios without serious loss of affinity for selenate. It needs to be mentioned that the feed solution used in this part of the study contained just 763 ppb Se. With low Se concentrations, surface loading appears to be the principal loading mechanism. Therefore, it is perhaps better to say that sulfate did not interfere with surface loading of selenate at up to 3,000 times of molar concentration of selenate.

In a study by Yang, selenite uptake by calcined Mg-Al LDH (20 ppb Se feed) was studied in the presence of various sulfate-to-selenite molar ratios [64]. At a sulfate-to-selenite molar ratio of 1,000, selenite loading dropped from 110 mg/kg to 20 mg/kg (81% reduction). Yang reported that the sulfate interference with selenite loading was much higher than the effects of sulfate on arsenate loading. At a sulfate-to-arsenate molar ratio of 1,000, arsenate loading did not change (~120 mg/kg for sulfate-free and sulfate-containing solutions). Only at an extremely high sulfate-to-arsenate molar ratio of 100,000 did arsenate loading drop from ~120 mg/kg to ~85 mg/kg. Arsenate loading by calcined Mg-Al LDH was strongly preferred over sulfate [64].

In a study by Suzuki, sulfate-to-selenite molar ratios of only up to 100 were tolerated by a chelating CMA resin preloaded with Zr(IV) [37]. Aged-FS loading of Se(VI) tolerates higher concentrations of sulfate than the Zr-CMA resin. The adsorption of selenate by the anion exchange resin Eporasu K-6 showed a 50% decrease in selenate loading at a sulfate-to-selenate molar ratio

of only 2:1 [34]. In conclusion, the sulfate tolerance of aged-FS during selenate loading (from ppb level solutions) was among the highest of any adsorbents reported in the literature.

6.3.2 Carbonate competition with selenate

The effect of carbonate oxyanion on selenate loading is shown with red triangles in Figure 39. As shown, for the adsorption of selenate by aged-FS, carbonate exhibited greater interference than sulfate oxyanion. At a carbonate-to-selenate molar ratio of 700, selenate adsorption dropped from 78.9% to 15.0% (81% reduction). For a similar reduction in selenite adsorption by calcined Mg-Al LDH, a carbonate-to-selenite molar ratio of 70,000 was required [64].

The order of oxyanions selectivity for aged-FS is $CO_3^{2-} > SeO_4^{2-} >> SO_4^{2-}$. An opposite interference order was observed for selenite adsorption by Mg-Al-Cl LDH [42]; the oxyanion interference order was $HPO_4^{2-} > SO_4^{2-} > CO_3^{2-} > NO_3^-$. As carbonate is interfering with selenate loading, it is advised to lower the carbonate content of the solution before the adsorption process. For this, a lime softening process is recommended for carbonate removal before usage of FS in industrial plants.

It is important to mention that oxyanions interference studies in this thesis were carried out with very low (ppb) concentration solutions; just $4.8X10^{-7}$ M Se. Such low concentration selenate solutions require only a small proportion of the aged-FS capacity, and as mentioned, surface loading is the dominant loading mechanism.

From the oxyanion studies in this thesis, two series of studies are recommended for further future investigations: firstly sulfate interference studies with selenate in ppm concentrations and secondly carbonate interference studies at a carbonate-to-selenate molar ratio of <700.

Study of the competition of chloride with selenate for adsorption on aged-FS is recommended. In a study by Dai, the competition of chloride with chromate for adsorption on Friedel's salt was performed using 2 mM Cr(VI) [33]. At this concentration, the principle loading mechanism was reported to be surface loading (based on the basal spacing changes obtained from the XRD patterns). Chloride showed no interference with the loading of chromate on Friedel's salt [33].

6.3.3 The effect of intercalated-carbonate content on Se loading (selenate adsorption by unaged-FS)

Aging of FS was shown to impose several physiochemical changes on the material including an increase in carbonate content and consequently an increase in the proportion of the chloro-carboaluminate hydrocalumite phase. Significant interference of carbonate on the loading of the majority of oxyanions on LDH materials has been extensively reported in the literature [44,64,66]. Hongo et al. showed that the adsorption percentage of phosphate, selenate, arsenate and chromate oxyanions by Mg-Al-CO_3 LDH was significantly lower than Zn-Fe-SO_4 LDH [66]. The carbonate oxyanion with a planar geometry (as shown in Figure 19), intercalates in the interlayer space and is not easily displaced by other oxyanions [25,30,70]. Therefore, it was of interest to study the effect of the increased intercalated carbonate during aging on selenate loading. For these experiments, aged-FS and unaged-FS were used as the two samples had different carbonate contents. The selenate adsorption experimental conditions were 219 ppm Se feed, initial pH 12.0, L/S 200, 30 °C, and 24 h. Each experiment was repeated three times.

In Table 29 the loading of selenate onto unaged- and aged-FS ($Se._L$) are compared under the same experimental conditions. The results showed that Se removal percentage by aged-FS and unaged-FS is an average of 71.2% (70.7-72.0%) and 70.9% (70.8-71.0%), respectively.

Surprisingly, both materials removed the same amounts of selenate from solution; about 71% loading. Similar extents of removal of Se from solution, is expected to result in similar Se loading capacities. However, when the mass losses of the two adsorbents are taken into consideration, amount of Se loaded at pseudo-equilibrium (Q_e) for unaged-FS was 40.8 mg Se/g while that of aged-FS was 35.4 mg Se/g.

Table 29 Selenate loading ($Se._L$) of aged-FS and unaged-FS (experimental condition: 219 ppm Se, initial pH 12.0, L/S 200, 30 °C, and 24 h)

Test #	**$Se._L$; Aged-FS**	**$Se._L$; Unaged-FS**
1	72.0	71.0
2	70.9	70.8
3	70.7	-
Average	71.2	70.9
Se available for loading in feed solution (mmol)	0.14	0.14
Mass of FS used (g), intercalated carbonate wt.%	0.25 g, 3.00 %	0.25 g, 1.15 %
Dissolution %, $Al._{LB}$	$Al._{LB}$: 12.1% (12.0-12.2)	$Al._{LB}$: 22.0% (21.9-22.1)

Based on Equation 6 (section 3.2.4.7.4), Se loading at pseudo-equilibrium (Q_e) in this thesis is defined by loaded Se (from solution analysis: $Se._L$) divided by final mass (W). In contrast to the polymeric ion exchangers, the unaged-FS and aged-FS dissolve. These FS materials have different dissolutions and therefore different W values. In these cases, the role of final mass on loading needs to be interpreted carefully. The unaged-FS has higher dissolution (smaller W), and similar loading ($Se._L$) to aged-FS. This combination of loading and dissolution will result in a higher loading for any material. In fact, the higher loading of unaged-FS is due to the higher dissolution and not higher $Se._L$ value. The remaining Se concentration in the effluent for both materials is

about the same. Besides this view, one can interpret the data, only with a focus on the theoretical capacity of two materials. The unaged-FS with higher theoretical capacity than aged-FS (based on the chloride contents) exhibited higher loading. In conclusion, one needs to be careful with calling the unaged-FS a material with a higher loading capacity than aged-FS. The capacity of materials with different dissolutions will be affected by both Se loading and degree of dissolution. There is a balancing point between these two variables. In an industrial plant both loading capacity and material dissolution need to be considered.

The feed solution contained 219 ppm Se and the L/S ratio was 200 (0.14 mmol Se). In both cases, 0.39 mmol/g of Se was loaded. The experimental maximum loading of aged-FS is 0.90 mmol Se/g. There was more than enough chloro-hydrocalumite phase available to accommodate the loaded Se. Under these conditions, carbonate did not inhibit loading. Apparently, the increased intercalated-carbonate during the aging process did not interfere with Se loading under the conditions studied. Higher-concentration Se solutions would, of course, result in decreased Se removal due to carbonate pre-loaded in the solid phase. It would be reasonable to expect that ppb-level solutions would be even less affected by the intercalated carbonate content of aged-FS (surface loading is dominant), though this would need to be verified experimentally. In summary, the complete nitrogen purging method is advised if one needs to use the maximum capacity of FS material (highly concentrated feed solutions). For industrial applications where the capacity of aged-FS is adequate for loading of selenate from wastewater (ppb level solution), a complete nitrogen purging method will be an unnecessary effort. Similarly, aging in a sealed container without nitrogen purging (the method used in this thesis) is suitable enough for industrial applications in ppb level Se feed solutions.

In Table 29, the average $Al._{LB}$ dissolution of unaged-FS and aged-FS during selenate adsorption are shown. The average $Al._{LB}$ dissolution of aged-FS was lower than average $Al._{LB}$ dissolution of unaged-FS (12.1% vs 22.0%). The aged-FS dissolved less Al^{3+} ions into the solution than unaged-FS). For mass loss calculations of aged-FS in this test, the molar mass value of aged-FS (639.61 g/mole) was used in Equation 3 (see 3.2.4.7.2). Similarly, for mass loss calculations of unaged-FS in this test, the molar mass of unaged-FS (579.76 g/mole) was used in Equation 3 (see 3.2.4.7.2). Note that dissolution of Ca were not used for mass loss data since Ca dissolution at initial pH 12.0 was almost the same for two materials (similar to Figure 18).

6.3.4 Analysis of complete nitrogen purging method and its effect on selenate loading

As explained in section 4.3.2, the carbonate content of unaged-FS was reduced from 1.15 to 1.01 wt.% by using the complete nitrogen purging preparation method. The improvement with respect to carbonate incorporation was modest. The results in Table 29, were obtained using a 219 ppm Se solution; probably much higher than most mining wastewaters. Nevertheless, loading with aged-FS containing 3.0% carbonate was still very good at a high liquid-solid ratio of solution-to-adsorbent. Therefore the difficult challenge of eliminating carbonate during the co-precipitation synthesis might not be worth the effort for a practical application. Of course, high carbonate concentrations in solution relative to selenate do adversely affect loading.

6.3.5 Importance of dissolution data inclusion/report in adsorption capacity from an engineering perspective

If loading of a Friedel's phase adsorbent is calculated on the basis of the amount of anion adsorbed and the initial mass of adsorbent, loading values will be erroneously low due to losses of adsorbent to dissolution. The higher the extent of dissolution, the greater the error. However, the more serious problem is simply the extent of dissolution of the adsorbent. In an industrial process higher losses

of adsorbent increase the operating costs of the associated process. Release of metal ions into effluent solutions might be unacceptably high, which would require either follow-up treatment, or it could make the process impractical. The partial solubility of LDH adsorbents remains one of the challenges to industrial implementation of these materials for oxyanions removal. In the next section, an industrial strategy is recommended to minimize material mass loss.

Assuming that one needs to choose between unaged-FS and aged-FS for usage in a wastewater treatment plant, there might be a desire to select unaged-FS as this material has slightly higher loading than aged-FS (40.8 mg Se/g vs 35.4 mg Se/g). However, considering the preference for using a less-soluble material, aged-FS will be a better candidate. One of the contributions of this thesis in LDH filed is bringing up attention to the importance of mass loss values in loading data.

6.3.6 Non-saturated calcium hydroxide solution experiments; a strategy for lowering dissolution

As mentioned earlier in 6.3.2, the lime softening process has been recommended for carbonate removal before usage of FS in industrial plants. Lime softening has the benefit of removing carbonate from solution as well as increasing pH. In this section, the effect of calcium hydroxide on the dissolution of FS and Se loading are discussed.

In section 5.5.1, the aging process was shown to reduce the metal ions dissolution depending on the initial pH. At initial pH 12.5, Al dissolution of aged-FS ($Al._{LB}$) was lower than that of unaged-FS material by a factor of ~45% ($Ca._{LB}$ was similar). At initial pH 8.0, Ca dissolution of aged-FS ($Ca._{LB}$) was lower than that of unaged-FS material by a factor of ~50%. $Al._{LB}$ was lowered by a factor of 23%. In general, the dissolution of FS was lowered by the aging process, but not fully eliminated. The deliberate addition of calcium (in the form of calcium hydroxide) to the adsorption solution was the second alternative strategy used for minimizing the

material loss and lowering the metal ions dissolution. Even without a lime-softening pre-treatment step, many Se-containing industrial effluents contain moderately high calcium concentrations (typically associated with either carbonate or sulfate). The dissolution of aged-FS is expected to be lowered in a saturated calcium hydroxide solution due to the common ion effect.

Selenate adsorption by aged-FS from calcium hydroxide solution was performed under following conditions: feed 498 ppb Se, 708 ppm Ca, pH 12.3, L/S 200, 24 h, 30 °C and 150 RPM (see 3.4.9). The calcium hydroxide addition increased the pH of DI water to 12.3, and therefore there was no need for another alkaline reagent such as sodium hydroxide for pH adjustment. Calcium concentration in solution could no longer be used for mass loss calculations of these experiments. The concentration of aluminum was monitored and mass loss was reported using $Al._{LB}$. The adsorption experiment was repeated twice. For two experiments, an average $Al._{LB}$ value of 0.78% (0.65-0.91%) was obtained. The $Al._{LB}$ value under the same experimental conditions from a regular solution (no calcium hydroxide in solution) was found to be measured to be 8.9% (initial pH 12.2). However, the XRD pattern of selenate-loaded FS from calcium hydroxide solution, however, showed that a new phase was precipitated (Figure 40). As shown, a calcium aluminum hydroxide phase, called katoite with a chemical formula of $Ca_3Al_2(OH)_{12}$ was formed (PDF number 96-100-8061). The formation of katoite was related to the precipitation of dissolved aluminum and excess calcium in solution. Therefore the actual mass of FS material left after the tests is not known. A QXRD analysis would be needed to ascertain how much was converted to katoite. It is also quite possible that the conversion of LDH material into katoite might continue to occur with longer reaction times. As mentioned earlier in 2.6.1, using the BC water quality criteria, the concentration of dissolved aluminum in freshwater aquatic life should not exceed 0.10 ppm when the pH is greater than or equal to 6.5 (the maximum at any time is called the instantaneous

maximum value) [78]. The average Al concentration in the calcium hydroxide solution experiments was 0.073 ppm (0.064-0.087 ppm). Compared to the BC guideline, the dissolved Al concentration value was lower than the instantaneous maximum value (0.10 ppm), and just above the permissible maximum monthly average value (0.05 ppm). This shows that usage of the lime softening process has the benefit of lowering the FS dissolution and controlling the Al concentration close to the guideline. The average Al concentration for the adsorption tests without calcium hydroxide addition was 50.6 ppm (45.0-57.0 ppm) under otherwise similar conditions.

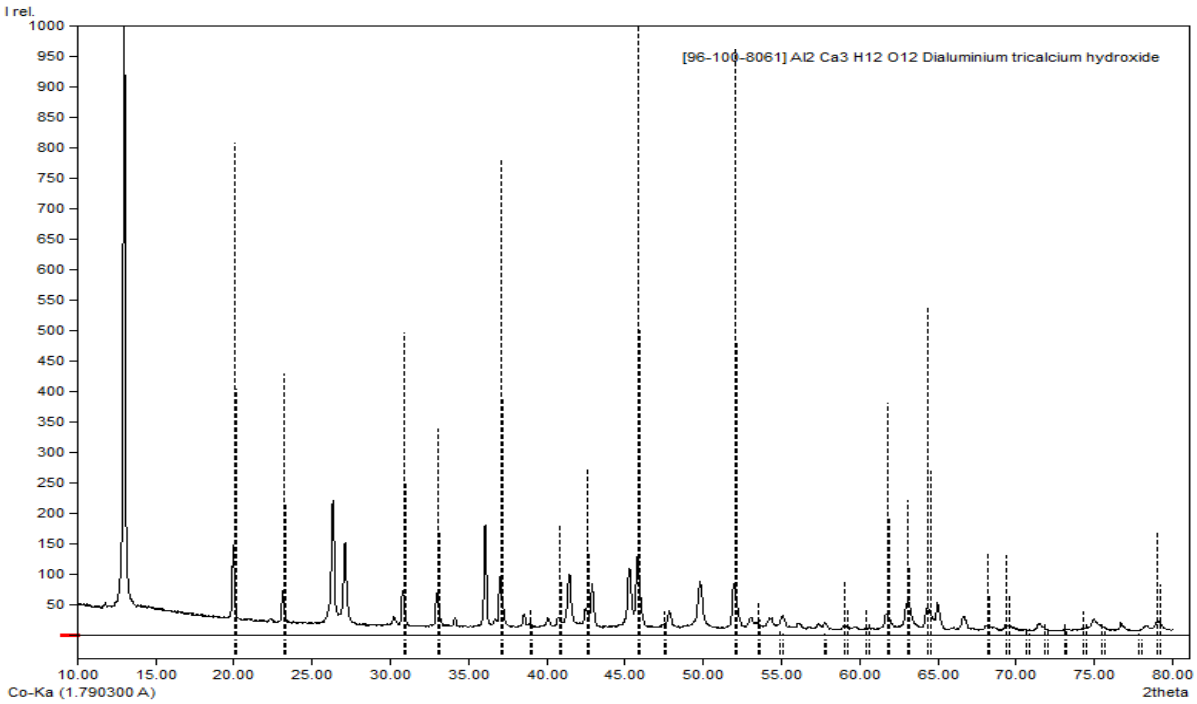

Figure 40 XRD pattern for selenate-loaded aged-FS from calcium hydroxide solution (498 ppb Se, 708 ppm Ca, pH 12.3, L/S 200, 24 h, 30 °C and 150 RPM). Katoite pattern is from Jade software.

Selenate loading from calcium hydroxide solution was calculated to evaluate whether lime softening would impact Se loading. For these experiments, the average selenate loading ($Se._L$) was 81.8% (79.0-84.6%). Selenate loading from a solution without added calcium hydroxide in

solution was measured to be 78.9%. This showed that aged-FS had about the same similar affinity for selenate when calcium hydroxide was present in solution.

6.3.7 Summary of oxyanion interference, intercalated-carbonate interference and calcium hydroxide matrix impact on the reduction of Al dissolution

In summary, added carbonate in solution significant interference with selenate loading onto aged-FS. Sulfate in the solution had very little effect on selenate loading. The oxyanion selectivity order for aged-FS is: CO_3^{2-}> SeO_4^{2-}>> SO_4^{2-}. The oxyanion selectivity of aged-FS for selenate over sulfate was 3000:1 selenate-to-sulfate. Therefore, aged-FS is a potentially selective ion exchange material for selenate removal from mining wastewaters with high sulfate contents. Most known ion exchangers exhibit little selectivity for selenate over sulfate [88]. In cases where carbonate is present in high concentrations, it may be possible to use a lime-softening pre-treatment prior to the application of the FS adsorption process. Such a pre-treatment would have the benefit of lowering the carbonate content as well as helping raise the pH.

Intercalated carbonate in the FS adsorbent does lower the total capacity for selenate. However, the materials prepared in this study still exhibited quite a suitable capacity for selenate.

In the case of using a lime softening process, the Al dissolution from aged-FS material will be lowered due to the high concentration of calcium ions in the matrix. $Al._{LB}$ dropped from 8.9 to 0.78% in the calcium hydroxide solution. However, this also appears to result in gradual conversion of FS into katoite. But, this did not appear to unduly compromise Se loading under the conditions employed in this work. There would be considerable cost savings associated with using lime for pH adjustment instead of NaOH. Furthermore, the use of lime softening as a pre-treatment to remove the carbonate content should minimize carbonate loading interference.

6.4 Calcination of aged-FS

The thermal treatment of the M-N LDH materials has been widely reported in the literature [44,49,64]. Generally, as the temperature is increased, dehydration, de-hydroxylation, and anion expulsion occur. The loosely held interlayer water, -OH groups from layers (M-OH-N), and interlayer anions are removed by calcination. Interestingly, the calcined sample is able to regenerate the layered structure on exposure to water and anions. This process is known as memory effect [44,58].

In this work, the aged-FS material was calcined in a furnace for 5 h at temperatures of 300-800 °C and the weight loss was recorded. The structural changes in the material were monitored by XRD analysis. By heating the samples, weight losses of 7.80, 25.7, 25.5, and 31.0 wt.% was observed at 300, 450, 600 and 800 °C, respectively. An XRD pattern of aged-FS and its calcined products are shown in Figure 41. The pattern at the bottom corresponds to aged-FS. The XRD patterns corresponding to increasing temperature for calcined samples follow from bottom to top (up to 600 °C). The XRD pattern of sample calcined at 300 °C showed a small shift in both sharp basal reflections at low 2θ and relatively weak non-basal reflections at high 2θ. These shifts are related to the dehydration and loss of interlayer water [44]. Further heating at 450 °C, resulted in the loss of crystallinity due to de-hydroxylation of the brucite layers. A largely X-ray amorphous phase was formed and resulted in a broad peak in the XRD pattern. The product recrystallizes at 600 °C, yielding a new metal oxide phase (top pattern in Figure 41). The XRD pattern of sample calcined at 800 °C was similar to that of sample calcined 600 °C.

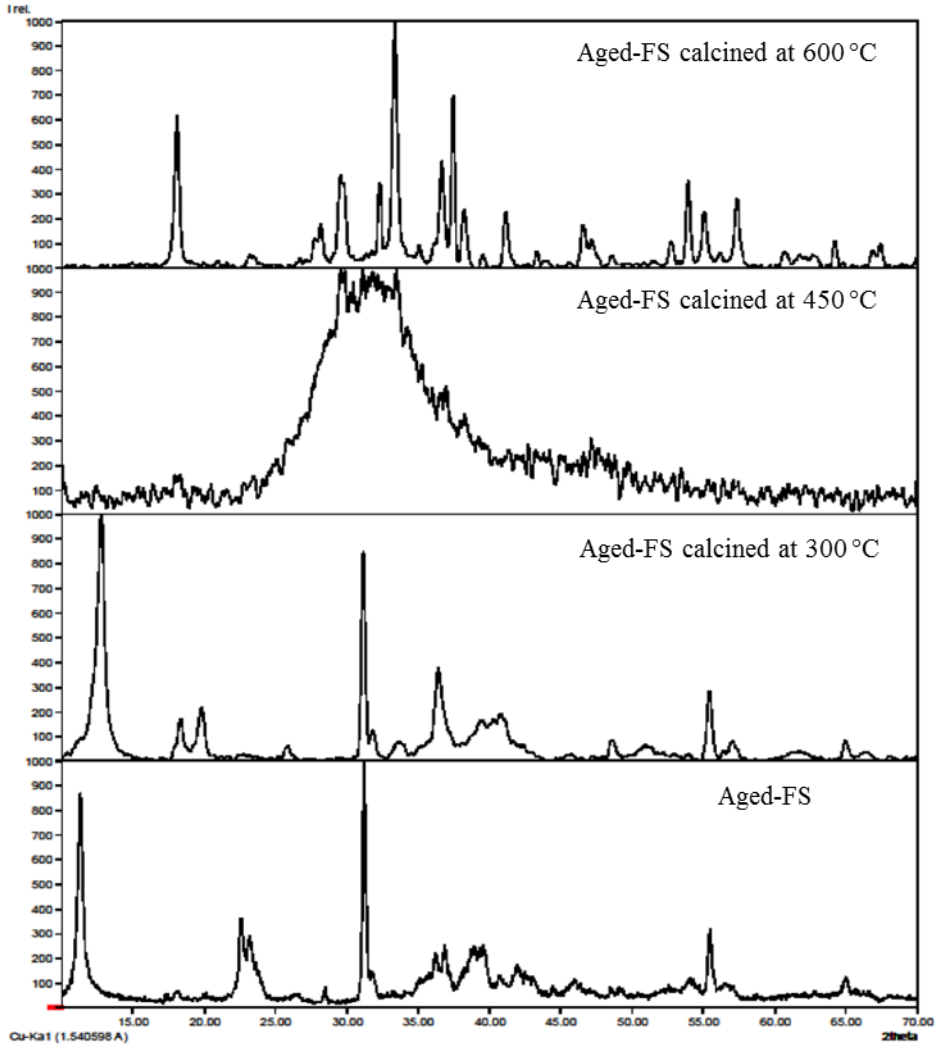

Figure 41 XRD pattern of aged-FS samples heated at different temperatures.

The XRD pattern of aged-FS calcined at 600 °C was further analyzed by Match software and the results are shown in Figure 42. The experimental pattern matches the mayenite phase ($Al_{14}Ca_{12}O_{33}$) with PDF number 96-210-2957 from the Match software. After subtraction of the pattern for the mayenite phase from the experimental pattern, the remaining phase (red pattern in Figure 42) matched with CaO with PDF number 96-900-8606 from Match software. The remaining XRD pattern after subtraction of patterns for both mayenite and CaO is shown in the

top pattern of Figure 42. This pattern did not match with any Ca or Al chloride-containing phase from the Match software database. However, this phase is believed to be a chloride-containing phase (Ca or Al) as there is no report of evaporation of chloride species from FS at high temperatures. The boiling temperature of $CaCl_2$ is reported to be 1650 °C [90]. Therefore, the aged-FS calcined at 600 °C is a mixture of mayenite, CaO, and a chloride-containing phase.

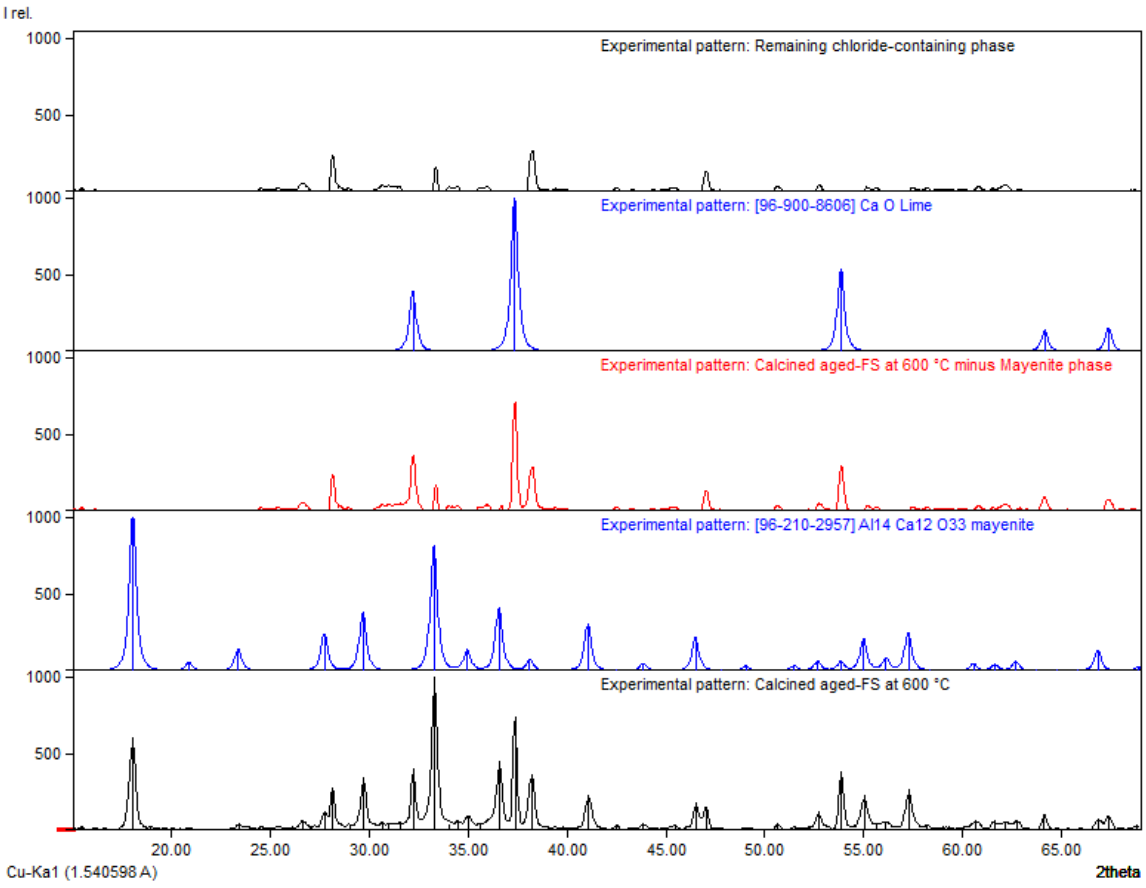

Figure 42 XRD pattern of calcined aged-FS at 600 °C matched with mayenite and calcium oxide from the Match software database.

The thermal analysis of Friedel's salt was studied by thermogravimetric analysis (TGA) [49,50]. Thermal studies performed by Birnin-Yauri showed three endothermic peaks at 120, 290, and 670 °C [49]. The thermal peak at 120 °C was attributed to the removal of interlayer water resulting in $3Ca(OH)_2 \cdot 2Al(OH)_3 \cdot CaCl_2$. Further heating to 290 °C formed an amorphous product

as a result of de-hydroxylation of layers. The amorphous phase turned to a crystalline phase with a chemical composition of ($11CaO{\cdot}7Al_2O_3{\cdot}CaCl_2$) at 670 °C. In another study by Vieille, the thermal behavior of Friedel's salt over the temperature ranges $25 \leq T \leq 280$ °C, $280 \leq T \leq 650$ °C, and $650 \leq T \leq 950$ °C was studied [50]. A similar three-step decomposition by heating was reported and followed by XRD measurements. The crystalline phase formed at 750 °C was related to a mixture of mayenite phase ($Ca_{12}Al_{14}O_{33}$) and CaO. The reports on phases formed at high temperatures in two studies are slightly different in terms of the Ca/Al molar ratios and chloride contents of the phases. For example, in Birnin-Yauri study, in addition to the $11CaO{\cdot}7Al_2O_3{\cdot}CaCl_2$ phase, a Ca-containing minor phase is expected to be present [49]. The Ca/Al molar ratio in $11CaO{\cdot}7Al_2O_3{\cdot}CaCl_2$ phase is 0.86, lower than that of Friedel's salt (unless the minor impurities of Friedel's salt are not reported). In Vieille's study, on the other hand, a chloride-containing phase is probably present [50]. As mentioned, chloride-species volatilization at this temperature is doubtful [90].

6.4.1 Effect of calcination on selenate adsorption

Studies on oxyanions removal by calcined and uncalcined LDHs in the literature report higher adsorption capacity for calcined LDHs [31,64]. Yang showed that selenite loading by calcined Mg-Al-CO_3 LDH was 140 mg Se/kg, while uncalcined Mg-Al-CO_3 had a loading of 70 mg Se/kg. The calcined Mg-Al LDH was obtained by heating of Mg-Al-CO_3 at 500 °C for 5 h [64].

In an attempt, to study the effect of calcination on the selenate loading behavior of aged-FS, adsorption tests were performed. Table 30 displays the selenate removal and loading (mmol/g) of calcined samples from 753 ppb Se feed solution (initial pH 12.1, L/S 200, 150 RPM, 24 h, and 30 °C, three tests each). The average of $Ca._{LB}$ and $Al._{LB}$ was used to estimate extents of dissolution. Selenate loading by aged-FS was performed under identical adsorption experiment.

The adsorption of selenate from a 753 ppb feed solution was carried out with samples calcined at all temperatures with the exclusion of the sample calcined at 450 °C. This sample was shown by XRD analysis to be an amorphous phase (see Figure 41) and in preliminary tests showed much lower adsorption capacity than the other samples.

The average selenate removal by samples calcined at 300 and 600 °C was 94.2% (92.6-95.5%) and 97.6% (95.8-98.6%), respectively. This showed that the calcination of material increased the affinity for Se loading. The reference material, aged-FS, removed 78.8% (78.5-79.0%) under similar experimental conditions. The calcined sample at 800 °C showed an average removal percentage of 99.8% (two tests both at 99.8%), higher than all of the other samples. The results showed that the calcination of the aged-FS sample at 800 °C increased the loading of selenate from 0.0160 mmol/g (for aged-FS) to 0.0207 mmol/g.

Table 30 Selenate loading percentage by calcined aged-FS (753 ppb Se feed, initial pH 12.1, L/S 200, 150 RPM, 24 h, and 30 °C)

		Aged-FS samples calcined at:			
	Aged-FS (not calcined)	**300 °C**	**450 °C**	**600 °C**	**800 °C**
Selenate loading (%)	78.8%	94.2% (92.6-95.5%)	Amorphous sample**	97.6% (95.8-98.6%)	99.8% (two tests both 99.8%)
Se loading (mmol/g)	0.0160	0.0190		0.0194	0.0207
FS dissolution* $Ca._{LB}$, $Al._{LB}$ (%)	7.10, 9.40	6.90, 7.01	-	6.01, 10.4	6.90, 10.6

*average LBM was used for Se-loading data**showed low Se-removal in preliminary tests

The higher loading capacity of calcined LDHs may be attributed to the larger surface area of these materials compared to the uncalcined LDHs [44]. The specific surface area of aged-FS as reported by Malvern Mastersizer laser instrument was 0.338 m^2/g (5.4.4). The porosity of material was ignored in the calculations of Malvern Mastersizer [86]. The surface area study of the calcined

aged-FS and aged-FS samples by Brunauer–Emmett–Teller (BET) method are recommended for future studies. In BET method, the surface area of a material is determined by the physical adsorption of a gas (typically nitrogen, krypton, or argon) onto the surfaces (internal and external) of the sample [91,92].

The average remaining selenium concentration in the final solution treated by aged-FS calcined at 800 °C was 1.84 ppb Se (1.70-1.98 ppb Se). This selenium level in a treated solution is lower than the maximum discharge limits set in 2016 by the US Environmental Protection Agency for lotic water (<3.1 ppb Se) [15]. As a result, the aged-FS sample calcined at 800 °C was a promising adsorbent for treatment of ppb level industrial wastewaters. As mentioned earlier in 6.2.7, the selenate removal from ppb levels has not been studied by Wu [25]. In this study, it was shown that the aged-FS sample calcined at 800 °C is a successful candidate for the treatment of ppb-level Se wastewaters.

Note that the dissolution of calcined aged-FS samples is similar to that of the aged-FS sample. The calcination process after aging has the benefit of higher loading and similar dissolution for the material. The structure and properties of aged-FS and calcined aged-FS samples are summarized in Table 35 (Appendix O).

6.4.2 The memory effect of calcined aged-FS sample

As shown in Table 30, the aged-FS calcined at 600 °C had higher loading than aged-FS. The XRD analysis of aged-FS calcined at 600 °C before and after selenate loading is shown in Figure 43. As seen, upon exposure of the calcined sample to selenate solution, the parent LDH structure of hydrocalumite is reconstructed (top pattern in Figure 43). The sharp basal reflection at low 2θ 11°, and weaker non-basal reflections at high 2θ 23°, all appeared in the top XRD pattern (a typical LDH pattern). The calcined aged-FS recovered its original layer structure through the structural

memory effect. Water is adsorbed to reform the hydroxyl layers and anions and water reconstruct the interlayer region. The adsorbed anions are most likely, selenate, hydroxyl, and chloride. The chemical composition of $[Ca_4Al_2(OH)_{12}]\cdot[Cl_{(2-2x-y)}(SeO_4)_x(OH)_y\cdot 4H_2O]$ is probably the best representation of the reconstructed phase. The memory effect has been used for the preparation of LDHs with desired inorganic or organic anions to fulfill specific applications [27,44,58].

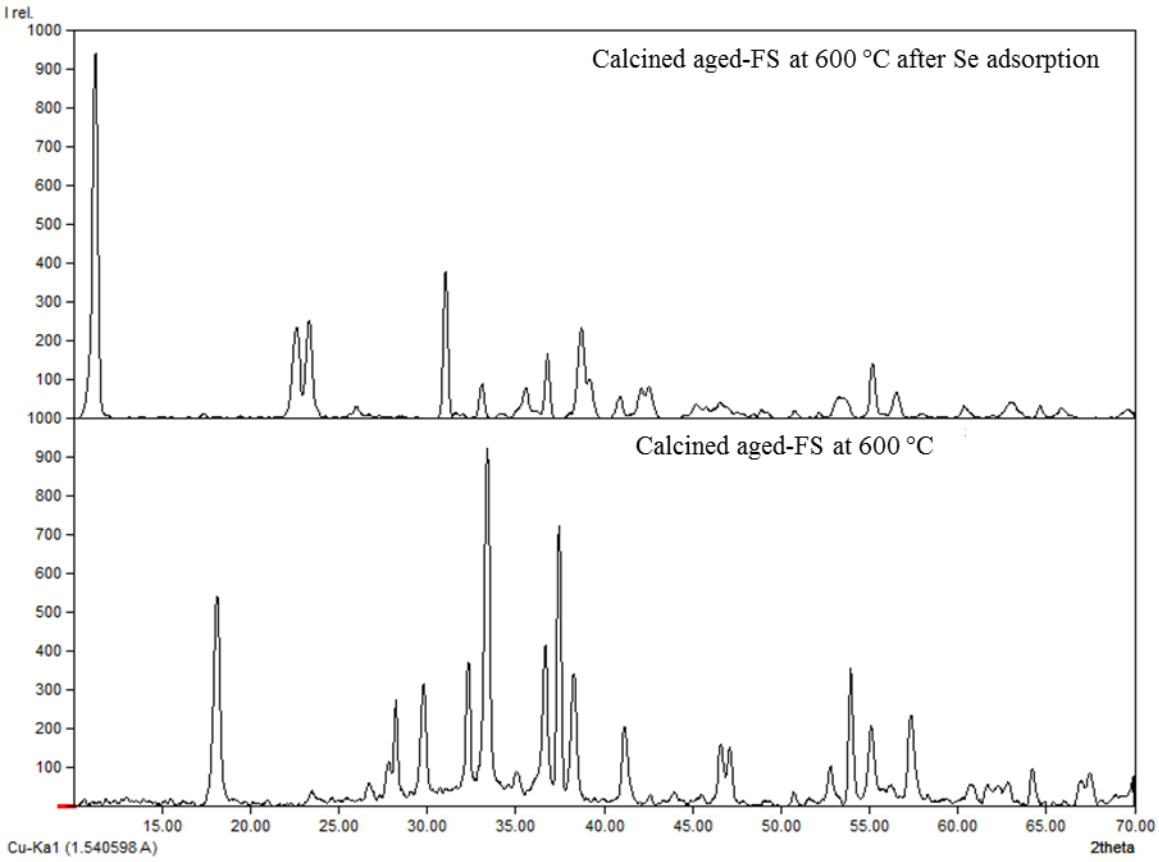

Figure 43 Reformation of the layered structure after selenate adsorption from 753 ppb Se feed (adsorption conditions: initial pH 12.1, L/S 200, 150 RPM, 24 h, and 30 °C). Bottom pattern: calcined aged-FS at 600 °C, and top pattern: calcined aged-FS at 600 °C after Se-adsorption.

Chapter 7: Conclusions

In this thesis, a partially carbonated Friedel's salt (unaged-FS) was synthesized and characterized. The carbonate content of the unaged-FS sample was lessened by variations in how a nitrogen atmosphere was employed. One selected aging condition was applied to minimize the dissolution of material during the selenate adsorption experiments. The aged-FS material was shown to have lower metal ions dissolution than unaged-FS, depending on initial pH. Therefore, the aged-FS material was used for selenate removal studies rather than unaged-FS material. The compositional changes associated with the aging process were tracked by various analytical methods. The lower dissolution of aged-FS was related to the observed compositional changes. The optimized adsorption condition was selected based on a trade-off between maximizing Se-loading and minimizing aged-FS dissolution. In the field of anion adsorption by LDH materials this thesis is a pioneer in reporting the dissolution of LDH material (aged-FS) connected with adsorption. For higher reliability, the mass loss was estimated by using the concentrations of calcium and aluminum in solution (LBM) rather than weighing the final mass of samples (SBM). The interferences of sulfate and carbonate oxyanions with selenate adsorption were investigated. The dissolution of aged-FS during the adsorption process was further minimized by using solutions saturated with calcium hydroxide.

The main conclusions are summarized in three sections: Section A: Synthesis process, Section B: Aging and dissolution studies and Section C: Selenate adsorption.

A. Synthesis process:

1. *Unaged-FS synthesis*: The unaged-FS sample was prepared by co-precipitation at nearly constant pH of 11.3 under partial nitrogen purging. The material was analyzed by XRD, QXRD, solid digestion, and carbon analysis. The QXRD results showed that the unaged-

FS contained multiple phases, including carbonated hydrocalumite; it was not a pure FS material. The unaged-FS material was composed of 74 wt.% chloro-hydrocalumite phase (a hexagonal crystal system with a chemical formula of $[Ca_4Al_2(OH)_{12}]\cdot[Cl_2\cdot 4H_2O]$), 24 wt.% chloro-carboaluminate hydrocalumite phase (a monoclinic crystal system with a chemical formula of $[Ca_4Al_2(OH)_{12}]\cdot[Cl(CO_3)_{0.5}\cdot 10.8H_2O]$), and 2 wt.% aluminum hydroxide ($Al(OH)_3$). Using QXRD analysis results, the unaged-FS was best represented by an experimental chemical formula of $[Ca_{3.88}Al_{2.09}(OH)_{12.1}]\cdot[Cl_{1.73}(CO_3)_{0.10}\cdot 5.27H_2O]$. The material had 1.15 wt.% carbonate. The carbonate content based on the preceding chemical formula worked out to be 1.06 wt.%. QXRD analysis showed that the carbonate was intercalated in the hydrocalumite phase and not physically adsorbed. The Ca and Al content (weight percent) calculated from QXRD results (26.8 and 9.71 % for Ca and Al, respectively) were in good agreement with the solid digestion data (25.3 and 9.03 % for Ca and Al, respectively).

2. *Lowering carbonate content by complete nitrogen purging:* Precautions to better exclude atmospheric CO_2 resulted in an unaged-FS material that contained 1.01 wt.% carbonate. In agreement with the carbon analysis, QXRD results (4.3.3.2) showed that the chloro-carboaluminate hydrocalumite phase with a chemical formula of $[Ca_4Al_2(OH)_{12}]\cdot[Cl(CO_3)_{0.5}\cdot 10.8H_2O]$) was reduced to 11 wt.% (more than 50% less than unaged-FS prepared under less rigorous inert-atmosphere conditions).

B. Aging and dissolution of aged-FS material:

1. *Aging tests:* The selected aging condition of initial pH 12.0, L/S 20, 65 °C and 7 days, was applied on unaged-FS material in a large batch. The variables of this aging process (L/S, temperature, and time) were selected to lower mass loss due to dissolution (5.2). Aging of

unaged-FS material at initial pH 12.0 resulted in the removal of the aluminum hydroxide impurity and formation of minor katoite phase (QXRD results, 5.4.1). In addition, the proportion of chloro-carboaluminate hydrocalumite phase increased (QXRD results, 5.4.1). The carbon analysis showed that the carbonate content increased as a result of the aging treatment (5.4.2). From QXRD results, the experimental chemical formula of aged-FS was found to be $[Ca_{4.02}Al_{2.03}(OH)_{12.1}]\cdot[Cl_{1.30}(CO_3)_{0.33}\cdot 8.40H_2O]$, (see 5.4.1.1). Aged-FS had an average experimental Ca/Al molar ratio of 2.02 (solid digestion).

2. *Quantification of the effect of aging on dissolution:* The aged-FS material was subjected to the conditions of a dissolution test, but without selenate being present (L/S 200, initial pH 12.5, RPM 150 and 24 h). The dissolution of Al from aged-FS was ~45% lower than that of unaged-FS. The dissolution of Ca from the two materials was about the same (5.5.1). In fact, the aging process assisted in removing the aluminum hydroxide impurity from the material prior to the adsorption process. Higher Al dissolution from unaged-FS was partly related to the presence of $Al(OH)_3$. Note that there was no $Al(OH)_3$ impurity in aged-FS material.

In the FS synthesis process, the formation of aluminum hydroxide impurity needs to be maintained at its minimum possible value (by careful pH control), and if not it will dissolve easily in the adsorption process and will cause the Al dissolution into water. More Al dissolution also means more material loss in the adsorption process. It needs to be added that both aluminum hydroxide and hydrocalumite phases were involved in Al dissolution from the unaged-FS sample (calculated from Al mass balance).

In summary, regardless of initial pH, the concentration of metal ions dissolved from aged-FS into solution was lower that of unaged-FS. In one hand, at high pH range (initial

pH 12.5), Al dissolution from aged-FS was lower than that of unaged-FS material by a factor of ~45%. On the other hand, at lower pH range (initial pH 8.0), Ca dissolution from aged-FS was lower than that of unaged-FS material by a factor of ~50%.

3. *Compositional change due to aging:* The higher stability of aged-FS (with respect to Al/Ca dissolution) was related to a combination of the physical/chemical changes in the material (5.5.2). First, the aluminum hydroxide impurity was removed and a stable minor phase of $Ca_3Al_2(OH)_{12}$ was formed. Secondly, the carbonate content was increased (from 1.15 to 3.00 wt.%) and more of chloro-carboaluminate hydrocalumite was formed. The insertion of carbonate with a planar geometry in the center of interlayer space was possibly forming more stable metal ions in the brucite layers. Over aging, particle agglomeration (5.4.4) and morphology changes into well-shaped hexagonal crystallites (5.4.3) were observed. It is hard to separate the impact of these variables from each other and therefore, lower dissolution of aged-FS is probably due to a combination of these factors. Undoubtedly, however, removal of the readily base-soluble $Al(OH)_3$ is significant.

C. Selenate adsorption:

1. The aged-FS material prepared by aging was used in adsorption studies. Dissolution data were reported for every adsorption experiment. To avoid the uncertainty associated with the collection of fine, powdery FS material (SBM), the concentration of Ca^{2+} and Al^{3+} ions in solution were used for mass loss estimates (LBM, using $Ca._{LB}$ and $Al._{LB}$). Selenate loading was referenced to the estimated actual mass of FS left at the end of adsorption tests. Loading isotherms were obtained. The loading isotherms are more accurate than those in the current literature due to the careful inclusion of mass loss impacts on the loading of

adsorbents. It is believed that this is the first investigation of LDH materials with consideration of partial dissolution of these materials in the adsorption process.

2. The adsorption experiments were performed to try to achieve the maximum selenate loading with the lowest dissolution of aged-FS. A maximum selenate loading of 71.1 mg Se/g equal to 0.90 mmol/g was achieved at initial pH 12.0, L/S 200, 24 h, 30 °C, and shaking rate 150 RPM. The theoretical capacity for this aged-FS material was 1.02 mmol Se/g (based on the exchangeable chloride ion). The highest selenate loading varied from 79% to 98% (depending on feed concentration). An average LBM dissolution of 11.0% was measured for aged-FS.
3. Selenate adsorption from ppb-level feed solutions was dominated by surface loading. With ppm-level feed solutions, the adsorption was dominated by an interlayer loading mechanism. The surface and interlayer loading mechanisms were confirmed by complete loading isotherm studies (Figure 36) and the XRD studies (Figure 37, and Figure 38).
4. Adsorption of selenate became close to equilibrium after 24 h (called pseudo-equilibrium) and at a stirring rate of 150 RPM. There was evidence of increased selenate adsorption as the temperature was increased from 30 to 60 °C.
5. Selenate loading by aged-FS was highly selective over sulfate loading. When the sulfate-to-selenate mole ratio was 3000 selenate loading dropped very little. The aged-FS material is considered to be a suitable and selective selenate adsorbent for sulfate-rich industrial wastewater solutions.
6. Carbonate had a greater impact on selenate adsorption than sulfate (Figure 39). Selenate loading was reduced from 78.9 to 15.0% at a carbonate-to-selenate molar ratio of 700. These experiments were performed using 763 ppb Se feed solution. Therefore, the

selectivity order for aged-FS loading is CO_3^{2-}> SeO_4^{2-}>>SO_4^{2-}. It is advised to reduce the carbonate concentration of a selenate-bearing solution by performing a lime softening pre-treatment process before the adsorption process. In addition to carbonate interference from solution, the interference of intercalated-carbonate was studied. Comparisons of selenate loading by two samples with different intercalated carbonate contents (unaged-FS and aged-FS), showed that the higher intercalated carbonate content in the aged-FS (3.00 vs 1.15%) did not interfere with selenate adsorption from ppm-level solutions, so long as the chloro-hydrocalumite capacity was greater than the amount of selenate available in solution (Table 29, 6.3.3). This indicates that it might not be necessary to prepare FS under rigorous nitrogen purging conditions; a suitably strong adsorbent for selenate can be readily obtained despite a moderate level of carbonate content. Intercalated carbonate does reduce the maximum possible Se loading from the theoretical value (1.78 mmol/g) for pure chloro-hydrocalumite. It is likely that moderate carbonate content in these LDH materials would not adversely affect loading from ppb-level solutions.

7. In pH 12.3 calcium hydroxide solution, aluminum dissolution from aged-FS was reduced drastically (from $Al._{LB}$: 8.9% to 0.78%). However, katoite ($Ca_3Al_2(OH)_{12}$) forms. Nevertheless, the final dissolved Al concentration of 0.07 ppm was just above the thirty-day average (<0.05 ppm Al), and below the instantaneous maximum (<0.10 ppm Al), indicated by the 2018 BC water quality guideline for aluminum [14,78]. The average Al concentration for regular adsorption tests (no calcium hydroxide), was 50.6 ppm. Therefore, in addition to the removal of carbonate and initial pH adjustment, pre-treatment with a lime-softening process will have the benefit of significantly suppressing the release of Al^{3+} ions into the treated water.

8. To achieve final selenium concentrations lower than both the BC Water Quality Guideline for freshwater in use for 2018 [14], and the 2016 US EPA guideline for lotic water, a calcined aged-FS sample was used. The calcination of aged-FS material at 800 °C increased the Se loading. The calcined aged-FS at 800 °C loaded 99.7 % of selenate from 753 ppb Se feed solution. This is a significant improvement over unaged-FS itself. The final aqueous Se concentration was 1.84 ppb, lower than the BC water quality guideline set in 2012 (2 ppb [14]), and the US EPA guideline set in 2016 for Se in lotic water (<3.1 ppb [78]). QXRD showed that the calcined aged-FS at 800 °C was mainly composed of mayenite ($Al_{14}Ca_{12}O_{33}$) with no layered structure. The mayenite phase was able to revert to the layered structure upon exposure to the selenate solution.
9. By using a lime-softening pre-treatment step, followed by selenium adsorption using calcined aged-FS, it is expected that it should be possible to achieve dissolved metals concentrations that would be very close to the current (2018) BC water quality guidelines for total aluminum and total selenium. As only a preliminary scoping test was performed for these conditions, it is possible that optimization of the experimental conditions could lead to final solutions where both the dissolved aluminum and selenium concentrations meet the current total metals guidelines.

   After the FS adsorption step, both the aluminum and selenium are still present in the solids phase so a solid-liquid separation step that is able to successfully handle the fine LDH solids would be required. (Note that the BC water quality guidelines for aluminum and selenium are based on total concentration, not just dissolved concentration.) Additionally, after solid-liquid separation, the solution pH will need to be adjusted down to levels acceptable for discharge (typically within a range of 6.5 – 9.0) [93].

7.1 Recommendations for future academic work

This section briefly describes some research topics that are worth investigating further.

A. Synthesis process:

1. Large amounts of impure tri-calcium aluminate are formed in the Bayer process, where it assists as a "filter aid". This material is considered waste and can be purchased from related industries. This inexpensive material can be used for the preparation of FS, but a low-quality FS is expected from this source. This material might still be good enough for some wastewater applications (e.g. high ppm Se concentrations).
2. For future studies, two series of co-precipitation tests at constant pH with the following nitrogen purging strategies are recommended. Firstly, co-precipitation should be conducted without any nitrogen purging. Secondly, the co-precipitation should be performed in a glove box with complete nitrogen purging to totally eliminate carbonate contamination of the FS. The analysis of FS prepared by the former method will quantify the maximum carbonate adsorbed from the air during synthesis in the absence of any nitrogen purging. The analysis of FS prepared by the latter method will determine if carbonate could be further reduced to values lower than 1.01%. In this method, the possibility for the synthesis of pure FS/close to pure FS material by co-precipitation method can be studied. Overall, the results of current data in this thesis in combination with these future studies will correlate the adsorbed-carbonate content from the air (and consequently chloro-carboaluminate phase proportion) to the nitrogen purging setups. Obviously, QXRD analysis of these FS samples for determination of chloro-carboaluminate phase proportion is required.

B. Aging and dissolution:

1. More aging tests at L/S ratios lower than 20 (e.g., 15, 10 and 5) and initial pH values higher than 12.0 (e.g., 12.5, 13.0, 13.5 and 14.0) are recommended for future works. The results of these experiments might provide a larger spectrum in the selection of an aging condition. It will be beneficial to age the material under the lowest possible mass-loss condition (e. g., L/S<20 or initial pH>12.0), and still get similar/better dissolution reduction to the selected aging condition of this thesis.
2. More studies on the role of chloro-carboaluminate phase proportion on FS dissolution are recommended. For this, the preparation of FS samples with different proportions of chloro-carboaluminate phase is recommended (e. g., 10 to 90 wt.% with the balance chloro-hydrocalumite FS). Next, these samples need to be exposed to an identical dissolution test (preferably initial pH 12.5, L/S 200, 30 °C, 24 h, 150 RPM, Se-free). From the dissolution results, the effect of intercalated carbonate on FS dissolution will be quantified.

C. Selenate adsorption:

1. It is recommended to study selenate desorption from loaded aged-FS. Various reagents such as sodium chloride, sodium carbonate, or sodium nitrate can be used for desorption studies. The concentration of anion in solution, time, and shaking rate effects can be the influential parameters.
2. Adsorption of selenate in the initial pH range of 12.0-<13.2, is recommended. The aged-FS dissolution in this range decreased drastically (Figure 23). An identical/similar selenate adsorption at this range to that of initial pH 12.0, will have a benefit for mass loss minimization.

3. More adsorption experiments by unaged-FS and aged-FS samples are recommended for ppb-level Se feed solutions and high ppm-level Se feed solution (>>219 ppm Se feed). The results of these future studies and the results of studies in this thesis (section 6.3.3), can be used to determine the actual effect of increased intercalated-carbonate during aging on the loading of selenate. Varying carbonate-content FS materials can also be added to this study.
4. Further studies on carbonate interference with carbonate-to-selenate molar ratios of <700 are recommended. The results will be helpful for industrial use of the material, to better quantify the interference effect. The sulfate interference studies for ppm levels Se feed solutions are also recommended. From the results of these studies, the competition of sulfate with selenate for interlayer sites loading will be clarified.
5. It is recommended to study the chloride anion interference with selenate loading on aged-FS in ppb-level Se solutions. Various sodium chloride contents can be added to the selenate solutions for this study. Since chloride is the host anion in aged-FS, the extent of interference of chloride will most likely be evident only in very dilute (ppb level) Se solutions. From higher ppm-level Se solutions, the principal selenate loading mechanism is ion exchange in the interlayer space, which occurs more readily at high Se concentration.
6. QXRD analysis of Se-loaded aged-FS samples from calcium hydroxide solution is recommended to determine the quantity of katoite phase, and how it accumulates with time.
7. The aged-FS sample calcined at 800 °C had higher loading than the aged-FS sample calcined at 600 °C (Table 30). Future QXRD studies on the analysis of aged-FS samples calcined at 600 °C and 800 °C are recommended. The surface area studies of aged-FS and calcined aged-FS samples at 600 °C and 800 °C by BET method are recommended for future studies.

8. Selenate adsorption by aged-FS from more complex synthetic solutions with different compositions of selenate, selenite, calcium sulfate and sodium carbonate is recommended to better understand the interaction of these various parameters.

7.2 Recommendations for applied R&D for potential industrial applications

In conclusion, the following steps are recommended for evaluating the applicability of FS to industrial wastewater solutions to achieve maximum selenate loading and minimum dissolution.

1) Determine if FS likely is a good option for the wastewater:
    - The initial pH of the water should be adjusted to 12.0 to minimize the dissolution of the adsorbent. If the pH of wastewater is lower, use calcium hydroxide to raise the pH. The usage of calcium hydroxide solution will be beneficial for minimization of Al release from FS and carbonate removal as well.

2) Perform scoping tests for FS:

- The unaged-FS preparation: Prepare unaged-FS by co-precipitation process at constant pH 11.3 (see 4.1 for synthesis details). The partial nitrogen purging method is adequate for treatment of ppm levels Se feed solutions. For extremely high ppm level-feeds the complete nitrogen purging method will be better, and the reason is that selenate capacity will be greater for a material with less carbonate.

Case study: 14 Kg FS material is needed for the treatment of 1000 m^3 wastewater containing 1000 ppb Se in solution based on the following calculations:

-Capacity of Se loading: 71 mg Se/g FS

-Se mass in wastewater: 1000 Kg

-FS needed: 1000/71: 14 kg

Several large batches of co-precipitation synthesis process under partial nitrogen purging, will provide the required mass for the treatment of this volume of water.

- The aged-FS preparation: After proper washing and drying of unaged-FS, run an aging process using the unaged-FS material in the decarbonated water, at initial pH 12.0, L/S 20, 65 °C and 7 days. The container needs to be sealed and no nitrogen purging is required.
- The calcined aged-FS preparation: Perform a calcination process on aged-FS material, at 800 °C for a minimum of 5 hours.
- Optimized selenate loading process: Use the calcined aged-FS to run the selenate removal experiments at initial pH 12.0, L/S 200, 150 RPM, 24 h, and 30 °C. This procedure ensures maximum loading and minimum dissolution (for full ppb to ppm concentration range feed solutions). In the case of direct usage of unaged-FS in adsorption process, a higher FS mass loss should be expected.
- Agitation needs to be energetic enough to ensure good contact between the FS particles and the solution.
- Effect of temperature: In this work, the temperature of 30 °C was recommended. However, most mining wastewater in cold areas will have temperatures lower than 30 °C. It is recommended that test work be done at various temperatures to determine the optimum operating temperature for the system. For hot wastewaters, some consideration would need to be given to the container type used for the experiments as the glass was shown to etch at 60 °C; HDPE might be more suitable.

3) Develop a research plan for scaling up the process:

- FS is a fine powder. The filtration of fine powders is an issue for their commercialization. Currently, research is being devoted to solving this issue. For this problem, the sorptive

flotation process [94] or filter candles inserted in the base of vessels integrated with powdered LDHs [95] are some of the recommended solutions. The latter is a commonly used method of separating microorganisms from drinking water in less-developed regions. These methods can run without getting into the solid/liquid separation and filter clogging issues. The mechanical stability of LDH can also be enhanced by using a network substrate with interconnected channels. In this method, LDH flakes are inserted and fixed in a macro-porous network. This method was used for the removal of thiosulfate from thiocyanate by a Ni-Al-LDH film [96].

- Evaluate continuous circuit design options to maximize selenate loading on FS. This thesis focused on batch tests. However, a full-scale application would likely require multiple reaction vessels in series with some type of countercurrent operation of the FS and the treated water. This will be particularly challenging due to the nature of the fine FS.
- It is recommended to optimize the experimental conditions for lime softening and adsorption by calcined aged-FS tests to ensure that the BC guideline values for both Al and Se are met.
- Further work would be required to evaluate elution and reactivation of material by calcination prior to reuse.

Bibliography

[1] W.C. Cooper, R.A. Zingaro, Selenium, in: Van Nostrand Reinhold, 1974: pp. 1–70.

[2] R. Bajpai, S. Banerji, Bioremediation of Soils Contaminated with Pentachlorophenol, Ann. N. Y. Acad. Sci. 665 (1992) 423–434.

[3] A.D. Lemly, Aquatic selenium pollution is a global environmental safety issue, Ecotoxicol. Environ. Saf. 59 (2004) 44–56.

[4] K. Smith, A.O. Lau, F.W. Vance, Evaluation of Treatment Techniques for Selenium Removal, in: Int. Water Conf., 2009: pp. 1–15.

[5] L. Moore, A. Mahmoudkhani, Methods for removing selenium from aqueous systems, Proc. Tailingd Mine Waste. (2011) 1–5.

[6] Treatment of Selenium-Containing Coal Mining Wastewater with Fluidized Bed Reactor Technology Proven Systems Provide Major Cost Advantages, An Envirogen Technol. Whitepaper. (2011) 1–15.

[7] P.D. Chamberlin, Selenium removal from wastewaters-an update, in: Randol Gold Forum, 1996: pp. 119–127.

[8] L.G. Twidwell, J. Mccloskey, H. Joyce, E. Dahlgren, A. Hadden, Removal of Selenium Oxyanions from Mine Waters Utilizing Elemental Iron and Galvanically Coupled Metals, Innov. Nat. Resour. Syst. Process. Jan D. Mill. Symp. (2005) 299–313.

[9] D.L. Hatfield, M.J. Berry, V.N. Gladyshev, Selenium: Its Molecular Biology and Role in Human Health, in: 2012: pp. 517–527.

[10] R. Jones, S. Brienne, S. Jensen, A. Tompkins, Selenium release from coal mines in the Elk valley, and treatment R&D plans, in: 2009 Br. Columbia Mine Reclam. Symp., n.d.

[11] P. Zhang, D.L. Sparks, Kinetics of Selenate and Selenite Adsorption/Desorption at the Goethite/Water Interface, Environ. Sci. Technol. 24 (1990) 1848–1856.

[12] J.F. Pumphrey, G. Gilron, Elk Valley Selenium Taskfroce (EVSTF) update and overview, Rep. by Teck Coal Limited,. (2009) 8.

[13] T. Sandy, C. DiSante, Review of Available Technologies for the Removal of Selenium from Water, in: North Am. Met. Counc., 2010: p. 10.

[14] Ministry of Environment & Climate Change Strategy British Columbia, British Columbia Approved Water Quality Guidelines for Aquatic Life, Wildlife & Agriculture: Summary Report, 2018.

[15] J. Beaman. U.S. Environmental Protection Agency, Aquatic life ambient water quality criterion for selenium in freshwater 2016 – Fact Sheet, (2016) 1–3.

[16] A. Ramana, A.K. Sengupta, Removing Selenium(IV) and Arsenic(V) Oxyanions with Tailored Chelating Polymers, J. Environ. Eng. 118 (1992) 755–775.

[17] T.D. Cooke, K.W. Bruland, Aquatic Chemistry of Selenium: Evidence of Biomethylation, Environ. Sci. Technol. 21 (1987) 1214–1219.

[18] M. Mokmeli, B. Wassink, D. Dreisinger, Kinetics study of selenium removal from copper sulfate-sulfuric acid solution, Hydrometallurgy. 139 (2013) 13–25.

[19] M. Misra, R. Nev., D. C. Nayak, Process for removal of selenium and arsenic from aqueous streams, US5603838A, 1995. https://patents.google.com/patent/US5603838A/en (accessed May 26, 1995).

[20] L.S. Balistrieri, T.T. Chao, Adsorption of selenium by amorphous iron oxyhydroxide and manganese dioxide, Geochim. Cosmochim. Acta. 54 (1990) 739–751.

[21] K.F. Hayes, A.L. Roe, G.E. Brown Jr, K.O. Hodgson, J.O. Leckie, G.A. Parks, In situ X-ray absorption study of surface complexes at oxide/water interfaces: selenium oxyanions on α-FeOOH, Science (80-.). 238 (1987) 783–786.

[22] G. Qin, Minor element behaviour in the Inco CRED process, University of British Columbia, 2005.

[23] L. Rosengrant, L. Fargo, Final best demonstrated available technology (BDAT) background document for K031, and P and U wastes containing arsenic and selenium listing constituents. Volume 1, Versar Inc., Springfield,VA (USA). (1990).

[24] K. Dorfner, Ion Exchangers, in: Walter de Gruyter Berlin, New York, 1935: pp. 7–170.

[25] Y. Wu, Y. Chi, H. Bai, G. Qian, Y. Cao, J. Zhou, Y. Xu, Q. Liu, Z.P. Xu, S. Qiao, Effective removal of selenate from aqueous solutions by the Friedel phase, J. Hazard. Mater. 176 (2010) 193–198.

[26] P.J. Marcantonio, Process for removing selenium from wastewater effluent, US4915928A, Assignee: Chevron Research and Technology Co, 1990.

[27] J. He, M. Wei, B. Li, Y. Kang, D.G. Evans, X. Duan, Preparation of layered double hydroxides, Struct. Bond. 119 (2005) 89–119.
[28] Y. Zhao, F. Li, R. Zhang, D.G. Evans, X. Duan, Preparation of layered double-hydroxide nanomaterials with a uniform crystallite size using a new method involving separate nucleation and aging steps, Chem. Mater. 14 (2002) 4286–4291.
[29] M. Chrysochoou, D. Dermatas, Evaluation of ettringite and hydrocalumite formation for heavy metal immobilization: Literature review and experimental study, J. Hazard. Mater. 136 (2006) 20–33.
[30] R. Salomão, L.M. Milena, M.H. Wakamatsu, V.C. Pandolfelli, Hydrotalcite synthesis via co-precipitation reactions using MgO and $Al(OH)_3$ precursors, Ceram. Int. 37 (2011) 3063–3070.
[31] Z.P. Xu, G.Q. (Max) Lu, Hydrothermal Synthesis of Layered Double Hydroxides (LDHs) from Mixed MgO and Al_2O_3 : LDH Formation Mechanism, Chem. Mater. 17 (2005) 1055–1062.
[32] Y. Jiang, Y. Yang, G. Qian, H. Hou, B. Xi, Y. Xu, Aqueous Cr (VI) removal by Friedel's salt adsorbent prepared from calcium aluminate-rich cementitious materials, Environ. Technol. 36 (2015) 2086–2093.
[33] Y. Dai, G. Qian, Y. Cao, Y. Chi, Y. Xu, J. Zhou, Q. Liu, Z.P. Xu, S.Z. Qiao, Effective removal and fixation of Cr(VI) from aqueous solution with Friedel's salt, J. Hazard. Mater. 170 (2009) 1086–1092.
[34] T. Nishimura, H. Hashimoto, M. Nakayama, Removal of selenium(VI) from aqueous solution with polyamine-type weakly basic ion exchange resin, Sep. Sci. Technol. 42 (2007) 3155–3167.
[35] T. Nishimura, R. Hata, F. Hasegawa, Chemistry of the M (M=Fe, Ca, Ba)-Se-H_2O systems at 25 °C, Molecules. 14 (2009) 3567–3588.
[36] M. Nakayama, K. Itoh, M. Chikuma, H. Sakurai, H. Tanaka, Anion-exchange resin modified with bismuthiol-II, as a new functional resin for the selective collection of selenium (IV), Talanta. 31 (1984) 269–274.
[37] T.M. Suzuki, D.A.P. Tanaka, M.A. Llosa-Tanco, M. Kanesato, T. Yokoyama, Adsorption and removal of oxo-anions of arsenic and selenium on the zirconium(IV) loaded polymer resin functionalized with diethylenetriamine-N,N,N',N'-polyacetic acid, J. Environ. Monit. 2 (2000) 550–555.
[38] I. Cardona, Selenium Removal by Nano-Magnetite Impregnated Diatomaceous Earth, Morgantown, West Virginia, 2010.
[39] I. Baur, C.A. Johnson, The solubility of selenate-AFt ($3CaO{\cdot}Al_2O_3{\cdot}3CaSeO_4{\cdot}37.5H_2O$) and selenate-AFm ($3CaO{\cdot}Al_2O_3{\cdot}CaSeO_4{\cdot}xH_2O$), Cem. Concr. Res. 33 (2003) 1741–1748.
[40] I. Baur, C.A. Johnson, Sorption of selenite and selenate to cement minerals, Environ. Sci. Technol. 37 (2003) 3442–3447.
[41] I. Bonhoure, I. Baur, E. Wieland, C.A. Johnson, A.M. Scheidegger, Uptake of Se(IV/VI) oxyanions by hardened cement paste and cement minerals: An X-ray absorption spectroscopy study, Cem. Concr. Res. 36 (2006) 91–98.
[42] Y. You, G.F. Vance, H. Zhao, Selenium adsorption on Mg-Al and Zn-Al layered double hydroxides, Appl. Clay Sci. 20 (2001) 13–25.
[43] D.G. Evans, R.C.T. Slade, Structural aspects of layered double hydroxides, Struct. Bond. 119 (2006) 1–87.
[44] K.-H. Goh, T.-T. Lim, Z. Dong, Application of layered double hydroxides for removal of oxyanions: A review, Water Res. 42 (2008) 1343–1368.
[45] B.D. Cullity, Elements of X-Ray diffraction, in: 1978: pp. 32–63.
[46] I. Rousselot, C. Taviot-Guého, F. Leroux, P. Léone, P. Palvadeau, J.P. Besse, Insights on the structural chemistry of hydrocalumite and hydrotalcite-like materials: Investigation of the series $Ca_2M^{3+}(OH)_6Cl{\cdot}2H_2O$ (M^{3+}: Al^{3+}, Ga^{3+}, Fe^{3+}, and Sc^{3+}) by X-ray powder diffraction, J. Solid State Chem. 167 (2002) 137–144.
[47] G. Renaudin, F. Kubel, J.P. Rivera, M. Francois, Structural phase transition and high temperature phase structure of Friedels salt, $3CaO{\cdot}Al_2O_3{\cdot}CaCl_2{\cdot}10H_2O$, Cem. Concr. Res. 29 (1999) 1937–1942.
[48] Y. Shao, M. Zhou, W. Wang, H. Hou, Identification of chromate binding mechanisms in Friedel's salt, Constr. Build. Mater. 48 (2013) 942–947.
[49] U.A. Birnin-Yauri, F.P. Glasser, Friedel's salt, $Ca_2Al(OH)_6(Cl,OH){\cdot}2H_2O$: Its solid solutions and their role in chloride binding, Cem. Concr. Res. 28 (1998) 1713–1723.
[50] L. Vieille, I. Rousselot, F. Leroux, J.P. Besse, C. Taviot-Guého, Hydrocalumite and Its Polymer Derivatives. 1. Reversible Thermal Behavior of Friedel's Salt: A Direct Observation by Means of High-Temperature in Situ Powder X-ray Diffraction, Chem. Mater. 15 (2003) 4361–4368.
[51] P.M. Friedel, Sur un chloro-aluminate de calcium hydraté se maclant par compression, Bull Soc Franç Minéral. 19 (1897) 122–136.
[52] A.K. Suryavanshi, J.D. Scantlebury, S.B. Lyon, Mechanism of Friedel's salt formation in cements rich in tri-calcium aluminate, Cem. Concr. Res. 26 (1996) 717–727.

[53] A. Mesbah, J.P. Rapin, M. Franąois, C. Cau-Dit-Coumes, F. Frizon, F. Leroux, G. Renaudin, Crystal structures and phase transition of cementitious Bi-anionic AFm-(Cl^-, CO_3^{2-}) compounds, J. Am. Ceram. Soc. 94 (2011) 261–268.
[54] F. Frizon, J. Ravaux, G. Renaudin, C. Cau-dit-Coumes, A. Mesbah, F. Leroux, A New Investigation of the Cl^--CO_3^{2-} Substitution in AFm Phases, J. Am. Ceram. Soc. 94 (2011) 1901–1910.
[55] V. Tóth, M. Sipiczki, A. Pallagi, Á. Kukovecz, Z. Kónya, P. Sipos, I. Pálinkó, Synthesis and properties of CaAl-layered double hydroxides of hydrocalumite-type, Chem. Pap. 68 (2014) 633–637.
[56] M. Zhang, E.J. Reardon, Removal of B, Cr, Mo, and Se from wastewater by incorporation into hydrocalumite and ettringite, Environ. Sci. Technol. 37 (2003) 2947–2952.
[57] J.M. Oh, S.H. Hwang, J.H. Choy, The effect of synthetic conditions on tailoring the size of hydrotalcite particles, in: Solid State Ionics, 2002: pp. 285–291.
[58] K.L. Erickson, T.E. Bostrom, R.L. Frost, A study of structural memory effects in synthetic hydrotalcites using environmental SEM, Mater. Lett. 59 (2005) 226–229.
[59] Ranko P. Bontchev, Shirley Liu, James L. Krumhansl, and James Voigt, T.M. Nenoff, Synthesis, Characterization, and Ion Exchange Properties of Hydrotalcite $Mg_6Al_2(OH)_{16}(A)_x(A')_{2-x}\cdot 4H_2O$ (A, A' = Cl^-, Br^-, I^-, and NO_3^-, $2 \geq x \geq 0$) Derivatives, (2003).
[60] M. Szabados, R. Mészáros, S. Erdei, Z. Kónya, Á. Kukovecz, P. Sipos, I. Pálinkó, Ultrasonically-enhanced mechanochemical synthesis of CaAl-layered double hydroxides intercalated by a variety of inorganic anions, Ultrason. Sonochem. 31 (2016) 409–416.
[61] Z. Ferencz, Á. Kukovecz, Z. Kónya, P. Sipos, I. Pálinkó, Optimisation of the synthesis parameters of mechanochemically prepared CaAl-layered double hydroxide, Appl. Clay Sci. 112–113 (2015) 94–99.
[62] C.F. Linares, J. Moscosso, V. Alzurutt, F. Ocanto, P. Bretto, G. González, Carbonated hydrocalumite synthesized by the microwave method as a possible antacid, Mater. Sci. Eng. C. 61 (2016) 875–878.
[63] J.W. Boclair, P.S. Braterman, Layered double hydroxide stability. 1. Relative stabilities of layered double hydroxides and their simple counterparts, Chem. Mater. 11 (1999) 298–302.
[64] L. Yang, Z. Shahrivari, P.K.T. Liu, M. Sahimi, T.T. Tsotsis, Removal of trace levels of arsenic and selenium from aqueous solutions by calcined and uncalcined layered double hydroxides (LDH), Ind. Eng. Chem. Res. 44 (2005) 6804–6815.
[65] P. Feng, C. Miao, J.W. Bullard, Factors Influencing the Stability of AF m and AF t in the Ca – Al – S – O – H System at 25 ℃, J. Am. Ceram. Soc. 99 (2016) 1031–1041.
[66] T. Hongo, T. Iemura, A. Yamazaki, Adsorption ability for several harmful anions and thermal behavior of Zn-Fe layered double hydroxide, Nippon Seramikkusu Kyokai Gakujutsu Ronbunshi/Journal Ceram. Soc. Japan. 116 (2008) 192–197.
[67] G. Renaudin, M. Francois, O. Evrard, Order and disorder in the lamellar hydrated tetracalcium monocarboaluminate compound, Cem. Concr. Res. (1999).
[68] M. Francois, G. Renaudin, O. Evrard, A cementitious compound with composition $3CaO.Al_2O_3$-$CaCO_3.11H_2O$, Acta Crystallogr. Sect. C Cryst. Struct. Commun. 54 (1998) 1214–1217.
[69] A. Fahami, G.W. Beall, S. Enayatpour, F. Tavangarian, M. Fahami, Rapid preparation of nano hexagonal-shaped hydrocalumite via one-pot mechanochemistry method, Appl. Clay Sci. 136 (2017) 90–95.
[70] F. Cavani, F. Trifirò, A. Vaccari, Hydrotalcite-type anionic clays: Preparation, properties and applications., Catal. Today. 11 (1991) 173–301.
[71] Z.P. Xu, G. Stevenson, C.Q. Lu, G.Q. Lu, Dispersion and size control of layered double hydroxide nanoparticles in aqueous solutions, J. Phys. Chem. B. 110 (2006) 16923–16929.
[72] F. Li, X. Jiang, D.G. Evans, X. Duan, Structure and basicity of mesoporous materials from Mg/Al/In layered double hydroxides prepared by separate nucleation and aging steps method, J. Porous Mater. 12 (2005) 55–63.
[73] E. Pérez-Barrado, M.C. Pujol, M. Aguiló, Y. Cesteros, F. Díaz, J. Pallarès, L.F. Marsal, P. Salagre, Fast aging treatment for the synthesis of hydrocalumites using microwaves, Appl. Clay Sci. 80–81 (2013) 313–319.
[74] N.N. Das, J. Konar, M.K. Mohanta, S.C. Srivastava, Adsorption of Cr(VI) and Se(IV) from their aqueous solutions onto Zr^{4+}-substituted ZnAl/MgAl-layered double hydroxides: Effect of Zr^{4+}substitution in the layer, J. Colloid Interface Sci. 270 (2004) 1–8.
[75] W.H. Goodman., Removal of selenium from water by ion-exchange, US005494582A, Assignee: Nalco Chemical Company, Naperville, Ill., 1996.
[76] J. Das, D. Das, G.P. Dash, K.M. Parida, Studies on Mg/Fe hydrotalcite-like-compound (HTlc): I. Removal of inorganic selenite (SeO_3^{2-}) from aqueous medium, J. Colloid Interface Sci. 251 (2002) 26–32.

[77] E. Álvarez-Ayuso, H.W. Nugteren, Purification of chromium(VI) finishing wastewaters using calcined and uncalcined Mg-Al-CO_3-hydrotalcite, Water Res. 39 (2005) 2535–2542.
[78] G. A. Butcher M. Sc., Water Quality Water Quality Criteria for Aluminum, Overv. Report, Prep. Purs. to Sect. 2(e) Environ. Manag. Act, 1981. 2 (2001).
[79] A. Gácsi, B. Kutus, Z. Kónya, Á. Kukovecz, I. Pálinkó, P. Sipos, Estimation of the solubility product of hydrocalumite–hydroxide, a layered double hydroxide with the formula of $[Ca_2Al(OH)_6]OH{\cdot}nH_2O$, J. Phys. Chem. Solids. 98 (2016) 167–173.
[80] A.O. Ferreira OP, De Moraes SG, Duran N, Cornejo L, Evaluation of boron removal from water by hydrotalcite-like compounds, Cienc. e Tecnol. Aliment. 26 (2006) 80–88.
[81] B.M. Mohamed, J.H. Sharp, Kinetics and mechanism of formation of tricalcium aluminate, $Ca_3Al_2O_6$, Thermochim. Acta. 388 (2002) 105–114.
[82] X. Sun, S.K. Dey, Insights into the synthesis of layered double hydroxide (LDH) nanoparticles: Part 2. Formation mechanisms of LDH, J. Colloid Interface Sci. 458 (2015) 160–168.
[83] X. Sun, E. Neuperger, S.K. Dey, Insights into the synthesis of layered double hydroxide (LDH) nanoparticles: Part 1. Optimization and controlled synthesis of chloride-intercalated LDH, J. Colloid Interface Sci. 459 (2015) 264–272.
[84] R.M. Cigala, C. De Stefano, A. Giacalone, A. Gianguzz, Speciation of Al^{3+} in fairly concentrated solutions (20 -200 $mmolL^{-1}$) at I=1 mol L^{-1} ($NaNO_3$), in the acidic pH range, at different temperatures, Chem. Speciat. Bioavailab. 23 (2011) 33–37.
[85] T.R. Jensen, A.N. Christensen, J.C. Hanson, Hydrothermal transformation of the calcium aluminum oxide hydrates $CaAl_2O_4{\cdot}10H_2O$ and $Ca_2Al_2O_5{\cdot}8H_2O$ to $Ca_3Al_2(OH)_{12}$ investigated by in situ synchrotron X-ray powder diffraction, Cem. Concr. Res. 35 (2005) 2300–2309.
[86] A. Rawle, Basic principles of particle size analysis, Surf. Coatings Int. 86 (2003) 58–65.
[87] HDPE and LDPE Resistance Chart by Chemical, Prof. Plast. (2019) 5–7. www.professionalplastics.com.
[88] F. Mohammandi, P. Littlejohn, A. West, A. Hall, Selen-IX$^{(TM)}$: Selenium Removal from Mining Affected Runoff using Ion Exchange Based Technology, in: Hydro 2014 Conf., 2014: pp. 1–13.
[89] A. E. Moore and H. F. W. Taylor, Crystal Structure of Ettringite, Acta Cryst. B26 (1970) 386–393.
[90] Source:ILO-ICSC 1184 - Calcium Chloride (ANHYDROUS). http://www.ilo.org/dyn/icsc/showcard.display?p_version=2&p_card_id=1184.
[91] Derivation of BET and Langmuir Isotherms, Https//Www.Uni-Ulm.de/Fileadmin/Website_uni_ulm/Nawi.Inst.251/Lehre/PC3-SS14/BET.Pdf. (n.d.).
[92] Https://Www.Particletechlabs.Com/Analytical-Testing/Gas-Adsorption-Porosimetry-Analyses/Bet-Specific-Surface-Area.
[93] C. McKean, N. Nagpal, Ambient Water Quality Criteria For pH, Technical Appendix, 1991. http://www.env.gov.bc.ca/wat/wq/BCguidelines/phtech.pdf.
[94] N.K. Lazaridis, A. Hourzemanoglou, K.A. Matis, Flotation of metal-loaded clay anion exchangers. Part II: The case of arsenates, Chemosphere. 47 (2002) 319–324.
[95] G.P. Gillman, A simple technology for arsenic removal from drinking water using hydrotalcite, Sci. Total Environ. 366 (2006) 926–931.
[96] X. Liu, W. Tian, X. Kong, M. Jiang, X. Sun, X. Lei, Selective removal of thiosulfate from thiocyanate-containing water by a three-dimensional structured adsorbent: A calcined NiAl-layered double hydroxide film, RSC Adv. 5 (2015) 87948–87955.
[97] K. Pyrzyńska, Separation of inorganic selenium species on anion-exchange resins, Analyst. 120 (1995) 1933–1936.
[98] M. Nakayama, M. Chikuma, H. Tanaka, T. Tanaka, Selective collection of selenium(IV) on anion-exchange resin with azothiopyrine disulphonic acid, Talanta. 30 (1983) 455–458.
[99] P. Taylor, T.M. Suzuki, M.L. Tanco, D.A.P. Tanaka, Adsorption characteristics and removal of oxo-anions of arsenic and selenium on the porous polymers loaded with monoclinic hydrous zirconium oxide, Sep. Sci. Technol. 36 (2001) 103–111.

Appendices

Appendix A Selenium adsorption with various basic anion exchangers, modified resins and exchangers loaded with metals

Basic Anion Exchangers						
Resin Name	**Se Species**	**pH dependency**	**Maximum Loading**	**Medium**	**Interfering species (molarity or tolerated limit)**	**Se feed concentration/ Regenerant**
Varion AT660 [97]	Selenite	Dependent (pH_{opt} 4-10)	1.85 g Se/g (99% recovery)	Water	Chloride (0.01 M for Cl form and 0.1 M For –OH form), sulfate (SO_4^{2-}/ SeO_3^{2-} ratio 5000 and SO_4^{2-}/ SeO_4^{2-} ratio 7500), Cu^{2+}, Fe^{3+} (1000 ppb)	20 ppb Se/ 0.01 M HNO_3
Purolite S-920 [75]	Selenite	Increase with pH raise	22 g/L(pH 7) and 29 g/L (pH 9.5)	Chloride, Sulfate	Not studied	600-700 ppm Se
	Selenate	Almost independent	31, 34, and 30 g/L (at pH 4.1, 7.0, and 9.2)	Chloride, Sulfate	Not studied	600-700 ppm Se
Eporasu K-6 [34]	Selenite	Increases with raise in pH 3-10, decrease at pH 13	36 g/L at pH 10	Water	Not studied	60 ppm Se/1 M HCl
	Selenate	Increases from pH 0-3, constant at pH 3-12, decrease at pH 13	46 g/L at pH 3-12, adsorption capacity 1.7 mmol/g*	Water	Sulfate (SO_4^{2-}/SeO_4^{2-} ratio 2), chloride (Cl^-/ SeO_4^{2-} ratio 20) leads to 50% drop in Se^{6+} removal	30-240 ppm Se/1 M HCl
Selen-IX™ [88]	Selenite, Selenate	Not studied, pH 7.6	0.3-0.5 meq/L	Sulfate, Nitrate, Carbonate	-	363 ppb total Se/ concentrated sodium sulfate
Modified Resins with Chelating Ligands						
Amberlite IRA-400-Bismuthiol-II [36]	Selenite	pH_{Opt}<2, decrease in sorption with increase in pH at 2-5	0.05 mmol/g (95% recovery)	0.3 M HCl	Strong interference Of Cu^{2+} at pH 0-5. Less interference for Fe^{3+}, Cr^{6+}, and Zn^{2+}	0.01-2 ppm Se/ Penicillamine Or Cysteine
Amberlite IRA-400-ATPS[98]	Selenite	Not studied	0.05 mmol/g	0.2 M HCl	Cu^{2+}(>10 ppm), Cd^{2+} (1-100 ppm) and I_2 (0.01 M) at 0-0.2 M HCl	6 ppm Se/ 10-13 M HNO_3
Exchangers Loaded with Immobilized Metal Cations						
Zr-CMA[37]	Selenite, Selenate	pH 2-7, pH_{opt} 3.5-5, SeO_4^{2-} pH<2	0.38 mmol/g* 100% recovery	-	$H_2PO_4^-$, 100 ratio of A/Se is tolerated for Selenite; where A: Sulfate, Nitrate, Acetate, or Chloride.	213.2 ppm Se/ 1M NaOH
Zr-Amberlite XAD-7[99]	Selenite Selenate	pH 2-8, pH_{opt} 4.5, SeO_4^{2-} pH<2	0.49 mmol/g* 100% recovery	-	$H_2PO_4^-$, F^-, 100 Ratio Of A/Se is tolerated for selenite; Where A: Sulfate, Nitrate, Acetate, or Chloride.	157.9 ppm Se/ 1M NaOH

*Calculated by Langmuir model

Appendix B Lattice crystal systems

In this appendix, a short introduction on crystal system families is provided to make the reader familiar with the concepts of monoclinic and hexagonal phases detected in QXRD analysis of FS samples. In a comprehensive study on X-ray crystallography of elements, by Cullity, a "crystal" is described as a solid composed of atoms arranged in a pattern periodic in three dimensions [45]. Imagine a crystalline unit cell illustrated in Figure 44. This unit cell is defined by three edge lengths (*a*, *b*, and *c*) and three angles of α, β, γ.

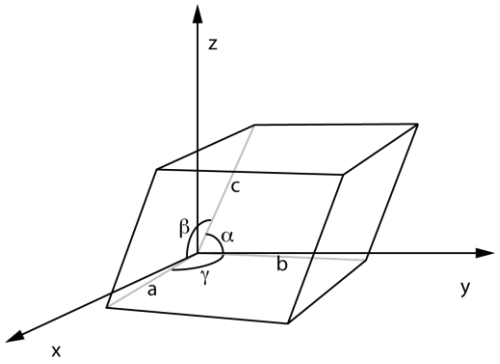

Figure 44 Lattice parameters in a unit cell of a crystal system.

Seven crystal classes (called point lattices as well) can be obtained by putting points at the corners of this unit cell. These crystal classes are cubic, tetragonal, hexagonal, rhombohedral, orthorhombic, monoclinic and triclinic (Table 31). As shown, the crystal classes differ in bond length and bond angles of crystal units. The simplest crystal system is cubic in which all the lengths are equal and all perpendicular (a=b=c, and α=β=γ=90°). For a hexagonal crystal system, the unit cell has two equal axes (*a* by *a*), an included angle of 120° (*γ*) and height (*c*), which is different from *a*) perpendicular to the two base axes (D_{6h} point group). The rhombohedral class is featured with a=b=c, α=β=γ≠90° and D_{3d} point group. The hexagonal and rhombohedral crystal classes belong to the same crystal family (hexagonal). For the monoclinic system, however, all three

coordination axes are different (a≠b≠c). Bonding angles are in the range of α= γ =90°, β≠ 90° (C_{2h} point group). The point groups of D_{6h}, D_{3d}, and C_{2h} are described in Appendix B with reference to a few familiar chemical compounds.

Table 31 Crystal family, crystal system and crystal classes [45]

Crystal family	Crystal system	Crystal class (point group)	Axis system	
Cubic		Cubic	a=b=c, α=β=γ=90°	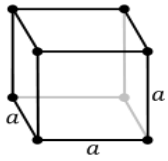
Tetragonal		Tetragonal	a=b≠c, α=β=γ=90°	
Hexagonal	Hexagonal	Hexagonal (D_{6h}) and 6 other point groups	a=b≠c, α=β=90°, γ=120°	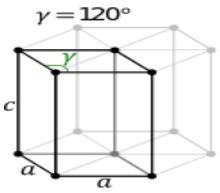
	Trigonal	Rhombohedral (D_{3d}) and 4 other point groups	a=b=c, α=β=γ≠90°	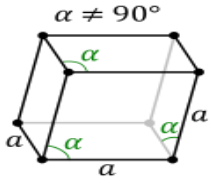
Orthorombic		Orthorhombic	a≠b≠c, α=β=γ=90°	
Monoclinic		Monoclinic (C_{2h})	a≠b≠c, α=γ=90°, β≠90°	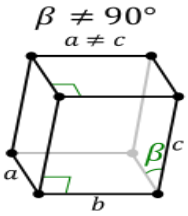
Triclinic		Triclinic	a≠b≠c, α≠β≠γ≠90°	

Ca and Al in the brucite layers of FS are coordinated to six -OH functional groups in an octahedral unit (the image on right side of Figure 45, M^{2+}:Ca^{2+} and M^{3+}:Al^{3+}). The two-dimensional infinite brucite layers are formed by edge-sharing of these octahedral units. The idealized arrangement for a hexagon is octahedral (O_h space group), however, the local geometry of metal ions is usually distorted [43]. In general, octahedral are compressed along the stacking axis (perpendicular to the brucite sheets), so that the local geometry of Ca or Al metal ions are D_{6h}, D_{3d}, and C_{2h} rather than O_h [43]. The D_{6h}, D_{3d}, and C_{2h} point groups belong to hexagonal, rhombohedral and monoclinic crystalline systems, respectively [45].

Ca or Al ion in the center of octahedral unit with the axis system of a=b≠c, α=β=90°, and γ=120°, belongs to a hexagonal system (D_{6h}) in the Friedel's salt. One can expect a monoclinic system for Ca or Al ion in the Friedel's salt, if the axis system of the octahedral unit cell follows a≠b≠c, α= γ =90°, and β≠90°. Note that a, b, c are the O-M-O bonding lengths, and α, β, γ are the bonding angles, where M: Ca or Al. The hexagonal and monoclinic systems reported for unaged-FS and aged-FS samples (by QXRD results), simply reflect the lattice system of Ca and Al, O-M-O bonding angles, and O-M-O bond lengths for Ca and Al ions, in the octahedral units of the brucite layers.

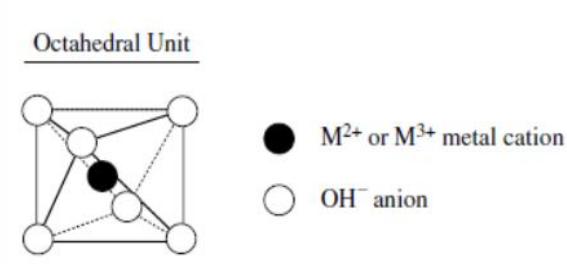

Figure 45 Hexagonal crystal class (left) and octahedral unit of divalent or trivalent metal ions in LDH (right). Reprinted with permission from [44].

Appendix C Description of point groups in FS

Ca or Al in an octahedral unit of brucite layers of FS is shown on the left side of Figure 46. The octahedral unit can be in hexagonal (D_{6h}), rhombohedral (D_{3d}), and monoclinic crystalline system (C_{2h}), depending on the symmetrical rotation axis of system. The hexagonal, rhombohedral, and monoclinic systems, have C_6, C_3 and C_2 axis, respectively. Some familiar chemical compounds are illustrated in Figure 46 to clarify the concept of D_{6h}, D_{3d}, and C_{2h} point groups in FS.

In $Cr(C_6H_6)_2$ compound the symmetric rotation axis of C_6 exists. An imaginary line goes through the center of a benzene ring (C_6H_6) about which the ring may be rotated with a C_6 rotation (360/6=60 °) and be brought back to the original position. A similar symmetrical C_6 axis can be imagined for an octahedral unit of Ca or Al FS in hexagonal system (D_{6h} point group). As shown in Figure 46, C_6 axis in the octahedral unit of Ca/Al, goes through the triangle plane. NH_3 and N_2F_2 compounds have the C_3 and C_2 axis, respectively. The C_3 axis is an imaginary line perpendicular to the NH_3 plane and rotates 120° to be brought back to original positions. A 180° rotation around C_2 axis in N_2F_2, brings the molecule back to its original position. Similar C_3 and C_2 symmetrical axis can be imagined for octahedral units in rhombohedral (D_{3d}) and monoclinic (C_{2h}) crystal classes of FS.

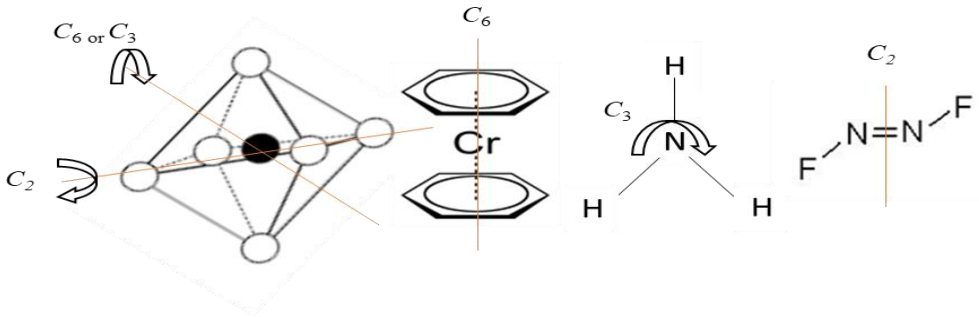

Figure 46 The octahedral unit of Ca or Al in FS (C_6, C_3, or C_2 axis), $Cr(C_6H_6)_2$ (C_6 axis), Ni-chelating complex (C_3 axis) and N_2F_2 (C_2 axis). The octahedral unit is reprinted with permission from [44].

Appendix D QXRD analysis of modified unaged-FS

Modified unaged-FS was analyzed by QXRD. As shown in Figure 47 the sample was composed of 85.7 wt.% chloro-hydrocalumite (hexagonal phase, ~86%) and 10.66 wt.% chloro-carboaluminate hydrocalumite (monoclinic phases, ~11%), respectively. Calcite and vaterite were the minor phases (0.98 and 1.49 %, respectively). Vaterite belongs to the hexagonal crystal system, whereas calcite is trigonal.

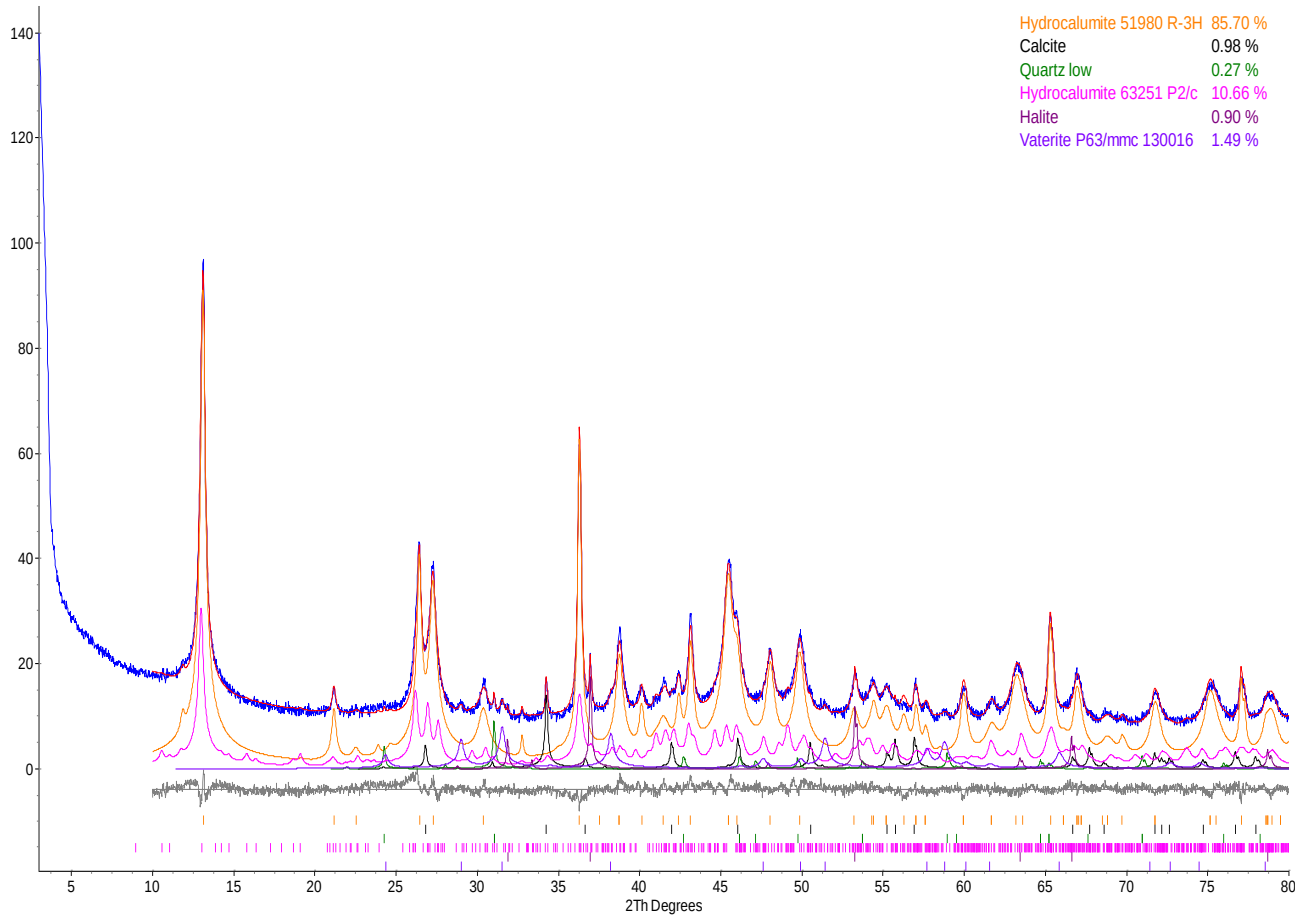

Figure 47 QXRD plot of the modified unaged-FS sample prepared with the constant-pH co-precipitation under complete nitrogen purging method. (Blue pattern: the experimental pattern, and detected phases in order; orange pattern: chloro-hydrocalumite (hexagonal phase), black pattern: calcite, green pattern: quartz, pink pattern: chloro-carboaluminate hydrocalumite (monoclinic phase), dark red pattern: halite, purple pattern: vaterite. Gray line: the difference between the experimental pattern and the detected phases.

Appendix E Reproducibility of L/S experiments in aging studies

Table 32 shows the reproducibility of six aging experiment at L/S 20, pH 8.0, 65 °C and 7 days. The average Ca and Al dissolution at L/S 20 was 3.10% (2.37-3.60%) and 2.37% (0.66-4.13%), respectively.

Table 32 Reproducibility data for FS dissolution in an aging test at L/S 20 **(**experimental condition: pH 8.0, 65 °C and 7 days)

Test number	**$Ca._{LB}$ %**	**$Al._{LB}$ %**
1	2.79	0.66
2	3.25	2.42
3	3.32	2.76
4	3.60	4.13
5	3.28	1.25
6	2.37	2.97
Average	3.10	2.37

Appendix F Ultrasound application on aged-FS and unaged-FS particles

Table 33 shows the particle size change of aged-FS and unaged-FS samples (for one sample each) with ultrasound application for one and two minutes. For example, after one- minute ultrasound application on aged-FS, the $d_{(0.9)}$ value of aged-FS was reduced from 73.2 to 52.6 μm. The ultrasound was breaking the agglomerate particles of aged-FS. The longer application of ultrasound for two minutes did not change the size of particles significantly. The $d_{(0.9)}$ value for aged-FS was 52.6 and 49.2 μm for one and two minutes, respectively.

Table 33 The particle size distribution of unaged-FS and aged-FS (selected aging: initial pH 12.0, L/S 20, 65 °C and 7 days) with and without ultrasound. Reference values are bolded for clarity.

	Unaged-FS (μm)			**Aged-FS (μm)**		
	No ultrasound	1-minute ultrasound	2 minutes ultrasound	No ultrasound	1-minute ultrasound	2 minutes ultrasound
$d_{(0.1)}$	4.1	3.7	3.6	3.8	3.3	3.1
$d_{(0.5)}$	19.9	17.2	16.7	26.4	18.8	17.0
$d_{(0.8)}$	37.4	31.1	30.5	55.0	40.3	37.5
$d_{(0.9)}$	**50.6**	**40.3**	**39.5**	**73.2**	**52.6**	**49.2**

The $d_{(0.9)}$ aged-FS value at one minute (52.6 μm) was close to the original $d_{(0.9)}$ of unaged-FS (50.6 μm). This showed that the coarse agglomerates formed through the aging process were broken by the application of ultrasound. In addition, as an indication of agglomeration during the 72-h synthesis process, the $d_{(0.9)}$ unaged-FS value was reduced from 50.6 to 40.3 μm by the one-minute ultrasound application. The longer application of ultrasound for two minutes did not change the size of particles significantly. The $d_{(0.9)}$ value for unaged-FS was 40.3 and 39.5 μm for one and two minutes, respectively.

Appendix G Phase transformations in literature

Table 34, summarizes the phase transformation of this study alongside with other phase transformations of Friedel's salt and carbonated Friedel's salt observed in the literature. The synthesis method, chemicals used for each synthesis procedure, the washing and drying methods, the crystalline phase and the phase transformations are described for each study. In this thesis, aged-FS with a chemical composition of $[Ca_{4.02}Al_{2.03}(OH)_{12.1}]\cdot[Cl_{1.30}(CO_3)_{0.33}\cdot 8.40H_2O]$ was synthesized by co-precipitation method at constant pH under partial nitrogen purging method followed by an aging process. As shown in Table 34, the solid sample before aging was mainly composed of hexagonal phase and monoclinic phase was a minor phase ($R\bar{3}$ >>$P2/c$). Over the aging process most of the hexagonal phase transformed into the monoclinic phase ($P2/c$>> $R\bar{3}$). During the aging process, more $CO_{2(g)}$ from the air was dissolved in solution and therefore the intercalated carbonate proportion was increased.

As shown in this thesis, the higher carbonate content favors the formation of monoclinic crystal phase. The phase transformation from rhombohedral to the monoclinic phase by increasing the intercalated-carbonate content of the chloro-carboaluminate phase was also reported by Mesbah [53]. In Mesbah's study, a series of $[Ca_2Al(OH)_6]\cdot[Cl_{1-x}(CO_3)_{x/2}\cdot\sim 2.25H_2O]$, with x=0.25, 0.5, and 0.75 were prepared with the co-precipitation method. From powder X-ray diffraction studies, the chloro-carboaluminate phase with lowest carbonate content was crystallized in a rhombohedral phase (x=0.25, $R\bar{3}$-c). A phase transformation from rhombohedral to monoclinic phase was reported as the carbonate content of hydrocalumite was increased. The chloro-carboaluminate with a chemical formula of $[Ca_2Al(OH)_6]\cdot[Cl_{1/2}(CO_3)_{1/4}]$ and $[Ca_2Al(OH)_6]\cdot[Cl_{1/4}(CO_3)_{3/8}]$, x=0.5 and 0.75, respectivley, were composed of almost equal proportions of rhombohedral and monoclinic phases [53]. In an agreement, with Mesbah's study,

in this work, a higher monoclinic phase proportion was favored by the aging process in which a higher carbonate content was available in solution. The difference between this study and Mesbah's study was the source of carbonate for hydrocalumite material. In this work, it was shown that the carbon dioxide gas from air dissolved in alkaline solution was adsorbed as carbonate in the interlayered composition. In Mesbah's study, carbonate was added deliberately to the sintering-precipitation process in various proportions.

A pure single crystal of Friedel's salt were prepared using the hydrothermal method [47]. The XRD data at low temperature (0 °C) showed that Friedel's salt crystallizes in the monoclinic phase (LT-phase). From the temperature variation results, a phase transformation from monoclinic (LT-phase) to rhombohedral phase (HT-phase) was recorded over a temperature range from 0 to 40 °C. The high-temperature structure (HT-phase) of the Friedel's salt was determined from X-ray single crystal diffraction intensities measured at elevated temperature (+37 °C). The rhombohedral phase with $R\bar{3}$-c space group was the only stable phase at high temperature +37 °C. The phase transformation in pure single crystal was triggered by temperature change.

Table 34 The chloro-carboaluminate and chloro-hydrocalumite phases; chemical formula, synthesis methods, crystal phase, and phase transformations

Material form/ Chemical formula	**Synthesis method/Chemicals used**	**Washing/Drying conditions**	**Crystal phase**	**Phase transformation/ cause**	**Reference**
Powder XRD Aged-FS $[Ca_{4.02}Al_{2.03}(OH)_{12.1}]\cdot[Cl_{1.30}(CO_3)_{0.33}\cdot 8.40H_2O]$	Co-precipitation method under partial nitrogen purging followed by aging process/ $CaCl_2\cdot 6H_2O$, $AlCl_3\cdot 6H_2O$, NaOH (partial N_2 purging)	Washing with cold water and drying in the oven at 100 °C	Two main phases ($R\bar{3}$ & *P2/c*)*	From $R\bar{3}$ >>*P2/c* to *P2/c*>> $R\bar{3}$/ carbonate intercalation in aging process**	This work
Powder XRD Chloro-carboaluminate phase $[Ca_2Al(OH)_6]\cdot[Cl_{1-x}(CO_3)_{x/2}\cdot 2.25H_2O]$ x=0.25, 0.5, and 0.75	Sintering-precipitation C_3A, $CaCl_2\cdot 6H_2O$, and $CaCO_3$	Washing with iso-propanol and drying over potassium acetate	x=0.25 single phase ($R\bar{3}$-c)*, x=0.5 & 0.75 two phases ($R\bar{3}$-c & *P2/c*)	From $R\bar{3}$-c to ($R\bar{3}$-c + *P2/c*)/ carbonate intercalation	Mesbah [53]
Friedel's salt single crystal $[Ca_4Al_2(OH)_{12}]\cdot[Cl_2\cdot 4H_2O]$	Hydrothermal synthesis/$Ca(OH)_2$, $Al(OH)_3$, and $CaCl_2\cdot 6H_2O$	-	Single phase $R\bar{3}$-c (at 37 °C)	*P2/c* to $R\bar{3}$-c/ temperature change	Renaudin [47]

*$R\bar{3}$, *P2/c*, and R$\bar{3}$-c: hexagonal, monoclinic and rhombohedral phases, respectively

** aging at initial pH 12.0, L/S 20, 65 °C, and 7 days

Appendix H Comparisons of $Ca._{LB}$ and $Al._{LB}$ dissolutions using pure FS and aged-FS (carbonated-FS) molar masses (561.34 and 639.61 g/mole, respectively) in initial pH studies of adsorption tests

Figure 48 shows the mass loss differences between two methods using pure FS and aged-FS molar masses for initial pH studies of adsorption tests. As seen, at selected initial pH of 12.0, the mass loss data calculated by two methods are close (e.g., 13.5 and 11.9 % $Ca._{LB}$ using aged-FS and pure FS, respectively).

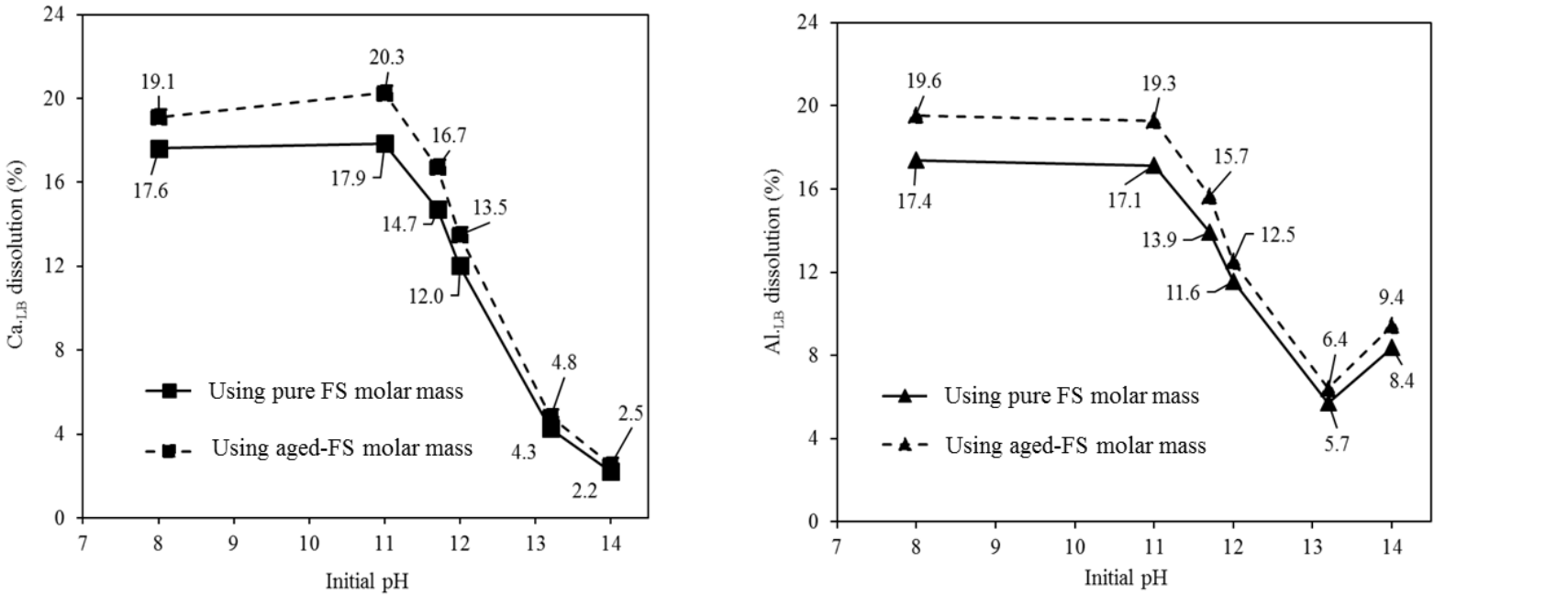

Figure 48 The mass loss differences in initial pH studies of adsorption tests using the molar mass of pure FS and aged-FS (Se 134 ppm, L/S 200, 150 RPM, 24 h, and 30 °C)

Appendix I Comparisons of $Ca._{LB}$ and $Al._{LB}$ dissolutions using FS and aged-FS (carbonated-FS) molar masses (561.34 and 639.61 g/mole, respectively) in L/S studies of adsorption tests

Figure 49 shows the mass loss differences between two methods using pure FS and aged-FS molar masses in L/S studies of adsorption tests. As seen, at selected L/S of 200, the mass loss data calculated by two methods are close (e.g., 13.5 and 12.1 % $Ca._{LB}$ using aged-FS and pure FS, respectively).

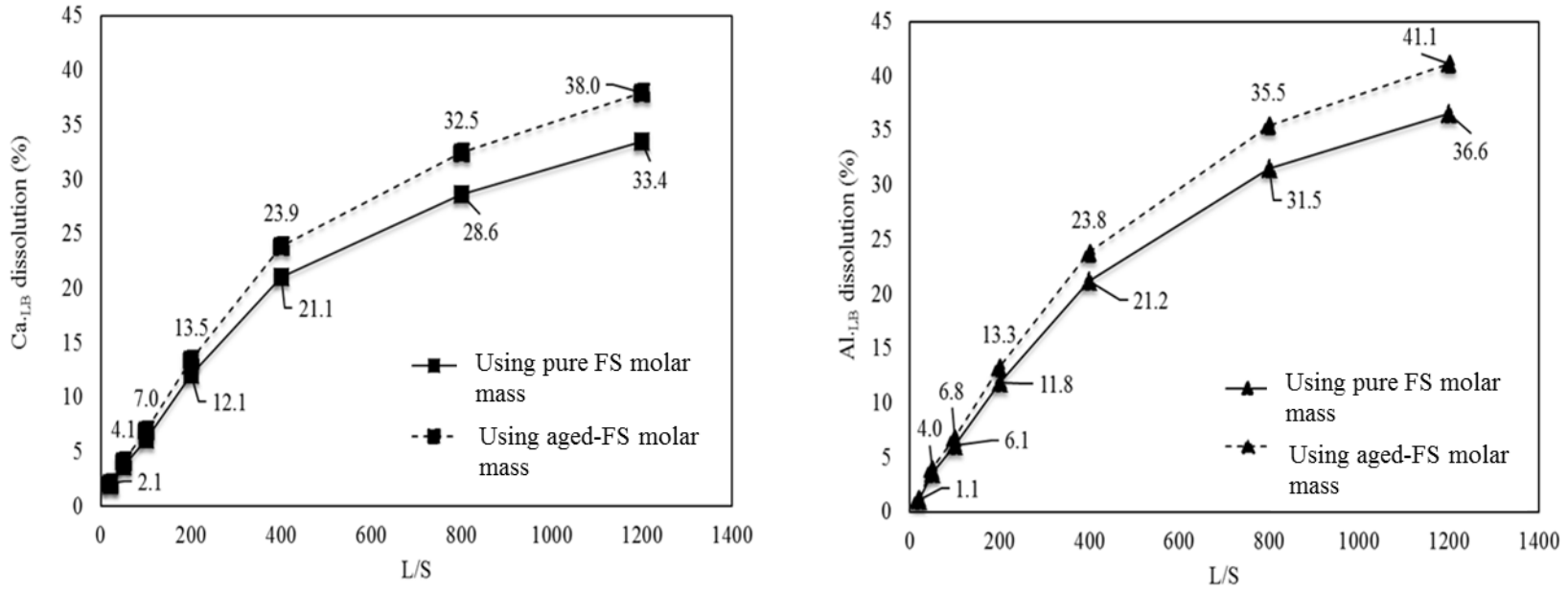

Figure 49 The mass loss differences in L/S studies of adsorption tests using the molar mass of pure FS and aged-FS (460 ppb Se, initial pH 12.0, 150 RPM, 24 h, and 30 °C)

Appendix J Adsorption experiment summary for initial pH experiments (experimental condition: L/S 200, 150 RPM, 24 h, and 30 °C)

Se feed: 847 ppb											
		$Se_{.L}/Ca_{.LB}$	$Se_{.L}/Al_{.LB}$	$Se_{.L}/Ca_{.LB}$	$Se_{.L}/Al_{.LB}$	$Se_{.S}$					
Initial pH	$Se_{.L}$%	Q_e (mg Se/g)	Q_e (mg Se/g)	Q_e (mmol/g)	Q_e (mmol/g)	Q_e (mg/g)	$Ca_{.LB}$%	$Al_{.LB}$%	SBM%	Final pH	MB*
8.0	45.5	0.10	0.09	$1.21X10^{-3}$	$1.19X10^{-3}$	-	16.5	15.4	20.3	11.30	-
8.0	49.9	0.10	0.10	$1.32X10^{-3}$	$1.31X10^{-3}$	-	16.4	15.4	18.4	11.21	-
11.7	53.9	0.10	0.10	$1.28X10^{-3}$	$1.21X10^{-3}$	-	12.8	8.31	19.5	11.50	-
12.2	61.0	0.11	0.11	$1.40X10^{-3}$	$1.40X10^{-3}$	-	9.01	8.90	10.6	11.81	-
13.2	54.6	0.090	0.10	$1.19X10^{-3}$	$1.22X10^{-3}$	-	3.60	6.01	5.60	12.60	-
Se feed: 460 ppb											
8.0	42.8	0.05	0.05	$5.95X10^{-4}$	$6.01X10^{-4}$	0.034	16.5	17.3	16.1	12.20	105
8.0	56.2	0.06	0.06	$8.02X10^{-4}$	$8.05X10^{-4}$	0.035	18.5	18.8	19.1	12.21	99
12.0	80.6	0.09	0.09	$1.09X10^{-3}$	$1.09X10^{-3}$	0.050	13.6	13.8	10.7	12.20	92
12.0	77.1	0.08	0.08	$1.03X10^{-3}$	$1.03X10^{-3}$	0.043	13.0	13.0	12.9	12.51	96
12.0	83.2	0.09	0.09	$1.10X10^{-3}$	$1.09X10^{-3}$	0.042	11.7	11.6	9.50	12.50	108
12.0	78.1	0.08	0.08	$1.03X10^{-3}$	$1.03X10^{-3}$	0.047	11.8	12.1	9.40	12.50	-
Se feed: 134 ppm											
8.0	95.3	31.4	31.2	0.40	0.39	-	17.9	17.4	-	10.50	-
11.0	95.0	31.3	30.8	0.40	0.39	-	18.2	17.1	-	11.51	-
11.0	96.4	31.2	30.8	0.40	0.39	-	-	-	-	11.53	-
11.7	97.4	30.8	30.4	0.39	0.38	-	15.0	13.9	-	11.68	-
11.7	97.5	30.7	30.3	0.39	0.38	-	-	-	-	11.70	-
12.0	98.0	30.3	29.9	0.38	0.38	-	12.1	11.1	-	12.20	-
12.0	97.7	29.2	28.8	0.37	0.37	-	11.9	12.0	-	12.61	-
13.2	91.7	25.9	26.3	0.33	0.33	-	4.30	5.70	-	12.75	-
14.0	11.2	3.17	3.39	0.040	0.040	-	2.30	8.40	-	13.20	-

$Se_{.L}$: from solution analysis, $Se_{.S}$: from solid digestion, *MB: mass balance from $Se_{.L}$ and LBM (average of $Al_{.LB}$ and $Ca_{.LB}$)

Appendix K Adsorption experiment summary for L/S experiments (experimental condition: 460 ppb Se, initial pH 12.0, 150 RPM, 24 h and 30 °C)

L/S	$Se._L$%	$Se._L/Ca._{LB}$	$Se._L/Al._{LB}$	$Se._L/Ca._{LB}$	$Se._L/Al._{LB}$	$Se._S$					
		Q_e (mg Se/g)	Q_e (mg Se/g)	Q_e (mmol/g)	Q_e (mmol/g)	Q_e (mg Se/g)	$Ca._{LB}$%	$Al._{LB}$%	SBM%	Final pH	MB*
20	96.8	0.009	0.009	$1.15X10^{-4}$	$1.14X10^{-4}$	0.009	1.93	1.09	0.16	12.1	101
50	94.0	0.022	0.022	$2.84X10^{-4}$	$2.83X10^{-4}$	0.024	3.70	3.53	1.05	12.1	110
100	89.0	0.044	0.043	$5.51X10^{-4}$	$5.50X10^{-4}$	0.032	6.25	6.06	6.21	12.2	76
200	78.7	0.082	0.082	$1.04 X10^{-3}$	$1.04X10^{-3}$	0.068	12.1	11.8	14.7	12.3	107
400	35.0	0.082	0.081	$1.04X10^{-3}$	$1.03X10^{-3}$	0.069	21.5	21.2	27.9	12.3	92
800	18.5	0.072	0.074	$9.16X10^{-4}$	$9.41X10^{-4}$	0.058	29.5	31.4	36.9	12.3	91
1200	13.2	0.073	0.076	$9.29X10^{-4}$	$9.65X10^{-4}$	0.074	34.1	36.6	43.3	12.4	94
200 (repeat #1)	77.1	-	-	-	-	0.07	-	-	-	-	-
200 (repeat #2)	80.6	-	-	-	-	0.09	-	-	-	-	-
200 (repeat #3)	83.2	-	-	-	-	0.08	-	-	-	-	-
200 (repeat #4)	78.1	-	-	-	-	0.07	-	-	-	-	-
200 (repeat #5)	75.7		-	-	-	0.08	-	-	-	-	-
400 (repeat #1)	31.5	-	-	-	-	0.08	-	-	36.2	-	93

$Se._L$: from solution analysis, $Se._S$: from solid digestion *MB: mass balance from $Se._S$ and LBM (average of $Al._{LB}$ and $Ca._{LB}$)

Appendix L Adsorption experiment summary for time experiments (experimental condition: 637 ppb Se, initial pH 12.0, L/S 200, 150 RPM, and 30 °C)

Time	$Se._L$%	$Se._L/Ca._{LB}$	$Se._L/Al._{LB}$	$Se._L/Ca._{LB}$	$Se._L/Al._{LB}$	$Se._S$				
		Q_e (mg Se/g)	Q_e (mg Se/g)	Q_e (mmol/g)	Q_e (mmol/g)	Q_e (mg Se/g)	$Ca._{LB}$%	$Al._{LB}$%	SBM%	MB*
20 min	27.8	0.037	0.037	$4.66X10^{-4}$	$4.72X10^{-4}$	0.017	3.66	4.94	-	85
45 min	47.8	0.064	0.064	$8.06X10^{-4}$	$8.15X10^{-4}$	0.027	4.38	5.39	0.16	72
2 h	51.5	0.069	0.070	$8.75X10^{-4}$	$8.82X10^{-4}$	0.029	5.00	5.71	8.53	70
3 h	62.4	0.084	0.084	$1.07X10^{-3}$	$1.06X10^{-3}$	0.042	6.13	5.67	6.26	69
6 h	72.3	0.103	0.102	$1.30X10^{-3}$	$1.29X10^{-3}$	0.061	10.5	9.86	3.84	71
12 h	85.2	0.120	0.120	$1.52X10^{-3}$	$1.51X10^{-3}$	0.071	9.87	9.33	11.2	65
24 h	88.0	0.129	0.128	$1.63X10^{-3}$	$1.62X10^{-3}$	0.071	13.0	12.4	12.0	119
48 h	91.7	0.137	0.137	$1.74X10^{-3}$	$1.74X10^{-3}$	0.082	14.8	14.8	6.80	63

$Se._L$: from solution analysis, $Se._S$: from solid digestion, *MB: mass balance from $Se._L$ and SBM

Appendix M Adsorption experiment summary for temperature experiments (experimental condition: 468 ppb Se, initial pH 12.0, L/S 200, 150 RPM, and 24 h)

Temperature (°C)	$Se._L$%	$Se._L/Ca._{LB}$	$Se._L/Al._{LB}$	$Se._L/Ca._{LB}$	$Se._L/Al._{LB}$				
		Q_e (mg/g)	Q_e (mg/g)	Q_e (mmol/g)	Q_e (mmol/g)	$Ca._{LB}$%	$Al._{LB}$%	SBM%	Final pH
60	98.6	0.105	0.097	$1.33X10^{-3}$	$1.23X10^{-3}$	12.4	5.18	21.6	-
60	99.1	0.106	0.097	$1.34X10^{-3}$	$1.22X10^{-3}$	12.4	4.29	22.9	-
60	99.5	0.106	0.096	$1.34X10^{-3}$	$1.22X10^{-3}$	12.4	3.83	20.9	-
85	96.7	0.100	0.092	$1.27X10^{-3}$	$1.17X10^{-3}$	9.95	2.44	27.0	11.33
85	97.5	0.101	0.093	$1.27X10^{-3}$	$1.18X10^{-3}$	10.1	2.82	24.4	11.38
85	96.8	0.100	0.093	$1.27X10^{-3}$	$1.18X10^{-3}$	10.4	3.34	22.8	11.38

$Se._L$: from solution analysis, $Se._S$: from solid digestion

Appendix N Adsorption experiment summary for concentration experiments (experimental condition: initial pH 12.0, L/S 100, 24 h, and 150 RPM)

Se concentration (ppm)	$Se._L$%	$Se._L$/SBM	$Se._L$/LBM	$Se._L$/SBM	$Se._L$/LBM	LBM (%)	SBM%
		Q_e (mg Se/g)	Q_e (mg Se/g)	Q_e (mmol/g)	Q_e (mmol/g)		
0.5	89.0	0.0450	0.0500	0.00	0.00	0.64	-
2	91.1	0.200	0.200	0.00	0.00	5.49	-
5	92.5	0.487	0.48	0.01	0.01	4.05	5.49
10	95.2	1.00	1.01	0.01	0.01	4.52	4.05
20	97.2	2.00	2.01	0.03	0.03	2.62	4.52
50	98.5	5.12	5.05	0.06	0.06	3.64	2.62
100	99.1	10.3	10.3	0.13	0.13	3.83	3.64
200	99.2	20.5	20.7	0.26	0.26	2.58	3.83
514	95.3	50.6	50.3	0.64	0.64	3.42	2.58
870	73.3	64.4	64.3	0.82	0.81	1.16	3.29
1258	53.9	70.7	70.2	0.90	0.89	4.21	1.16
1539	43.9	71.2	71.2	0.90	0.90	2.24	4.21

$Se._L$: from solution analysis

Appendix O Structural and properties relationship of FS samples

Table 35 shows the structural and properties relationship of all FS materials prepared in this thesis with respect to aged-FS.

Table 35 Structural and properties relationship of all FS samples prepared in this thesis

	Unaged-FS	**Aged-FS**	**Calcined aged-FS at 300 °C**	**Calcined aged-FS at 800 °C**	**Modified unaged-FS**
Synthesis	Co-precipitation (partial nitrogen purging)				Co-precipitation (complete nitrogen purging)
Aging	No aging	Aged*			No aging
Phase analysis	Chloro-hydrocalumite (74 wt.%), Chloro-carboaluminate hydrocalumite (24 wt.%) and $Al(OH)_3$ (2 wt.%)	Chloro-hydrocalumite (28 wt.%), Chloro-carboaluminate hydrocalumite (70 wt.%) and $Ca_3Al_2(OH)_{12}$ (2 wt.%)	Dehydrated-FS	Mayenite, CaO and chloride containing phase	Chloro-hydrocalumite (86 wt.%), Chloro-carboaluminate hydrocalumite (11 wt.%) and $CaCO_3$ (2 wt.%), and NaCl (1 wt.%)
Experimental chemical formula	$[Ca_{3.88}Al_{2.09}(OH)_{12.1}]\cdot[Cl_{1.73}(CO_3)_{0.10}\cdot 5.27H_2O]$	$[Ca_{4.02}Al_{2.03}(OH)_{12.1}]\cdot[Cl_{1.30}(CO_3)_{0.33}\cdot 8.40H_2O]$			
QXRD/ SEM studies	Crystalline/ broken plates	Crystalline/ well- shaped hexagonal particles	Crystalline/-	-	Crystalline/-
Selenate loading	Similar to aged-FS	79% to 98% **	Higher than aged-FS	Much higher than aged-FS	-
Dissolution during adsorption	Higher than aged-FS	11.0%***	Similar to aged-FS	Similar to aged-FS	-

*aging at initial pH 12.0, L/S 20, 65 °C and 7 days **depending on feed concentration *** average LBM dissolution